Joint PhD degree in Environmental Technology

Docteur de l'Université Paris-Est
Spécialité: Science et Technique de l'Environnement

Dottore di Recerca in Tecnologie Ambientali

Degree of Doctor in Environmental Technology

Thèse – Tesi di Dottorato – PhD thesis

Sandra Viviana BOLAÑOS BENÍTEZ

Understanding of (bio)geochemical processes which control chromium release, speciation and isotopic fractionation in ultramafic environments impacted by mining activities

To be defended July 12th, 2018

In front of the PhD committee

Prof. Balz KAMBER	Reviewer
Dr. Hab. Gaël LE ROUX	Reviewer
Prof. Marc BENEDETTI	Examiner
Prof. Cécile QUANTIN	Examiner
Dr. Hab. Eric van HULLEBUSCH	Promotor
Dr. Hab. Yann SIVRY	Co-promotor
Prof. Dr. Ir. Piet LENS	Co-promotor
Prof. Giovanni ESPOSITO	Co-promotor

Erasmus Joint doctorate programme in Environmental Technology for Contaminated Solids, Soils and Sediments (ETeCoS^3)

ABSTRACT

Ultramafic systems are often synonym with high chromium (Cr) content in rocks, which is naturally leached to surface and groundwater. Due to this natural enrichment, in ultramafic areas chromium and nickel are widely mined. The mining process includes exploitation and beneficiation activities, in which large amounts of metal-rich residues, such as overburden, waste rock and tailings, stored in open air, are produced. These processes may considerably increase the amount of both trivalent (Cr(III)) and hexavalent chromium (Cr(VI)) released to the environment. The later (Cr(VI)) is known to be highly soluble in water, bioavailable and toxic. Within these mining residues, many chemical and biological processes may take place, which will control Cr speciation, mobility and availability. The present work was conducted on i) the nickel exploitation and metallurgic area of Barro Alto (BA, Goiás state, Brazil); ii) the historical chromite exploitation area of Cromínia (CA, Goiás State, Brazil) and iii) the current chromite mine in the Sukinda valley (Odisha, India). *The main focus of this research is the identification of the impact of mining activities (nickel and chromium mining) on Cr mobility and availability in ultramafic environments, through the use of isotopic techniques.*

The chemically and isotopically exchangeable pools of Cr(VI) ($E_{Cr(VI)}$) were higher in BA ore samples, where the enrichment in light chromium isotopes (-0.76 to -0.16‰) was attributed to the loose of isotopically heavy and exchangeable Cr(VI) during weathering. Astonishingly, heavy δ^{53}Cr values were also found in saprolitic ores in BA and in mining-affected soils in CA up to +3.9‰, strongly enriched in Cr(III). *The main causes are attributed to the existence of hydrothermal chromite in CA and/or to natural weathering followed by Cr(VI) reduction that induces reprecipitation of mobile and isotopically heavy Cr. In such a mining context, accelerated weathering would play an important role in this process.*

Chromium in the leachate of BA lateritic and saprolitic ores samples was present as Cr(VI), isotopically enriched in heavy isotopes (up to +4.84‰), consistent with the exchangeable Cr ($E_{Cr(VI)}$) (up to +4.37‰). These values were in the same range as isotopic compositions measured in the fresh waters (streams and ponds) in the ultramafic area. These results imply that Cr is mainly released as the toxic Cr(VI) species, whose availability increases from i) the soil profile to ii) the ores and iii) the mining residues. *This also suggests that δ^{53}Cr could be used as a tracer of Cr leaching in environmental studies in the dissolved phase.*

In bioleaching tests on tailings with *Acidithiobacillus thiooxidans* (pH ~ 2) or *Pseudomonas putida* (pH ~ 9), Cr was initially extracted as Cr(VI) and later reduced to Cr(III). In the experiments with *A. thiooxidans* Cr reduction is due to the production of a series of sulfur compounds with high reducing power, while for *P. putida* probably uses a variety of electron acceptor for chromate reduction, enhanced by the presence of extracellular polymeric substances. *Those mechanisms together with the increase of natural organic matter (NOM) and mineral carbonation, could explain the lower exchangeable pool of Cr(VI) in stockpiled chromite tailings compared to fresh tailings.*

Through the use of isotopic exchange, the contribution of suspended particulate matter (SPM) to the transport of exchangeable Cr and the impact of colloids containing Cr-bearing phases on the determination of the exchangeable pool of Cr associated to SPM (E^{W}_{Cr}) was highlighted. Larger particles (>0.2 µm) were dominant in the impacted area, while chromium was mainly associated with colloids (1 kDa–500 kDa) in the pristine area. *The presence of organic and inorganic colloids containing non-exchangeable Cr induces an overestimation of the E^{W}_{Cr} values, which can be over-come with a worst-case scenario correction.*

Keywords: Ultramafic systems, weathering, mining residues, chromium mobility, Cr isotopes, isotopic exchange.

ACKNOWLEDGEMENT

Undertaking this PhD has been a truly life-changing experience for me and it would not have been possible to do without the support and guidance that I received from many people.

First, I want to thank God, because during all my life I have been feeling that God gave me an angel, an angel that always protects me and give me patience, motivation and perseverance. My angel also fills my life of beautiful opportunities and people, and I am so grateful for that!!

To my life-coaches, my grandparents Monchito and Lety. I always want them to be proud of me and that became one of my biggest incentive to work hard… I know that every achievement in my life makes them happy!!

I am grateful to my parents, Oscar and Gloria and my brother Juancho, who have provided me through moral and emotional support in my life. I am also grateful to my beloved niece Valeria, because she is one of the biggest motivations in my life. I am also grateful to all my family members and Colombian friends who always gave me positive energy and love!!

Heartfelt thanks go to my Rapha and his family, because they became my family in France and always upheld me.

I would like to thank the EteCoS^3 committee members, Eric, Piet and Giovanni, to give me the opportunity to be part of this program. I can firmly say that is an experience that changed my life!!

A very special gratitude to my supervisors Yann, Eric and Piet, because without them this research would not be possible.

Anaelle and Evelyne, master students, gave me invaluable help with sample collection, analysis and interpretation. Thank you girls!!!

I would like to thank Jéremie Garnier, for his help during sampling and data analysis of Brasilian samples. I am also grateful to Cécile Quantin and Alexandre Gelabert for the opportunity of working in the synchrotron. It was an amazing experience.

My sincere thanks to Bibi (Jean-Loius Birk) for all his patience while teaching me the Cr isotopic techniques, and for the longer journeys in the Neptune. I am also greateful to Pascale Louvat for her support in the Neptune sessions.

My research would have been not possible with the aid of the lab staff in IPGP: Mickael Tharaud with the ICP-MS, Laure Cordier with the ICP-OES and ion chromatography, Emmanuelle Raimbault and Hassiba Lazar with carbon measurements. And also the lab staff in IHE-Delft, where I spent 6 unforgettable months: Peter Heerings, Ferdi Battes, Berend Lolkema, Fred Kruis, Lyzette Robbemont and Jack van de Vossenberg.

My sincere thanks to Nadia Saraoui for all the administrative support for the preparation of field trips and conferences. Thanks to Remi Losno for the "Integlec", Microsoft Visual Basic environment program and Eric Viollier for his explanations of the ferrozine method. Stephan Borensztajn for the assistance during measurements with the MEB and FEB. Sophie Nowak for XRF and XRD.

Thanks to all the lab members of “Biogéochimie environnementale” that in one way or another supported me during my PhD. And to my office mattes Damien, Claire and Virginia.

To my latin family in IPGP: Andreina, Sara, Virginia, Fernando, Thaïs and Kanshana and to my international family in IHE-Delft Teju, Samy, Shrutica, Joseph, Mirko, Angelo, Chris and Grabrielle. Thanks to you guys I laughed and laughed and laughed!!! And thank you to all the students of the Erasmus Mundus program EteCoS^3 and ABWET, specially Douglas, Jairo, Grabrielle, Kirki and Paolo. I will never forget the summer schools in Paris, Delft and Gaeta!!!

My sincere thanks to Jean Riotte, Sajeev Krishnan, Praveen Ramamurthy and Sankaran Subramanian for the collaboration during sampling and sample processing collected in Sukinda valley. And also to the Anglo American mining company for the accompaniment on sampling in Barro Alto mine (Goiás state, Brazil).

Finally, I would like to thank several institutions involved in my PhD. The Institute de Physique du Globe de Paris, IPGP, where I performed most of my experiments and the Institute for Water Education, IHE-Delft, where I spent six months of my PhD. And also the Indian Institute of sciences and the University of Brasilia, UnB, for their support during preparation, sampling and analysis of samples collected in the mines.

TABLE OF CONTENTS

INTRODUCTION

i. BACKGROUND

Areas with occurrence of ultramafic rocks are known as potential ore deposits of nickel-copper, platinum group metals, chromium and asbestos. One of the metals highly concentrated in those areas is chromium (Cr), which average content ranges between 1000 and 3000 mg kg^{-1}. Due to this natural enrichment, ultramafic areas are heavily mined to meet the increasing demands of metals for economic growth. The mining process includes exploitation and beneficiation activities, in which large amount of metal-rich residues, stored in open air, are produced, as well as stripped as void opencast exploited areas (Raous et al., 2013).

This research focuses on the mine residues including overburden and waste rock of the nickel exploitation and metallurgic area of Barro Alto (Goiás state, Brazil), affected and non-affected soils of the historical chromite exploitation area of Cromínia (Goiás State, Brazil) and chromite tailings from the current chromite exploitation and beneficiation area from a typical chromite mine in Sukinda valley (India).

The chemical weathering of ultramafic rocks has been studied extensively (Berger and Frei, 2014; Cooper, 2002; Garnier et al., 2009), because it is a natural source of metals, including Cr, to the environment. Rocks can be naturally weathered, however, this process occurs at a slow rate, but in mining areas, this weathering process can be accelerated, increasing concentration of Cr in the surrounding soils, surface and ground waters. Special attention has been paid to the waste generated by mining activities. Chromium has been included in the list of the priority pollutants regulated by the US Environment Protection Agency (EPA, Sueker, 1964). The EPA proposes several hazardous properties, including the threat to the environment, for the identification of the hazardous waste (EPA, 2015). They categorized tailings as “Hazardous”(MH) which is in agreement with the classification proposed by Beukes et al. (2017) for hexavalent chromium (Cr(VI)) containing wastes, generated by chromite mining. From the three groups proposed by Beukes et al. (2017) “recycled within the process”, “re-used in other applications” and “hazardous” chromite tailings belong to the third. In contrast, EPA (2001) classified waste from mineral metalliferous excavation (overburden and waste rock) as “Absolute non-hazardous (AN)”. However, several works have already shown the potential release of metals, including Cr in its hexavalent form, in

spoil nickel materials and soils in ultramafic areas (Garnier et al., 2013, 2009, 2006; Raous et al., 2013, 2010).

ii. PROBLEMS OF STATEMENT

Ultramafic waste mining residues stored in open air contain significant amount of Cr that can be mobilized to the environment by erosion (rain, water, and wind), representing a source of toxic species such as Cr(VI), as well as potentially oxidizable Cr(III). Cr(VI) is a highly oxidizing agent that can damage plant tissue cell membranes through the induction of oxidative stress (Mei et al., 2002). Besides, due to its high solubility, Cr(VI) is accumulated in plant biomass, subsequently leading to the death of the plant (Choppala et al., 2013). For the human body, Cr(VI) is a cancer agent by inhalation, while the dermal contact with Cr(VI) can develop skin lesions.

In laterite mines, the leaching of metallurgical products (bauxite processing residue and slag) have shown the presence of Cr(VI) in the dissolved fraction at concentration as high as 2100 µg L^{-1} (Economou-Eliopoulos et al., 2016). Moreover, Raous et al. (2013) concluded that Cr concentrations in waters leached from soil heaps of laterite mines can be expected to exceed the World Health Organization (WHO) guideline concentration for drinking water of 0.05 mg L^{-1} for total Cr. In a typical chromite mine, for each ton of chromite extracted, ten tons of overburden and waste rock are produced, and Cr(VI) released to the environment per year can be as high as 12 tons (Dhal and Nanda, 2011). Dhal et al. (2013) estimated the Cr(VI) production in chromite mine overburden (COB) close to 500 mg kg^{-1}, promoted by the presence of Mn oxides. Chromite tailings, containing several Cr-bearing phases, are also produced in large amount (3.7×10^5 ton yr^{-1}), during the beneficiation process. No study related with their potential chemical and biological leachability has been reported so far.

Besides studies focusing on anthropogenic environments, several authors have focused on rock weathering in ultramafic areas as the main source of Cr in rivers. The corresponding estimated contribution is 5×10^8 mol $year^{-1}$ compared to 2×10^9 mol $year^{-1}$, from anthropogenic discharges (Mcclain and Maher, 2016). Also, the use of fertilizers in ultramafic areas can worsen Cr(VI) mobility in soils, because chromate anions could be desorbed owing to competition with phosphates (Garnier et al., 2013). The impact of natural weathering on the chromium isotopic composition has also been evaluated (Crowe et al., 2013; D'Arcy et al., 2016; Ellis et al., 2002; Paulukat et al., 2015; Schauble et al., 2004; Wang et al., 2015).

Economou-Eliopoulos et al. (2016) evaluated the Cr leachability in metallurgical residues (slag and red mud, respectively) and measured the Cr isotopic composition in the leachate to follow chromium's pathway to the sea. The measurement of stable Cr isotopes has been proposed as a tool to track Cr(VI) migration in groundwater (Berger and Frei, 2014; Ellis et al., 2002; Frei and Polat, 2013; Izbicki et al., 2012) and for assessment of sources of contamination (Novak et al., 2017, 2014). However, for the second case most of studies have focused on environments affected by Cr-electroplating, where Cr in the effluents is mainly present in its hexavalent form. Meanwhile, none of the previous work has focused on the impact of mining activities on the Cr isotopic composition and its relation to redox processes and Cr mobility.

iii. OBJECTIVES

This study used isotopic techniques to identify the impact of mining activities on Cr mobility and availability in ultramafic environments. The main goal was to establish the processes which govern Cr fate in the mining context and its link with Cr isotopic composition. The specific objectives can be outlined as follows:

1. To establish the role of suspended matter on Cr mobility in the mining context as well as the impact of colloids on the determination of the Cr exchangeable pool;
2. To assess the impact of mining activities on the Cr isotopic composition of the material extracted in the mine and its relation with Cr mobility and availability in ultramafic areas;
3. To study the fate of Cr during lateritic and saprolitic ore weathering;
4. To determine the influence of pH on bioleaching of chromite tailings through incubation with *Acidithiobacillus thiooxidans* and *Pseudomonas putida*, respectively.

iv. SCOPE OF THE STUDY

The overall research was planned as five main phases (Figure 1): Phase I: Sample collection, Phase II: Samples characterization, Phase III: Cr mobility, Phase IV: Chemical leaching and Phase V: Bioleaching. Phase I consisted of samples collection in three different ultramafic areas, corresponding to an active nickel exploitation and metallurgic area (Barro Alto, Goiás state (Brazil)), a historical chromite exploitation area (Cromínia, Goiás State (Brazil)) and finally an active chromite exploitation and beneficiation area (Sukinda valley, India). This phase was decisive because samples were collected in specific sites to achieve the objectives of the study. After liquid and solid sample collection, Phase II consisted of their characterization, to serve as the main foundation of the whole laboratory research before stepping into further phases.

Once all the background information was collected from Phase II, the research activities in the following phases were initiated. Phase III consisted of the study of Cr mobility using isotopic techniques. In the first place, isotopic exchange was used to determine the isotopically exchangeable pool of Cr in suspended particulate matter in pristine and mining ultramafic areas. Also the role of colloids in the E^{W}_{Cr} determination was established, therefore achieving the first objective. In the second place, Cr isotopic measurements and fractionation in solid (bedrock, ores, soils, sediments) and liquid samples (surface and groundwater) in the active nickel mine, Barro Alto, and in the historical chromite exploitation mine, Cromínia, were used to assess the impact of mining activities and its relation with Cr fate, as described in the second objective.

The results from earlier research phases provided valuable information for sample selection for Phase IV, which consisted of the chemical leaching of lateritic and saprolitic ores collected in Barro Alto mine. Several major (Na, Ca, K, Mg, Si) and traces (Fe, Mn, Al, Cr, Ni) elements of interest were monitored during the leaching experiment. This set of experiments was focused on the understanding of Cr fate during weathering in ultramafic areas. So far, experiments were conducted with waste residues remaining after the exploitation process, however, in Phase V chromite tailings were used. Phase V consisted of bioleaching of chromite tailings, a residue obtained in large amount after the beneficiation processes in chromite mines. Acidic and alkaline conditions were obtained through the use of *Acidithiobacillus thiooxidans* and *Pseudomonas putida*, respectively. In addition, the role of bacteria in the leachability of chromite tailings was evaluated as it is described in the fifth objective.

Samples collection in Brazil was carried out in collaboration with the Universidade de Brasilia and Anglo American for access to their field facilities and help during sampling. In India, the sampling activities were supported by the Indian Institute of Sciences in Bangalore and a private chromite mine in Sukinda valley. In general, the research and experimental work related to the first four phases of the research was mainly conducted in France (Institut de Physique du Globe de Paris – Université Paris-Diderot) as well as in the Netherlands (IHE Delft Institute for Water Education) during a 6 months mobility.

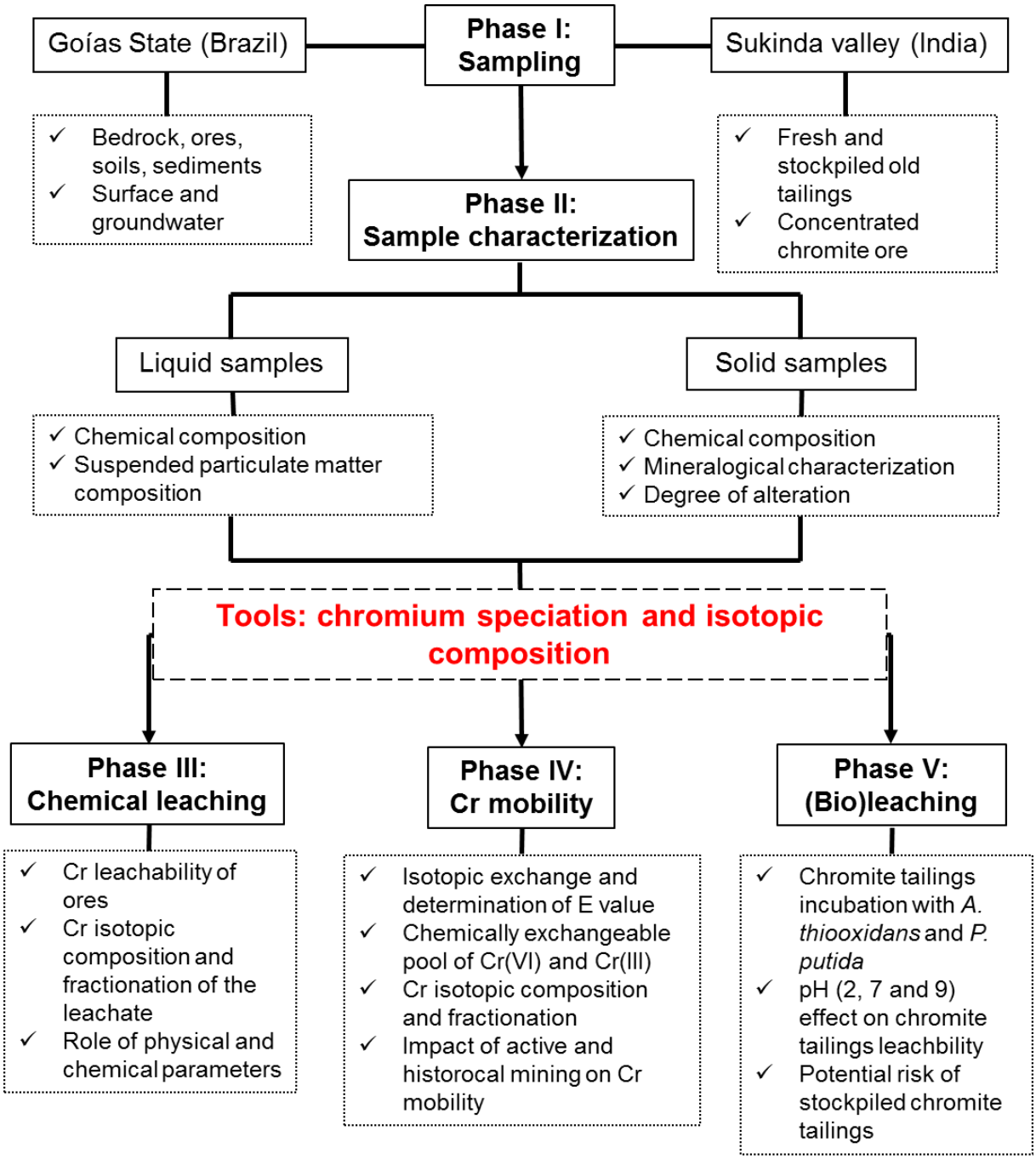

Figure 1 Research framework

v. STRUCTURE OF THE THESIS

This thesis is composed by an introduction, eight chapters and a summary and perspectives section:

Introduction: Gives an overview of the research to understand the structure of the thesis. It includes the background, problem statement, research objectives and structure of the thesis.

Chapter 2: Literature review. The review focuses on the Cr fate and availability in the environment. It compiles natural and anthropogenic sources, with emphasis on mining

activities, the processes governing Cr fate during weathering in ultramafic areas and the Cr isotopic system.

Chapter 3: Materials and methods. This chapter gives the detailed information about the sample collected, sample characterization (XRF, XRD, SEM, ICP-OES, ICP-MS) and isotopic techniques (isotopic exchange and Cr isotopic composition), as well as the leaching and bioleaching protocols used.

Chapter 4: Assessing chromium mobility in natural surface waters: colloidal contribution to the isotopically exchangeable pool of chromium (E^{W}_{Cr} value). This chapter focuses on three main aspects: i) assessing the impact of the cut-off used for the isotopic dilution technique to determine the chromium E value in water SPM, ii) determining the distribution of the chromium E value in the dissolved, particulate and colloidal fractions, and iii) proposing a calculation method to assess the contribution of the non-exchangeable colloidal Cr fraction to the chromium E value.

Chapter 5: Availability and mobility of chromium in ultramafic areas affected by mining activities: An isotopic study. This chapter investigates the impact of mining activities in the chromium mobility, availability and isotopic composition in ultramafic areas. The potential use of Cr isotopes as tracers of sources in mining areas was also evaluated.

Chapter 6: Chromium availability and mobility in soils affected by mineral extraction. This chapter outlines the Cr behavior in soils affected by historical mining activities in a small chromite mine. Exchangeable pool of Cr and Cr isotopic composition were studied in soils profiles and along a toposequence to identify the Cr behavior in areas directly affected, indirectly affected and non-affected by the mineral extraction.

Chapter 7: Saprolitic and lateritic ore alteration in mining environments. This chapter investigates the leaching behavior of saprolitic and lateritic ores, in which Cr content and mineralogical composition vary. Several physical and chemical parameters were monitored to understand its role in chromium fate and the Cr isotopic signature was measured in the leachate.

Chapter 8: (Bio)leaching behavior of chromite tailings. This chapter identifies the influence of pH and the effect of bacteria on the leachability of chromite tailings in batch experiments, where acidic and alkaline conditions were obtained through the incubation with *Acidithiobacillus thiooxidans* and *Pseudomonas putida*, respectively.

Summary and perspectives. The final chapter gives a summary and conclusions of the main results obtained, but also recommendations for further development and future research directions.

REFERENCES

Berger, A., Frei, R., 2014. The fate of chromium during tropical weathering: A laterite profile from central madagascar. Geoderma 213, 521–532. doi:10.1016/j.geoderma.2013.09.004

Beukes, J.P., du Preez, S.P., van Zyl, P.G., Paktunc, D., Fabritius, T., Päätalo, M., Cramer, M., 2017. Review of Cr(VI) environmental practices in the chromite mining and smelting industry – Relevance to development of the Ring of Fire, Canada. J. Clean. Prod. 165, 874–889. doi:10.1016/j.jclepro.2017.07.176

Choppala, G., Bolan, N., Park, J.H., 2013. Chromium Contamination and Its Risk Management in Complex Environmental Settings, Advances in Agronomy. Elsevier. doi:10.1016/B978-0-12-407686-0.00002-6

Cooper, G.R.C., 2002. Oxidation and toxicity of chromium in ultramafic soils in Zimbabwe. Appl. Geochemistry 17, 981–986. doi:10.1016/S0883-2927(02)00014-8

Crowe, S.A., Døssing, L.N., Beukes, N.J., Bau, M., Kruger, S.J., Frei, R., Canfield, D.E., 2013. Atmospheric oxygenation three billion years ago. Nature 501, 535–538. doi:10.1038/nature12426

D'Arcy, J., Babechuk, M.G., Døssing, L.N., Gaucher, C., Frei, R., 2016. Processes controlling the chromium isotopic composition of river water: Constrains from basaltic river catchments. Geochim. Cosmochim. Acta 186, 296–315. doi:10.1016/j.gca.2016.04.027

Dhal, B., Nanda, N., 2011. Environmental Quality of the Boula-Nuasahi Chromite Mine Area in India. Mine water Environ. 30, 191–196. doi:10.1007/s10230-010-0134-0

Dhal, B., Thatoi, H.N., Das, N.N., Pandey, B.D., 2013. Chemical and microbial remediation of hexavalent chromium from contaminated soil and mining/metallurgical solid waste: A review. J. Hazard. Mater. 250–251, 272–291. doi:10.1016/j.jhazmat.2013.01.048

Economou-Eliopoulos, M., Frei, R., Megremi, I., 2016. Potential leaching of Cr (VI) from laterite mines and residues of metallurgical products (red mud and slag): An integrated approach. J. Geochemical Explor. 162, 40–49. doi:10.1016/j.gexplo.2015.12.007

Ellis, A.S., Johnson, T.M., Bullen, T.D., 2002. Chromium Isotopes and the Fate of Hexavalent Chromium in the Environment. Science (80-.). 295, 2060–2062. doi:10.1126/science.1068368

EPA, 2015. Waste Classification Guide [WWW Document]. Guid. Classif. Assess. waste. URL https://www.sepa.org.uk/media/162490/waste-classification-technical-guidance-wm3.pdf (accessed 8.20.04).

Frei, R., Polat, A., 2013. Chromium isotope fractionation during oxidative weathering — Implications from the study of a Paleoproterozoic (ca. 1.9 Ga) paleosol, Schreiber Beach, Ontario, Canada. Precambrian Res. 224, 434–453.

doi:10.1016/j.precamres.2012.10.008

Garnier, J., Quantin, C., Echevarria, G., Becquer, T., 2009. Assessing chromate availability in tropical ultramafic soils using isotopic exchange kinetics. J. Soils Sediments 9, 468–475. doi:10.1007/s11368-009-0062-4

Garnier, J., Quantin, C., Guimarães, E.M., Vantelon, D., Montargès-Pelletier, E., Becquer, T., 2013. Cr(VI) genesis and dynamics in Ferralsols developed from ultramafic rocks: The case of Niquelândia, Brazil. Geoderma 193–194, 256–264. doi:10.1016/j.geoderma.2012.08.031

Garnier, J., Quantin, C., Martins, E.S., Becquer, T., 2006. Solid speciation and availability of chromium in ultramafic soils from Niquelândia, Brazil. J. Geochemical Explor. 88, 206–209. doi:10.1016/j.gexplo.2005.08.040

Izbicki, J.A., Bullen, T.D., Martin, P., Schroth, B., 2012. Delta Chromium-53/52 isotopic composition of native and contaminated groundwater, Mojave Desert, USA. Appl. Geochemistry 27, 841–853. doi:10.1016/j.apgeochem.2011.12.019

Mcclain, C.N., Maher, K., 2016. Chromium fluxes and speciation in ultramafic catchments and global rivers. Chem. Geol. 426, 135–157. doi:10.1016/j.chemgeo.2016.01.021

Mei, B., Puryear, J.D., Newton, R.J., 2002. Assessment of Cr tolerance and accumulation in selected plant species. Plant Soil 247, 223–231. doi:10.1023/A:1021509115343

Novak, M., Chrastny, V., Cadkova, E., Farkas, J., Bullen, T.D., Tylcer, J., Szurmanova, Z., Cron, M., Prechova, E., Curik, J., Stepanova, M., Pasava, J., Erbanova, L., Houskova, M., Puncochar, K., Hellerich, L.A., 2014. Common occurrence of a positive δ53Cr shift in central european waters contaminated by geogenic/industrial chromium relative to source values. Environ. Sci. Technol. 48, 6089–6096. doi:10.1021/es405615h

Novak, M., Kram, P., Sebek, O., Andronikov, A., Chrastny, V., Martinkova, E., Stepanova, M., Prechova, E., Curik, J., Veselovsky, F., Myska, O., Stedra, V., Farkas, J., 2017. Temporal changes in Cr fluxes and δ53Cr values in runoff from a small serpentinite catchment (Slavkov Forest, Czech Republic). Chem. Geol. 472, 22–30. doi:10.1016/j.chemgeo.2017.09.023

Paulukat, C., Døssing, L.N., Mondal, S.K., Voegelin, A.R., Frei, R., 2015. Oxidative release of chromium from Archean ultramafic rocks, its transport and environmental impact – A Cr isotope perspective on the Sukinda valley ore district (Orissa, India). Appl. Geochemistry 59, 125–138. doi:10.1016/j.apgeochem.2015.04.016

Raous, S., Becquer, T., Garnier, J., Martins, É.D.S., Echevarria, G., Sterckeman, T., 2010. Mobility of metals in nickel mine spoil materials. Appl. Geochemistry 25, 1746–1755. doi:10.1016/j.apgeochem.2010.09.001

Raous, S., Echevarria, G., Sterckeman, T., Hanna, K., Thomas, F., Martins, E.S., Becquer, T., 2013. Potentially toxic metals in ultramafic mining materials: Identification of the main

bearing and reactive phases. Geoderma 192, 111–119. doi:10.1016/j.geoderma.2012.08.017

Schauble, E., Rossman, G.R., Taylor, H.P., 2004. Theoretical estimates of equilibrium chromium-isotope fractionations. Chem. Geol. 205, 99–114. doi:10.1016/j.chemgeo.2003.12.015

Sueker, J.K., 1964. Chromium, in: Murphy, B. (Ed.), Environmental Forensics: Contaminant Specific Guide. Academic Press, Burlington, pp. 82–93. doi:https://doi.org/10.1016/B978-012507751-4/50027-6

Wang, X., Johnson, T.M., Ellis, A.S., 2015. Equilibrium isotopic fractionation and isotopic exchange kinetics between Cr(III) and Cr(VI). Geochim. Cosmochim. Acta 153, 72–90. doi:10.1016/j.gca.2015.01.003

CHAPTER 1

Literature review: Chromium fate and availability in the environment

CHAPTER 1.

1.1 INTRODUCTION

Chromium (Cr) is a hard, steel-grey metallic element listed as one of the priority pollutants regulated by the Environmental Protection Agency, EPA (Sueker, 1964). In the environment, it can be present as trivalent chromium (Cr(III)) and hexavalent chromium (Cr(VI)). In neutral or basic conditions, Cr(III) is the most common form of naturally occurring Cr as $Cr(OH)_3(s)$ and has a limited mobility (Apte et al., 2006). Cr(III) can also be sorbed onto iron and clay minerals. Sorption of Cr(III) increases when pH rises, because the clay surface becomes more negatively charged and it also increases when the organic matter content increases in the soil (Choppala et al., 2013). Although Cr(III) is not highly toxic, it can be oxidized to Cr(VI) leading to the formation of its anionic forms (CrO_4^{2-}, $HCrO_4^-$ and $Cr_2O_7^{2-}$) that are highly mobile and soluble. It can be toxic to both plants and animals, being a strong oxidizing agent, corrosive and a potential carcinogen (Fendorf, 1995). Cr(VI) can be produced after the oxidation of Cr(III) to Cr(VI) in soils. It has been demonstrated that easily reducible Mn oxides are able to oxidize Cr in ordinary soils, and that such oxides are the only known oxidants of Cr(III) at pH < 9 (Cooper, 2002). Bacteria can also play an important role in Cr oxido-reduction processes, through enzymatic or non-enzymatic pathways (Hansel et al., 2003; Kraemer, 2004; Thatoi et al., 2014).

In ultramafic areas, which are characterized by a high content of heavy metals including Cr (1000 – 3000 mg kg^{-1}), weathering processes represent a natural source of Cr(VI) for the aquatic system. A first dissolution of Cr(III) takes place, followed by Cr(III) oxidation by the reduction of easily reducible Mn oxides (pH < 9) (Cooper, 2002). Not only natural rocks are affected by weathering, but also residues or altered rocks, resulting from mining activities (ultramafic systems are economically valuable for Cr and Ni ores exploitation) are exposed to open air and rainfall, and consequently some metals can be dissolved.

Besides natural sources, anthropogenic sources represent the biggest input of Cr to the environment, and Cr is mainly released in its toxic hexavalent form (Guertin, 2005). Environmental pollution due to toxic metals is one of the major concerns in mining areas around the world. As a result of Cr mining, a large volume of overburden, comprising of chromite ores and waste rock material generated which are dumped in the open ground. During the wet season, heavy metals are leached, from these dumps, which contaminates

the surface water as well as ground water bodies (Das et al., 2013). Several studies have shown the potential release of Cr(VI) from mining materials (Becquer et al., 2003; Garnier et al., 2013, 2009b, 2008, Raous et al., 2013, 2010). Once Cr ore is mined, it is converted to ferrochromium, chromium chemicals and incorporated in chromite-containing refractories, which represent other sources of chromium in the environment (Papp, 1994).

The oxidation-reduction changes of Cr have been of special interest, because they promote isotopic fractionation. Cr has four stables isotopes ^{50}Cr (4.345%), ^{52}Cr (83.789%), ^{53}Cr (9.501%) and ^{54}Cr (2.365%), where ^{52}Cr and ^{53}Cr are the most abundant. The measured variations of ^{53}Cr/^{52}Cr in different material have been used to provide information on Cr sources, transport mechanisms, and fate in the environment (Ellis et al., 2002; Izbicki et al., 2012). Weathering is a Cr source in the environment and in addition oxidative rock weathering is accompanied by isotopic fractionation, where the mobilized Cr(VI) released to runoff is enriched in isotopically heavy Cr, leaving behind an isotopically light Cr(III) pool in the soil (Paulukat et al., 2015). Some studies have shown that soils can be also enriched in heavy Cr isotopes (Crowe et al., 2013; Farkaš et al., 2013; Frei and Polat, 2013; Wang et al., 2015).

Considering the toxicity of Cr and its presence in ultramafic systems impacted by mining activities, this chapter presents an introduction to the understanding of the biogeochemical processes which control Cr release, speciation and isotopic fractionation in such specific systems.

1.2 CHROMIUM SOURCES IN THE ENVIRONMENT

Chromium is present in various environmental media including surface and ground water, seawater, air, soils, sediments and rocks. Chromium can enter into the environment via natural sources and through anthropogenic pathways (Choppala et al., 2013).

1.2.1 Natural sources

Bedrocks, such as ultramafic rocks are naturally enriched in light elements including silica (Si) and magnesia (Mg), and are depleted in Cr and other heavy metals. Those rocks are susceptible to weathering, because the light elements (Si and Mg), which are the main chemical components, are preferentially leached by meteoric waters, with a consequent enrichment in heavy elements such as Fe (laterite) and Cr hydroxides. In ultramafic soils derived from ultramafic rocks, nutrient content is poor, Ca:Mg ratio is low and Cr is highly concentrated. It is important to highlight that the Cr content in soils is largely dependent on parent materials. In granitic rocks, limestones and sandstones, Cr levels average from 20 to 35 mg kg^{-1}, in basaltic rock the average Cr content is 220 mg kg^{-1} and in ultramafic rocks it

increases up to 1800 mg kg^{-1} (Choppala et al., 2013). Table 1.1 presents the average Cr stoichiometry in relevant minerals and Table 1.2 presents an average Cr content in some materials. Chromite ($FeCr_2O_4$) is the main Cr mineral and it can be commonly found in ultramafic areas. Chromite is of igneous origin and formed in peridotite. Other Cr-bearing minerals are mainly oxides such as magnetite and to a lower extent silicate phases like serpentine and pyroxenes (Garnier et al., 2009b).

Table 1.1 Chromium minerals (Burns and Burns, 1975).

Mineral	Formula	Structure type
Chromite	$FeCr_2O_4$	Spinel (Normal)
Crocoite	$PbCrO_4$	Own
Phoenicochroite	$Pb_2O(CrO_4)$	Lanarkite
Magnesiochromite	$MgCr_2O_4$	Spinel (Normal)
Picotite	$(Fe, Mg)(Al, Cr, Fe)_2O_4$	Spinel
Grimaldiite	$HCrO_2$	$HCrO_2$
Silicates / Knorringite	$Mg_3(Cr, Al)_2(SiO_4)_3$	Garnet
Chromatite	$CaCrO_4$	Zircon

Despite the presence of geogenic Cr mainly as chromite which is reported to be extremely insoluble (Becquer et al., 2003), various studies have been conducted to evaluate Cr mobility, availability and potential toxicity in the environment. Garnier et al. (2009) used isotopic exchange kinetics to assess the chromate availability in tropical ultramafic soils collected in Niquelândia (Goiás, Brazil).

Table 1.2 Concentration of Cr in some materials (Choppala et al., 2013).

Material	Chromium content	
	Range (mg kg^{-1})	Average (mg kg^{-1})
Ultramafic and serpentine	1100 – 3400	1800
Phosphorites	30 – 3000	300
Basalts and gabros	60 – 420	220
Clay and shales	1 – 200	90
Andesites, diorites	10 – 200	50
Soil	10 – 150	40
Sandstones	20 – 35	35
Limestone and dolomites	-	11
Coal	-	10
Granitic rocks	2 – 60	5

Garnier et al. (2009) reported that there is a large quantity of labile Cr(VI) (up to 1000 mg kg^{-1} which represents 10 wt% of total Cr) in ferroalsols, in which behaviour is controlled by amorphous iron oxides and pH. A significant positive correlation ($p<0.05$) between the readily labile Cr with the Cr associated to amorphous or poorly crystallized Fe-oxides and with pH

($p<0.05$) were obtained by Garnier et al. (2009). Sequential extraction was performed in the same Brazilian soils, showing that most of the Cr is within the well crystalized Fe-oxides (50-85%) and the residual fraction (5-30%). Cooper (2002) performed Cr extraction with ammonium acetate in ultramafic subsoils in Zimbabwe, which was identified as Cr(VI) using S-diphenylcarbazide, whereas Becquer et al. (2003) used KH_2PO_4 and KCl to extract Cr(VI) and Cr(III), respectively in soils from New Caledonia. Becquer et al. (2003) observed a large part of Cr associated with Fe-oxides, due to isomorphic substitution of Fe by Cr.

Table 1.3 Total Cr concentration (µg L^{-1}) in surface and ground waters located in ultramafic areas.

Study areas	Water bodies	Range of variation of total Cr concentration (µg L^{-1})	References
Worldwide	Surface water	0.25 – 100	Mcclain and Maher (2016)
Sukinda valley (India)	Groundwater	1220 – 1260	Paulukat et al. (2015)
	Surface water	0.292 – 120	
	Seawater	0.3	
Central Euboea and the Assopos basin (Greece)	Groundwater	41 – 230	Economou-Eliopoulos et al. (2014)
Leon valley (Mexico)	Groundwater	31.6 – 11070	Villalobos-Aragón et al. (2012)
Mohelno (Czech Republic)	Surface water	7.8 – 23.3	Farkaš et al. (2013)
Sukinda valley (India)	Surface water	740	DAS et al. (2013)
Sukinda valley (India)	Surface water	17 – 68	Godgul and Sahu (1995)
	Well	17	
	Quarry	17 – 1791	

Chromium potentially released from soils reaches surface and groundwater. Rock weathering (crustal rocks typically have Cr concentrations of 100 mg kg^{-1}) represents the main natural sources of Cr to river (Mcclain and Maher, 2016). Other sources include wet precipitation, dry fallout from the atmosphere and runoff from the terrestrial system (Kotaś and Stasicka, 2000). Continental dust flux is the main natural source of chromium in the atmosphere, and volcanic dust and gas flux are minor natural sources. Approximately one-third of the atmospheric releases of Cr are in the hexavalent form (Fendorf, 1995). In freshwater, total Cr concentration generally ranges from 0.1 to 6.0 µg L^{-1} with an average of 1.0 µg L^{-1} and in seawater the average is 0.3 µg L^{-1} with values from 0.2 to 50.0 µg L^{-1} (Bowen, 1979 in Choppala et al., 2013). However, in water bodies crossing ultramafic areas, the Cr concentration can be higher. Table 1.3 presents a compilation of Cr concentration in surface and groundwater located in ultramafic systems. Values presented in Table 1.3 not only correspond to pristine environments, because due to the Cr enrichment in ultramafic

areas, different anthropogenic activities such as mining are carried out with a consequent heavy metal pollution of water bodies.

In natural waters, Cr occurs in two oxidation states, as Cr(III) and Cr(VI). The concentration of Cr(III), which is sparingly soluble in natural waters, is limited by adsorption on mineral surfaces and incorporation into minerals such as chromite, Fe(III) containing minerals, Al hydroxides and clays. In contrast, Cr(VI) is more soluble and mobile, persists in polyatomic anionic form as CrO_4^{2-} under strong oxidizing conditions, and its concentration is affected by adsorption onto Fe oxides and hydroxides at acid to neutral pH conditions (Choppala et al., 2013; Fendorf, 1995; Oze et al., 2004).

1.2.2 Anthropogenic sources

The utilization of Cr by many industries including electroplating, chrome tannery processing, wood-pulp preserving, petroleum refining, pigment production and nuclear power plants, has been increasing (Choppala et al., 2013). All those activities have in common the potential production of Cr in its hexavalent form which is highly mobile and toxic.

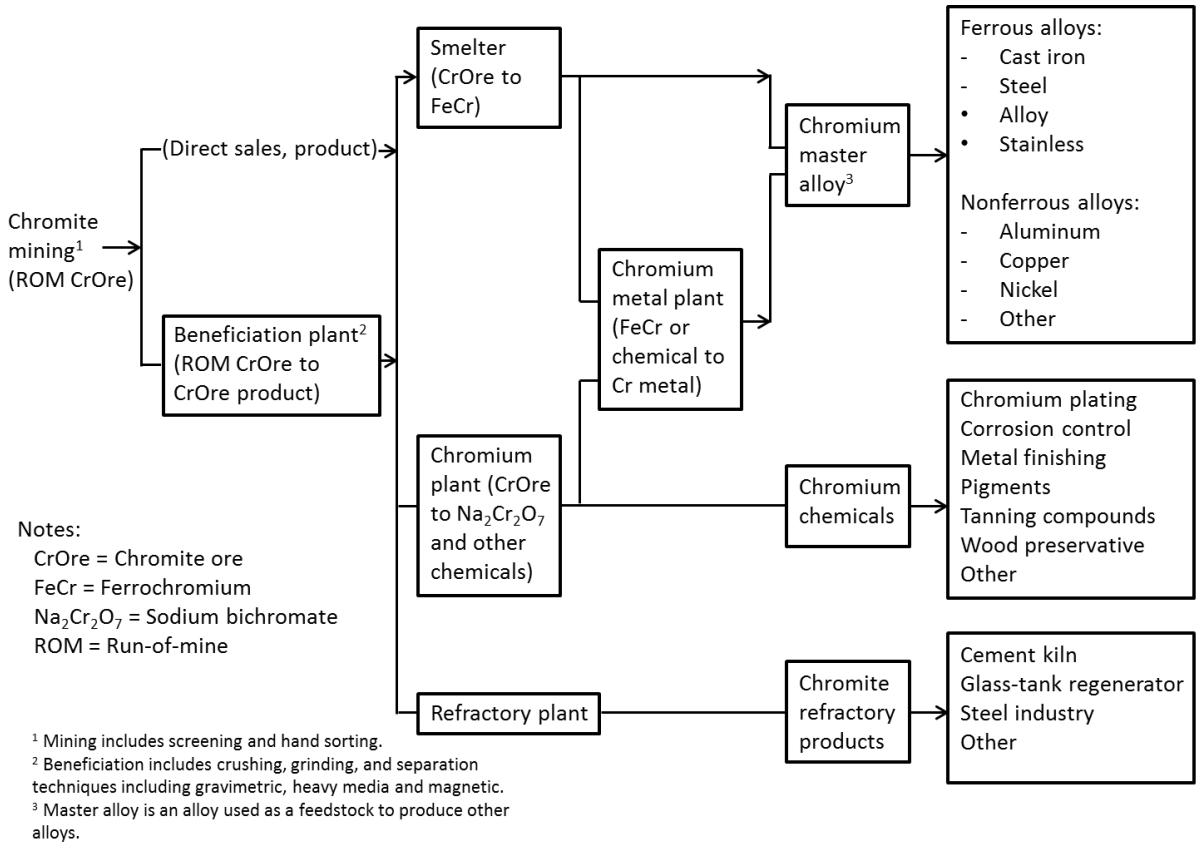

Figure 1.1 Industrial chromium material flow (Papp, 1994).

Figure 1.1 shows the flow of chromium from mine production through to end uses. In this sense, the first anthropogenic source of Cr is mining, when chromite ore is extracted.

Afterwards, the ore extracted is converted to ferrochromium, Cr chemicals and incorporated in chromite-containing refractories, which represent other sources of Cr in the environment.

1.2.2.1 Chromite mining

Chromium is extensively used in the manufacture of paint pigments and chemicals, as oxidizing agents in organic syntheses, as electrolytes in chromium plating baths, and as agents for the tanning of leather (Nafziger, 1982). The source of chromium for the manufacturing of the products mentioned previously is mining, where chromite is extracted. Figure 1.2 shows the main chromite producers in the world.

In contrast to the Cr anthropogenic sources explained above, in most of the cases mining activities does not release Cr(VI) directly to the environment, because in minerals, such as chromite, Cr is present in its trivalent form. However, mining which can include blasting and the crushing leaves open-air materials that were previously buried. Rocks can be naturally weathered, however, this process occurs at a slow rate. In mining area, this weathering process can be accelerated, increasing concentration of Cr in the surrounding soils, surface and ground waters. The mining process is divided in two main phases: exploitation and beneficiation.

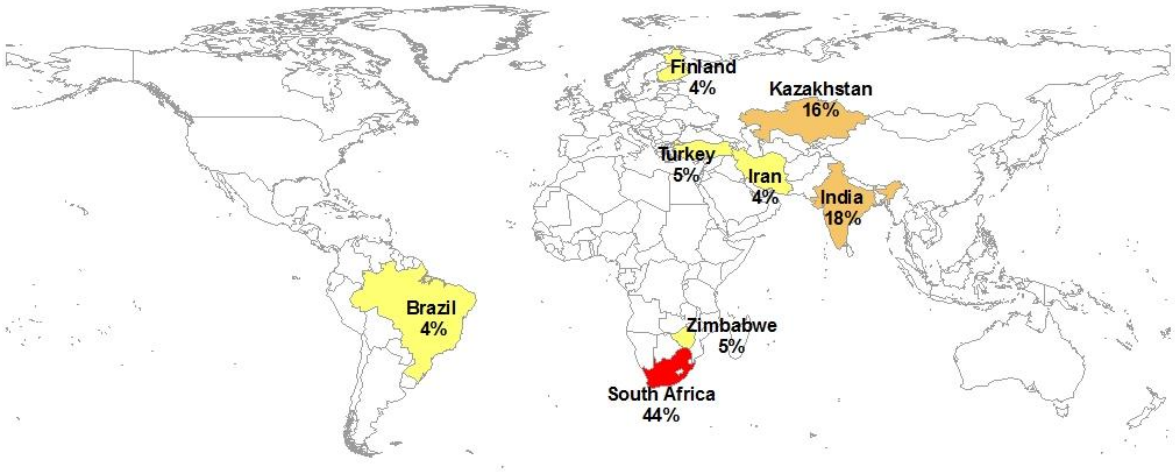

Figure 1.2 Chromite production worldwide. South Africa, India and Kazakhstan produce 78% of chromite in the world.

1.2.2.1.1 Exploitation

The exploitation consists in the actual recovery of minerals which will depend on the characteristics of the mineral deposit and the limitations imposed by safety, technology, environment concerns and economics. Chromite can be extracted by both traditional exploitation methods that are surface and underground mining. Figure 1.3 shows an overview of surface mining, which can be open pit and open cast (strip mining). In Figure 1.3 the dark pink represents the ore deposit, which in the case of chromium is chromite. Chromium ore is a ferrous alloy, which basically means that there is a high content of Fe while Cr remains concentrated reaching 50 to 70% by weight. In “mining terminology”, ore is a mineral deposit that has sufficient utility and value to be mined at a profit (Arndt et al., 2015). In order to gain access to the ore deposit, different materials are extracted including overburden and waste rock. Overburden basically corresponds to the soil on top of the deposit and waste rock is the material associated with the ore deposit that must be mined to get access to the ore, but is discarded. One particular type of waste rock is the gangue which are valueless minerals within an ore deposit (Tripathy et al., 2012).

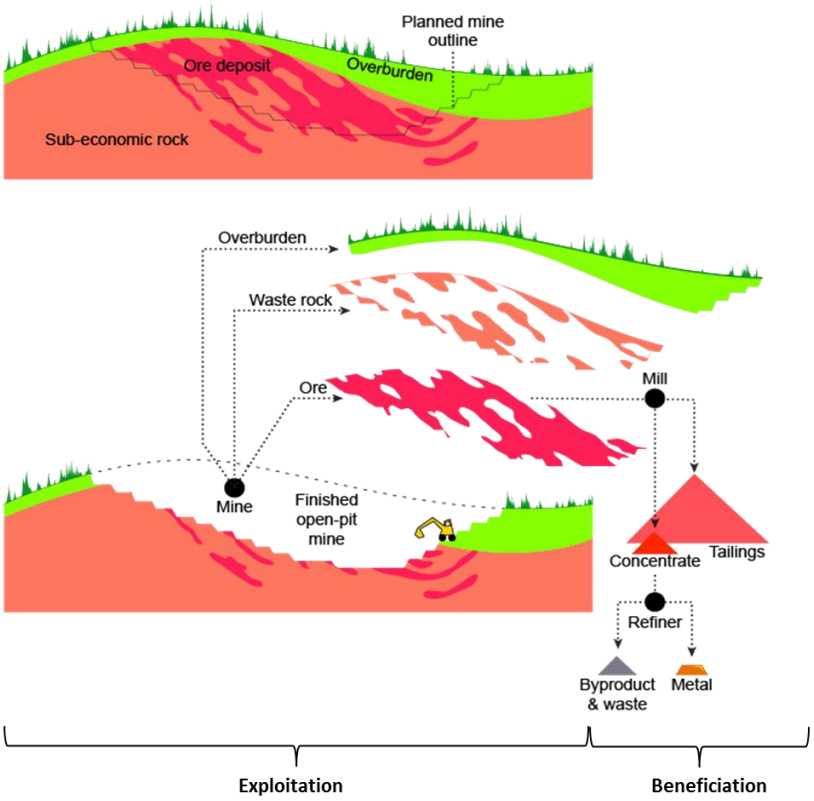

Figure 1.3 Overview of component of a mineral deposit and mining phases: exploitation and beneficiation (Higman, n.d.).

Both overburden and waste rock are stored as open air stockpiles, representing a source of Cr and other heavy metals to the environment. Chromite oxidation in overburden dumps represents one source of Cr(VI). In Sukinda (India), more than seven decades of open-cast chromite ore mining has resulted in massive holes and the accumulation of mountains of waste rock and soil (Dhal et al., 2013).

For each ton of chromite extracted, ten tons of overburden and waste rock are typically produced. It is estimated that approximately 7.6 million tons of overburden are stored per year, releasing in the environment 12 tons of Cr(VI) per year (Dhal and Nanda, 2011). This is the reason why Sukinda is in the top ten of the world's 30 most polluted places. Due to this concern, Dhal et al. (2013) estimated the Cr(VI) production close to 500 mg kg^{-1} in the chromite mine overburden (COB) dump of Sukinda. This promoted promoted by the presence of Mn oxides. Dhal and Nanda (2011) also observed that the microbial population in overburden samples was low as well as the nutrient (N, P, K) which were leached to nearby agriculture land, making them less fertile. Cr(VI) produced can migrate until groundwater, however, Tiwary et al. (2005) observed that poor permeability of the seepage could limit the Cr(VI) migration to groundwater. Cr(VI) not only migrates to groundwater, surface water also ends up affected specially during the Monsson season (Das et al., 2013).

Elzinga and Cirmo (2010) determined the Cr speciation in marsh soils developed in weathering chromite ore processing residue (CORP). The sequential extraction revealed that Cr was associated with reducible and oxidizable soil components, and significant non-extractable residual Cr. Micro-sized chromite particles were found in the CORP matrix. Cr leaching and repartition into secondary $Fe(OH)_3$ phases and organics, from the CORP was observed when comparing weathered material (200-850 ppm) with unweathered material (20,000-60,000 ppm).

Taking into consideration the enormous production of chromite overburden, studies have focused on the recovery of elements such as Ni, which can be present in concentrations between 0.5 and 1.0 wt%. Since Ni is embedded in goethite, Behera et al. (2012) performed microbial reduction of ferric iron with *A. ferrooxidans*, reaching and extraction of 41% of Ni from COB of 1% nickel grade. Esther et al. (2013) used a dissimilatory iron reducing bacterial consortium (DIRB) to recover Ni and Co from COB, with a maximum yield of 69% and 81%, respectively (using 8M H_2SO_4). DIRB utilized Fe(III) as terminal electron acceptor reducing it to Fe(II), with a consequent reduction of goethite to hematite and magnetite. Fungal assisted bioleaching also has been evaluated by Biswas and Bhattacharjee (2014) to recover Ni and Co from COB with a maximum recovery of 70.49 and 66.93%, respectively.

1.2.2.1.2 Beneficiation

Ores can be divided in two broad categories according to the content of the mineral of interest in low-grade ore or high-grade ore. The highest-grade chromites are those having a Cr/Fe ratio of more than 2.0 (approximately 2.8) and those containing a minimum of 46 to 48 wt% of Cr_2O_3 (Nafziger, 1982). Low-grade chromites are those with lower Cr/Fe ratio and smaller Cr_2O_3 content (less than 40%). India possesses huge quantities of low-grade chromite reserves (Kumar Bhandary et al., 2016). High-grade chromites are apt to be used directly in the metallurgical industry, however, low-grade chromites have to be concentrated through a process called beneficiation. The beneficiation process includes crushing to decrease particle size and to facilitate the following steps, grinding and gravity recovery. In India, chromites can be concentrated by conventional ore-dressing techniques owing to the difference in relative density between the ore and gangue materials (Nafziger, 1982). As a product of the beneficiation process, concentrated chromite is obtained with a Cr/Fe ratio close to 2.0 and tailings are produced as a residue. The most essential issue of every gravity separation circuit in mineral processing plants, is the loss of large fraction of the valuable minerals into tailings (Murthy et al., 2011). Nearly 50% of total feed is lost as a tailings in Indian chromite beneficiation plant. Tripathy et al. (2013) performed a characterization of an Indian chromite beneficiation plant tailing. Tailings were composed of Cr_2O_3 (17%), $Fe_{(T)}$ (23.9%), Al_2O_3 (24.4%), SiO_2 (11.3%), MgO (3.6%) and loss on ignition (8.7%). About 80% (by weight) of the particles are <260 µm and 50% < 190 µm, where Cr_2O_3 content increases up to 37 µm and decreases below that. The main mineral phases present on tailings are chromite, goethite, hematite, gibbsite, quartz and kaolinite. Despite the high content of Cr in the tailings, no detailed studies dealing with the risk of Cr(VI) leaching on the tailings have been conducted, because chromite is considered a refractory mineral resistant to alteration.

Regardless of the lack of study dealing with environmental risks associated to chromite tailings storage, several studies have been conducted to evaluate the potential re-use of chromite tailings. Özgen (2012) evaluated the combination of hydrocyclone and multigravity separator (MGS) for the beneficiation of fine chromite tailings to produce concentrated chromite (48%). Tripathy et al. (2013) produced a concentrated chromite with a Cr/Fe ratio of 2.3 and a Cr_2O_3 content of 45% using a flow sheet comprised by conventional gravity concentration, magnetic separation and flotation. Mine tailings contain base transition metals such as iron, copper, nickel and zinc, in relative high concentration, and occasionally precious metals such as gold and silver (Falagán et al., 2017). So far, the potential recovery of metals contained in chromite tailings has not yet been evaluated.

1.2.2.2 Ni laterite mining

Ultramafic soil are a natural source of Cr(VI) in the environment (section 1.2.1). Those ultramafic areas can contain an important reservoir of Ni, and consequently Ferro-nickel mining takes place, as is the case of Niquelândia and Barro Alto in Goiás state (Brazil). In ultramafic rocks, the mineral phases to which Ni is associated are mainly olivine (in particular forsterite), spinel, amphiboles, serpentine, pentlandite and Cr-magnetite (Kierczak et al., 2007; Quantin et al., 2008; Zelano et al., 2015). In Niquelândia and Barro Alto in Goiás state (Brazil), Cr is present in the soil (overburden) and ores. Raous et al. (2013) studied the potential toxic metals, including Cr, in ultramafic mining materials. They found that in garneritic and limonitic samples and their corresponding spoil material, Ni and Cr are the main secondary metals. In garnerite, Cr presented a low availability, which can be linked to its sequestration into chromiferous spinels but also as an element in the octaheadral sheet in the smectite structure. However, 0.7% of total Cr was extracted as a Cr(VI) which corresponds to Cr linked to complexed on the silanol and aluminol peripheral groups of smectite. In limonite the presence of goethite explained the presence of Cr(VI). Raous et al. (2013) concluded that Cr concentrations in waters leaching from soil heaps can be expected to exceed the WHO guideline concentration for drinking water of 0.05 mg L^{-1} for total Cr. In Niquelândia (Brazil), a Ferro-nickel mine, Raous et al. (2010) performed lixiviation experiments on limonite and revealed Cr concentration, mainly Cr(VI) (CrO_4^{2-} or $HCrO_4^-$), in waters exceeding this limit. Economou-Eliopoulos et al. (2014) studied the potential leaching of Cr(VI) from laterite mines and residues of metallurgical products (red mud and slag) in Greece and found Cr(VI) concentrations as high as 2100 µg L^{-1}. Even if there is a lack of studies dealing with Ni and Cr speciation and mobility in temperate climate are even rarer (Kierczak et al., 2007).

1.2.2.3 Chrome tannery

In the leather industry, Cr(III) salts are the most widely used materials in tanning processes and are known to be highly toxic and affects cellular compounds in organisms (Pasco et al., 2000 in Mwinyihija, 2010). Cr remains in the tannery wastewater, which subsequently discharges into the treatment plant and ultimately goes into the excess sludge. As a result, about 1 to 4% of Cr(III) remains in the dry tannery sludge (Ma et al., 2017). However, in most of the countries the tanning wastewater is discharged without treatment into the sewerage system causing serious environmental impact (Ahmed et al., 2016). Cr(III) is the most expected species in tanning effluents, however, redox reactions occurring in the sludge increase the content of Cr(VI). The pH of this wastewater is slightly acidic or neutral and $Cr(OH)_3$ should be the dominant form, but a high content of organic matter originating from hide/skin material processing is effective in forming soluble Cr(III) complexes (Mwinyihija,

2010). Stein and Schwedt (1994) studied Cr speciation, toxicity and eco-chemical behaviour in the wastewater from a tannery. They observed that Cr(VI) was not stable in the samples collected and Cr(III) was mainly associated with colloids. When effluents from tannery and treatment plants containing Cr(VI) are discharged in water bodies, sediments act as a reservoir of Cr(VI).

Considering the presence of Cr(VI), river sediment acts as a reservoir of Cr(VI). Dredging operations is an alternative to removed polluted sediments, however Cr(VI) can be potentially mobilized into the water column. Burbridge et al. (2012) studied the Cr speciation in river sediment pore waters contaminated by tannery effluent. To avoid changes in the native chemical conditions and chemical speciation, they used peepers (dialysis cells to collect sediment pore water samples) for pore water extraction. They did not find Cr(VI) in the pore water, concluding that Cr(VI) reduction was favoured. Groundwater polluted by tannery was studied in Chennai city, India by Kumar and Riyazuddin (2010) and they found Cr mainly in its hexavalent form and trivalent chromium forming organic complexes.

Traditionally, precipitation methods are used for Cr removal from tannery wastewater. Ahmed et al. (2016) found that remediation of Cr from a tannery in a microcosm with the actinomycete strain *Kitasatosporia* sp and the later recycling of Cr(III) is a promising strategy for economic and environmentally friendly industry. Bioleaching from tannery sludge driven by *Acidithiobacillus* species, exhibited large amounts of Cr(III) and Fe, also contained Ca, Na, Mg and K. This bio-leachate can be later recycled as a Cr-iron tanning agent, which can reduce the usage of Cr during the tanning process (Ma et al., 2017). A consortium of four Cr-resistant ascomycetous fungi (*Cladosporeum perangustum*, *Penicillium commune*, *Paecilomyces lilacinus* and *Fusarium equiseti*) was used by Sharma and Malaviya (2016) for detoxification of industrial wastewaters through extracellular enzymes production and biosorption by fungal biomass. Chromium nanofiltration and the influence of the chloride/sulfate ions ratio also has been studied Religa et al. (2011).

1.2.2.4 Electroplating

Next to tannery, electroplating industries are also a major source of Cr in the environment. Electroplating consists on the deposition of a fine layer of one metal on another metal or material through electrolysis. The goal of the process is to produce a surface with desired properties such as corrosion protection, enhanced surface hardness, color, among others (Machado et al., 2010). Chrome plating can be achieved by using salts of both trivalent and hexavalent chromium, however, the most commonly used is chromic oxide (CrO_3). Washing and rinsing generate wastewater enriched in Cr(VI) species, with low concentrations of

soluble forms of various metal salts at low pH (3-5) (Liu et al., 2016). India is one of the countries with most electroplating industries with over 3 million industries, which are operating as small scale sectors (Chitraprabha and Sathyavathi, 2018). In Australia, nearly 6 million copper-chrome-arsenate (CCA)-treated posts are disposed annually, thus constituting the major source of Cr(VI) in soil and groundwater. In the past, Cr-wastewater, containing mainly Cr(VI), was disposed into dry wells (Choppala et al., 2013).

As a result of Cr(VI) production by electroplating several studies have been conducted to reduce Cr(VI) to a nontoxic form. Traditional plating wastewater treatments include two main steps: i) Cr(VI) reduction and ii) precipitation of Cr(III) and other metal ions as hydroxides. Cavaco et al. (2007) used a chelating exchange resin (Diaion CR11) and a weak cationic resin (Amberlite IRC86) to retain Cr(VI). Despite the recovery of Cr with resins the cost are elevated and for those reasons further studies with biomaterial have been carried out. Liu et al. (2016) proposed a wastewater treatment replacing the first conventional step (Cr(VI) reduction) by biosorption with exhausted coffee, which eliminated totally Cr(VI) in solution. Sibi (2016) used dried algal biomass of *Chlorella vulgaris* as a biosorbent of Cr(VI), displaying a potential use of this technology in a wide range of pH and salinity. Chitraprabha and Sathyavathi (2018) performed phytoextraction of Cr from electroplating effluent using *Tagetes erecta* (L.), with a successful metal translocation in the plant from soil-to-root-to-shoot and a tolerance of Cr concentration up to 6 mg kg^{-1}.

1.3 CHROMIUM DISTRIBUTION AND SPECIATION IN THE ENVIRONMENT

Chromium can exist in several oxidation states, displaying numbers from 0 to VI, however only trivalent (Cr(III)) and hexavalent chromium (Cr(VI)) are stable enough to occur in the environment (Choppala et al., 2013; Fendorf, 1995; Kotaś and Stasicka, 2000). Figure 1.4 presents the hydrolysis speciation and valence state of Cr over a range of Eh and pH values. In neutral and basic aquatic environments, Cr(III) binds with adjacent molecules of the same species to form poly nuclear complexes and finally precipitates as $Cr(OH)_3$ (Salem et al., 1989). According to Choppala's et al. (2013) thermodynamic model, Cr(III) can exist as hydroxyl species in an aquatic environment as $Cr(III)^{+}$, $Cr(OH)^{2+}$, $Cr(OH)_3$, $Cr(OH)^{4-}$, $Cr_2(OH)_2^{4+}$, $Cr_3(OH)_4^{5+}$ and $Cr_4(OH)_6^{6+}$ at pH> 3.5. Under reductive conditions of water and soil, trivalent chromium is the most stable form and in the absence of complexing agents, other than H_2O or OH^-, Cr(III) exists as hexa-aquachromium (3+) and its hydrolysis products (Kotaś and Stasicka, 2000):

$$\mathrm{Cr(H_2O)_6^{3+}} + H_2O \leftrightarrow \mathrm{Cr(OH)(H_2O)_5^{2+}} + H_3O^+ \quad \textbf{(1.1)}$$

$$\mathrm{Cr(OH)(H_2O)_5^{2+}} + H_2O \leftrightarrow \mathrm{Cr(OH)_2(H_2O)_4^{+}} + H_3O^+ \quad \textbf{(1.2)}$$

$$\mathrm{Cr(OH)_2(H_2O)_4^{+}} + H_2O \leftrightarrow \mathrm{Cr(OH)_3.aq} + \mathrm{H_3O^+} \quad \textbf{(1.3)}$$

The formation of Cr(III) hydrolysis products at low pH has important implications on the sorption, solubility and bioavailability of this ion. This is due to the disruption of their symmetric water coordination sphere, which greatly enhances the ions reactivity (Schindler and Stumm, 1987 in Fendorf, 1995). This reactivity promotes Cr(III) ion retention on soil minerals under most pH values encountered. Cr(III) also readily sorbs on surfaces of Fe(III) oxides and (oxy)hydroxides via inner-sphere surface complexes and form low solubility precipitates (Oze et al., 2004). Sass and Rai (1987) as reported in Oze et al. (2004) have attributed the low concentration of Cr(III) in soil solution to the low solubility of Fe(III)-Cr(III) amorphous hydroxides.

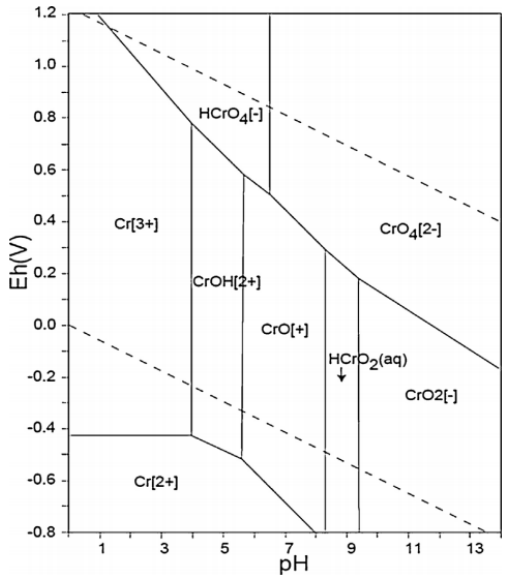

Figure 1.4 Diagram of the thermodynamic stability of aqueous Cr species over a range of Eh and pH values of the surface environment (Fendorf, 1995).

On the other hand, hexavalent chromium (Cr(VI)) is a strong oxidant and is stable under high redox potentials, in the absence of reductants (Choppala et al., 2013). In water, Cr(VI) forms several anionic species and the relative proportions depend on pH and total Cr concentration (Kotaś and Stasicka, 2000). In a pH range between 1 and 6, $HCrO_4^-$ is the predominant form of Cr(VI), and above 7 only CrO_4^{2-} exists in solution (Figure 1.4). Within the normal pH range (4 - 9) in natural waters, CrO_4^{2-}, $Cr_2O_7^{2-}$ and $HCrO_4^-$ are the forms expected (Kotaś and Stasicka, 2000). At acid to neutral pH conditions, Cr(VI) has a limited thermodynamic redox stability and it can be easily adsorb onto Fe oxide and hydroxides, whereas at high pH

conditions is more mobile (Stefánsson et al., 2015). Due to its anionic nature, Cr(VI) is not retained appreciably on negatively charged colloids of soils or sediments. In addition, hydrous oxides of Al and Fe commonly have a net positive charge and therefore a potential affinity for Cr(VI) oxyanions (Fendorf, 1995). Cr(VI) anions can be leached into deeper soils and eventually reach groundwater or can be taken up by plants. To understand the mobility and fate of chromium in the environment, three groups of reactions have to be considered: oxidation-reduction, sorption-desorption and precipitation-dissolution.

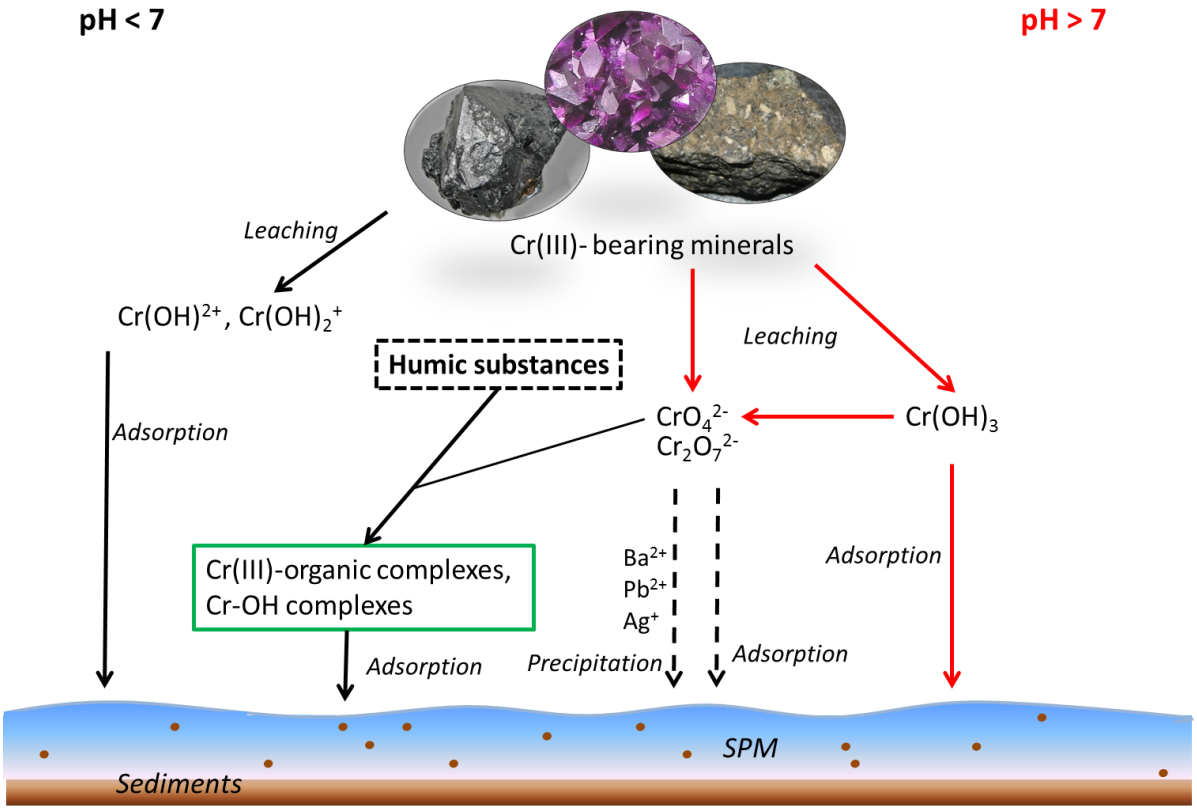

Figure 1.5 Schematic model for chromium circulation in natural waters under alkaline and acidic conditions (Modified from Saputro et al., 2014).

Saputro et al. (2014) proposed a schematic model for chromium cycling (Figure 1.5). Cr bearing minerals are the source of Cr in the environment. Cr is first leached as Cr(VI) from Cr(III)-minerals under neutral to alkaline conditions by oxidation with dissolved oxygen. Sediments and suspended matter adsorb Cr(III), as hydroxo complexes such as $CrOH^{2+}$ and $Cr(OH)_2^+$, leached from the rock or produced after Cr(VI) reduction. Under acidic conditions, Cr(III) tends to form complexes with naturally occurring organic matter, such as fulvic or humic acids.

1.3.1 Oxidation-reduction reactions

Oxidation and reduction reactions can convert Cr(VI) to Cr(III) and vice versa, and the processes depend on pH, O concentration and presence of reducers and mediators acting as ligands or catalysts. Figure 1.6 shows the coupling of Cr oxidation and reduction in soils. Cr(VI) mobile forms ($HCrO_4^-$ and CrO_4^{2-}) can be reduced in the presence of Fe(II) and S^{2-}. The Cr(III) produced is transported by mobile ligands like fulvate and citrate to the oxidation site where Mn(III) and Mn(IV) are reduced to form Mn(II) and in parallel Cr(III) is oxidized to Cr(VI) (Kotaś and Stasicka, 2000). Oxidation of Cr(III) to Cr(VI) represents a hazard, since a rather innocuous species is transformed into a toxic one. The role of Mn-oxides on Cr(III) oxidation has been studied by Fandeur et al. (2009) in a lateritic regolith in ultramafic rocks of New Caledonia. The largest amount of Cr(VI) was observed in the vicinity of Mn-oxides. Cr(VI) distribution suggested Cr(III) oxidation by Mn-oxides with a consequent re-adsorption on Fe-oxides. Ultramafic soils with a high clay and total Cr content are likely to contain labile Cr(III) capable of oxidation to toxic Cr(VI). In addition, wetting-drying cycles promotes this process (Cooper, 2002).

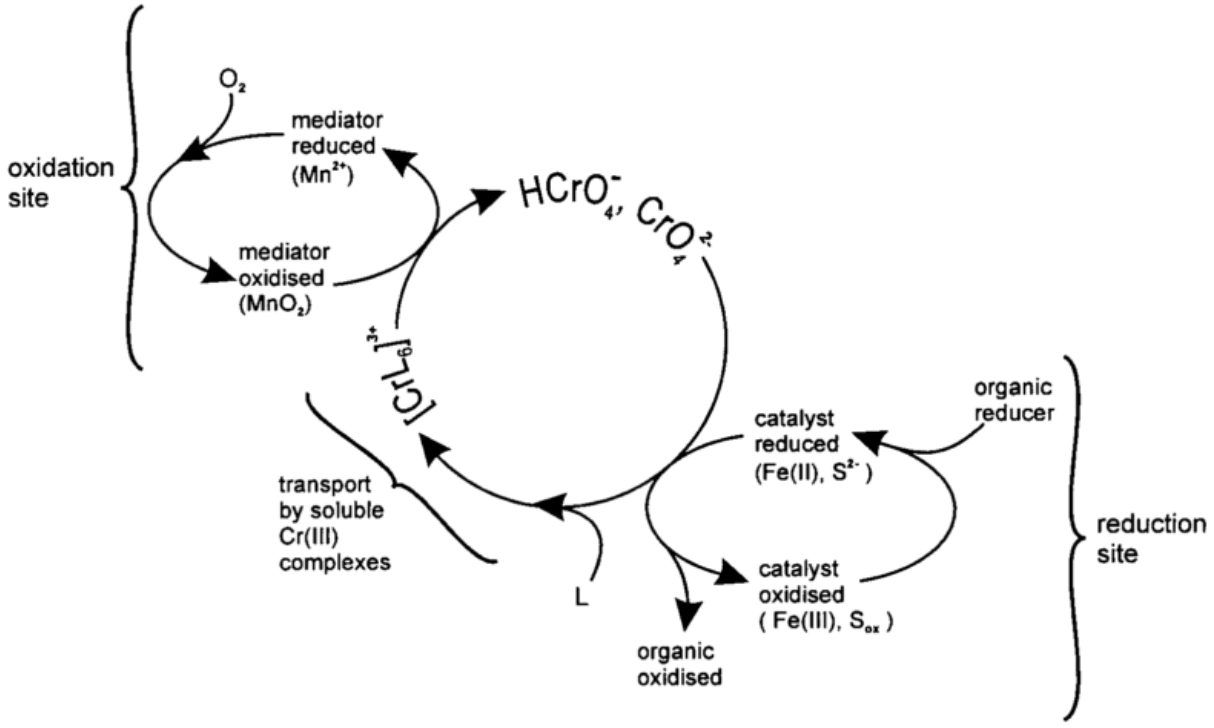

Figure 1.6 The oxidation-reduction chromium (Cr) in soils (Kotaś and Stasicka, 2000).

The oxidation of Cr(III) by manganese oxide-containing minerals such as hausmannite, manganite, birnessite, asbolane, lithiophorite and cryptomelane occurs by the following reaction, which occurs at pH 5 approximately:

$$2\mathrm{Cr(OH)_3} + 3\mathrm{MnO_2} \rightarrow 2\mathrm{CrO_4^{2-}} + 3\mathrm{Mn^{2+}} + 2H_2O + 2OH^- \quad \textbf{(1.4)}$$

Cooper (2002) identified lower Mn oxides such as hausmannite (Mn_3O_4) and manganite (MnOOH) as capable of oxidizing Cr(III), because the reduction of these oxides provides the most free energy for Cr(III) oxidation. Later, Stepniewska et al. (2004) studied the effect of MnO_2 on sorption and oxidation of Cr(III) by soils. The sorption of Cr(III) on soils decreases in presence of Mn(IV) oxide. It is probably caused by the competitive reaction, which is oxidation of Cr(III) to Cr(VI) by MnO_2 and also by Mn(III) sorption on the soil. The rate of Cr(III) oxidation by δ-MnO_2 with different Cr(III) concentration over a range of pH from 3 to 5 in a matrix of 0.1 $NaNO_3$ was studied by Fendorf and Zasoski (1992). Figure 1.7 shows that at pH smaller than 3.5, MnO_2 has a higher oxidizing capacity. At pH ≥4 and initial concentration of Cr(III) > 77 µM, reactants remained upon reaching steady state.

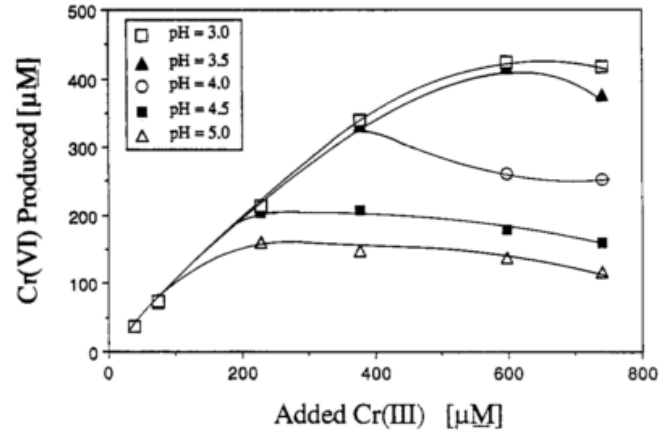

(a)

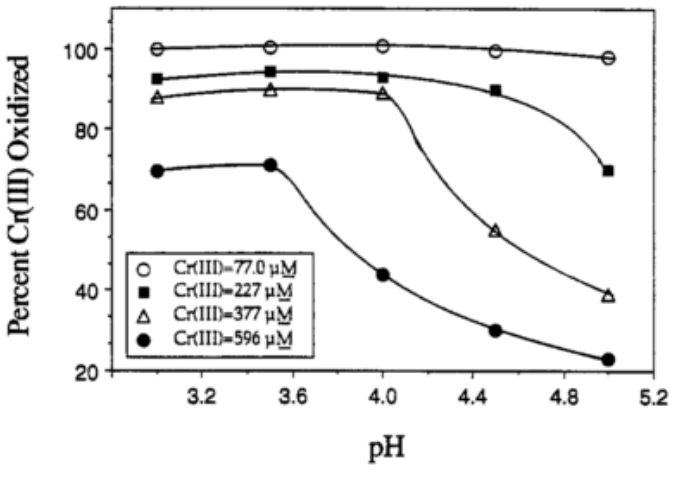

(b)

Figure 1.7 Cr(III) oxidized by δ-MnO_2 (initial concentration of 0.1 g L^{-1}): a) as a function of added Cr(III) concentration at various pH values, and b) as a function of pH at various Cr(III) concentrations (Fendorf and Zasoski, 1992).

Remediation schemes of contaminated soils with Cr(VI) are treated to reduce the carcinogenic, soluble and mobile Cr(VI) (pH ~ 2) to the less toxic and less mobile Cr(III)

which forms insoluble or sparingly soluble precipitates (pH ~ 9-10). Cr(VI) reduction is known to be promoted by the presence of living organism and organic material (soluble or insoluble), sulfides and ferrous iron. Sulfides (pyrite), oxides (goethite and hematite) and silicates (olivine and fayalite) are some of the Fe(II)-containing minerals involved in this process (Choppala et al., 2013). Cr(VI) adsorption and reduction can occur in the presence of Fe(II)-bearing minerals such as magnetite (Døssing et al., 2011). For magnetite, the Cr(VI) occur at the mineral surface with structural Fe(II) as the electron donor, most likely leading to the formation of maghemite (Peterson et al., 1996). The general reaction of Cr(VI) reduction with Fe(II) was described by Eary and Rai (1989) (Pettine et al., 1998):

$$H_j CrO_4^{j-2} + 3Fe^{2+} \rightarrow Cr(OH)_m^{3-m} + 3Fe(OH)_k^{3-k} + nH_2O + qH^+ \quad \textbf{(1.5)}$$

Where the possible hydrolyzed species are defined by j = 0 to 2, K= 0 to 4, n = 4 – (3k + m), and q = j – (3k + m + 2n). Salem et al. (1989) studied Cr transformations under typical environmental conditions using batch, microcosm and column experiments. Instantaneous reduction of Cr(VI) was observed by the presence of Fe^{2+} and S^{2-} under anaerobic conditions, while Cr(III) oxidation promoted by MnO_2 was much slower (oxidation rate 2.1 x 10^{-4} $days^{-1}$) and exhibited kinetic control. Clay minerals, such as vermiculite and montmorillonite have also shown influence on Cr reduction on soils. Until 60% Cr(VI) reduction was observed by Fe(II) adsorbed and released from the clay minerals on aqueous phase (Kwak et al., 2018). Once Cr(VI) has been reduced to Cr(III), Cr(III) can be adsorbed onto suspended particulate matter and river sediments (Saputro et al., 2014).

1.3.2 Role of bacteria on Cr oxidation and reduction

Although abiotic reductions are 100 times faster than the biotic reduction rate, the biotic reduction process is more common in soils and is associated with the fact that some bacteria possess chromate reductase activity. This pathway is called enzymatic Cr(VI) reduction, however, there is also non-enzymatic Cr(VI) reduction in which Cr(VI) is reduced to Cr(III) in presence of different chemicals produced by bacterial metabolic processes (Thatoi et al., 2014) (Figure 1.8). One of the main differences between these processes is the stability of the Cr(III) complexes formed. For instance, enzymatic reduction of chromate may result in a soluble Cr(III) organic complexes that can be stable for extended periods of time, whereas reduction by Fe(II) and S results in insoluble precipitates (Hansel et al., 2003). Hansel et al. (2003) investigated the fate of Cr followed by a coupled biotic-abiotic reduction by dissimilatory iron-reducing bacteria. First Fe(II), a microbial metabolite, was produced with a consequent Cr(VI) reduction to Cr(III) as $Cr(OH)_3$. Siderophores can also promote the presence of Fe(II) in solution, with a consequent role in Cr(VI) reduction. Siderophores are

low molecular weight organic ligands with high affinity and specificity for iron binding, and are produced by microorganisms to overcome limitations due to the lack of iron (Kraemer, 2004). The siderophores production has been studied in *Pseudomonas fluorescens* and *P. putida* (Budzikiewicz, 1996; Sayyed et al., 2005) as well as *P. aeruginosa* (Jenifer et al., 2015) among others.

Within natural environments, the reduction pathway, and subsequent fate of Cr(VI), will be defined by the operating reactions kinetics of competing microbial and chemical reactions (Hansel et al., 2003). In bioremediation processes, the effectiveness of Cr(VI) reduction depends on the formation of Cr(III) species as hydroxide which can be easily immobilized and precipitated. Das et al. (2014) isolated, from mine soil of Sukinda, *Bacillus amyloliquefaciens*, a bacterial strain with a high tolerance to Cr(VI) (< 900 mg L^{-1}) and fast reduction rate 2.22 mg Cr(VI) L^{-1} h^{-1} in 45 hours (100 mg L^{-1} Cr(VI), pH 7, temperature 35°C).

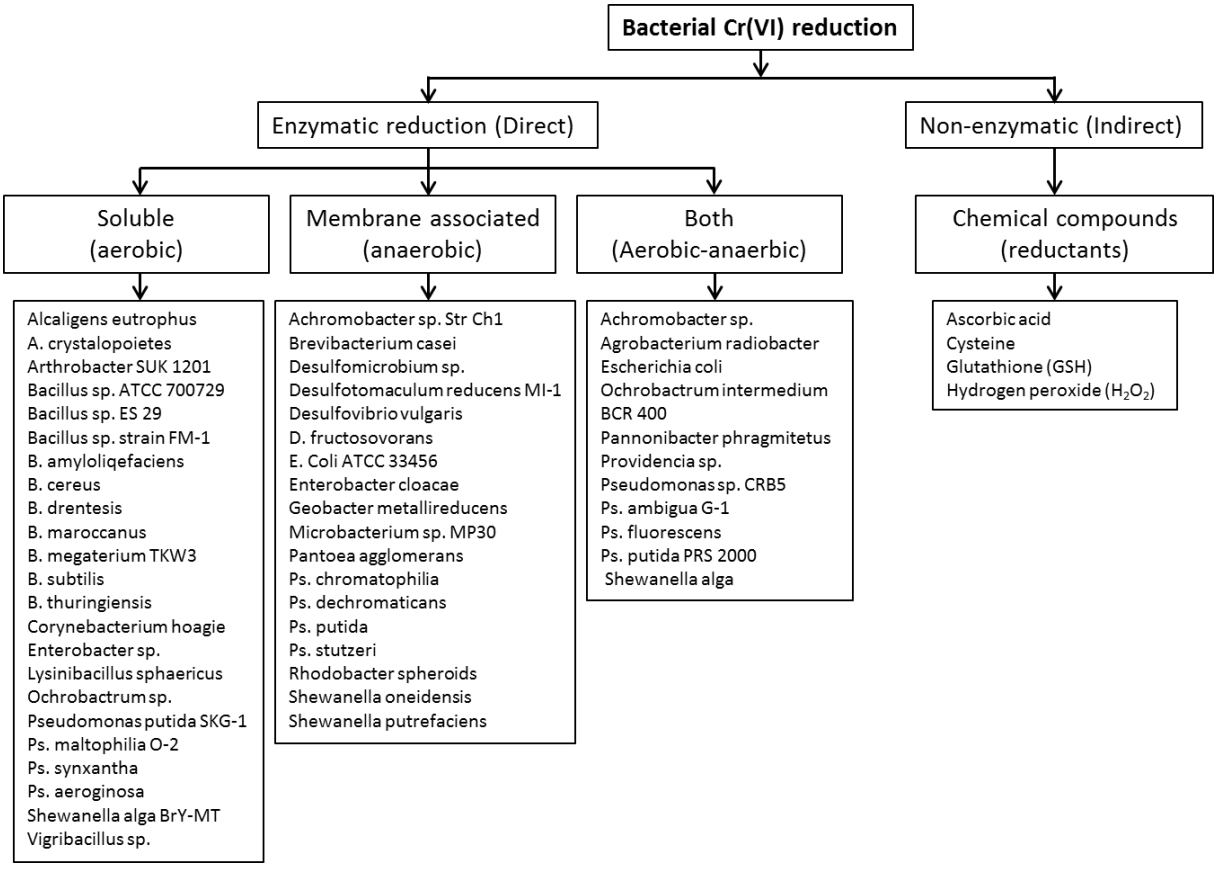

Figure 1.8 Bacterial Cr(VI) direct and indirect reduction (Thatoi et al., 2014).

Das et al. (2014) determined that Cr(VI) removal mechanism included surface immobilization and intracellular accumulation of Cr(III). Gan et al. (2018) performed reduction experiments of pyrite, and in S/FeS_2 ratio 1:1 condition, they reported 4.42 fold higher reduction with a

biological treatment with *Acidithiobacillus ferrooxidans* compared to the chemical treatment. Also *Acidithiobacillus thiooxidans* in sulfuric acid, using S as energy source, was used to indirectly reduce Cr(VI) promoted by intermediate products such as sulfite and thiosulfate (Viera et al., 2003). Later on Allegretti et al. (2006) highlighted the role of polythionates ($S_xO_6^{2-}$) for Cr(VI) reduction using *Acidiothiobacillus* and *Thiobacillus* cultures. Chen et al. (2012) reported that cells of *Bacillus cereus* could reduce Cr(VI), and the Cr(III) could coordinate with the supernatant, cell debris and cytoplasm through carboxyl and amino functional groups.

1.3.3 Precipitation-dissolution reactions

Chromium (III) species do not occur naturally and are less stable in the environment. These species can precipitate readily in the form of mixed Fe-Cr hydroxide, in waters at neutral pH levels (Choppala et al., 2013). Anions of Cr(VI) as CrO_4^{2-} and $Cr_2O_7^{2-}$ are soluble in water at all pH, but the rate of precipitation and dissolution change depending on the pH. For water treatment, Cr(III) is usually precipitated as hydroxide using alkaline materials like NaOH, Na_2CO_3 and NH_4OH, and lime (Karale et al., 2007). Some studies have reported that precipitation is more effective at pH 8.5-9.5, due to the solubility of chromic hydroxide in that range (Choppala et al., 2013). In the case of Cr(VI), its removal from industrial effluents can be achieved with a two-step treatment: first reduction of Cr(VI) to Cr(III) and followed by precipitation of Cr(III). Scrap iron is a cheap material, which has successfully been tested for the reduction of Cr(VI) to Cr(III) (Gheju and Balcu, 2011).

1.3.4 Sorption-desorption reactions

Cr(III) is specifically, strongly and rapidly adsorbed by soil Fe and Mn oxides, clay minerals and sand. The process increase when the pH rises, because the clay surface becomes more negatively charged (Choppala et al., 2013). The content of organic matter increases this adsorption as well. In contrast, the adsorption decreases when other inorganic cations or dissolved organic ligands are present in the solution (Richard and Bourg, 1991). Fendorf and Zasoski (1992) observed that Cr(III) sorption increases with increased pH and Cr(III) concentrations as shown in Figure 1.9.

Chromate ions can be adsorbed by Mn, Al, Fe oxides, clay minerals and natural soils and colloids. Adsorption of Cr(VI) is a surface complexation reaction between aqueous chromates and hydroxyl-specific surface sites. According to Richard and Bourg (1991), at diluted concentrations, the adsorption increase when the pH decreases. Meanwhile, concentration of K^+, Ca^{2+}, Mg^{2+}, have only slight influence on the adsorption process. Abdel-Samad and Watson (1997) demonstrated that chromate adsorption on goethite increases with decreasing pH, with a maximum at pH 6.5. X-ray photoelectron spectroscopy (XPS)

indicated that a small amount of Cr adsorbs in the trivalent oxidation state via redox reaction mediated by the presence of Fe(II) present on the oxide surface, however, the large majority remains as hexavalent Cr. In serpentine sediments, the presence of magnetite contributed to 50% of Cr(VI) removal through Cr(VI) reduction in a pH 3-7, while adsorption was dominated by finer sediment fraction (<0.075 mm). Cr(VI) adsorption was constant in the pH range 3 – 7 and decreased sharply at pH 8.5 (Mpouras et al., 2017).

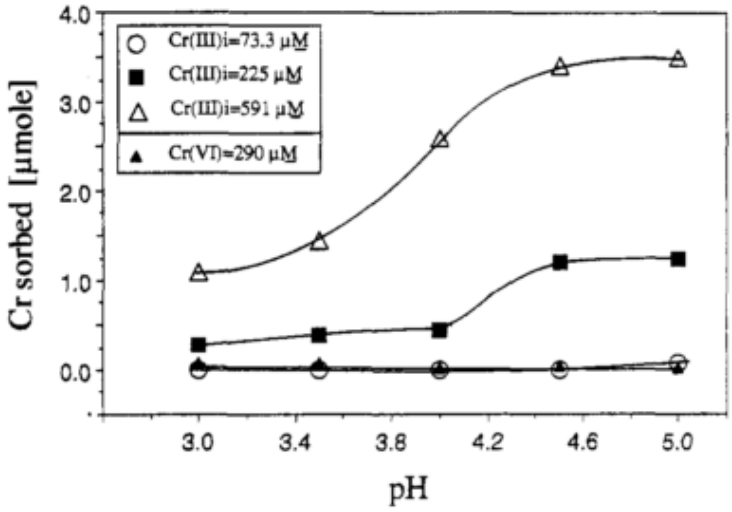

Figure 1.9 Sorption of Cr on δ-MnO_2 in a matrix of 0.1 M $NaNO_3$ (Fendorf and Zasoski, 1992).

1.3.5 Chromium interaction with water colloids

Because of the high solubility of chromate ions and their high oxidizing power, Cr(VI) is unlikely to be bound to organic matter or adsorbed on colloidal particles (Osaki, 1983). On the contrary, Cr(III) can be sorbed by hydrous Fe oxides which involves, adsorption, surface precipitation and co-precipitation phenomena (Charlet and Manceau, 1992). In particular, the adsorption of Cr(III) ions onto goethite or hydrous ferric oxide occurs through the formation of inner-sphere surface complexes. Colloids have been shown to have a strong interaction with trace metals, thereby determining their speciation over space and time and affecting their bioavailability and toxicity to microorganisms. A large portion of trace metals will be adsorbed on colloidal materials through covalent, electrostatic, or hydrophobic interactions (Carreira et al., 2015). Colloidal particles include organic matter, comprising biopolymers and humic substances, and inorganic matter, including natural iron and manganese oxides and clays, and now also engineered nanoparticles (Carreira et al., 2015). Ren et al. (2010) assessed the distribution of metal partitioning among particulate, colloidal and truly dissolved fractions in the polluted Yongdingxin River (Tianjin, China). They classified the metals into three groups: (1) organic colloidal pool-borne elements (Cu, Cr), (2) inorganic colloidal pool-borne metals (Fe, Mn) and (3) metals with varying complexation patterns (Zn, Hg).

Fukushima et al. (1995) found that the binding capacity of Cr(III) species and humic acids are in the range of 0.8 to 2.4 mmol g^{-1} of C, and the Cr(III) binding capacities are correlated to the carboxylic content of humic acids (HAs). Cr^{3+} binding capacity is similar to those of Ca^{2+} and Zn^{2+} and the one binding capacity of $CrOH^{2+}$ is comparable to the one of Pb^{2+}, Cu^{2+} and Ni^{2+}. Ren et al. (2010) found that in the Yongdingxin River (China), Cr is strongly bound to very low molecular weight organic ligands and it cannot be complexed by larger size colloids (100 kDa to 0.22 µm) such as fulvic and/or humic acids, cell fragments or bacteria. Similarly, Pokrovsky and Schott (2002) showed that in organic and Fe-rich boreal rivers, Cr is associated with small-size (< 10 kDa) organic colloids or with Fe colloids (10 kDa–0.8 µm), which can contribute up to 50% of its dissolved fraction.

Specifically for Cr(VI), the formation of a Cr(VI)-HAs micelles via supramolecular chemical processes could explain the persistence of Cr(VI) in soils enriched in humic substances (Leita et al., 2009). However, in soils where clay minerals are negatively charged, Cr(VI) anions like CrO_4^{2-} and $HCrO_4$, are highly mobile because of the repulsion between clay and Cr(VI), consequently Cr(VI) species can be transported into aquifers. Thacher et al. (2015) modelled the influence of organic matter on the transport and bioreduction of Cr(VI) in aquifers. They demonstrated that humic acids promote extracellular redox reactions and enhance metal reduction.

1.4 CHROMIUM COMPORTMENT DURING WEATHERING IN THE ULTRAMAFIC SYSTEM

Ultramafic rocks, and the soils derived from them (less than 1% of the Earth's land surface), are widely distributed throughout the globe across all climatic zones. The mineralogy of tropical soils derived on ultramafic rocks is dominated by Fe-oxides and (oxy)hydroxides, whereas clay minerals are nearly absent (Garnier et al., 2013). They are characterized by having low concentrations of nutrients like N, P, K and Ca, strong chemical fertility limitation due to the low Ca/Mg ratio and the presence of metals in harmful concentrations for the environment. Chromium and Ni are the most representative heavy metals of soils developed from ultramafic rocks, also known as serpentine soils. Chromium is commonly present either as Cr(III) and Cr(VI) and concentration of Cr of 15000 mg kg^{-1} have been reported (Oze et al., 2004). In addition, specialized habitats with extreme edaphic conditions are produced in ultramafic soils and frequently host unique plant communities and 'islands' of biodiversity with many restricted and endemic taxa (Chiarucci and Baker, 2007).

A standardized geochemical profile of residual laterites derived from ultramafic rocks is shown in the Figure 1.10. The bedrock is enriched in light elements such as Si and Mg, and

depleted in heavy ones like Fe, Cr and Ni. Relatively high ambient temperatures and rainfall cause intense weathering, which promotes the formation of laterite. During weathering, light elements are leached which leaves the more insoluble ions, predominantly Fe and Al. The mechanism of leaching involves acid dissolution, hydrolysis and precipitation of insoluble oxides and sulfates. An essential feature for the formation of laterite is the repetition of wet and dry seasons where rocks are leached by percolating rain water during the wet season. The resulting solution containing the leached ions is brought to the surface by capillary action during the dry season. These ions form soluble salt compounds which dry on the surface and are washed away during the next wet season (Fagoyinbo and Adeola, 2017).

The enrichment of chrome-spinels in the laterite is caused by leaching of Si and Mg from the ultramafic parent rock. The lateritic weathering process, which causes the enrichment of the chrome spinels, can be subdivided into 3 phases: (a) Hydration of the ultramafic parent rock, (b) Leaching of Mg and Si by unsaturated descending meteoritic waters. Relative enrichment of weathering resistance chrome spinels, Fe and Al hydroxides and (c) Al and Si may be enriched in the upper limonitic horizon due to precipitation from ascending capillary waters or due to re-sedimentation of Al and Si bearing materials (Rodríguez-Clemente and Tardy, 1987).

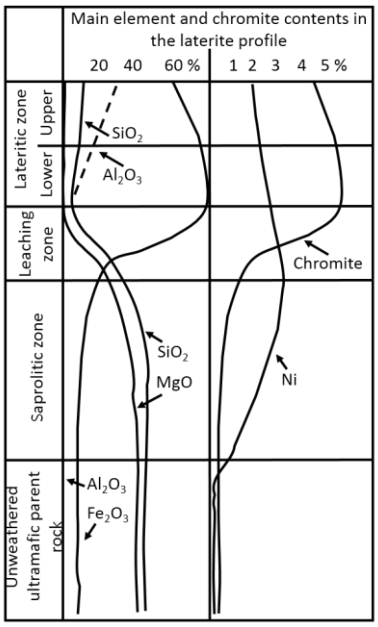

Figure 1.10 Vertical distribution of Al, Fe, Cr, Ni, Mg and Si in an ultramafic weathering profile (Rodríguez-Clemente and Tardy, 1987).

Garnier et al. (2006) reported KH_2PO_4 extractable Cr, up to 960 mg kg^{-1} of Cr(VI) in Niquelândia soils (Goiás, Brazil). In addition, in the same area, Garnier et al. (2009) studied the availability of chromate through the application of isotopic exchange kinetics (IEK), and

they found high chromate available and consequently, potential chromate toxicity in soil organism. Similarly, In New Caledonia, Becquer et al. (2003) observed Cr concentrations higher than 5 µmol L^{-1} under heavily P-fertilized crops as a result of Cr(VI) desorption from the soil iron oxide surfaces under the influence of phosphate ions. In this area, Cr(VI) extracted with KH_2PO_4 reported concentrations up to 90 mg kg^{-1}, whereas Cr(III) extracted with KCl was very low. These authors identified the Cr-substituted goethite and chromite as the main Cr sources. Those studies show that Cr can be released from ultramafic areas, and weathering is the main process involve.

During weathering, the main physical and mechanical processes which take place are abrasion and comminution of rocks and minerals as a result of erosive forces, and hydration along grain boundaries (Chesworth, 2008). The apparent resistance of Cr-spinels to weathering, evident from extraction experiments, and its insolubility suggests that these minerals are not large inputs of Cr in soil solutions and vegetation associated with serpentine soils. Chromium-bearing igneous and metamorphic silicates in the protolith and Cr-bearing clay minerals in the soil are more likely sources of chemically mobile and bioavailable Cr.

The chemical weathering of ultramafic rocks has been studied extensively. According to Garnier et al. (2009), ultramafic rocks rich in Ni and Cr could release toxic elements to the ecosystem, and particularly to the hydrosphere during mineral weathering. There are two main factors that affect the weathering processes: in the first place, the mineral composition of the rock and its physical properties (e.g., porosity) and, in the second place, the physical and chemical characteristics of the water, which are controlled by the climate, vegetation and the morphology of the landscape (Berger and Frei, 2014). However, it is important to know that primary minerals (chromite and Cr-magnetite) are not fully dissolved, instead they are partially transformed into secondary minerals (clay and Fe (hydr)oxides), which are more stable under intensive weathering conditions (Berger and Frei, 2014). Cooper (2002) proposed a two-stage mechanism for chromite weathering: (a) In subsoils, slow hydrolysis under moist field conditions of Cr(III) from isomorphically substituted Cr, to $Cr(OH)_3$ and (b) slow oxidation of $Cr(OH)_3$ to Cr(VI) by the reduction of easily reducible Mn oxides. Kimball (1990) described the formation of magnetite rims formed around chromite grains as either an alteration product of the original chromite or precipitation of a secondary overgrowth around the original chromite formed by partial dissolution of Fe from silicates minerals. There rims could limit the dissolution of Cr during weathering, however, Morrison et al. (2015) observed visible etching along the grain edge and dissolution embayment textures within magnetite rim and across the magnetite-chromite boundary.

During weathering, Cr(III) can be oxidized to soluble Cr(VI). Compound such as Mn oxides and hydroxides and oxygen can oxidize significant amounts of Cr(III) to Cr(VI) during their reduction (Leita et al., 2009). Fandeur et al. (2009) observed that the highest concentrations of Cr(VI) extracted were observed in the laterite unit (27 m) where Mn concentrations (as Mn(IV)) were the highest (Figure 1.11). This result strongly suggests that Cr(VI) is produced through Cr(III) oxidation in the presence of Mn oxide. The $Cr(OH)_3$ initially on the surfaces of chromite particles, is likely to become adsorbed on the surface of Mn oxides as well, since these have a high affinity for heavy metals (Cooper, 2002). This process, which is produced during tropical weathering of ultramafic rocks and provided by alternating oxidizing-reducing conditions because of the fluctuating seasonal water table, enhances the Cr mobility along the stratigraphy column.

In the southern Sacramento valley, Mills et al. (2011) found that the major mechanism for Cr(VI) mobilization is the weathering of Cr(III) from ultramafic rocks and its subsequent oxidation on Mn oxides. Cr(VI) (on the order of 100 mg kg^{-1}) is associated with Fe oxides and clay minerals, which represent a small fraction of total Cr, but is high enough to impact groundwater quality. Western Sacramento valley soils present a regional Cr and Ni enrichment as a result of erosion, transport and weathering of ultramafic rocks in the Coast Range (Morrison et al., 2015).

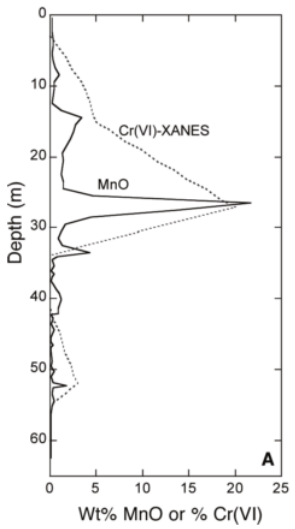

Figure 1.11 Comparison between the fraction of Cr(VI) (expressed as percentage of Cr(VI)) and the Mn concentration (expressed as wt% MnO) in a lateritic regolith (Fandeur et al., 2009).

1.5 CHROMIUM ISOTOPIC SYSTEM

Chromium has four stables isotopes: ^{50}Cr (4.345%), ^{52}Cr (83.789%), ^{53}Cr (9.501%) and ^{54}Cr (2.365%). Among these four isotopes, ^{50}Cr, ^{52}Cr and ^{54}Cr are non-radiogenic, whereas ^{53}Cr is a radiogenic product of the extinct nuclide ^{53}Mn (Qin and Wang, 2017). Because ^{52}Cr and

^{53}Cr are the most abundant chromium isotopes, n(^{53}Cr)/n(^{52}Cr) ratios usually are measured and expressed as δ^{53}Cr value, relative to NIST SRM 979 chromium nitrate (Coplen, 2002).

$$\delta^{53}Cr = \left[\frac{(^{53}Cr/^{52}Cr)_{Sample}}{(^{53}Cr/^{52}Cr)_{SRM-979}} - 1\right] X\ 1000‰ \quad \textbf{(1.6)}$$

On Earth, chromites and unaltered igneous rocks have a restricted range of Cr isotope composition that is commonly referred to as the “igneous inventory,” with reported mean (±2SD) $\delta^{53/52}$Cr values of −0.12 ± 0.10 (Schoenberg et al., 2008), −0.08 ± 0.13 (Farkaš et al., 2013), −0.12 ± 0.13 ‰ (Wang et al., 2015) and −0.14 ± 0.09 (Schoenberg et al., 2016). Table 1.4 presents the isotopic composition of some materials including Cr(VI) and Cr(III) standards, weathering profiles, supernatant of leaching experiments, surface and groundwater and industrial solutions. The isotopic spread across those materials is explained by isotopic fractionation. According to Bullen (2013), isotopic fractionation is a set of processes, which can divide an isotopically homogenous pool of an element into multiples fractions that have different isotopic composition. Both inorganic and microbial mediated reduction of Cr(VI) to Cr(III) have been shown to result in isotopic fractionation, and this is one of the main reasons why Cr isotopic fractionation is considered as a promising tool to detect redox changes in aqueous environments.

Stable isotope fractionation in natural samples can be divided into kinetic and equilibrium effects. Kinetic isotope effects are caused by different reaction rates between light and heavy isotopes and equilibrium isotope effect occur when two phases react with forward and backward reactions proceeding at equal rates (Wiederhold, 2015). Cr fractionation due to oxidation-reduction processes is an example of the kinetic isotope effect, which can be described by the Rayleigh model, which is often used to model the evolution of isotope ratios during incomplete unidirectional reactions within closed systems. Cr fractionation during reaction occurs because the bonds of O with light Cr isotopes are easier to break than those of heavy isotopes, resulting in greater reaction rates of lighter Cr isotope composition and thus in Cr(III) enrichment in the product (Schauble et al., 2004). The solid is separated from the liquid, which prevents backward reaction, otherwise the imprint of kinetic isotope effect during the process would be erased and isotope ratios of products are identical to initial reactants (Wiederhold, 2015).

According to Qin and Wang (2017) due to the contrasting behavior of Cr(III) and Cr(VI), and the redox sensitivity of Cr, Cr isotopic fractionation can be used for different purposes. Small natural variations in the ratio of ^{53}Cr to ^{52}Cr can be used to identify chemical processes

involving Cr or the sources of Cr. According to Izbicki et al. (2008) , in areas with high natural Cr content, determining the bulk concentration of Cr does not permit to distinguish the origin of Cr, however, Cr isotopes have shown to be effective.

Table 1.4 Chromium isotopic composition in different compartments.

Type	Substance	Minimum δ^{53}Cr value	Maximum δ^{53}Cr value	Reference
Standard	$K_2Cr_2O_7$ – Cr(VI)	+0.6*	+0.56*	Ellis (2002)
	$Cr(NO_3)_3$ – Cr(III)	0.0 ±0.2	0.0 ±0.2	Ellis (2002)
Soils and weathering profiles	Lateritic soil	-0.34*	-0.44*	Berger and Frei (2014)
	Tonalitic bedrock	-0.14*	-0.14*	Berger and Frei (2014)
	Banded iron formations (BIFs)	+0.9*	+4.9*	Frei et al. (2009)
	Bidar laterite profile	-0.85*	+0.36*	Wille et al. (2018)
	Chhindwara saprolite profile	-0.19*	-0.01*	Wille et al. (2018)
	Flin flon paleosol	-0.11*	+2.38*	Babechuk et al. (2017)
	Basaltic weathering profile	+0.28 ±0.14		Crowe et al. (2013)
	Basaltic weathering profile	-0.27 ±0.03	-0.15 ±0.04	Wu et al. (2017)
	Ultramafic - Weathering profile	-0.43 ±0.02	+0.89 ±0.10	Paulukat et al. (2015)
	Hydrothermal lead chromates	+0.640*	+1.037*	Schoenberg et al. (2008)
Leachate	Acid leachate (0.2N HCl) of tonalitic bedrock	-0.12 ±0.02		Berger and Frei (2014)
	Basic leachate (0.1N NaOH) of tonalitic bedrock	-0.48 ±0.03		Berger and Frei (2014)
	Leachate (MQ water) of tonalitic bedrock	+0.21 ±0.05		Berger and Frei (2014)
	Leachate highly serpentinized peridotite	+0.56*	+0.96*	Economou-Eliopoulos et al. (2014)
	Soil leachate	+0.33*	+0.59*	Economou-Eliopoulos et al. (2014)
Surface and ground water	River water	+0.38*		Frei et al. (2014)
	River water	+0.67 ±0.11	+1.33 ±0.04	Paulukat et al. (2015)
	River – basaltic catchment	-0.17 ±0.3	+1.68 ±0.3	D'Arcy et al. (2016)
	River – basaltic catchment	+0.16 ±0.06	+1.02 ±0.05	Wu et al. (2017)
	Ground water	+1.1*	+5.8*	Ellis (2002)
	Ground water	+0.84*	+1.98*	Economou-Eliopoulos et al. (2014)
	Seawater	+0.55 ±0.08		Paulukat et al. (2015)
Industrial solutions	Draining water from a chromite mine	+0.003 ±0.003		Paulukat et al. (2015)
	Plating bath	+0.5*		Novak et al. (2014)
	Hard plating bath	-0.1 ±0.03	+0.5 ±0.01	Novak et al. (2017)
	Chromating bath	-0.1 ±0.06	+0.9 ±0.06	Novak et al. (2017)

* Uncertainty was not reported

** Values for δ^{53}Cr given per mil relative to SRM 979 chromium nitrate.

Other applications of Cr isotopes include monitoring of Cr in contaminated sites and examination of oxygenation in the Precambrian. The use of Cr stable isotopes for monitoring groundwater has been reported by Ellis (2002), Sikora et al. (2008), Izbicki et al. (2008), Zink et al. (2010), Economou-Eliopoulos et al. (2016) and Novak et al. (2014).

In comparison to natural environments, in anthropogenic sources such as electroplating, tanning, chemical industry where Cr is released mainly in its hexavalent form, a significantly higher extend of fractionation has been reported (5.8‰) (Novak et al., 2014). In groundwater polluted by Cr-electroplating the high δ^{53}Cr is associated with Cr(VI) reduction (Novak et al., 2017).

The differences on the chromium isotopic composition between natural and industrial contamination sources can be potentially used to distinguish the two (Ellis, 2002; Izbicki et al., 2012; Novak et al., 2014; Wang et al., 2015).

1.5.1 Isotopic Exchange in aqueous systems

The use of Cr isotopic data to trace Cr redox reactions demands knowledge about Cr(VI) and Cr(III) exchange. In natural systems with Cr(VI) and Cr(III) that are not at isotopic equilibrium initially, the Cr(VI) and Cr(III) will tend to evolve toward isotopic equilibrium, though possibly at extremely slow rates (Wang et al., 2015). Isotopic exchange between Cr(III) and Cr(VI) can occur when they interact and transfer electrons. Cr(III) preferentially forms octahedrally coordinated hydroxide complexes, whereas Cr(VI) forms tetrahedrally coordinated ions with very strong Cr-O bonds (Zink et al., 2010). The strongly contrasted bonding environments of Cr(VI) and Cr(III) mean that three electron transfers are required, and that is reflected in a slow isotopic exchange (Schauble et al., 2004; Zink et al., 2010). In contrast to Cr, elements such as iron are known to undergo rapid isotopic exchange on time scales of several minutes via one-electron-transfer mechanism (Johnson et al., 2002). Wang et al. (2015) proposed the Cr exchange via the following reactions:

$$^{53}Cr(VI) + {}^{52}Cr(VI) = {}^{53}Cr(IV) + {}^{52}Cr(V) \quad \textbf{(1.7)}$$

$$^{53}Cr(IV) + {}^{52}Cr(V) = {}^{53}Cr(V) + {}^{52}Cr(IV) \quad \textbf{(1.8)}$$

$$^{53}Cr(V) + {}^{52}Cr(IV) = {}^{53}Cr(VI) + {}^{52}Cr(III) \quad \textbf{(1.9)}$$

$$^{53}Cr(III) + {}^{52}Cr(VI) = {}^{53}Cr(VI) + {}^{52}Cr(III) \quad \textbf{(1.10)}$$

As intermediate species, Cr(V) and Cr(IV) are unstable and present only at very low concentrations. Equation (1.10) gives the overall isotope reaction. It is important to consider that the occurrence of three electron transfer during a single Cr(VI)-Cr(III) collision is

extremely unlikely (Zink et al., 2010). This simplified model shows that electron transfer in individual reaction (1.7, 1.8 and 1.9) occurs when there is a collision of the intermediate species, however in natural settings Cr species interaction is more complicated (Wang et al., 2015). Zink et al. (2010) studied isotopic exchange kinetics between soluble Cr(III) and Cr(VI) by means of enriched isotope tracer experiments, in a pH environment of 5.5 to 7. Over a reaction time of 120h none of the experiments reveals detectable Cr isotopic fractionation, which demonstrates the lack of isotopic exchange between Cr(III) and Cr(VI) for those conditions. However, after several weeks, visible coagulation of Cr(III)-hydroxides precipitated, which resulted in a small change in Cr composition for Cr(III) and Cr(VI). In low concentration, neutral-pH experiments Wang et al. (2015) observed that the rate of isotopic exchange should be controlled by the abundance of Cr(VI) species adsorbed onto Cr(III) surfaces. The adsorbed Cr(VI) and the dissolved Cr(VI) are expected to equilibrate isotopically over a time scale shorter than between adsorbed Cr(VI) and Cr(III) (oxy)hydroxide. They observed that whereas adsorption reaches equilibrium with respect to concentration within a few hours, isotopic shift due to Cr(VI)-Cr(III) exchange occurred over tens of days.

In natural settings, isotopic exchange is potentially important where Cr(III) (oxy)hydroxide with large exposed surface area are present and Cr(VI) stays in contact with the Cr(III) for several years or longer (Wang et al., 2015). This can be the case for groundwater and aquifers, where the isotope exchange rates between Cr(III) and Cr(VI) will depend on several parameters, including the form in which the different Cr species are present, their concentration, the ambient temperature and the prevailing pH conditions (Zink et al., 2010).

1.5.2 Changes in the Cr isotopic composition during weathering

Several studies performed on soils profiles (Berger and Frei, 2014; Crowe et al., 2013; Frei and Polat, 2013; Paulukat et al., 2015) demonstrated that oxidative rock weathering is accompanied by isotopic shifts. The mobilized Cr(VI) released to runoff is enriched in isotopically heavy Cr, leaving behind an isotopically light Cr(III) pool in the soil (Paulukat et al., 2015). D'Arcy et al. (2016) concluded that Cr isotope composition of soils is a function of the modal abundance and weathering rates of Cr-bearing minerals. For instance, the accumulation of Cr-spinels in soils presents a Cr pool enriched in $\delta^{53}Cr$ similar to the local bedrock (-0.21 ± 0.12 ‰), whereas dissolution of easily weathered Cr-silicates results in depletion of heavy isotopes of Cr (-0.32 ± 0.04 ‰) relative to the local bedrock. The overall effect of Cr redox reactions in the weathering environments leads to heavy Cr(VI) that is ultimately exported to the ocean by rivers (Crowe et al., 2013). The reduced soil pool has shown to reach values on the order of -3 to -4 ‰ (Døssing et al., 2011; Ellis et al., 2002).

Døssing et al. (2011) suggested that the variations in the Cr isotopic fractionation, could be related to the reaction rates because they observed larger fractionation in the batch experiments and lower fractionation in the constant addition experiments, where Fe was slowly added. Nevertheless, Ellis, (2002) observed considerable Cr isotopic fractionation by Cr(VI) reduction by magnetite, over a couple of days. Biotic reduction of Cr(VI) also generates isotopic shifts up to -4.1 ‰ (Sikora et al., 2008), comparable to those produced by abiotic reduction (Frei et al., 2009).

Several Cr isotopic composition studies, including two highly ferruginous modern profiles developed on tonalite, have been conductedin subtropical and tropical region (Berger and Frei, 2014; D'Arcy et al., 2016; Frei et al., 2014; Paulukat et al., 2015). Wille et al. (2018) confirmed two emerging models: (a) Cr loss may reflect leaching and small-scale redistribution of Cr(III) under low Eh and pH conditions with no evidence of isotopic fractionation; (b) Partial oxidation of Cr(III) to Cr(VI) at comparatively higher Eh and pH conditions leads to loss of soluble and isotopically heavy Cr(VI) species. This means that Cr mobilization as Cr(III) does not present isotopic fractionation, however, the subsequent oxidation of Cr(III) to Cr(VI) induces isotopic fractionation, which is stored in the weathering profile. Nevertheless, Wille et al. (2018) observed that oxidative weathering under modern atmospheric conditions does not necessarily imprint changing Cr isotopic signatures, because the large unfractionated pool of Cr(III) masks Cr isotopic signatures generated through pedogenic processes.

Contrary to the expected removal of isotopically heavy Cr(VI) that is observed in modern oxidative weathering environments, Babechuk et al. (2017) found in oxidized paleosol horizons a significant enrichment in ^{53}Cr (Table 1.4). The authors explained this as the result of reintroduction of isotopically heavy Cr(VI), after initial Cr loss. Farkaš et al. (2013) described this process as reductive sequestration of ^{53}Cr-enriched Cr(VI) from the weathering fluid. Similarly, Crowe et al. (2013) reported sediments which captured a mobile, ^{53}Cr-enriched Cr(VI) pool originating from oxidative continental weathering. They reported oxidative weathering in the Mesoarchaean which led to a δ^{53}Cr of 1.26‰ in Polonga rocks, which is more than six times the range observed in igneous rocks. Their data revealed extensive mobilization of redox sensitive elements through oxidative weathering such as Cr and U. Frei and Polat (2013) found positively fractionated δ^{53}Cr values higher than the Earth's magmatic inventory in reddish hyoloclastites and weathered red basalts (red soil). These authors explained this as a result of heavy Cr re-deposition, associated with enrichment of iron (presence of hematite), together with other redox sensitive elements such as U, Ce and V. Besides iron, organic matter is a potential Cr-trap for surface water run-off,

which immobilizes positively fractionated Cr liberated from elsewhere in the profile (Berger and Frei, 2014; Wang et al., 2015).

Farkaš et al. (2013) found that weathering products of processes involving oxidative weathering and aqueous alteration, i.e., serpentinization, become progressively enriched in heavy Cr isotopes. However, they did not find any correlation with the index of weathering, suggesting that Cr isotopic enrichment in the studied ultramafic rocks is primarily due to aqueous alteration phenomena and complex redox cycling of Cr in the near-surface environment during oxidative weathering and perhaps partly due to kinetic isotope effects linked to diffusion and metasomatism. One possibility to generate heavy $\delta^{53/52}$Cr in altered ultramafic minerals and rocks is related to the meteoric/serpentinizing fluids carrying dissolved Cr(VI) species with heavy isotope signatures, which would come in contact with reduced magmatic Fe(II)-bearing minerals that, in turn, would facilitate an efficient reduction of the dissolved Cr(VI) to Cr(III). It creates the opportunity for transferring heavy $\delta^{53/52}$Cr signatures to newly formed secondary minerals (Farkaš et al., 2013). Frei et al. (2009) proposed a pathway:

$$Cr(VI)_{(AQ)} + 3Fe(II)_{(MIN/AQ)} \rightarrow Cr(III)_{(MIN/AQ)} + 3Fe(III)_{(AQ)} \quad \textbf{(1.11)}$$

This pathway involves oxidation of iron during alteration, producing secondary Fe(III)-bearing minerals. One of the most common serpentine group minerals, lizardite, contains about 50 to 90% of total iron as Fe(III) species. This oxidizing serpentinization reaction produces hydrogen gas (H_2) which acts as a reducing agent of Cr(VI). Other mechanism suggested by Bigeleisen and Mayer (1947) and Urey (1947) in Farkaš et al. (2013), is based on the preferential breaking of the weaker Cr(III)-bonds associated with lighter Cr isotopes during weathering. A subsequent oxidation and mobilization of this isotopically light Cr fraction occurs, which might be transported away, and thus the remaining Cr(III) in the altered mineral/rocks would be enriched in heavy Cr isotopes.

Wang et al. (2015) confirmed that the fractionation of solid Cr(III) is expected to be small due to a “rind effect”. Each micro-layer of the Cr(III) (oxy)hydroxide particles is essentially completely oxidized leading to limited isotopic fractionation. Even if the natural oxidation of solid Cr(III) is expected to be small due to a “rind effect”, which limits the isotope fractionation, isotopic exchange involving Cr(III) (oxy)hydroxide may be rapid enough to cause significate effects over a time scale of months (Wang et al., 2015). Conversely, soluble Cr(VI) can be reduced back to insoluble Cr(III). Organic material, sulfides, and ferrous species appear to be the dominant reductants (Fendorf, 1995). During reduction, ^{52}Cr

exhibits greater reactions rates, due to its higher vibrational frequencies, and thus there is an enrichment in the produced Cr(III) (Schauble et al., 2004; Qin and Wang, 2017).

1.6 BIBLIOGRAPHY

Abdel-Samad, H., Watson, P.R., 1997. An XPS study of the adsorption of chromate on goethite (α-FeOOH). Appl. Surf. Sci. 108, 371–377. doi:10.1016/S0169-4332(96)00609-5

Ahmed, E., Abdulla, H.M., Mohamed, A.H., Ahmed, D., 2016. Remediation and recycling of chromium from tannery wastewater using combined chemical – biological treatment system. Process Saf. Environ. Prot. 104, 1–10. doi:10.1016/j.psep.2016.08.004

Allegretti, P., Furlong, J., Donati, E., 2006. The role of higher polythionates in the reduction of chromium(VI) by Acidithiobacillus and Thiobacillus cultures. J. Biotechnol. 122, 55–61. doi:10.1016/j.jbiotec.2005.08.031

Apte, A.D., Tare, V., Bose, P., 2006. Extent of oxidation of Cr(III) to Cr(VI) under various conditions pertaining to natural environment. J. Hazard. Mater. 128, 164–174. doi:10.1016/j.jhazmat.2005.07.057

Arndt, N., Kesler, S., Ganino, C., 2015. Classification, Distribution and Uses of Ores and Ore Deposits, in: Metals and Society. Springer, Cham, pp. 15–40. doi:10.1007/978-3-319-17232-3

Babechuk, M.G., Kleinhanns, I.C., Schoenberg, R., 2017. Chromium geochemistry of the ca. 1.85 Ga Flin Flon paleosol. Geobiology 15, 30–50. doi:10.1111/gbi.12203

Becquer, T., Quantin, C., Sicot, M., Boudot, J.P., 2003. Chromium availability in ultramafic soils from New Caledonia. Sci. Total Environ. 301, 251–261. doi:10.1016/S0048-9697(02)00298-X

Behera, S.K., Panda, S.K., Pradhan, N., Sukla, L.B., Mishra, B.K., 2012. Extraction of nickel by microbial reduction of lateritic chromite overburden of Sukinda, India. Bioresour. Technol. 125, 17–22. doi:10.1016/j.biortech.2012.08.076

Berger, A., Frei, R., 2014. The fate of chromium during tropical weathering: A laterite profile from central madagascar. Geoderma 213, 521–532. doi:10.1016/j.geoderma.2013.09.004

Biswas, S., Bhattacharjee, K., 2014. Fungal assisted bioleaching process optimization and kinetics: Scenario for Ni and Co recovery from a lateritic chromite overburden. Sep. Purif. Technol. 135, 100–109. doi:10.1016/j.seppur.2014.07.055

Budzikiewicz, H., 1996. Siderophores from fluorescent pseudomonas. Stud. Nat. Prod. Chem. 19, 793–835. doi:10.1016/S1572-5995(96)80019-6

Bullen, T.D., 2013. Metal Stable Isotopes in Weathering and Hydrology, Treatise on Geochemistry. doi:10.1016/B978-0-08-095975-7.00511-8

Burbridge, D.J., Koch, I., Zhang, J., Reimer, K.J., 2012. Chemosphere Chromium speciation in river sediment pore water contaminated by tannery effluent. Chemosphere 89, 838–843. doi:10.1016/j.chemosphere.2012.05.005

Burns, V.M., Burns, R.G., 1975. Mineralogy of chromium. Geochim. Cosmochim. Acta 39, 903–910. doi:10.1016/0016-7037(75)90036-8

Carreira, S., Domingos, R.F., Ge, A., Cordeiro, A., Sivry, Y., Benedetti, M.F., 2015. Metals in the Aquatic Environment — Interactions and Implications for the Speciation and Bioavailability : Aquat. Geochemistry 21, 231–257. doi:10.1007/s10498-014-9251-x

Cavaco, S.A., Fernandes, S., Quina, M.M., Ferreira, M., 2007. Removal of chromium from electroplating industry effluents by ion exchange resins. J. Hazard. Mater. 144, 634–638. doi:10.1016/j.jhazmat.2007.01.087

Charlet, L., Manceau, A., 1992. X-Ray Absorption Spectroscopic Study of the Sorption of Cr (lll) at the Oxide-Water Interface. J. Colloid Interface Sci. 148, 443–458.

Chen, Z., Huang, Z., Cheng, Y., Pan, D., Pan, X., Yu, M., Pan, Z., Lin, Z., Guan, X., Wu, Z., 2012. Cr(VI) uptake mechanism of Bacillus cereus. Chemosphere 87, 211–216. doi:10.1016/j.chemosphere.2011.12.050

Chesworth, W., 2008. Encyclopedia of soil sciences. Springer. doi:10.1007/978-1-4020-3995-9

Chiarucci, A., Baker, A.J.M., 2007. Advances in the ecology of serpentine soils. Plant Soil 293, 1–2. doi:10.1007/s11104-007-9268-7

Chitraprabha, K., Sathyavathi, S., 2018. Phytoextraction of chromium from electroplating ef fl uent by Tagetes erecta (L .). Sustain. Environ. Res. 1–7. doi:10.1016/j.serj.2018.01.002

Choppala, G., Bolan, N., Park, J.H., 2013. Chromium Contamination and Its Risk Management in Complex Environmental Settings, Advances in Agronomy. Elsevier. doi:10.1016/B978-0-12-407686-0.00002-6

Cooper, G.R.C., 2002. Oxidation and toxicity of chromium in ultramafic soils in Zimbabwe. Appl. Geochemistry 17, 981–986. doi:10.1016/S0883-2927(02)00014-8

Coplen, T.B., 2002. Compilation of minimum and maximum isotope ratios of selected elements in naturally occurring terrestrial materials and reagents, U.S. Geol. Surv. Water Resour. Invest. Rep.

Crowe, S.A., Døssing, L.N., Beukes, N.J., Bau, M., Kruger, S.J., Frei, R., Canfield, D.E., 2013. Atmospheric oxygenation three billion years ago. Nature 501, 535–538. doi:10.1038/nature12426

D'Arcy, J., Babechuk, M.G., Døssing, L.N., Gaucher, C., Frei, R., 2016. Processes controlling the chromium isotopic composition of river water: Constrains from basaltic river catchments. Geochim. Cosmochim. Acta 186, 296–315. doi:10.1016/j.gca.2016.04.027

Das, S., Mishra, J., Das, S.K., Pandey, S., Rao, D.S., Chakraborty, A., Sudarshan, M., Das, N., Thatoi, H., 2014. Investigation on mechanism of Cr(VI) reduction and removal by Bacillus amyloliquefaciens, a novel chromate tolerant bacterium isolated from chromite mine soil. Chemosphere 96, 112–121. doi:10.1016/j.chemosphere.2013.08.080

Das, S., Patnaik, S.C., Sahu, H.K., Chakraborty, A., Sudarshan, M., Thatoi, H.N., 2013. Heavy metal contamination, physico-chemical and microbial evaluation of water samples collected from chromite mine environment of Sukinda, India. Trans. Nonferrous Met. Soc. China 23, 484–493. doi:10.1016/S1003-6326(13)62489-9

Dhal, B., Nanda, N., 2011. Environmental Quality of the Boula-Nuasahi Chromite Mine Area in India. Mine water Environ. 30, 191–196. doi:10.1007/s10230-010-0134-0

Dhal, B., Thatoi, H.N., Das, N.N., Pandey, B.D., 2013. Chemical and microbial remediation of hexavalent chromium from contaminated soil and mining/metallurgical solid waste: A review. J. Hazard. Mater. 250–251, 272–291. doi:10.1016/j.jhazmat.2013.01.048

Døssing, L.N., Dideriksen, K., Stipp, S.L.S., Frei, R., 2011. Reduction of hexavalent chromium by ferrous iron: A process of chromium isotope fractionation and its relevance to natural environments. Chem. Geol. 285, 157–166. doi:10.1016/j.chemgeo.2011.04.005

Economou-Eliopoulos, M., Frei, R., Atsarou, C., 2014. Application of chromium stable isotopes to the evaluation of Cr(VI) contamination in groundwater and rock leachates from central Euboea and the Assopos basin (Greece). Catena 122, 216–228. doi:10.1016/j.catena.2014.06.013

Economou-Eliopoulos, M., Frei, R., Megremi, I., 2016. Potential leaching of Cr (VI) from laterite mines and residues of metallurgical products (red mud and slag): An integrated approach. J. Geochemical Explor. 162, 40–49. doi:10.1016/j.gexplo.2015.12.007

Ellis, A.S., Johnson, T.M., Bullen, T.D., 2002. Chromium Isotopes and the Fate of Hexavalent Chromium in the Environment. Science (80-.). 295, 2060–2062. doi:10.1126/science.1068368

Elzinga, E.J., Cirmo, A., 2010. Application of sequential extractions and X-ray absorption spectroscopy to determine the speciation of chromium in Northern New Jersey marsh soils developed in chromite ore processing residue (COPR). J. Hazard. Mater. 183, 145–154. doi:10.1016/j.jhazmat.2010.06.130

Esther, J., Panda, S., Behera, S.K., Sukla, L.B., Pradhan, N., Mishra, B.K., 2013. Bioresource Technology Effect of dissimilatory Fe (III) reducers on bio-reduction and nickel – cobalt recovery from Sukinda chromite-overburden. Bioresour. Technol. 146, 762–766. doi:10.1016/j.biortech.2013.07.103

Fagoyinbo, C.V.O., Adeola, A.J., 2017. Relative Abundance of Minerals in Parent Rock and their Effects on Laterite Properties. J. Sci. Eng. Res. 4, 41–50.

Falagán, C., Grail, B.M., Johnson, D.B., 2017. New approaches for extracting and recovering metals from mine tailings. Miner. Eng. 106, 71–78. doi:10.1016/j.mineng.2016.10.008

Fandeur, D., Juillot, F., Morin, G., Livi, L., Cognigni, A., Webb, S.M., Ambrosi, J.P., Fritsch, E., Guyot, F., Brown, G.E., 2009. XANES evidence for oxidation of Cr(III) to Cr(VI) by Mn-oxides in a lateritic regolith developed on serpentinized ultramafic rocks of New Caledonia. Environ. Sci. Technol. 43, 7384–7390. doi:10.1021/es900498r

Farkaš, J., Chrastný, V., Novák, M., Čadkova, E., Pašava, J., Chakrabarti, R., Jacobsen, S.B., Ackerman, L., Bullen, T.D., 2013. Chromium isotope variations (δ53/52Cr) in mantle-derived sources and their weathering products: Implications for environmental studies and the evolution of δ53/52Cr in the Earth's mantle over geologic time. Geochim. Cosmochim. Acta 123, 74–92. doi:10.1016/j.gca.2013.08.016

Fendorf, S.E., 1995. Surface reactions of chromium in soils and waters. Geoderma 67, 55–71. doi:10.1016/0016-7061(94)00062-F

Fendorf, S.E., Zasoski, R.J., 1992. Chromium(Iii) Oxidation By Delta-Mno2 .1. Characterization. Environ. Sci. Technol. 26, 79–85.

Frei, R., Gaucher, C., Poulton, S.W., Canfield, D.E., 2009. Fluctuations in Precambrian atmospheric oxygenation recorded by chromium isotopes. Nature 461, 250–253. doi:10.1038/nature08266

Frei, R., Poiré, D., Frei, K.M., 2014. Weathering on land and transport of chromium to the ocean in a subtropical region (Misiones, NW Argentina): A chromium stable isotope perspective. Chem. Geol. 381, 110–124. doi:10.1016/j.chemgeo.2014.05.015

Frei, R., Polat, A., 2013. Chromium isotope fractionation during oxidative weathering — Implications from the study of a Paleoproterozoic (ca. 1.9 Ga) paleosol, Schreiber Beach, Ontario, Canada. Precambrian Res. 224, 434–453. doi:10.1016/j.precamres.2012.10.008

Fukushima, M., Nakayasu, K., Tanaka, S., Nakamura, H., 1995. Chromium (III) binding abilities of humic acids. Anal. Chim. Acta 317, 195–206.

Gan, M., Li, J., Sun, S., Cao, Y., Zheng, Z., Zhu, J., Liu, X., Wang, J., Qiu, G., 2018. The enhanced effect of Acidithiobacillus ferrooxidans on pyrite based Cr(VI) reduction. Chem. Eng. J. 341, 27–36. doi:10.1016/j.cej.2018.02.014

Garnier, J., Quantin, C., Echevarria, G., Becquer, T., 2009a. Assessing chromate availability in tropical ultramafic soils using isotopic exchange kinetics. J. Soils Sediments 9, 468–475. doi:10.1007/s11368-009-0062-4

Garnier, J., Quantin, C., Guimaraes, E., Becquer, T., 2008. Can chromite weathering be a source of Cr in soils? Mineral. Mag. 72, 49–53.

Garnier, J., Quantin, C., Guimarães, E., Garg, V.K., Martins, E.S., Becquer, T., 2009b. Understanding the genesis of ultramafic soils and catena dynamics in Niquelândia,

Brazil. Geoderma 151, 204–214. doi:10.1016/j.geoderma.2009.04.020

Garnier, J., Quantin, C., Guimarães, E.M., Vantelon, D., Montargès-Pelletier, E., Becquer, T., 2013. Cr(VI) genesis and dynamics in Ferralsols developed from ultramafic rocks: The case of Niquelândia, Brazil. Geoderma 193–194, 256–264. doi:10.1016/j.geoderma.2012.08.031

Garnier, J., Quantin, C., Martins, E.S., Becquer, T., 2006. Solid speciation and availability of chromium in ultramafic soils from Niquelândia, Brazil. J. Geochemical Explor. 88, 206–209. doi:10.1016/j.gexplo.2005.08.040

Gheju, M., Balcu, I., 2011. Removal of chromium from Cr(VI) polluted wastewaters by reduction with scrap iron and subsequent precipitation of resulted cations. J. Hazard. Mater. 196, 131–138. doi:http://dx.doi.org/10.1016/j.jhazmat.2011.09.002

Godgul, G., Sahu, K.C., 1995. Chromium Contamination from Chromite Mine. Environ. Geol. 25, 251–257. doi:10.1007/BF00766754

Guertin, J., 2005. Toxicity and Health Effects of Chromium (All Oxidation States). Chromium Handb. 215–234. doi:doi:10.1201/9780203487969.ch6

Hansel, C.M., Wielinga, B.W., Fendorf, S.R., 2003. Structural and compositional evolution of Cr/Fe solids after indirect chromate reduction by dissimilatory iron-reducing bacteria. Geochim. Cosmochim. Acta 67, 401–412. doi:10.1016/S0016-7037(02)01081-5

Higman, B., n.d. Basic Mining Terminology [WWW Document]. Gr. Truth Trekking. URL http://www.groundtruthtrekking.org/Graphics/Mining-terms.html

Izbicki, J.A., Bullen, T.D., Martin, P., Schroth, B., 2012. Delta Chromium-53/52 isotopic composition of native and contaminated groundwater, Mojave Desert, USA. Appl. Geochemistry 27, 841–853. doi:10.1016/j.apgeochem.2011.12.019

Izbicki, J. a., Ball, J.W., Bullen, T.D., Sutley, S.J., 2008. Chromium, chromium isotopes and selected trace elements, western Mojave Desert, USA. Appl. Geochemistry 23, 1325–1352. doi:10.1016/j.apgeochem.2007.11.015

Jenifer, C., Sharmili, A., Anbumalarmathi, J., Umamaheswari, K., Shyamala, K., 2015. Studies on siderophore production by microbial isolates obtained from aquatic environment. Eur. J. Exp. Biol. 5, 41–45.

Johnson, C.M., Skulan, J.L., Beard, B.L., Sun, H., Nealson, K.H., Braterman, P.S., 2002. Isotopic fractionation between Fe(III) and Fe(II) in aqueous solutions. Earth Planet. Sci. Lett. 195, 141–153. doi:10.1016/S0012-821X(01)00581-7

Karale, R.S., Wadkar, D. V, Nangare, P.B., 2007. Removal and Recovery of Hexavalent Chromium From Industrial Waste Water By Precipitation With Due Consideration To Cost Optimization. J. Environ. Res. Dev. 2, 209–216.

Kierczak, J., Neel, C., Bril, H., Puziewicz, J., 2007. Effect of mineralogy and pedoclimatic variations on Ni and Cr distribution in serpentine soils under temperate climate.

Geoderma 142, 165–177. doi:10.1016/j.geoderma.2007.08.009

Kimball, K.L., 1990. Effects of hydrothermal alteration on the compositions of chromian spinels. Contrib. to Mineral. Petrol. 105, 337–346. doi:10.1007/BF00306543

Kotaś, J., Stasicka, Z., 2000. Chromium occurrence in the environment and methods of its speciation. Environ. Pollut. 107, 263–283. doi:10.1016/S0269-7491(99)00168-2

Kraemer, S.M., 2004. Iron oxide dissolution and solubility in the presence of siderophores 66, 3–18. doi:10.1007/s00027-003-0690-5

Kumar, A.R., Riyazuddin, P., 2010. Chromium speciation in groundwater of a tannery polluted area of Chennai City , India 579–591. doi:10.1007/s10661-008-0720-9

Kumar Bhandary, A., Gupta, P., Mukherjee, S., Ghosh Chaudhuri, M., Dey, R., 2016. Beneficiation of Low Grade Chromite Ore and Its Characterization for the Formation of Magnesia-Chromite Refractory by Economically Viable Process. Int. J. Chem. Mol. Eng. 10, 1083–1091.

Kwak, S., Yoo, J.C., Moon, D.H., Baek, K., 2018. Role of clay minerals on reduction of Cr(VI). Geoderma 312, 1–5. doi:10.1016/j.geoderma.2017.10.001

Leita, L., Margon, A., Pastrello, A., Arčon, I., Contin, M., Mosetti, D., 2009. Soil humic acids may favour the persistence of hexavalent chromium in soil. Environ. Pollut. 157, 1862–1866. doi:10.1016/j.envpol.2009.01.020

Liu, C., Fiol, N., Poch, J., Villaescusa, I., 2016. Journal of Water Process Engineering A new technology for the treatment of chromium electroplating wastewater based on biosorption. J. Water Process Eng. 11, 143–151. doi:10.1016/j.jwpe.2016.05.002

Ma, H., Zhou, J., Hua, L., Cheng, F., Zhou, L., Qiao, X., 2017. Chromium recovery from tannery sludge by bioleaching and its reuse in tanning process. J. Clean. Prod. 142, 2752–2760. doi:10.1016/j.jclepro.2016.10.193

Machado, M.D., Soares, E. V, Soares, H.M.V.M., 2010. Removal of heavy metals using a brewer ' s yeast strain of Saccharomyces cerevisiae : Chemical speciation as a tool in the prediction and improving of treatment efficiency of real electroplating effluents. J. Hazard. Mater. 180, 347–353. doi:10.1016/j.jhazmat.2010.04.037

Mcclain, C.N., Maher, K., 2016. Chromium fluxes and speciation in ultramafic catchments and global rivers. Chem. Geol. 426, 135–157. doi:10.1016/j.chemgeo.2016.01.021

Mills, C.T., Morrison, J.M., Goldhaber, M.B., Ellefsen, K.J., 2011. Applied Geochemistry Chromium (VI) generation in vadose zone soils and alluvial sediments of the southwestern Sacramento Valley , California : A potential source of geogenic Cr (VI) to groundwater. Appl. Geochemistry 26, 1488–1501. doi:10.1016/j.apgeochem.2011.05.023

Morrison, J.M., Goldhaber, M.B., Mills, C.T., Breit, G.N., Hooper, R.L., Holloway, J.A.M., Diehl, S.F., Ranville, J.F., 2015. Weathering and transport of chromium and nickel from

serpentinite in the Coast Range ophiolite to the Sacramento Valley, California, USA. Appl. Geochemistry 61, 72–86. doi:10.1016/j.apgeochem.2015.05.018

Mpouras, T., Chrysochoou, M., Dermatas, D., 2017. Investigation of hexavalent chromium sorption in serpentine sediments. J. Contam. Hydrol. 197, 29–38. doi:10.1016/j.jconhyd.2016.12.009

Murthy, Y.R., Tripathy, S.K., Kumar, C.R., 2011. Chrome ore beneficiation challenges & opportunities - A review. Miner. Eng. 24, 375–380. doi:10.1016/j.mineng.2010.12.001

Mwinyihija, M., 2010. Main Pollutants and Environmental Impacts of the Tanning Industry, in: Ecotoxicological Diagnosis in the Tanning Industry. pp. 17–35. doi:10.1007/978-1-4419-6266-9

Nafziger, R.H., 1982. A review of the deposits and beneficiation of lower-grade chromite. J . S . Afr . Inst. Min. Met. 205–226.

Novak, M., Chrastny, V., Cadkova, E., Farkas, J., Bullen, T.D., Tylcer, J., Szurmanova, Z., Cron, M., Prechova, E., Curik, J., Stepanova, M., Pasava, J., Erbanova, L., Houskova, M., Puncochar, K., Hellerich, L.A., 2014. Common occurrence of a positive δ53Cr shift in central european waters contaminated by geogenic/industrial chromium relative to source values. Environ. Sci. Technol. 48, 6089–6096. doi:10.1021/es405615h

Novak, M., Chrastny, V., Sebek, O., Martinkova, E., Prechova, E., Curik, J., Veselovsky, F., Stepanova, M., Dousova, B., Buzek, F., Farkas, J., Andronikov, A., Cimova, N., Houskova, M., 2017. Chromium isotope fractionations resulting from electroplating, chromating and anodizing: Implications for groundwater pollution studies. Appl. Geochemistry 80, 134–142. doi:10.1016/j.apgeochem.2017.03.009

Osaki, S., 1983. The effect of organic matter and colloidal particles on the determination of chromium (VI) in natural waters. Talanta 30, 523–526.

Oze, C., Fendorf, S., Bird, D.K., Coleman, R.G., 2004. Chromium Geochemistry of Serpentine Soils. Int. Geol. Rev. 46, 97–126. doi:10.2747/0020-6814.46.2.97

Özgen, S., 2012. Modelling and optimization of clean chromite production from fine chromite tailings by a combination of multigravity separator and hydrocyclone. J. South. African Inst. Min. Metall. VO - 112 112, 387.

Papp, J.F., 1994. Chromium life cycle study.

Paulukat, C., Døssing, L.N., Mondal, S.K., Voegelin, A.R., Frei, R., 2015. Oxidative release of chromium from Archean ultramafic rocks, its transport and environmental impact – A Cr isotope perspective on the Sukinda valley ore district (Orissa, India). Appl. Geochemistry 59, 125–138. doi:10.1016/j.apgeochem.2015.04.016

Peterson, M., Brown, G., Parks, G., 1996. Direct XAFS evidence for heterogeneous redox reaction at the aqueous chromium/magnetite interface, Colloids and Surfaces A: Physicochemical and Engineering Aspects. doi:10.1016/0927-7757(95)03345-9

Pettine, M., D'Ottone, L., Campanella, L., Millero, F.J., Passino, R., 1998. The reduction of chromium (VI) by iron (II) in aqueous solutions. Geochim. Cosmochim. Acta 62, 1509–1519. doi:10.1016/S0016-7037(98)00086-6

Pokrovsky, O.S., Schott, J., 2002. Iron colloids/organic matter associated transport of major and trace elements in small boreal rivers and their estuaries (NW Russia). Chem. Geol. 190, 141–179.

Qin, L., Wang, X., 2017. Chromium Isotope Geochemistry. Rev. Mineral. Geochemistry 82, 379–414.

Quantin, C., Ettler, V., Garnier, J., Šebek, O., 2008. Sources and extractibility of chromium and nickel in soil profiles developed on Czech serpentinites. Comptes Rendus - Geosci. 340, 872–882. doi:10.1016/j.crte.2008.07.013

Raous, S., Becquer, T., Garnier, J., Martins, É.D.S., Echevarria, G., Sterckeman, T., 2010. Mobility of metals in nickel mine spoil materials. Appl. Geochemistry 25, 1746–1755. doi:10.1016/j.apgeochem.2010.09.001

Raous, S., Echevarria, G., Sterckeman, T., Hanna, K., Thomas, F., Martins, E.S., Becquer, T., 2013. Potentially toxic metals in ultramafic mining materials: Identification of the main bearing and reactive phases. Geoderma 192, 111–119. doi:10.1016/j.geoderma.2012.08.017

Religa, P., Kowalik, A., Gierycz, P., 2011. Application of nanofiltration for chromium concentration in the tannery wastewater. J. Hazard. Mater. 186, 288–292. doi:10.1016/j.jhazmat.2010.10.112

Ren, H., Liu, H., Qu, J., Berg, M., Qi, W., Xu, W., 2010. The influence of colloids on the geochemical behavior of metals in polluted water using as an example Yongdingxin River, Tianjin, China. Chemosphere 78, 360–367. doi:10.1016/j.chemosphere.2009.11.018

Richard, F.C., Bourg, A.C.M., 1991. Aqueous geochemistry of chromium: A review. Water Res. 25, 807–816. doi:10.1016/0043-1354(91)90160-R

Rodríguez-Clemente, R., Tardy, Y., 1987. Geochemistry and mineral formation in the earth surface: proceedings of the international meeting "Geochemistry of the earth surface and processes of mineral formation." Centre national de la recherche scientifique, Madrid.

Salem, F.Y., Parkerton, T.F., Lewis, R. V., Huang, J.H., Dickson, K.L., 1989. Kinetics of chromium transformations in the environment. Sci. Total Environ. 86, 25–41. doi:10.1016/0048-9697(89)90190-3

Saputro, S., Yoshimura, K., Matsuoka, S., Takehara, K., Narsito, Aizawa, J., Tennichi, Y., 2014. Speciation of dissolved chromium and the mechanisms controlling its concentration in natural water. Chem. Geol. 364, 33–41.

doi:10.1016/j.chemgeo.2013.11.024

Sayyed, R.Z., Badgujar, M.D., Sonawane, H.M., Mhaske, M.M., Chincholkar, S.B., 2005. Production of microbial iron chelators (siderophores) by fluorescent Pseudomonads. Indian J. Biotechnol. 4, 484–490.

Schauble, E., Rossman, G.R., Taylor, H.P., 2004. Theoretical estimates of equilibrium chromium-isotope fractionations. Chem. Geol. 205, 99–114. doi:10.1016/j.chemgeo.2003.12.015

Schoenberg, R., Merdian, A., Holmden, C., Kleinhanns, I.C., Haßler, K., Wille, M., Reitter, E., 2016. ScienceDirect The stable Cr isotopic compositions of chondrites and silicate planetary reservoirs. Geochim. Cosmochim. Acta 183, 14–30. doi:10.1016/j.gca.2016.03.013

Schoenberg, R., Zink, S., Staubwasser, M., von Blanckenburg, F., 2008. The stable Cr isotope inventory of solid Earth reservoirs determined by double spike MC-ICP-MS. Chem. Geol. 249, 294–306. doi:10.1016/j.chemgeo.2008.01.009

Sharma, S., Malaviya, P., 2016. Bioremediation of tannery wastewater by chromium resistant novel fungal consortium. Ecol. Eng. 91, 419–425. doi:10.1016/j.ecoleng.2016.03.005

Sibi, G., 2016. Biosorption of chromium from electroplating and galvanizing industrial effluents under extreme conditions using Chlorella vulgaris. Green Energy Environ. 1, 172–177. doi:10.1016/j.gee.2016.08.002

Sikora, E.R., Johnson, T.M., Bullen, T.D., 2008. Microbial mass-dependent fractionation of chromium isotopes. Geochim. Cosmochim. Acta 72, 3631–3641. doi:10.1016/j.gca.2008.05.051

Stefánsson, A., Gunnarsson, I., Kaasalainen, H., Arnórsson, S., 2015. Chromium geochemistry and speciation in natural waters, Iceland. Appl. Geochemistry 62, 200–206. doi:10.1016/j.apgeochem.2014.07.007

Stein, K., Schwedt, G., 1994. Speciation of chromium in the waste water from a tannery. Anal. Chem. 350, 38–43.

Stepniewska, Z., Buciora, K., Bennicellia, R.P., 2004. The effects of MnO2 on sorption and oxidation of Cr(III) by soils. Geoderma 112, 291–296. doi:10.1016/j.geoderma.2004.01.015

Sueker, J.K., 1964. Chromium, in: Murphy, B. (Ed.), Environmental Forensics: Contaminant Specific Guide. Academic Press, Burlington, pp. 82–93. doi:https://doi.org/10.1016/B978-012507751-4/50027-6

Thacher, R., Hsu, L., Ravindran, V., Nealson, K.H., 2015. Modeling the transport and bioreduction of hexavalent chromium in aquifers : Influence of natural organic matter. Chem. Eng. Sci. 138, 552–565. doi:10.1016/j.ces.2015.08.011

Thatoi, H., Das, S., Mishra, J., Rath, B.P., Das, N., 2014. Bacterial chromate reductase, a

potential enzyme for bioremediation of hexavalent chromium: a review. J. Environ. Manage. 146, 383–99. doi:10.1016/j.jenvman.2014.07.014

Tiwary, R.K., Dhakate, R., Ananda Rao, V., Singh, V.S., 2005. Assessment and prediction of contaminant migration in ground water from chromite waste dump. Environ. Geol. 48, 420–429. doi:10.1007/s00254-005-1233-2

Tripathy, S.K., Murthy, Y.R., Singh, V., 2013. Characterisation and separation studies of Indian chromite beneficiation plant tailing. Int. J. Miner. Process. 122, 47–53. doi:10.1016/j.minpro.2013.04.008

Tripathy, S.K., Singh, V., Ramamurthy, Y., 2012. Improvement in Cr:Fe Ratio of Indian Chromite Ore for Ferro Chrome Production. Int. J. Min. Miner. Process. 1, 101–106. doi:10.5923/j.mining.20120103.01

Viera, M., Curutchet, G., Donati, E., 2003. A combined bacterial process for the reduction and immobilization of chromium. Int. Biodeterior. Biodegrad. 52, 31–34. doi:10.1016/S0964-8305(02)00103-8

Villalobos-Aragón, A., Ellis, A.S., Armienta, M. a., Morton-Bermea, O., Johnson, T.M., 2012. Geochemistry and Cr stable isotopes of Cr-contaminated groundwater in León valley, Guanajuato, México. Appl. Geochemistry 27, 1783–1794. doi:10.1016/j.apgeochem.2012.02.013

Wang, X., Johnson, T.M., Ellis, A.S., 2015. Equilibrium isotopic fractionation and isotopic exchange kinetics between Cr(III) and Cr(VI). Geochim. Cosmochim. Acta 153, 72–90. doi:10.1016/j.gca.2015.01.003

Wiederhold, J.G., 2015. Metal Stable Isotope Signatures as Tracers in Environmental Geochemistry. Environ. Sci. Technol. 49, 2606–2624. doi:10.1021/es504683e

Wille, M., Babechuk, M.G., Kleinhanns, I.C., Stegmaier, J., Suhr, N., Widdowson, M., Kamber, B.S., Schoenberg, R., 2018. Silicon and chromium stable isotopic systematics during basalt weathering and lateritisation: A comparison of variably weathered basalt profiles in the Deccan Traps, India. Geoderma 314, 190–204. doi:10.1016/j.geoderma.2017.10.051

Wu, W., Wang, X., Reinhard, C.T., Planavsky, N.J., 2017. Chromium isotope systematics in the Connecticut River. Chem. Geol. 456, 98–111. doi:10.1016/j.chemgeo.2017.03.009

Zelano, I., Sivry, Y., Quantin, C., Gélabert, A., Tharaud, M., Nowak, S., Garnier, J., Malandrino, M., Benedetti, M.F., 2015. Study of Ni exchangeable pool speciation in ultramafic and mining environments with isotopic exchange kinetic data and models. Appl. Geochemistry 64, 146–156. doi:10.1016/j.apgeochem.2015.09.021

Zink, S., Schoenberg, R., Staubwasser, M., 2010. Isotopic fractionation and reaction kinetics between Cr(III) and Cr(VI) in aqueous media. Geochim. Cosmochim. Acta 74, 5729–5745. doi:10.1016/j.gca.2010.07.015

CHAPTER 2

Material and methods

CHAPTER 2

2.1 STUDY AREAS

One of the characteristics of ultramafic areas is their enrichment in chromium (Cr). Although all ultramafic areas have this point in common, Cr mobility and availability will depend on the Cr bearing phases. Indeed, Cr speciation plays an important role on Cr mobility, while the trivalent state (Cr(III)) is the most stable form under reduced conditions (pH 4 - 8), under oxidized conditions hexavalent Cr (Cr(VI)) if often the termodinamically most stable oxidation state of Cr. All the Cr(VI) species will be anionic, thus exhibiting a much greater mobility and bioavailability than Cr(III) in soils and waters (Fendorf, 1995). This PhD focuses on the study of Cr in three different contexts: Nickel exploitation (Barro Alto, Goiás State, Brazil), historical chromite exploitation (Cromínia, Goiás State, Brazil) and current chromite exploitation and beneficiation (Sukinda valley, India).

2.1.1 Barro Alto (Goiás State, Brazil) – Nickel exploitation and metallurgic area

Starting from 2012, Barro Alto has produced 36.000 tons per year of ferronickel and this production will be maintained over the 25 years of mine life (Ettler et al., 2015). The climate of the area is tropical, with mean temperatures ranging between 18 and 22°C and an annual precipitation of approximately 1500 mm with a wet season from October to March (Zelano et al., 2013). Natural vegetation is dominated by the Brazilian Savannah, i.e. “Cerrado”. Barro Alto is part of the same granulite belt that includes the Niquelândia and Caña Brava complexes (Goiás state, Brazil) and is a major mafic-ultramafic layered intrusion that was subjected to granulite facies metamorphism. It is composed mainly of gabbronorite with minor dunite, peridotite, norite, gabbro, anorthosite and banded clinopyroxene-garnet amphibolite (Moraes and Fuck, 2000). In this area, weathering of ultramafic rocks has formed important nickel lateritic reserves that are being mined. The main Ni-bearing minerals are phyllosilicates (serpentine, chlorite, smectite, sepiolite) and Fe-oxides (Colin et al., 1990; Ratié et al., 2015). The mixture of saprolitic and lateritic ore is subjected to a pyrometallurgical processing to produce ferronickel (Zelano et al., 2013). Other mafic minerals containing large amount of Ni include olivine ($(Mg, Fe)_2SiO_4$) and pyroxene ($XY(Si, Al)_2O_6$), where X represents Ca, Na, Fe or Mg and Y represents ions of smaller size such as Cr, Al or Mn.

With the aim of understanding Cr dynamics in ultramafic areas and the impact on Cr speciation and isotopic fractionation associated to mining activities, water and solid samples

were collected in June 2015 (Table 2.1) in an active Ni mine and former metallurgical area in the Barro Alto complex (Goiás state, Brazil). Nine water samples from streams, ponds and groundwater were collected. Stream 1 was located in the ultramafic area but outside the mine and it was used as a reference, while stream 2 was located inside the mine. The three ponds are localized inside the mine and are used to store runoff water. Finally, the groundwater was collected in four piezometers, before (Piezo 1) and after (Piezo 2) the mine and before (Piezo 3) and after (Piezo 4) the smelter area (Figure 2.1).

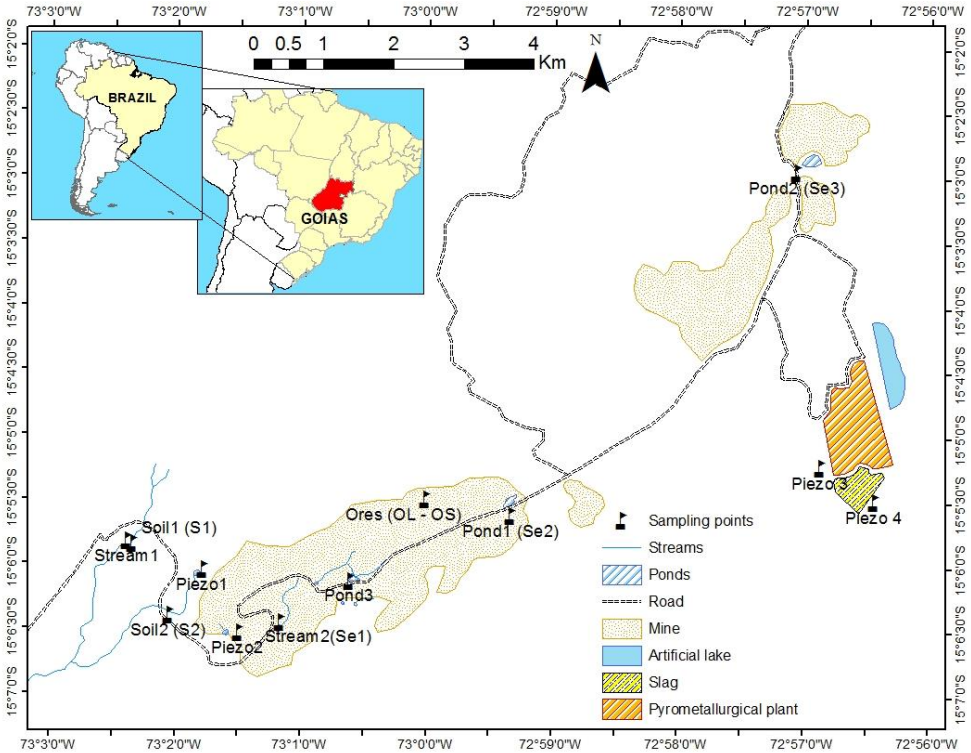

Figure 2.1 Map of the study area in Barro Alto mine and location of the sampling sites. (Names in parenthesis are the ones used for the solid samples).

In addition, solids such as soils, ores, sediments and bedrocks were sampled. Two soil profiles were collected: soil 1 profile (S1) had three layers between 0-10 cm, 10-40 cm and 80-100 cm and soil 2 profile (S2) had two layers between 0-15 cm and 15-40 cm. Eight lateritic ores (OL1 – OL8) and three saprolitic ores (OS1 – OS3) were collected in the mine exploitation area. Bottom sediment samples were collected in stream 2 (Se1), pond 1 (Se2) and pond 2 (Se3) (Figure 2.1). The bedrock B1 is a serpentinite collected in the area, while B2 and B3 were provided by the Anglo American mining company and come from two cores that were drilled through the lateritic regolith at 27 m and 28 m depths, respectively and correspond to samples C1 and C2 of Ratié et al. (2015).

Table 2.1 Water, soils, ores, bedrock and sediments sampling points in Barro Alto (Goiás state, Brazil).

Sample type	Sample name	Description	Coordinates		Altitude (m.a.s.l)
			E	N	
Water	Stream1	Stream located in pristine area	710672	8329997	728
	Stream2	Stream in the mine	712850	8328843	802
	Pond1	Sediment pond	716040	8330501	938
	Pond2	Sediment pond	720234	8335221	695
	Pond3	Sediment pond	713850	8329425	903
	Piezo 1	Piezometer before mining area	711752	8329590	767
	Piezo 2	Piezometer after mining area	712260	8328693	762
	Piezo 3	Piezometer before smelter	720565	8331014	684
	Piezo 4	Piezometer after smelter	712147	8330904	599
Soil	S1(0-10 cm)	Soil	710751	8329966	743
	S1(10-40 cm)	Soil	710751	8329966	743
	S1(80-100 cm)	Soil	710751	8329966	743
	S2(0-15 cm)	Soil	711264	8328944	748
	S2(15-40 cm)	Soil	711264	8328944	748
Ores	OL1	Lateritic ores	715781	8330582	963
	OL2	Lateritic ores	715781	8330582	963
	OL3	Lateritic ores	715781	8330582	963
	OL4	Lateritic ores	715781	8330582	963
	OL5	Lateritic ores	715781	8330582	963
	OL6	Lateritic ores	715781	8330582	963
	OL7	Lateritic ores	715781	8330582	963
	OL8	Lateritic ores	715781	8330582	963
	OS1	Saprolitic ores	715781	8330582	963
	OS2	Saprolitic ores	715781	8330582	963
	OS3	Saprolitic ores	715781	8330582	963
Bedrock	B1	Serpentinite	-	-	-
	B2	Core drilled – lateritic regolith 27m	-	-	-
	B3	Core drilled – lateritic regolith 28m	-	-	-
Sediment	Se1	Stream in the mine	712850	8328843	802
	Se2	Sediment pond	716040	8330501	938
	Se3	Sediment pond	720234	8335221	695

A great variety of Cr-bearing minerals has been described in both Barro Alto and Niquelândia massifs: goethite (FeO(OH)), Cr-rich magnetite ($Fe^{2+}(Fe^{3+}, Cr)_2O_4$), chromite [$(Fe,Mg)(Cr,Al)_2O_4$] and other mixed-composition spinels, talc ($Mg_3Si_4O_{10}(OH)_2$), chlorite ($(Mg, Fe)_5\ Al[(OH)_8\ AlSi_3O_{10}]$) and smectite (Garnier et al., 2009; Garuti et al., 2012). In addition, Raous et al. (2013) identified nontronite, a clay mineral that may represent a significant Ni and Cr-bearing phase in the first stage of ultramafic rock weathering. Weathering of ultramafic rocks is known to produce soil and sediments with high

concentrations of Ni and Cr associated with Al, Mn and Fe (Kumar and Maiti, 2013; Oze et al., 2003).

Several authors have been studying Barro Alto for the identification of the main carriers and reactive phases (Raous et al., 2013) in ores and spoils, the fate of metals (Raous et al., 2010) in spoils and the leaching of slag and fly ash from laterite ore (Ettler et al., 2015). In similar ultramafic systems such as Niquelândia, the fate of Cr during ultramafic weathering has been studied (Garnier et al., 2009) as well as the Cr solid speciation and availability (Garnier et al., 2006).

2.1.2 Cromínia (Goiás State, Brazil) – Historic chromite exploitation area

Cromínia (Goiás state, Brazil) soils derived from metamorphic rocks. Cromínia is part of the Araxa Group which comprises mostly micaschists, quartzites and carbonate-bearing schists. The most abundant rock types are garnet-feldspar-biotite-muscovite schist, kyanite-garnet-biotite-muscovite schist, garnet quartzite and chlorite-muscovite schist (Piuzana et al., 2003). Climate is characterized by average annual precipitation of 1384 mm, with a wet season occurring from November to February and an average annual temperature of 23.6°C.

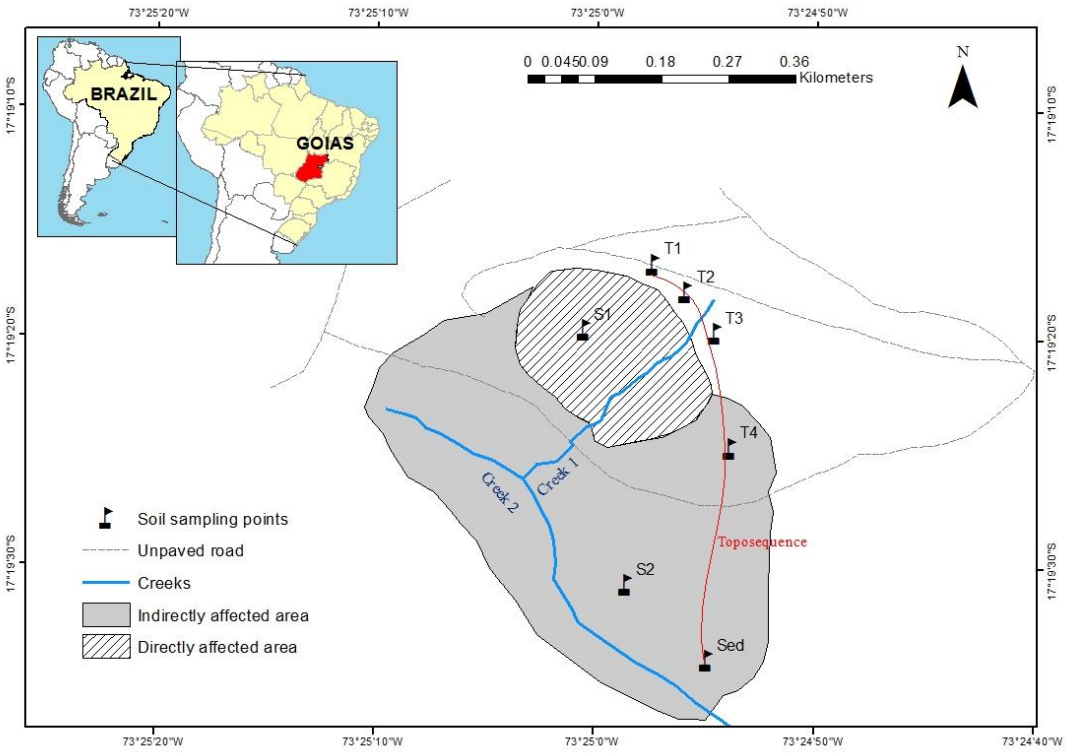

Figure 2.2 Map of the study area in Cromínia antique mine and location of the sampling sites.

In Cromínia-Mairipotaba, chromite has been extracted intermittently. The chromite concentrations in the chromitite seams reach 70 to 85% by volume of rock. The crystals are

dispersed in the matrix, which are composed essentially of serpentine, and subordinately of chlorite and talc (Angeli et al., 2010). Chromite deposits are predominantly of a high-refractory-grade that can be used without further processing. In general, the one is coarse grain, with nodules up to 2 mm of diameter. It occurs in compact masses and also disseminated in a serpentine matrix that generally grades between 20 and 40vol% Cr_2O_3.

Table 2.2 Water, soil and sediments sampling points in Cromínia (Goiás state, Brazil).

Sample type		Sample name	Type	Coordinates		Altitude (m.a.s.l.)
				E	N	
Water		Creek1	Stream	668301	8084074	730
		Creek2	Stream	668243	8083656	705
Soil	Non-affected area	T1	Soil	668351	8084176	763
		T2	Soil	668356	8084159	761
		T3(0-20 cm)	Soil	668333	8084107	742
		T3(20-70 cm)	Soil	668333	8084107	742
		T3Y(70-110 cm)	Soil	668333	8084107	742
		T3W(70-110 cm)	Soil	668333	8084107	742
		T3R(70-110 cm)	Soil	668333	8084107	742
		T3O(70-110 cm)	Soil	668333	8084107	742
		T3(130-160 cm)	Soil	668333	8084107	742
	Directly affected area	S1(0-30 cm)	Soil	668379	8084141	752
		S1(30-40 cm)	Soil	668379	8084141	752
		S1(40-100 cm)	Soil	668379	8084141	752
		S1(100-150 cm)	Soil	668379	8084141	752
		S1(>150 cm)	Soil	668379	8084141	752
	Indirectly affected area	T4	Soil	-	-	-
		S2	Soil	-	-	-
Sediment		Sed	Sediment	668342	8083643	711

In order to study the mobility of Cr through the soil in natural profiles and to determine how it has been affected by historic mining activities, in June 2015, solid samples were collected at different points based on the degree of exposure to mining activities (Figure 2.2).

In Crominía, three areas were defined: non-affected area, directly affected area and indirectly affected area. The non-affected area is located at the top of the hill and around the upper terrace, where sampling points T1, T2 and T3 are located. The directly affected area corresponds basically to the area of exploitation on the terraces where a soil profile (S1) was collected. And finally, the indirectly affected area corresponds to where material produced by exploitation activities has been deposited. For this area, one superficial soil (S2) and one sediment (Sed) sample were collected (Figure 2.2).

In addition, a toposequence (T1, T2, T3, T4 and Sed) including non-affected and indirectly affected soils and sediments was collected. The toposequence coved altitudes between 763 and 711 m.a.s.l. and there is a total distance of 300 m between the pedon T1 located in the upper part of the hill and Sed which is sediment of creek 2. From the sampling point mentioned previously, two soil profiles representing non-affected (T3) and affected soils (S1) were studied. The soil profile in T3 was 140 cm depth and between 70 and 110 cm, 4 subsamples were collected, due to the presence of different colors, which later were associated with contrasted mineralogical and chemical composition. The soil profile in S1 was 150 cm depth, and 5 subsamples through the profile were collected. We also sampled water of two creeks, named creek 1 and creek 2, which cross the area.

2.1.3 Sukinda valley, India – Chromite exploitation and metallurgic area

Chromite mine tailings were collected from materials generated in a typical beneficiation plant of Sukinda valley, Jajpur district, Odisha, India (Figure 2.3). Sukinda valley is located in the eastern part of the Indian peninsula, in the humid tropics where the average annual precipitation is about 2400 mm. Most of the rain occurs during the monsoon season between May and October. It is primarily drained by the Damsala nala River and it flows westward through the central valley to meet the major river, Brahmani, which flows at a distance of 15 km downstream of the mining belt (Paulukat et al., 2015).

Most of the mines are located in the central part of the valley and are operated for various companies including Orissa Mines Corporation (OMC), Tata Iron and Steel Company (TISCO) and Ferro Alloys Corporation (FACOR). The Sukinda ultramafic complex is composed of alternate band of chromite, dunite, peridotite and orthopyroxenite, which are extensively lateralized (Allegretti et al., 2006; Wang et al., 2007). The chromite bands in Sukinda valley present different composition. When the Cr_2O_3 content is higher than 48%, the ore is high grade and is directly marketable, between 32 and 45% is medium grade and finally lower than 30% is low grade (Kumar and Nagendran, 2009; Marrero et al., 2017). For the last case, the presence of gangue minerals such as goethite, serpentine, olivine and talc has led to the utilization of lean ore after beneficiation. The beneficiation process majorly consists of comminution to physically liberate the minerals followed by physical separation to generate the concentrate of chromite ore (Kumar et al., 2009). During the comminution process, large quantities of fines are generated. The fines are commonly de-slimed using hydro-cyclone and cyclone underflow processed using gravity concentrator like spirals and tables. As a results, chromite concentrated ore is obtained, and roughly 50 to 70% of the

chromite losses are in the fine fractions (tailings), where the fraction below 75 µm contain about 9-20% Cr_2O_3 (Dwari et al., 2018; Murthy et al., 2011).

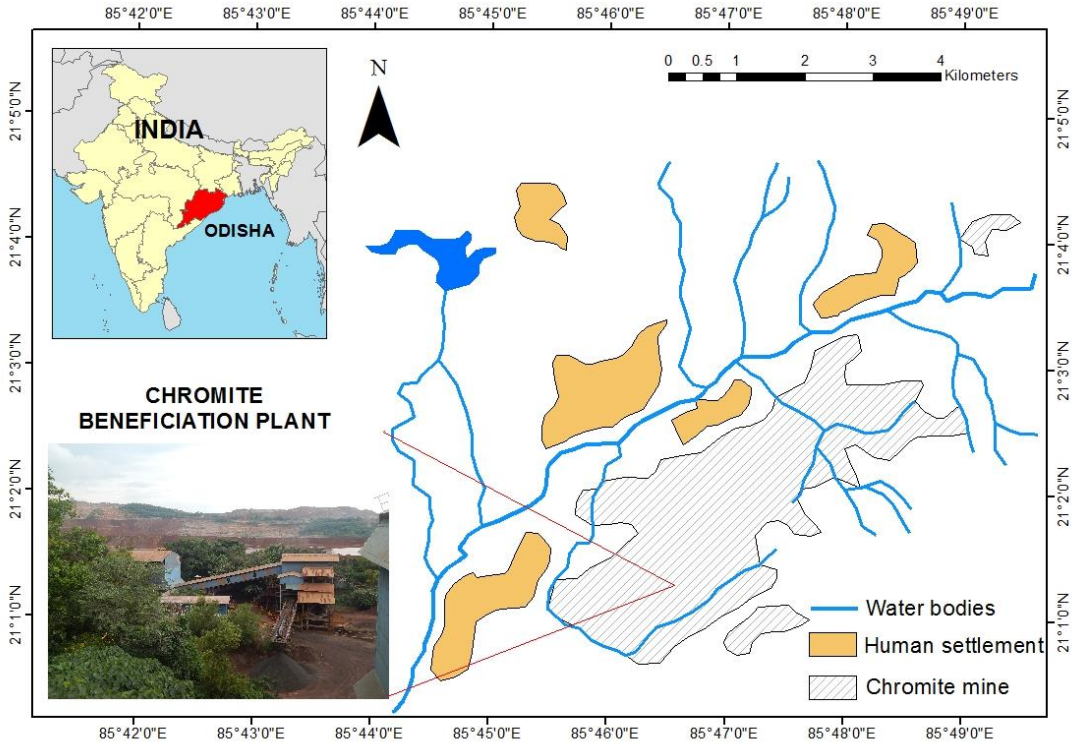

Figure 2.3 Map of the study area in the Sukinda valley (India).

Studies in Sukinda valley have focused on beneficiation improvement (Dhal and Pandey, 2013; Dwari et al., 2018; Kumar et al., 2009; Murthy et al., 2011; Tripathy et al., 2012), and on the recovery of chromite from beneficiation plant tailing (Tripathy et al., 2013). Also the migration of contaminant from chromite waste dump (Economou-Eliopoulos et al., 2016; Tiwary et al., 2005) has been of interest and the remediation of Cr(VI) contamination (Beukes et al., 2017; Dhal et al., 2013; Thatoi et al., 2014).

2.2 SAMPLES COLLECTION AND CHARACTERIZATION

2.2.1 Liquid samples

In water bodies, *in situ* parameters including temperature, pH and electrical conductivity were measured directly on the field using a WTW 3410 Set 2 multiparameter probe. Superficial and groundwater waters were collected in each sampling point and bulks were stored in pre-cleaned acid washed polyethylene bottles at 4°C (Figure 2.4).

(a)

(b)

(c)

Figure 2.4 Sampling of (a) surface water, (b) sediment ponds and (c) ground water in Barro Alto mine.

Samples were filtered using 0.22 µm PES (Polyethersulfone) syringe filters, and acidified with ultrapure concentrated HNO_3 for major (Na, Ca, K, Mg, Si) and trace (Fe, Mn, Al, Cr, Ni) elements analyses with ICP-AES (ICAP 6200, Thermo Fisher) or High-Resolution ICP-MS (Element II, ThermoScientific) for concentrations under 10 µg L^{-1}. Detection limits for the ICP-AES were typically between 10 and 200 µg L^{-1} and for the ICP-MS between 0.6 and 74 ng L^{-1}. The standard deviation (1σ) associated to the measurements was smaller than 5%.

Part of the filtered sample was stored in amber glass bottles and acidified with H_3PO_4 for dissolved organic carbon (DOC) analyses with a Shimadzu total organic carbon TOC-VCSH analyzer. Suspended particulate matter (SPM) and carbon were determined in GFF filters of 0.7 µm. An aliquot of the filtrated non acidified sample was used for anions (F^-, Cl^-, NO_3^-, SO_4^{2-}) measurements by ion chromatography (ICS 1100, Thermo Fisher) equipped with a column Ionpac thermos AS14 and a pre-column Ionpac thermos AG14. The mobile phase

consisted in a mixture of Na_2CO_3 and $NaHCO_3$. The injection volume was 20 µL and the flow rate was 1.2 mL min^{-1}. For the analysis of Cr isotopes in liquid samples, nearly 3 L of sample previously filtered and acidified with ultrapure HNO_3 were evaporated and concentrated up to a minimum of 100 ng Cr.

The Fe speciation was measured with the ferrozine method (Viollier et al., 2000). The ferrozine method consists in recording the absorbance of a Fe(II) colored complex before and after a Fe(III) reduction step. The ferrozine reagent forms a stable magenta complex with Fe(II). The maximum absorbance was recorded at 562 nm. When Fe(III) is also present in solution, it can react with ferrozine, thereby interfering with the coloration of the ferrous complex (Viollier et al., 2000). A mixture of dissolved Fe(II) and Fe(III) reacting with the ferrozine leads to the following absorbance:

$$A_1 = \varepsilon_{Fe(II)}\, l C_{Fe(II)} + \varepsilon C_{Fe(III)} l C_{Fe(III)} \quad \textbf{(2.1)}$$

Where A_1 is the measured absorbance before the reduction step, $\varepsilon_{Fe(II)}$ and $\varepsilon_{Fe(III)}$ are molar absorption coefficients, l is the optic path length (1 cm) and $C_{Fe(II)}$ and $C_{Fe(III)}$ are the Fe species concentrations. After the reduction of Fe(III) to Fe(II) the concentration of Fe(II)-ferrozine complex increases and according to the Beer-Lamber law.

$$A_2 = \varepsilon_{Fe(II)}\, l(C_{Fe(II)} + C_{Fe(III)})\alpha \quad \textbf{(2.2)}$$

Where A_2 is the measured absorbance after the reduction step and α is the dilution factor due to addition of the reducing agent and buffer. The Fe(II) and Fe(III) concentrations were calculated with the following equations:

$$C_{Fe(II)} = \frac{A_1 \varepsilon_{Fe(II)} l\alpha - A_2 \varepsilon_{Fe(III)} l}{\varepsilon_{Fe(II)} l\alpha(\varepsilon_{Fe(II)} l - \varepsilon_{Fe(III)} l)} \quad \textbf{(2.3)}$$

$$C_{Fe(III)} = \frac{A_2 - A_1\alpha}{\alpha(\varepsilon_{Fe(II)} l - \varepsilon_{Fe(III)} l)} \quad \textbf{(2.4)}$$

2.2.2 Solid samples

Solid samples including soils, ores and sediments were collected in Barro Alto and Cromínia. In addition, chromite tailings from the beneficiation plant in Sukinda valley were sampled. In the field, samples were stored in plastic bags and later dried in an oven at 60°C for 24h and sieved at 2 mm.

Total metal concentration in the solid samples was determined by X-ray fluorescence (XRF), using a PANalytical X fluorescence spectrometer equipped with Energy Dispersive Minipal 4 (Rh X Ray tube-30kV-9W), at a resolution of 150 eV (Mn Kα). Measurements were performed according to the thin-layer hypothesis. Considering the importance of the characterization of the main metals bearing phases to predict their mobility in ultramafic materials (Tina et al., 2006), the mineralogical composition was determined using X-ray diffraction (XRD) analysis on a PANalytical diffractometer and using the Cu Kα radiation (at 45 kV – 40 mA), in grazing incidence in the 5°-70° 2θ range with a scan step of 0.013°.

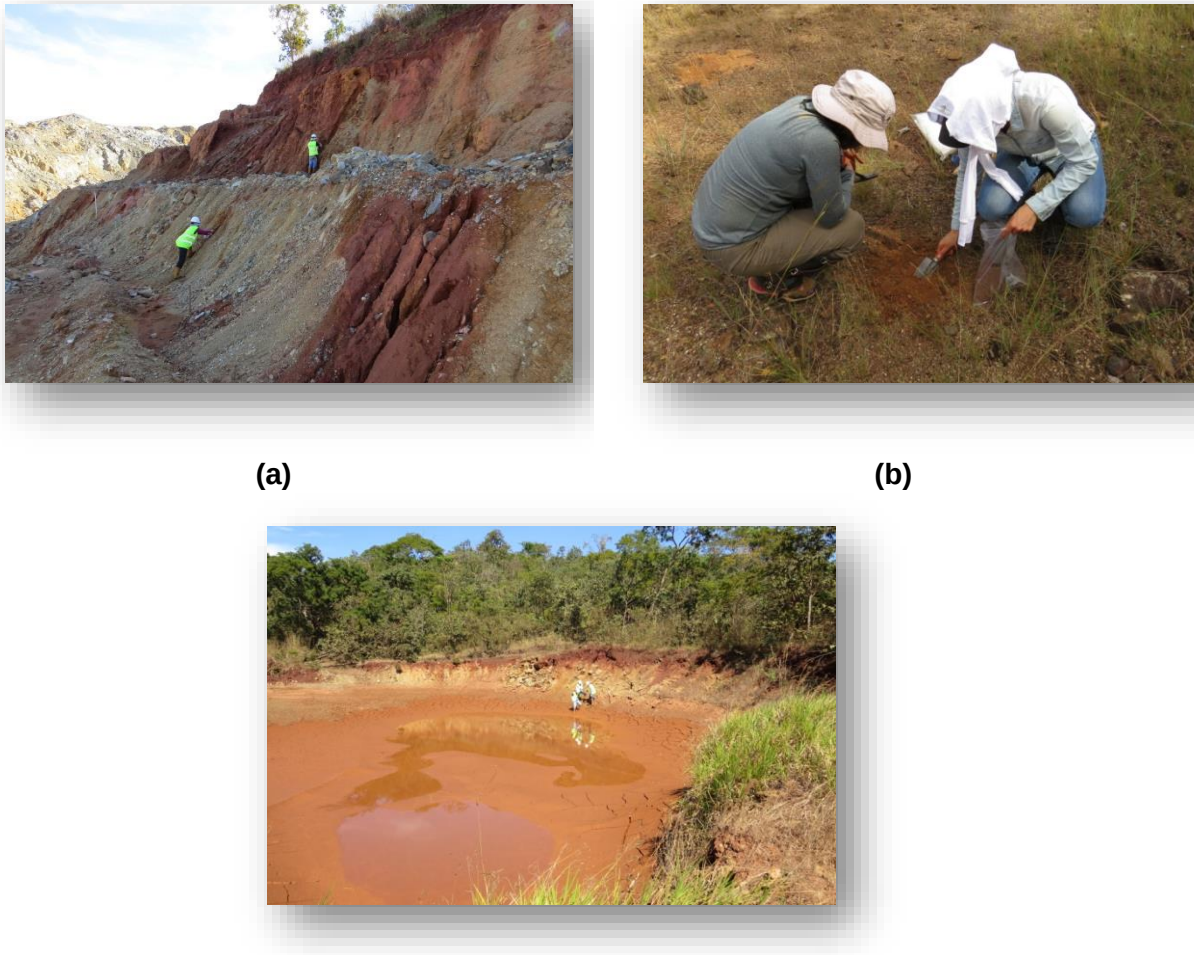

(a) **(b)**

(c)

Figure 2.5 Sampling of (a) ores, (b) soils and (c) sediments in Barro Alto mine.

In addition, acid digestions with ultrapure distilled HNO_3, HCl and HF were done in order to fully dissolve the solid samples. This procedure was performed in the clean room, in savillex previously cleaned with distilled HNO_3 and HCl (24 hours each). The refractory black residue (characteristic of samples containing minerals as chromite), after the acid digestion, was treated in a second step with acid digestion with $HClO_4$. Hence, it was important to dissolve

this fraction to know the total concentration of this element as well as to determine the real isotopic composition. After the dissolution of the samples, dilutions with 2% ultrapure HNO_3 were done and analyses of major (Na, K, Mg, Ca, Si) and trace (Fe, Mn, Al, Cr, Ni) elements were performed with ICP-AES (ICAP 6200, Thermo Fisher). The detection limits were between 10 and 200 µg L^{-1}.

2.3 CHROMIUM AVAILABILITY: THE EXCHANGEABLE POOL OF CHROMIUM

2.3.1 Chemical extraction

In order to measure the exchangeable pool of Cr(VI) ($E_{Cr(VI)}$-KH_2PO_4) and Cr(III) ($E_{Cr(III)}$-KCl), the protocol of Bartlett and James (1996) was applied (Figure 2.6). The principle of this protocol is based on the fact that Cr(VI) is mainly present in the anionic form, which can form labile surface complexes with Fe oxides and can be displaced by phosphates (Bartlett and James, 1996). Similarly, trivalent chromium species can be extracted through exchange with potassium.

For the extraction, to one gram of non-crushed sample sieved at 2 mm, was added 25 mL of 0.1 M KH_2PO_4 for Cr(VI) extraction, while for Cr(III) extraction were performed with 25 mL 1 M KCl. The mix was placed in a horizontal shaker for 1 hour at 20°C. After that, the sample was centrifuged to separate the solid from the liquid phase, and the supernatant was extracted and filtered with a 0.22 µm syringe PES (Polyethersulfone) filter. Total Cr concentration was measured with the ICP-AES (ICAP 6200, Thermo Fisher) or High-Resolution ICP-MS (Element II, ThermoScientific) for concentrations under 10 µg L^{-1}. Detection limits for the ICP-AES were typically between 10 and 200 µg L^{-1} and for the ICP-MS between 0.6 and 74 ng L^{-1}. Extractions were performed in triplicate and average is reported with its correspondent standard deviation. The data treatment of ICP-MS results was performed with uFREASI (Tharaud et al., 2015).

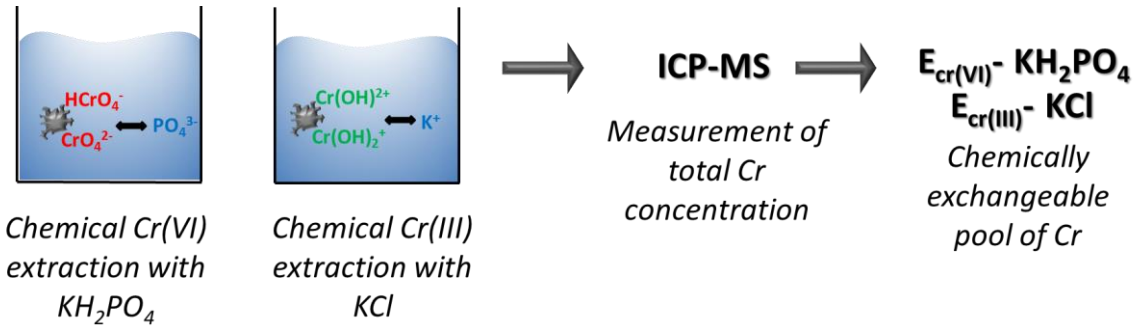

Figure 2.6 Protocol for chemical extraction of Cr(VI) with KH_2PO_4 and Cr(III) with KCl.

2.3.2 Isotopic exchange

The principle of this technique is based on the assumption that all the isotopes of the same element have the same macroscopic chemical behavior (Figure 2.7). Given this property, when two compartments with two different isotopic signatures are in contact, isotopes will tend to equilibrate between solid and liquid phases through isotopic exchange (Hamon et al., 2008).

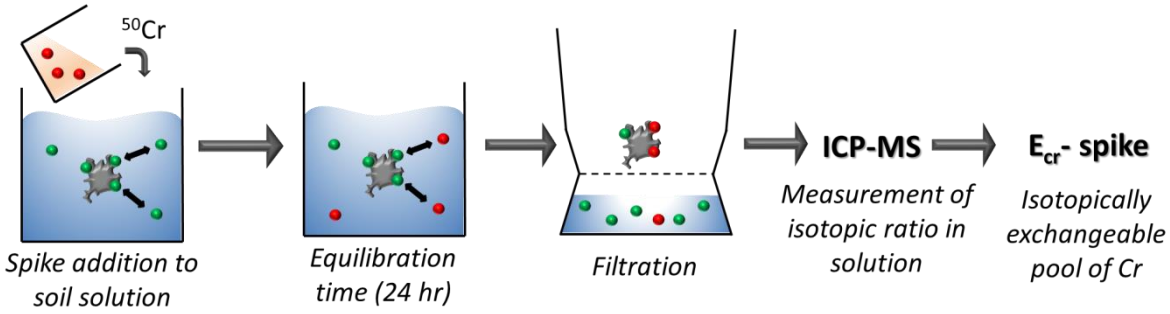

Figure 2.7 Isotopic exchange principle.

Isotopic dilution techniques have been recognized as a useful tool to investigate a variety of processes related to the bioavailability and mobility of trace elements and contaminants, while determining the concentration of isotopically exchangeable elements (E value) (Collins et al., 2006; Collins and Waite, 2009; Gäbler et al., 2007; Hamon et al., 2008; Lombi et al., 2003; Marzouk et al., 2013; Rodríguez-González et al., 2005; Sivry et al., 2011). The spiking solution used for the present study was obtained by the dissolution of metal Cr (Euriso-top®, atomic abundance: 98.31%, 1.55%, 0.08% and 0.05% of ^{53}Cr, ^{52}Cr, ^{54}Cr and ^{50}Cr, respectively) in 6N HCl, then dilution with MQ water to obtain a 357 mg L^{-1} stock solution of ^{53}Cr(III) in 1.57 N HCl.

For elements with more than one oxidation state, the importance of evaluating speciation in the E value calculation has been highlighted. Johnson et al. (2002) and Collins and Waite (2009) demonstrated that the isotopic exchange between Fe(II) and Fe(III) hydroxide species occurred within only a few minutes, so that Fe speciation does not need to be considered when determining the E_{Fe} value. In contrast, Collins et al. (2006) found that SeO_3^{2-} and SeO_4^{2-} were not isotopically self-exchangeable during 24 h of isotope exchange, concluding that Se speciation must be considered in the determination of the E_{Se} value.

The redox kinetics of the Cr(III) and Cr(VI) species in aquatic media have been investigated by Wang et al. (2015) and Zink et al. (2010). These authors found that there is no significant isotopic exchange between Cr(VI) and Cr(III) species over a timescale of days to weeks in

natural systems, while isotopic exchange inside the Cr(VI) pool is much faster (from 1 minute to 24 hours) (Garnier et al., 2009a). This may be explained by the preferential formation of Cr(III) complexes as octahedrally coordinated hydroxide, whereas Cr(VI) form tetrahedrally coordinated ions with very strong Cr-O bonds. This marked difference in the binding environment of Cr species with different oxidation states, but especially the very strong oxygen bonds in dissolved Cr(VI) complexes, are evidently responsible for the lack of both chromium and oxygen isotopic exchanges, of chromate and dichromate, with the prevailing surrounding environment. In addition, the isotopic exchange between Cr(VI) and Cr(III) requires three electron transfers, with the result that the rate of isotopic exchange is much lower (Apte et al., 2006; Wang et al., 2015b).

Based on the statements given above, after the addition of ^{53}Cr(III) or ^{50}Cr(VI) spiking solution to natural water samples or soil solution, it will redistribute itself within the solution and exchangeable pool similarly to the other Cr(III) (^{50}Cr(III), ^{52}Cr(III), and ^{54}Cr(III)) or Cr(VI) (^{52}Cr(VI), ^{53}Cr(VI), and ^{54}Cr(VI)) isotopes, respectively. The detail of the isotopic exchange experiments with ^{53}Cr(III) in water samples and with ^{50}Cr(VI) in soil solution, is given in chapters 3 and 4 of this PhD, respectively. The information obtained will be related to the isotopically exchangeable pool of Cr(III) or Cr(VI) only.

2.3.2.1 E^W_{Cr} determination

All of the filtrates from experiments #E1 and #E2, the un-spiked solutions of each sample, the standard solutions as well as the spike mother solution were analyzed using a High-Resolution ICP-MS (ThermoScientific Element II). All of the Cr isotopes were measured: ^{50}Cr, ^{52}Cr, ^{53}Cr and ^{54}Cr in medium resolution (R > 4000) in order to eliminate potential polyatomic interferences, as well as ^{47}Ti, ^{51}V and ^{57}Fe to correct for possible isobaric interferences. The calculated ^{53}Cr/^{52}Cr isotopic ratio corresponds to the average of 20 runs with an analytical reproducibility better than 1% (2SD, n = 520). Samples were divided by blocks using bracketing with standard and natural un-spiked solutions in order to verify and correct, if necessary, drift in the signal and intensity.

The term E^W was introduced by Zelano et al. (2013) and is defined as the product of the concentration of suspended particulate matter (mg L^{-1}) and the isotopically exchangeable pool of metal E_{Me} (Sivry et al., 2011). On this basis, the amount of isotopically exchangeable chromium per liter of solution (E^W_{Cr}) was calculated as follows (1):

$$\boldsymbol{E^{w}_{Cr}} = Q\,.\,CSPM.\ \frac{M_{STD}}{M_s}.\frac{A_s}{A_{STD}}.\left[\frac{IR_{Spike} - IR_{Sample}}{IR_{Sample} - IR_{UN}}\right] \qquad \textbf{(2.5)}$$

where *Q* represents the amount of ^{53}Cr spike solution added (µg per kg of SPM), CSPM is the concentration of suspended particulate matter (kg of SPM per L of sample), M_{STD} and M_S represent the atomic mass of Cr in the standard and spike solutions (in g/mol), A_{STD} and A_S represent the abundance in percentage of ^{52}Cr in the standard and spike solutions, respectively; IR_{Spike}, IR_{Sample} and IR_{UN} represent the isotopic ratio $^{53}Cr/^{52}Cr$ in the spike solution, in the sample after spike addition and in the sample without spike addition, respectively. To assess the reproducibility of the method for experiments #E1 and #E2, the triplicates were analyzed for three cut-offs (0.7 µm, 0.2 µm and 500 kDa) and one particle size range (1–500 kDa), respectively. Three filtration blanks were also prepared to determine the filter and reagent contributions. The error propagation was used to calculate the uncertainty in the E^w_{Cr} values. The fractional uncertainties of the isotopic $^{53}Cr/^{52}Cr$ ratio in the spiked and un-spiked samples as well as in the spike solution were included in the error calculation. Each isotopic ratio results from the average of 20 runs of five scan each, with their associated standard deviation.

2.3.3 Chromium speciation in liquid samples

In order to determine the chromium liquid speciation, a chromatography column was coupled to the High-Resolution ICP-MS (ThermoScientific Element II). This is an on-line method which allows the determination of Cr(VI) and Cr(III) content at a single run and within one analytical unit. On-line methods are often applied by using flow injection analysis (FIA) techniques. The sample is injected into a carrier stream passing through a column which retains certain species. The carrier stream composition is changed and the species retained on the sorbents are directly eluted from the column into the detection systems (Świetlik, 1998).

The column used was part of a speciation kit (CF-KIT-Cr36) of Elemental Scientific specially designed to separate Cr(VI) and Cr(III) species, which were subsequently eluted into the High-Resolution ICP-MS (Figure 2.8(a)). The speciation column was added to an existing SC-DX-FAST system for separation of Cr species by isocratic elution anion exchange chromatography. The HPLC separation of chromium species was performed with a mobile phase, at pH 2, constituted by 68% HNO_3, 25% NH_3 and 10 ppm Tm. The flow rate through the column was between 170 and 180 µL min^{-1} (10 rpm on the peristaltic pump). Prior to using the column, mobile phase was allowed to flow through the column for 30 minutes in order to condition the column with the ion-pair reagent. After use column was rinsed with MQ water and was stored wet to prevent drying out. The detection limit for Cr(VI) is 4 ng L^{-1} and for Cr(III) is 3 ng L^{-1}. Figure 2.8(b) shows a chromatogram of a mixture of Cr(VI) and Cr(III) (5 µg L^{-1} each) acquired while monitoring ^{52}Cr. Chromium standards, ranging from 10 ppt to 10

ppb, were prepared from 1000 mg L^{-1} stock solution of Cr(III) (PerkinElmer, $Cr(NO_3)_3.9H_2O$) and Cr(VI) (Merk, CrO_4^{2-}). The calibration curve for Cr(III) and Cr(VI) was done considering the area down the curve, which was estimated with a curve integration program ("Integlec", Microsoft Visual Basic environment, R. Losno, personal communication) using trapeze integration method with a user defined baseline and a graphical front-end. The noise reduction was calculated with a Hamming filter. To estimate the Cr(III) and Cr(VI) concentrations in the samples, the area down the curve was calculated for each sample the concentration was estimated using the calibration curve.

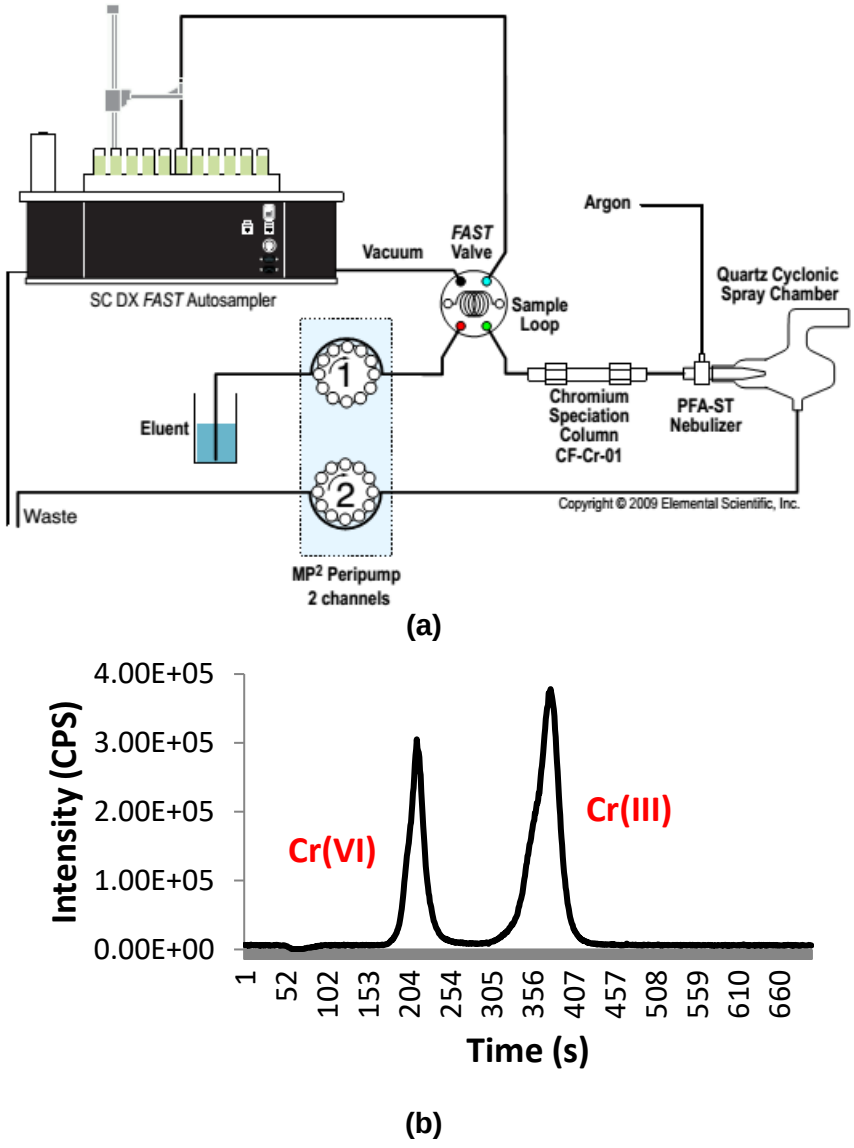

Figure 2.8 Diagram of the Cr speciation system (Sullivan and Wiederin, 2018) (a) and Cr speciation spectra of standard containing Cr(III) and Cr(VI) (b).

2.4 CHROMIUM MOBILITY: ALTERATION OF CHROMIUM BEARING PHASES

Environmental exposure period of ores and mine residues, such as tailings, resulting in alteration of minerals, could affect the release process of heavy metals (Jin et al., 2014). To study the dynamic leaching of heavy metals, batch experiments were carried out. Ores from Barro Alto (Goiás State, Brazil) and chromite tailings from Sukinda valley (Odisha, India) were leached for an approximated period of two weeks.

2.4.1 Chemical leaching of Barro Alto ores

From the solid samples collected in Barro Alto mine, ores had the highest content of exchangeable pool of Cr(VI). This was the main criteria considerer for the samples selection (Ores OL1, OL3, OL5, OS3, OL8), as well as the mineralogical composition. Ores OL3, OL5 and OL8 were characterized for a high content of iron oxides including Goethite and Hematite, ores OL1 and OL8 also contained spinel, while ore 9 with a lower exchangeable pool or Cr(VI) was mainly constituted by serpentine.

About 15 g of the sample previously sieved through a 2.0 mm mesh, were mixed with 300 mL of the electrolyte, 10^{-3} M $NaNO_3$. This corresponds to a 20:1 solid-liquid ratio, as used in previous works (Liu et al., 2013) and closely to the field land conditions. Sodium azide (NaN_3 0.02% w/v), an antimicrobial agent, was added to prevent biological activity in the system. The mixture was shaken with a magnetic bar at a speed of 120 rpm for 11 days. In order to establish the leaching kinetic, several subsamples were collected: 1 h, 4 h, 7 h, 11 h, 1 d, 2 d, 3 d, 4 d, 5 d, 7 d, 9 d and 11 d. Subsamples of 30 mL were collected in the middle of the water level with a plastic tube that was installed on the side of the batch reactor. To limit the collection of particles and the consequent modification of the solid liquid ratio, the shaker was stopped about 30 minutes before the sample collection. In addition; the volume sampled was replaced immediately by an equivalent volume of the leaching solution (10^{-3}M $NaNO_3$) to keep the same solid-liquid ratio. Figure 2.9 shows the configuration of the batch reactor.

2.4.1.1 Leachate characterization

In situ parameters such as pH, dissolved oxygen, temperature and electrical conductivity was permanently monitored (Figure 2.9). Samples were filtered using 0.22 µm syringe PES (Polyethersulfone) filters, and acidified with ultrapure concentrated HNO_3 for major (Na, Ca, K, Mg, Si) and trace (Fe, Mn, Al, Cr, Ni) elements analyses with ICP-AES (ICAP 6200, Thermo Fisher) or High-Resolution ICP-MS (Element II, ThermoScientific) for concentrations under 10 µg L^{-1}. Detection limits for the ICP-AES were typically between 10 and 200 µg L^{-1} and for the ICP-MS between 0.6 and 74 ng L^{-1}. The standard deviation (1σ) associated to the measurements was smaller than 5%.

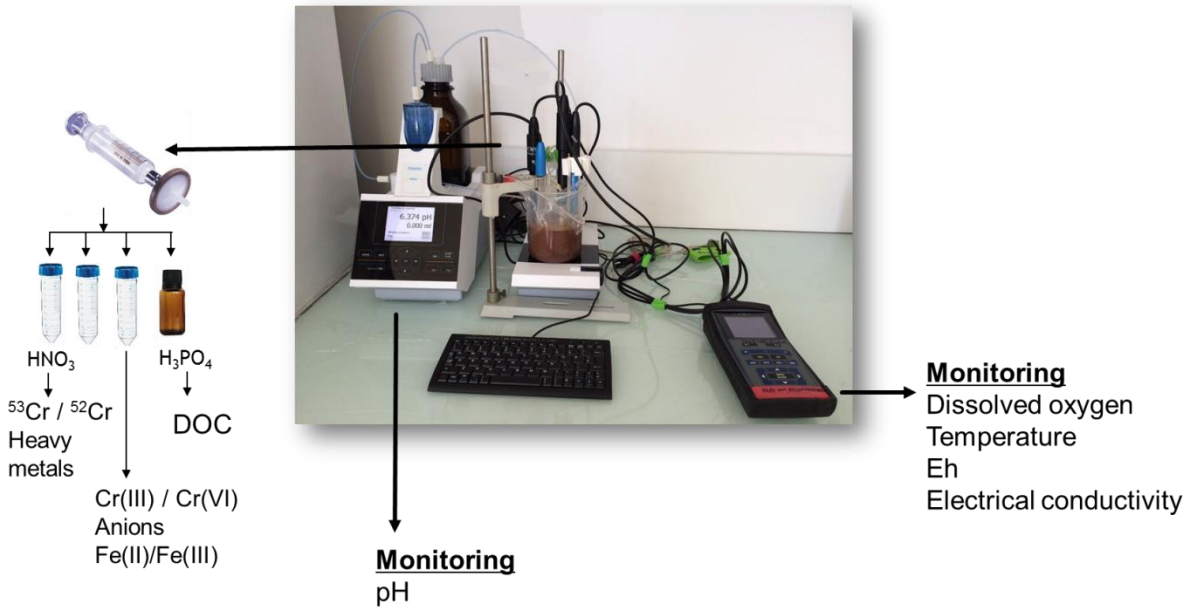

Figure 2.9 Batch reactor configuration for chemical leaching of Barro Alto ores.

Part of the filtered sample was stored in amber glass bottles and acidified with H_3PO_4 for dissolved organic carbon (DOC) analyses with Shimadzu total organic carbon TOC-VCSH analyzer. An aliquot of the filtrated non acidified sample was used for anions (F^-, Cl^-, NO_3^-, SO_4^{2-}) measurements by ion chromatography (ICS 1100, Thermo Fisher) equipped with a column Ionpac thermos AS14 and a pre-column Ionpac thermos AG14. For the analysis of Cr isotopes in liquid samples, nearly 20 mL of sample previously filtered and acidified with ultrapure HNO_3 were evaporated and concentrated up to a minimum of 50 or 100 ng Cr. Alkalinity was measured in the first and the last samples. Fe speciation was determined with the ferrozine method (Viollier et al., 2000) and Cr speciation was done with the method described in the section 2.3.3.

2.4.2 Chromite tailings bioleaching

Bioleaching experiments were performed at IHE Delft Institute for Water Education (Delft, The Netherlands) to determine the leaching behavior of chromite tailings under the influence of two bacterial strains: *Pseudomonas putida* and *Acidithiobacillus thiooxidans*. In parallel, the effect of pulp density (5, 10 and 30 g L^{-1}) was studied. The experiments were carried out in glass bottles. All the material was sterilized at 121 °C for 20 minutes prior to use. The reactors were closed using a cotton plug and placed in an orbital shaker at 190 rpm and 30 °C. Around ten subsamples of 20 mL each were collected during two weeks. The same volume of sample collected was replaced with fresh sterile medium (Figure 2.10).

Figure 2.10 Bio-leaching batch experiments with *P. putida* and *A. thiooxidans*.

2.4.2.1 Leaching with distilled water

The growth media (for *A. thiooxidans* and *P. putida*) effect on tailings leachability was evaluated. To avoid bacterial growth, sterilization of the sample was needed. For this purpose, tailings were heated at 160 °C for 5 hours. However, this temperature could affect the leachability of the tailings. In order to verify this, a test with distilled water was performed. Tailings with and without sterilization at 160 °C were leached with distilled water at 190 RPM and 30°C. Three pulp densities were included (5, 10 and 30 g L^{-1}).

2.4.2.2 Bio-leaching with A. thiooxidans and P. putida

The bioleaching experiments with *A. thiooxidans* and *P. putida* were performed in solutions containing the same components of the growth media where bacteria were pre-grown. The initial pH was set at 3.5 for *A. thiooxidans* and 7 for *P. putida*. 1% (v v^{-1}) of the pre-grown bacterial culture was inoculated to the batch reactors. Sterilized tailings and media were considered as a control and sodium azide (NaN_3) was added to avoid bacterial growth.

Medium composition for *P. putida*

The gram-negative *P. putida* (WCS 358) bacterial strain was provided by Peter Bakker, University of Utrecht (The Netherlands). For siderophore production iron free succinate medium (SM) consisting of g L^{-1}: K_2HPO_4 6.0, KH_2PO_4 3.0, $MgSO_4$ $7H_2O$ 0.2, $(NH_4)_2SO_4$ 1.0 and succinic acid 4.0, pH 7.0 was used to inoculate *P. putida* at a rate of 1% (v/v) inoculum.

Medium composition for *A. thiooxidans*

The gram-negative *A. thiooxidans* (DSM 9463) bacterial strain was grown in a medium composed of 2 g ammonium sulfate ($(NH_4)_2SO_4$), 0.25 g of magnesium sulfate ($MgSO_4$ $7H_2O$), 0.1 g of dipotassium hydrogen phosphate (K_2HPO_4), 0.1 g of potassium chloride (KCl) and 11% (wt v^{-1}) of elemental sulfur previously sterilized. The medium pH was adjusted to 3.5 before sterilization, and after the sterilized sulfur was added together with the inoculum.

The culture was maintained at 30 °C. The size of the culture was increased gradually in separated Erlenmeyer.

2.4.2.3 Chemical leaching

In addition to the experiments done with *A. thiooxidans* and *P. putida*, chemical leaching of tailings with distilled water at pH 2 (adjusted with H_2SO_4) and distilled water at pH 9 (adjusted with NaOH) were carried out at 30 g L^{-1}. The leachability of chromite was studied through the leaching of the concentrated ore coming from the beneficiation plant. Distilled water at pH 2 adjusted with H_2SO_4 was used.

2.4.2.4 Leachate characterization

Dissolved oxygen, electrical conductivity and pH were monitored after sampling. Part of the sample was frozen at -20 °C to determine protein and siderophores content (in the case of *P. putida*). The rest of the sample was filtered at 0.2 µm using PES filters, for the determination of major and traces element concentrations (Fe, Cr, Al, Ni, Mn, Mg) in the leachate. Concentration of major elements in filtered samples was determined using ICP-AES (ICAP 6200 Thermo Fisher), whereas HR-ICP-MS (Thermo Scientific Element II) was used for trace elements analysis. Detection limits were typically between 0.6 and 74 ng L^{-1} and the standard deviation (1σ) associated to the measurements was smaller than 5%. The solid sample was collected at the end of the experiment and dried at 60°C for 24 hours for XRF measurements.

2.4.2.5 Siderophores and protein content determination

In order to establish the growth of the bacterial community, the Lowry protein test was performed in the supernatant collected in the leaching experiments. The Lowry method is the most commonly employed procedure for the assay of protein because of its sensitivity, simplicity and reproducibility (Rodríguez-Vico et al., 1989). In this method peptide bonds of proteins reacts with copper under alkaline conditions to produce Cu^+. The Cu^+ produced reacts with the Folin reagent. In essence phosphomolybdotungstate is reduced to heteropolymolybdenum blue by the copper-catalyzed oxidation of aromatic amino acids. The reaction results in a strong blue color, which depends on the tyrosine and tryptophan content (Waterborg and Matthews, 1984).

The complex-forming reagent was prepared just before use by the mixing of the stock solution in a proportion of 100:1:1 (by volume) respectively: Solution A: 2% (w v^{-1}) Na_2CO_3 in distilled water; Solution B: $CuSO_4 \cdot 5H_2O$ in distilled water; solution C: 2% (w v^{-1}) sodium potassium tartrate in distilled water. 2N NaOH and folin regent 1N were also required. For

the calibration curve, protein standards were prepared with bovine serum albumin with concentrations between 10 and 500 µg mL^{-1}.

0.1 mL of 2N NaOH was added to 0.1 mL of sample or standard. The mixture was hydrolyze at 100°C for 10 minutes in a boiling water bath. After cool the hydrolysate to room temperature, 1mL of the complex-forming reagent was added and the solution was left for 10 minutes at room temperature. After that 0.1 mL of Folin reagent was added to the mix, using a vortex mixer. After 30 to 60 minutes, the absorbance was read at 750 nm for protein concentration below 500 µg mL^{-1} (Waterborg and Matthews, 1984).

Quantitative estimation of siderophores produced by *P. putida* was done by CAS-shuttle assay. Various assays have been developed to detect different phenotypes of siderophores. Schwyn and Neilands (1987) developed an universal method to detect and determine siderophores by using their high affinity for iron(III). The following chemical equation explains the principle:

$$FeDye^{3-\lambda} + L^{k-} \rightarrow FeL^{3-k} + Dye^{\lambda-} \quad \textbf{(2.6)}$$

A strong ligand L (e.g., siderophore) is added to a highly colored iron dye complex. When the iron ligand complex is formed, the release of the free dye is accompanied by a color change from blue to orange (Schwyn and Neilands, 1987). Quantitative estimation of siderophores produced by *P. putida* was done by CAS-shuttle assay (Payne, 1994).

The next solutions were required for the preparation of the CAS reagent: (a) 0.06 g of CAS in 50 mL of distilled water; (b) 0.0027 g of $FeCl_3 \cdot 6H_2O$ in 10 mL of 10 mM HCl; (c) 0.073 g of HDTMA in 40 mL of distilled water. Solution (a) was mixed with 9 mL of solution (b) and after with solution (c). The CAS reagent was autoclaved and stored in a plastic bottle (Lynne et al., 2011).

For the quantification of the siderophores, 0.5 mL of supernatant (sample) was mixed with 0.5 mL of CAS reagent, and absorbance was measured at 630 nm. Siderophore content was calculated by using the equation (2.7) proposed by Sayyed et al. (2005).

$$\%\ siderophore\ units = \frac{A_r - A_s}{A_r} * 100 \quad \textbf{(2.7)}$$

Where A_r and A_s correspond to the absorbance of the reference and sample at 630 nm, respectively.

2.5 CHROMIUM ISOTOPIC MEASUREMENTS

2.5.1 Reagents and isotopic standards

Prior to use, super pure grade nitric (HNO_3), hydrochloric (HCl) and hydrofluoric (HF) acids bought from Merk Inc. (Germany) were purified by sub-boiling distillation in the Institut de Physique du Globe de Paris (IPGP). Solutions were prepared with the distilled acids and ultra-pure water (≥ 18.2 MΩ cm), prepared by de-ionization of reverse osmosis water using a Milli-Q® system (Millipore, USA).

The savillex used for the collection of eluted samples were cleaned, in the IPGP's clean room, with concentrated HNO_3 and HCl, 24 hours each at 100°C with three rinses with ultra-pure water between them and at the end of the cleaning process. Savillex were dried under the laminar flow cabinet. The polypropylene plastic tubes, to store the samples dilutions prior analysis, were cleaned with distilled 1% HCl during 24 hours and rinsed three times with ultra-pure water.

The reference material used was BHVO-2 which is basalt from the Hawaiian Volcanic Observatory containing 280 µg g^{-1} of chromium. Home standards (IPGP standards) were prepared from NIST SRM-979 and NIST SRM-3112a.

2.5.2 Sample preparation

For isotopic measurements the ideal is to have at least 100 ng of chromium. It is feasible to find this quantity in few mg of solid samples, however liquid samples could require several liters. Chromium concentration in liquid samples was measured to calculate the volume needed to reach at least 100 ng of Cr. Samples were concentrated through evaporation in previously acid washed savillex. Once the sample was totally dry, 0.15 mL of distilled 6 N HCl was added to dissolve the residue after evaporation. Just before the first elution, 1 mL of MQ water was added to decrease the concentration of the HCl to less than 0.1 N.

For solid samples, Cr concentration in the solution after acid digestion (section 2.2.2) was determined to calculate the volume of the solution to have at least 100 ng of Cr in a 10 mL solution. The sample was dried then and 0.5 mL of 6 N HCl was added to dissolve the residue. Just before the first elution 3 mL of MQ water were added to decrease the concentration of the HCl to less than 0.1 N.

2.5.3 Column chemistry

The valence states of Cr impart different ion chromatographic properties on the ionic species used for the separation (Frei and Rosing, 2005). Under this consideration, all Cr was

converted to Cr(III) prior to chemical separation by reduction in 6 M HCl at 100°C (Trinquier et al., 2008). It is important to consider that species elute in order of increasing selectivity. According to Larsen et al. (2016) Cr(III) species are expected to elute in the order $Cr(H_2O)_3Cl_3$, $Cr(H_20)_4Cl_2^+$, $Cr(H_2O)_5Cl^{2+}$ and $Cr(H_2O)_6^{3+}$. The protonated functional groups on the resin (R-), while the positively charged species exchange according to equations (2.8), (2.9) and (2.10) where R- represents the sulfonated functional group in the cation exchanger (Larsen et al., 2016).

$$Cr(H_2O)_4Cl_2^+ + R-H \leftrightarrow R-Cr(H_2O)_4Cl_2 + H^+ \quad \textbf{(2.8)}$$

$$Cr(H_2O)_5Cl^{2+} + 2[R-H] \leftrightarrow R_2-Cr(H_2O)_5Cl + 2H^+ \quad \textbf{(2.9)}$$

$$Cr(H_2O)_6{}^{3+} + 3[R-H] \leftrightarrow R_3-Cr(H_2O)_6Cl + 3H^+ \quad \textbf{(2.10)}$$

The extremely slow reaction kinetics of Cr redox reactions and Cr(III)-Cl complexation at ambient conditions likely invokes kinetic isotope effect (Johnson and Bullen, 2004). The abundance of Cr(III) species, which could limit the Cr recovery, was avoided with a sample pre-treatment, exposing the sample matrix to concentrated HCl solution at 100°C. Afterward the samples was loaded in diluted acid where the relative differences in distribution coefficients on a cation exchanger are really large, providing sufficient resolution for elemental separation (Larsen et al., 2016).

For the third elution, pre-treatment was done with HNO_3. Figure 2.11 shows that complete transformation of Cr into Cr(III) form was obtained after equilibration of Cr samples in diluted HNO_3 at about room temperature.

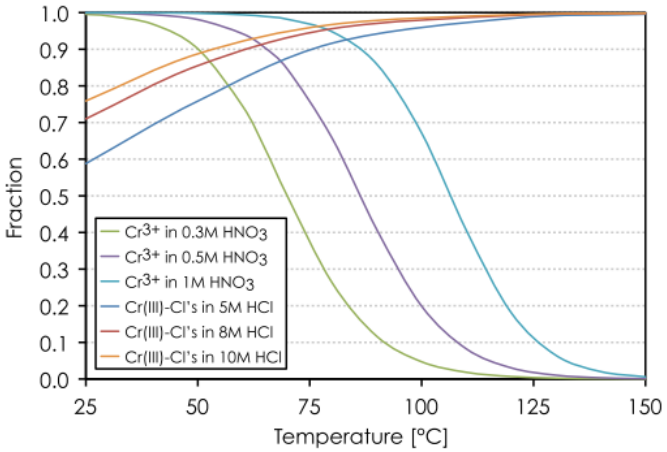

Figure 2.11 Cr speciation model showing the predominance of the Cr^{3+} specie in dilute HNO_3 and Cr(III)-Cl complexes in 5–10 M HCl as a function of temperature (Larsen et al., 2016).

2.5.3.1 Chromatography column separation of Cr

The chromium purification was performed in three steps in a cation exchange resin (AG 50 X8) and is displayed in Figure 2.12.

First elution: Chromium purification from matrix.

- ✓ The sample was loaded into the column and the elution was collected in savillex **1**.
- ✓ After that 5 mL of distilled 1N HCl were added and the elution was collected in savillex 1, together with the sample load.
- ✓ A second savillex (2) was used to collect the elution of 2 mL distilled 6 N HCl. With the 1 N HCl around 95% of Cr is eluted, for that reason the 5% remaining is eluted with the 6 N HCl.
- ✓ The columns were washed with 5 mL of distilled 6 N HCl and 2 mL of MQ water.

Second elution: In order to recover the 5% of Cr present in savillex **2**, the first elution was repeated.

- ✓ Content of savillex 2 was dried. Afterwards 0.15 mL of 6 N HCl was added and the mix was heated for 10 min at 100°C.
- ✓ Once the mix was at room temperature, 1 mL of MQ water was added.
- ✓ The sample was loaded into the column and it was collected in savillex **3** together with the elution of 5 mL 1 N HCl.
- ✓ The mix of the two elutions was collected in savillex **4** and then dried. Once the sample was dried, 60 µL of distilled 12 N HNO_3 was added until the residue was dissolved. After that 2 mL of MQ water was added and the mix was heated at 100°C for 24 h (savillex **5**).
- ✓ The columns were washed with 5 mL of distilled 6 N HCl and 2 mL of MQ water.

Third elution: Chromium separation from residual Al, Ti, and Na.

- ✓ The sample contained in savillex **5** was loaded into the column. This elution was not collected (trash).
- ✓ After that 5 mL of 0.5 N HF was loaded and, the elution was discarded.
- ✓ 22 mL of 1 N HCl was loaded and discarded.
- ✓ Finally Cr(III) was eluted with 10 mL of 2 N HCl and collected in savillex **6**.
- ✓ The columns were washed three times with 5 mL of distilled 6 N HCl and one time with 2 mL of MQ water.

After elution, the collected samples were evaporated until dryness in order to eliminate the HCl. The concentration was adjusted to 100 ppb or 50 ppb of Cr with 0.6% $HN0_3$.

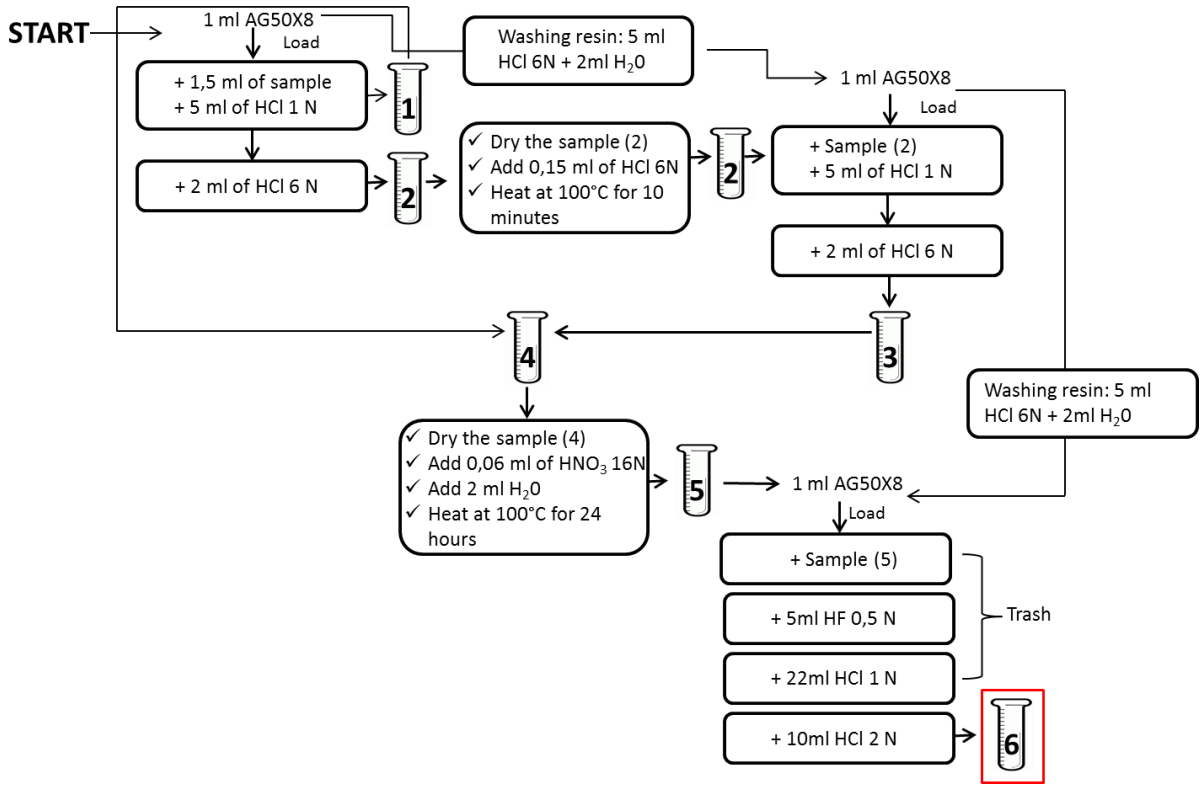

Figure 2.12 Chromium purification in a chromatography column.

2.5.4 Mass spectrometry

Chromium isotopic compositions were measured on a Multicollector ICP-MS (Neptune, and Neptune Plus Thermo Scientific) hosted at the IPGP. Purified Cr samples were dissolved in 0.5% HNO_3 with concentrations of 100 ppb or 50 ppb for solid and water samples, respectively. Dilute samples were introduced in the plasma with a PFA µFlow nebulizer (100 µL min^{-1}) coupled with an Apex IR desolvation introduction system (Elemental scientific) without additional gas or membrane desolvatation. With a jet sample cone and H skimmer cone and under high-resolution mode, the obtained sensitivity was 2.8 – 4.9 V ^{52}Cr per 100 ppb Cr. All ion beams were measured on Faraday detectors connected to 10^{11} Ω amplifiers. The isotopes ^{50}Cr, ^{52}Cr, ^{53}Cr and ^{54}Cr were simultaneously measured with ^{49}Ti, ^{51}V and ^{56}Fe to correct for isobaric interferences of ^{50}Ti, ^{50}V and ^{54}Fe, ^{54}Fe.

The base-line calibration was performed before every analytical session. The detailed parameters selected for Cr isotopes measurements as well as the configuration of both Neptune and Neptune Plus within one particular analytical session are summarized in Table 2.3.

2.5.4.1 Isotopic analyses and $\delta^{53}Cr$ value calculation

Isotopic measurements in each sample were done in 5 blocks of 15×10 s integrations. The NIST SRM-979 was measured every three samples to monitor potential drift, which was

< 0.1% within each analytical session. On-peak blanks were measured before and after every sample/standard. The analytical accuracy and precision were assessed by repeatedly processing and measuring USGS reference material BHVO-2 standard (-0.11 ± 0.02‰, 2SD, n=3), as it was done for previous Cr isotopes studies (Ellis et al., 2002; Schoenberg et al., 2008; Wille et al., 2018). The analytical results are expressed in the conventional δ notation in part per mil (‰) (equation (2.11)).

$$\delta^{53}Cr(‰) = \left[\left(\frac{^{53}Cr/^{52}Cr_{sample}}{^{53}Cr/^{52}Cr_{SRM\ 979}}\right) - 1\right] * 1000 \quad \textbf{(2.11)}$$

Table 2.3 Operating conditions and collector configuration used on the Neptune and Neptune plus.

Parameters	Values	
Skimmer and sampler cones	Ni	
Dry plasma	APEX HF (ESI)	
Heater temperature (°C)	100 to140	
Cooler temperature (°C)	-3 to 2	
Flow rate (µL min^{-1})	100	
Inlet system		
Cool gas (L min^{-1})	16.0	
Auxiliary gas (L min^{-1})	1.2	
Sample gas (L min^{-1})	1.0	
Torch position		
X (mm)	0.1	
Y (mm)	-3.8	
Z (mm)	-0.5	
RF coil power (W)	1200	
Zoom optics		
Focus quad (V)	-17.6	
Dispersion (V)	0.5	
Source lenses		
Extraction (V)	-2000	
Focus (V)	-615.5	
X-deflection (V)	5.44	
Y-deflection (V)	-2.26	
Shape (V)	198	
Rot quad (V)	2.7	
Source offset	3.0	
Mass resolution	High resolution	
Cup configuration		
Cup name	**Isotope**	**Distance (mm)**
L4-F	49Ti	82.545
L3-F	50Cr	72.400
L2-F		21.790
L1-F	52Cr	21.300
C-F	52.937	
H1-F	54Cr	20.400
H2-F	55Mn	43.300
H3-F	57Fe	94.300
H4-F		55.159

2.5.4.2 Polyatomic interferences in Cr isotopic measurements

A major challenge when measuring Cr isotopes with Ar based plasma is the isobaric molecular interferences resulting from the Ar gas. Table 2.4 presents all the polyatomic interferences for Cr isotopes. In particular, $^{40}Ar^{16}O$ and $^{40}Ar^{14}N$ are difficult because they

produce interferences on the masses 54 and 56 and, thus, resolving these interferences is necessary for acquiring precise and accurate ^{54}Cr data (Schiller et al., 2014). In order to minimize the contribution of the molecular argon species to the Cr mass array, a Jet sampler cone and H skimmer cone were used. Schiller et al. (2014) affirmed that this cone configuration can result in a decrease of sensitivity (~ 30%) however, the oxide and nitride production rate are reduced by a factor of 2-3, effectively improving the sample over oxide and nitride signal. Halicz et al. (2008) affirmed that polyatomic interferences, such as $^{34}S^{16}O^{+}$, $^{36}Ar^{14}N^{+}$, $^{40}Ar^{12}C+$, $^{36}Ar^{16}O^{+}$, $^{37}Cl^{16}O^{+}$, $^{40}Ar^{13}C^{+}$, $^{35}Cl^{18}O^{+}$, $^{36}Ar^{16}O^{1}H^{+}$, can be minimized by the use of medium or high resolution mass spectrometry, as it was done in the present study. The medium resolution mode of the Neptune (R ~ 3000) provides an effective means of avoiding polyatomic overlap originated from Ar, S and O containing species (Schiller et al., 2014).

Because Ar plasma has a very high ionization efficiency, another critical step in acquiring accurate Cr isotope data by MC-ICP-MS is an effective correction for the atomic isobaric interferences with ^{49}Ti, ^{51}V and ^{56}Fe which cannot be resolved. The effect of these isobars is slightly different because the presence of Ti and V interferes with the mass bias correcting isotope ^{50}Cr and affects all measured Cr isotope ratios, while the presence of Fe solely affects the ^{54}Cr data (Schiller et al., 2014). The first step to avoid isobaric interferences from ^{5O}Ti, ^{50}V and ^{56}Fe on ^{50}Cr and ^{54}Cr, and to prevent matrix effects, is a separation procedure as the one used in the present study with a cation exchange resin.

The correction of a potential vanadium contribution to the ^{50}Cr signal was conducted by calculating a ^{50}V signal based on 51V Assuming a natural $^{50}V/^{51}V$ of $2.425x10^{-3}$. The correction of any contribution of ^{54}Fe to the ^{54}Cr signal is non-trivial because the geometry of the Neptune Plus does not allow the measurement of the relatively interference-free ^{57}Fe simultaneously with all Cr isotopes and ^{49}Ti. Instead this correction must be based on ^{56}Fe. A Fe correction using ^{56}Fe is complicated by the typically large isobaric $^{40}Ar^{16}O$ interference and hence requires careful assessment. While the mass resolution of the Neptune allows in principle the full resolution of ^{56}Fe and $^{40}Ar^{16}O$, the interference is significantly larger than the ^{56}Fe signal by orders of magnitude. Thus, even small tailing contributions of $^{40}Ar^{16}O$ can lead to overcorrection and additional noise in the calculated ^{54}Fe signal (Taylor et al., 1992). Because no Fe isotope interferes with the ^{50}Cr and ^{52}Cr signals, the contribution of ^{54}Fe to the ^{54}Cr signal was calculated using a Ti and V corrected $^{50}Cr/^{52}Cr$ for mass bias correction and a natural isotope abundance fraction of 0.05845 and 0.91754 for ^{54}Fe and ^{56}Fe, respectively, as it was reported by Schiller et al. (2014).

Table 2.4 List of polyatomic interferences for Cr isotopes (May et al., 1998).

Isotope	Abundance	Interference
^{50}Cr	4.35	$^{34}S^{16}O^{+}$, $^{36}Ar^{14}N^{+}$, $^{35}Cl^{15}N^{+}$, $^{36}S^{14}N^{+}$, $^{32}S^{18}O^{+}$, $^{33}S^{17}O^{+}$
^{52}Cr	83.76	$^{35}Cl^{16}O^{1}H^{+}$, $^{40}Ar^{12}C^{+}$, $^{36}Ar^{16}O^{+}$, $^{37}Cl^{15}N^{+}$, $^{34}S^{18}O^{+}$, $^{36}S^{16}O^{+}$, $^{38}Ar^{14}N^{+}$, $^{36}Ar^{15}N^{1}H^{+}$, $^{35}Cl^{17}O^{+}$
^{53}Cr	9.51	$^{37}Cl^{16}O^{+}$, $^{38}Ar^{15}N^{+}$, $^{38}Ar^{14}N^{1}H^{+}$, $^{36}Ar^{17}O^{+}$, $^{36}Ar^{16}O^{1}H^{+}$, $^{35}Cl^{17}O^{1}H^{+}$, $^{35}Cl^{18}O^{+}$, $^{36}S^{17}O^{+}$, $^{40}Ar^{13}C^{+}$
^{54}Cr	2.38	$^{37}Cl^{16}O^{1}H^{+}$, $^{40}Ar^{14}N^{+}$, $^{38}Ar^{15}N^{1}H^{+}$, $^{36}Ar^{18}O^{+}$, $^{38}Ar^{16}O^{+}$, $^{36}Ar^{17}O^{1}H^{+}$, $^{37}Cl^{17}O^{+}$, $^{19}F_{2}{}^{16}O^{+}$

2.6 THERMODYNAMIC MODELING AND STATISTICAL ANALYSIS

The chemical equilibrium code Visual MINTEQ v3.0 was used to calculate the saturation index and to identify possible phases controlling solubility. The total elemental concentration, as well as Cr(VI) and Fe(II) measured from the different bio-leaching and chemical leaching, were input into the model.

Linear regression analyses were carried out with the software SigmaPlot version 12.0 from Systat Software, INC., San Jose California USA, which yielded regression slopes, coefficients of determination (R^2), P values, and standard errors of the regression (S.E.).

2.7 BIBLIOGRAPHY

Allegretti, P., Furlong, J., Donati, E., 2006. The role of higher polythionates in the reduction of chromium(VI) by Acidithiobacillus and Thiobacillus cultures. J. Biotechnol. 122, 55–61. doi:10.1016/j.jbiotec.2005.08.031

Angeli, N., Rafael, G., Navarro, B., 2010. Caracterização Química de Cromitas nos Maciços de Cromínia e. Geol. série Cient. USP 10, 87–99.

Apte, A.D., Tare, V., Bose, P., 2006. Extent of oxidation of Cr(III) to Cr(VI) under various conditions pertaining to natural environment. J. Hazard. Mater. 128, 164–174. doi:10.1016/j.jhazmat.2005.07.057

Bartlett, R., James, B., 1996. Chromium, in: Sparks DL, E. (Ed.), Methods of Soil Analysis, Part 3, Chemical Methods. Madison, WI, USA, pp. 683–701.

Beukes, J.P., du Preez, S.P., van Zyl, P.G., Paktunc, D., Fabritius, T., Päätalo, M., Cramer, M., 2017. Review of Cr(VI) environmental practices in the chromite mining and smelting industry – Relevance to development of the Ring of Fire, Canada. J. Clean. Prod. 165, 874–889. doi:10.1016/j.jclepro.2017.07.176

Colin, F., Nahon, D., Trescases, J.J., Melfi, A.J., 1990. Lateritic Weathering of Pyroxenites at Niquelandia, Goias, Brazil: The Supergene Behaviour of Nickel. Econ. Geol. 85, 1010–

1023.

Collins, R.N., Tran, N.D., Bakkaus, E., Avoscan, L., Gouget, B., 2006. Assessment of isotope exchange methodology to determine the sorption coefficient and isotopically exchangeable concentration of selenium in soils and sediments. Environ. Sci. Technol. 40, 7778–7783.

Collins, R.N., Waite, T.D., 2009. Isotopically exchangeable concentrations of elements having multiple oxidation states: The case of Fe(II)/Fe(III) isotope self-exchange in coastal lowland acid sulfate soils. Environ. Sci. Technol. 43, 5365–5370.

Dhal, B., Pandey, B.D., 2013. International Journal of Mineral Processing Process optimization for bio-beneficiation of a chromite concentrate by a Cr (VI) reducing native microbe (Bacillus sp.). Int. J. Miner. Process. 123, 129–136. doi:10.1016/j.minpro.2013.05.011

Dhal, B., Thatoi, H.N., Das, N.N., Pandey, B.D., 2013. Chemical and microbial remediation of hexavalent chromium from contaminated soil and mining/metallurgical solid waste: A review. J. Hazard. Mater. 250–251, 272–291. doi:10.1016/j.jhazmat.2013.01.048

Dwari, R.K., Angadi, S.I., Tripathy, S.K., 2018. Studies on flocculation characteristics of chromite's ore process tailing: Effect of flocculants ionicity and molecular mass. Colloids Surfaces A Physicochem. Eng. Asp. 537, 467–477. doi:10.1016/j.colsurfa.2017.10.069

Economou-Eliopoulos, M., Frei, R., Megremi, I., 2016. Potential leaching of Cr (VI) from laterite mines and residues of metallurgical products (red mud and slag): An integrated approach. J. Geochemical Explor. 162, 40–49. doi:10.1016/j.gexplo.2015.12.007

Ellis, A.S., Johnson, T.M., Bullen, T.D., 2002. Chromium Isotopes and the Fate of Hexavalent Chromium in the Environment. Science. 295, 2060–2062. doi:10.1126/science.1068368

Ettler, V., Kvapil, J., Šebek, O., Johan, Z., Mihaljevič, M., Ratié, G., Garnier, J., Quantin, C., 2015. Leaching behaviour of slag and fly ash from laterite nickel ore smelting (Niquelândia, Brazil). Appl. Geochemistry 64, 118–127. doi:10.1016/j.apgeochem.2015.09.019

Fendorf, S.E., 1995. Surface reactions of chromium in soils and waters. Geoderma 67, 55–71. doi:10.1016/0016-7061(94)00062-F

Frei, R., Rosing, M.T., 2005. Search for traces of the late heavy bombardment on Earth—Results from high precision chromium isotopes. Earth Planet. Sci. Lett. 236, 28–40. doi:10.1016/j.epsl.2005.05.024

Gäbler, H.E., Bahr, A., Heidkamp, A., Utermann, J., 2007. Enriched stable isotopes for determining the isotopically exchangeable element content in soils. Eur. J. Soil Sci. 58, 746–757. doi:10.1111/j.1365-2389.2006.00863.x

Garnier, J., Quantin, C., Echevarria, G., Becquer, T., 2009a. Assessing chromate availability

in tropical ultramafic soils using isotopic exchange kinetics. J. Soils Sediments 9, 468–475. doi:10.1007/s11368-009-0062-4

Garnier, J., Quantin, C., Guimarães, E., Garg, V.K., Martins, E.S., Becquer, T., 2009b. Understanding the genesis of ultramafic soils and catena dynamics in Niquelândia, Brazil. Geoderma 151, 204–214. doi:10.1016/j.geoderma.2009.04.020

Garnier, J., Quantin, C., Martins, E.S., Becquer, T., 2006. Solid speciation and availability of chromium in ultramafic soils from Niquelândia, Brazil. J. Geochemical Explor. 88, 206–209. doi:10.1016/j.gexplo.2005.08.040

Garuti, G., Zaccarini, F., Proenza, J.A., Thalhammer, O.A.R., Angeli, N., 2012. Platinum-Group Minerals in Chromitites of the Niquelândia Layered Intrusion (Central Goias, Brazil): Their Magmatic Origin and Low-Temperature Reworking during Serpentinization and Lateritic Weathering. Minerals 2, 365–384. doi:10.3390/min2040365

Halicz, L., Yang, L., Teplyakov, N., Burg, A., Sturgeon, R., Kolodny, Y., 2008. High precision determination of chromium isotope ratios in geological samples by MC-ICP-MS. J. Anal. At. Spectrom. 23, 1622. doi:10.1039/b808351g

Hamon, R.E., Parker, D.R., Lombi, E., Donald, L.S., 2008. Chapter 6 Advances in Isotopic Dilution Techniques in Trace Element Research: A Review of Methodologies, Benefits, and Limitations. Adv. Agron. Volume 99, 289–343. doi:10.1016/s0065-2113(08)00406-9

Jin, Z., Liu, T., Yang, Y., Jackson, D., 2014. Leaching of cadmium, chromium, copper, lead, and zinc from two slag dumps with different environmental exposure periods under dynamic acidic condition. Ecotoxicol. Environ. Saf. 104, 43–50. doi:10.1016/j.ecoenv.2014.02.003

Johnson, C.M., Skulan, J.L., Beard, B.L., Sun, H., Nealson, K.H., Braterman, P.S., 2002. Isotopic fractionation between Fe(III) and Fe(II) in aqueous solutions. Earth Planet. Sci. Lett. 195, 141–153. doi:10.1016/S0012-821X(01)00581-7

Johnson, T.M., Bullen, T.D., 2004. Mass-Dependent Fractionation of Selenium and Chromium Isotopes in Low-Temperature Environments. Rev. Mineral. Geochemistry 55, 289–317. doi:10.2138/gsrmg.55.1.289

Kumar, A., Maiti, S.K., 2013. Availability of Chromium , Nickel and Other Associated Heavy Metals of Ultramafic and Serpentine Soil / Rock and in Plants. Int. J. Emerg. Technol. Adv. Eng. 3, 256–268.

Kumar, C.R., Tripathy, S., Rao, D.S., 2009. Characterisation and Pre-concentration of Chromite Values from Plant Tailings Using Floatex Density Separator. J. Miner. Mater. Charact. Eng. Raghu Kumar Sunil Tripathy 88, 367–378.

Kumar, N., Nagendran, R., 2009. Fractionation behavior of heavy metals in soil during bioleaching with Acidithiobacillus thiooxidans. J. Hazard. Mater. 169, 1119–1126. doi:10.1016/j.jhazmat.2009.04.069

Larsen, K.K., Wielandt, D., Schiller, M., Bizzarro, M., 2016. Chromatographic speciation of Cr(III)-species, inter-species equilibrium isotope fractionation and improved chemical purification strategies for high-precision isotope analysis. J. Chromatogr. A 1443, 162–174. doi:10.1016/j.chroma.2016.03.040

Liu, S., Chen, L., Gao, Y., 2013. Hexavalent Chromium Leaching Influenced Factors in the Weathering Chrome Slag. Procedia Environ. Sci. 18, 783–787. doi:http://dx.doi.org/10.1016/j.proenv.2013.04.105

Lombi, E., Hamon, R.E., Mcgrath, S.P., Mclaughlin, M.J., 2003. Lability of Cd, Cu, and Zn in Polluted Soils Treated with Lime, Beringite, and Red Mud and Identification of a Non-Labile Colloidal Fraction of Metals Using Isotopic Techniques. Environ. Sci. Technol. 37, 979–984.

Lynne, A.M., Haarmann, D., Louden, B.C., 2011. Use of Blue Agar CAS Assay for Siderophore Detection. J. Microbiol. Biol. Educ. 12, 51–53. doi:10.1128/jmbe.v12i1.249

Marrero, J., Coto, O., Schippers, A., 2017. Anaerobic and aerobic reductive dissolutions of iron-rich nickel laterite overburden by Acidithiobacillus. Hydrometallurgy 168, 49–55. doi:10.1016/j.hydromet.2016.08.012

Marzouk, E.R., Chenery, S.R., Young, S.D., 2013. Measuring reactive metal in soil : a comparison of multi-element isotopic dilution and chemical extraction. Eur. J. Soil Sci. 64, 526–536. doi:10.1111/ejss.12043

May, T.W., Wiedmeyer, R.H., Chaudhary-webb, M., Paschal, D.C., Elliott, W.C., Hopkins, H.P., Ghazi, a M., Ting, B.C., Romieu, I., Vicente, O., Pelfort, E., Martinez, L., Olsina, R., Marchevsky, E., Chen, H.P., Miller, D.T., Morrow, J.C., 1998. A table of polyatimic interferences in ICP-MS. At. Spectrosc. 19, 150–155.

Moraes, R., Fuck, R.A., 2000. Ultra-high-temperature metamorphism in Central Brazil: The Barro Alto complex. J. Metamorph. Geol. 18, 345–358. doi:10.1046/j.1525-1314.2000.00262.x

Murthy, Y.R., Tripathy, S.K., Kumar, C.R., 2011. Chrome ore beneficiation challenges & opportunities - A review. Miner. Eng. 24, 375–380. doi:10.1016/j.mineng.2010.12.001

Oze, C.J., Laforce, M.J., Wentworth, C.M., Hanson, R.T., Bird, D.K., Coleman, R.G., Bird, K., Coleman, R.G., 2003. Chromium geochemistry of serpentinous sediment in the Willow core , Santa Clara County , CA.

Paulukat, C., Døssing, L.N., Mondal, S.K., Voegelin, A.R., Frei, R., 2015. Oxidative release of chromium from Archean ultramafic rocks, its transport and environmental impact – A Cr isotope perspective on the Sukinda valley ore district (Orissa, India). Appl. Geochemistry 59, 125–138. doi:10.1016/j.apgeochem.2015.04.016

Payne, S.M., 1994. Detection, isolation, and characterization of siderophores. Methods Enzymol. 235, 329–344. doi:10.1016/0076-6879(94)35151-1

Piuzana, D., Pimentel, M.M., Fuck, R.A., Armstrong, R., 2003. SHRIMP U-Pb and Sm-Nd data for the Araxá Group and associated magmatic rocks: Constraints for the age of sedimentation and geodynamic context of the southern Brasília Belt, central Brazil. Precambrian Res. 125, 139–160. doi:10.1016/S0301-9268(03)00107-4

Raous, S., Becquer, T., Garnier, J., Martins, É.D.S., Echevarria, G., Sterckeman, T., 2010. Mobility of metals in nickel mine spoil materials. Appl. Geochemistry 25, 1746–1755. doi:10.1016/j.apgeochem.2010.09.001

Raous, S., Echevarria, G., Sterckeman, T., Hanna, K., Thomas, F., Martins, E.S., Becquer, T., 2013. Potentially toxic metals in ultramafic mining materials: Identification of the main bearing and reactive phases. Geoderma 192, 111–119. doi:10.1016/j.geoderma.2012.08.017

Ratié, G., Jouvin, D., Garnier, J., Rouxel, O., Miska, S., Guimarães, E., Vieira, L.C., Sivry, Y., Zelano, I., Pelletier, E.M., Thil, F., Quantin, C., 2015. Nickel isotope fractionation during tropical weathering of ultramafic rocks. Chem. Geol. 402, 68–76. doi:10.1016/j.chemgeo.2015.02.039

Rodríguez-González, P., Marchante-Gayón, J.M., García Alonso, J.I., Sanz-Medel, A., 2005. Isotope dilution analysis for elemental speciation: A tutorial review. Spectrochim. Acta - Part B At. Spectrosc. 60, 151–207. doi:10.1016/j.sab.2005.01.005

Rodríguez-Vico, F., Martínez-Cayuela, M., García-Peregrín, E., Ramírez, H., 1989. A procedure for eliminating interferences in the lowry method of protein determination. Anal. Biochem. 183, 275–278. doi:10.1016/0003-2697(89)90479-X

Sayyed, R.Z., Badgujar, M.D., Sonawane, H.M., Mhaske, M.M., Chincholkar, S.B., 2005. Production of microbial iron chelators (siderophores) by fluorescent Pseudomonads. Indian J. Biotechnol. 4, 484–490.

Schiller, M., Van Kooten, E., Holst, J.C., Olsen, M.B., Bizzarro, M., 2014. Precise measurement of chromium isotopes by MC-ICPMS. J. Anal. At. Spectrom. 29, 1406–1416. doi:10.1039/C4JA00018H

Schoenberg, R., Zink, S., Staubwasser, M., von Blanckenburg, F., 2008. The stable Cr isotope inventory of solid Earth reservoirs determined by double spike MC-ICP-MS. Chem. Geol. 249, 294–306. doi:10.1016/j.chemgeo.2008.01.009

Schwyn, B., Neilands, J.B., 1987. Universal chemical assay for the detection and determination of siderophore. Anal. Biochem. 160, 47–56.

Sivry, Y., Riotte, J., Munoz, M., Redon, P., Denaix, L., Dupr, B., Laboratoire, M., 2011. Multielementary (Cd , Cu , Pb , Zn , Ni) Stable Isotopic Exchange Kinetic (SIEK) Method To Characterize Polymetallic Contaminations. Environ. Sci. Technol. 45, 6247–6253.

Sullivan, P., Wiederin, D., 2018. Low-Pressure Chromium Speciation in Drinking Water using the SC-DX chromFAST System with ICPMS Detection [WWW Document]. Elem. Sci.

URL http://www.icpms.de/pdf/TN06-Chromium-Speciation-chromFAST-System.pdf

Świetlik, R., 1998. Speciation analysis of chromium in waters. Polish J. Environ. Stud. 7, 257–266.

Taylor, P.D.P., Maeck, R., De Bièvre, P., 1992. Determination of the absolute isotopic composition and Atomic Weight of a reference sample of natural iron. Int. J. Mass Spectrom. Ion Process. 121, 111–125. doi:10.1016/0168-1176(92)80075-C

Tharaud, M., Gardoll, S., Khelifi, O., Benedetti, M.F., Sivry, Y., 2015. UFREASI: User-FRiendly Elemental dAta procesSIng. A free and easy-to-use tool for elemental data treatment. Microchem. J. 121, 32–40. doi:10.1016/j.microc.2015.01.011

Thatoi, H., Das, S., Mishra, J., Rath, B.P., Das, N., 2014. Bacterial chromate reductase, a potential enzyme for bioremediation of hexavalent chromium: a review. J. Environ. Manage. 146, 383–99. doi:10.1016/j.jenvman.2014.07.014

Tina, S., Echevarria, G., Becquer, T., Ghanbaja, J., Leclerc-cessac, E., Morel, J., 2006. Control of nickel availability by nickel bearing minerals in natural and anthropogenic soils. Geoderma 136, 28–37. doi:10.1016/j.geoderma.2006.01.008

Tiwary, R.K., Dhakate, R., Ananda Rao, V., Singh, V.S., 2005. Assessment and prediction of contaminant migration in ground water from chromite waste dump. Environ. Geol. 48, 420–429. doi:10.1007/s00254-005-1233-2

Trinquier, A., Birck, J.-L., Allègre, C.J., 2008. High-precision analysis of chromium isotopes in terrestrial and meteorite samples by thermal ionization mass spectrometry. J. Anal. At. Spectrom. 23, 1565. doi:10.1039/b809755k

Tripathy, S.K., Murthy, Y.R., Singh, V., 2013. Characterisation and separation studies of Indian chromite beneficiation plant tailing. Int. J. Miner. Process. 122, 47–53. doi:10.1016/j.minpro.2013.04.008

Tripathy, S.K., Singh, V., Ramamurthy, Y., 2012. Improvement in Cr:Fe Ratio of Indian Chromite Ore for Ferro Chrome Production. Int. J. Min. Miner. Process. 1, 101–106. doi:10.5923/j.mining.20120103.01

Viollier, E., Inglett, P.W., Hunter, K., Roychoudhury, a. N., Van Cappellen, P., 2000. The ferrozine method revisited: Fe(II)/Fe(III) determination in natural waters. Appl. Geochemistry 15, 785–790. doi:10.1016/S0883-2927(99)00097-9

Wang, X., Johnson, T.M., Ellis, A.S., 2015a. Equilibrium isotopic fractionation and isotopic exchange kinetics between Cr(III) and Cr(VI). Geochim. Cosmochim. Acta 153, 72–90. doi:10.1016/j.gca.2015.01.003

Wang, X., Johnson, T.M., Ellis, A.S., 2015b. Equilibrium isotopic fractionation and isotopic exchange kinetics between Cr(III) and Cr(VI). Geochim. Cosmochim. Acta 153, 72–90. doi:10.1016/j.gca.2015.01.003

Wang, Y.S., Pan, Z.Y., Lang, J.M., Xu, J.M., Zheng, Y.G., 2007. Bioleaching of chromium

from tannery sludge by indigenous Acidithiobacillus thiooxidans. J. Hazard. Mater. 147, 319–324. doi:10.1016/j.jhazmat.2007.01.005

Waterborg, J.H., Matthews, H.R., 1984. The lowry method for protein quantitation. Methods Mol. Biol. 1, 1–3. doi:10.1385/1-59259-169-8:7

Wille, M., Babechuk, M.G., Kleinhanns, I.C., Stegmaier, J., Suhr, N., Widdowson, M., Kamber, B.S., Schoenberg, R., 2018. Silicon and chromium stable isotopic systematics during basalt weathering and lateritisation: A comparison of variably weathered basalt profiles in the Deccan Traps, India. Geoderma 314, 190–204. doi:10.1016/j.geoderma.2017.10.051

Zelano, I., Sivry, Y., Quantin, C., Gélabert, a., Tharaud, M., Jouvin, D., Montarges-Pelletier, E., Garnier, J., Pichon, R., Nowak, S., Miska, S., Abollino, O., Benedetti, M.F., 2013. Colloids and suspended particulate matters influence on Ni availability in surface waters of impacted ultramafic systems in Brazil. Colloids Surfaces A Physicochem. Eng. Asp. 435, 36–47. doi:10.1016/j.colsurfa.2013.02.051

Zink, S., Schoenberg, R., Staubwasser, M., 2010. Isotopic fractionation and reaction kinetics between Cr(III) and Cr(VI) in aqueous media. Geochim. Cosmochim. Acta 74, 5729–5745. doi:10.1016/j.gca.2010.07.015

CHAPTER 3

Assessing chromium mobility in natural surface waters: colloidal contribution to the isotopically exchangeable pool of chromium (E^{w}_{Cr} value)

This chapter has been published:

Bolaños-Benítez, V., van Hullebusch, E.D., Garnier, J., Quantin, C., Tharaud, M., Lens, P.N.L., Sivry, Y., 2018. Assessing chromium mobility in natural surface waters: Colloidal contribution to the isotopically exchangeable pool of chromium (E^{w}_{Cr}value). Appl. Geochemistry 92, 19–29. doi:10.1016/j.apgeochem.2018.02.007

CHAPTER 3

3.1 INTRODUCTION

One of the most invasive anthropogenic activities is represented by the mining and metallurgical industries, which are known to produce a large quantity of waste including tailings, slags, ashes and liquid discharges (Ji et al., 2016; Mishra and Sahu, 2013; Zhang et al., 2014). The mines are located in areas that are naturally enriched in heavy metals, such as Cr and Ni in ultramafic systems. Ultramafic rocks have a Cr concentration close to 2400 mg kg^{-1}, which is higher than the ones encountered in other types of rocks (upper crust = 30 mg kg^{-1}, (Taylor and McClennan, 1985)). These areas can represent an important source of Cr release into natural water bodies, with up to 30 µg L^{-1} and 339 mg kg^{-1} in the dissolved and particulate fractions, respectively, whereas world rivers average 0.7 µg L^{-1} and 130 mg kg^{-1}, respectively (Mcclain and Maher, 2016; Viers et al., 2008).

In ultramafic rocks and regolith, chromium-bearing minerals are mainly spinel and silicates in which Cr is mostly present as Cr(III), the less toxic Cr species. Chromite is the most abundant Cr-bearing mineral and is resistant to low-grade metamorphic processes related to serpentinization. Additionally, Fe-oxides and silicates are also Cr-containing minerals, where Cr(III) is substituted for Al and Fe(III).

During ultramafic rock weathering, the availability of elements such as Fe, Mn, Al, Ni and Cr increases and may be later released and transported in rivers and groundwater (Gaillardet et al., 2014; Mcclain and Maher, 2016). In addition, tropical soils developed on ultramafic rocks are known to be particularly rich in metals such as Cr, Co and Ni and, in some cases, a large amount is biologically available and therefore potentially toxic (Garnier et al., 2009). Mcclain and Maher (2016) found that riverine Cr concentrations and speciation in ultramafic catchments are governed by the balance between ultramafic rock weathering and elemental cycling along water flow paths in the Putah Creek watershed (California Coast Ranges, USA). In addition, dissolved Cr is exported not only as soluble hexavalent Cr(VI) species (CrO_4^{2-}, $MgCrO_4$), but also as trivalent Cr species ($Cr(OH)_3$, $CrOH(CO_3)_2^{2-}$).

Trace elements released during weathering (Fe, Mn, Al, Ni and Cr) can be present either in the particulate or dissolved fraction. The latter has been operationally defined by a filtration cut-off (0.45 or 0.2 µm). However, the denominated “dissolved” fraction is composed of free

metals, as well as complexed ions, metals bound to a variety of ligands, forming molecules with various dimensions and chemical characteristics, which may be further bound to larger colloidal-sized entities, both organic and inorganic (Dominik and Gue, 2003; Ren et al., 2010). Consequently, colloids can be defined as a third phase, which include particles with an intermediary size (from 1 kDa to 0.2 µm). In surface waters, colloids can be organic and/or inorganic. Inorganic colloids include Mn, Fe, Al and Si (oxy)hydroxides, as well as carbonates and clays, with sizes ranging from a few nanometers to micrometers (Schäfer et al., 2000). Hydrolyzed Cr(III) ions are predominantly bound to organic matter or adsorbed on colloidal particles due to low solubility. In contrast, Cr(VI) is unlikely to be bound to organic matter or adsorbed on colloidal particles because of its high solubility and high oxidizing power (Osaki, 1983). Ren et al. (2010) found that the total Cr is strongly bound to very low-molecular weight organic ligands (1-100 kDa) such as extracellular ligands, whereas there is no complexation of Cr by large-size colloids (100 kDa–0.2 µm) such as fulvic and/or humic acids, cell fragments or bacteria.

Given the importance of colloids associated with metal transport, availability and toxicity in natural ecosystems (Gallego-urrea et al., 2013), different methods such as ultrafiltration (Dupre et al., 2008) have been used to assess their role in aquatic environments. Ren et al. (2010) assessed the distribution of metal partitioning among particulate, colloidal and truly dissolved fractions in the polluted Yongdingxin River (Tianjin, China). They classified the metals into three groups: (1) organic colloidal pool-borne elements (Cu, Cr), (2) inorganic colloidal pool-borne metals (Fe, Mn) and (3) metals with varying complexation patterns (Zn, Hg). A similar study was carried out by Dominik and Gue (2003), who found that the highly saline residual waters of coal mine discharges in the Vistula River decrease the colloid concentration due to colloidal coagulation. As a result, the metal concentration (Co, Cu, Cr, Mn and Zn) in the colloidal fraction was lower than in the particulate one.

The isotopic dilution technique has been widely developed to determine the exchangeable pool of metals (E_{metal} value) in soils. This method consists of adding a known amount of an isotopically modified element, used as a tracer, to a soil suspension (Hamon et al., 2008). The potential impact of soil colloids on the determination of the E_{metal} value was assessed by Marzouk et al. (2013) through the use of cation exchange resin Chelex-100. The results showed that the E_{metal} value could be overestimated due to the presence of colloids. Similarly, Lombi et al. (2003) identified the non-labile colloidal fraction of metals using isotopic techniques. Up to now, studies of the impact of colloids on the techniques used to establish the reactive pool of metals have focused on soils and only one study has discussed

suspended particulate matter (SPM) and colloids in aquatic environments (Zelano et al., 2013), despite the important role of water in the long-distance transport of contaminants.

Therefore, this study focuses on three main aspects: i) assessing the impact of the cut-off used for the isotopic dilution technique to determine the chromium E value in water SPM from pristine and contaminated areas, ii) determining the distribution of the chromium E value in the dissolved, particulate and colloidal fractions, and iii) proposing a calculation method to assess the contribution of the non-exchangeable colloidal Cr fraction to the chromium E value.

3.2 MATERIAL AND METHODS

3.2.1 Water samples collection

Five sampling points including two small streams and three sediment ponds were chosen in the Barro Alto mining area (Goiás state, Brazil) (Figure 3.1) in order to have a wide range of variability in terms of the Cr and colloid content and composition. Stream #1 is located in the ultramafic system, but outside of the mining activity catchment; therefore, it was used as a reference and is labeled as the “pristine area” in this paper. Stream #2 passes through the mining area and collects water runoff that then flows into the sediment ponds.

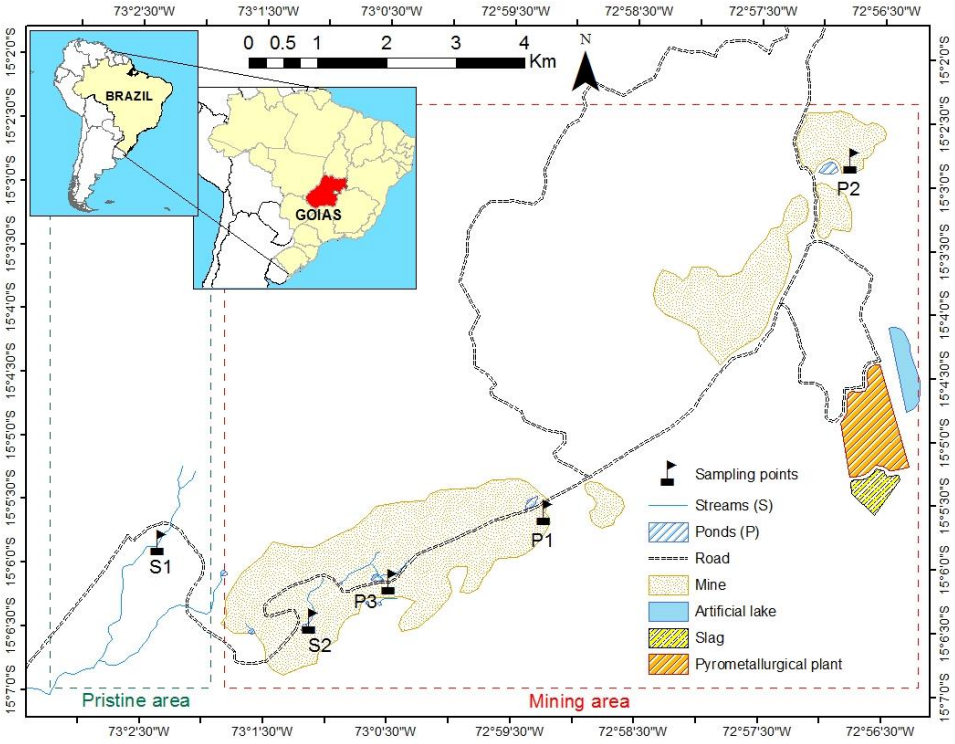

Figure 3.1 Map of the study area, location of the Barro Alto mine infrastructures and sampling points.

Finally, three ponds that collect sediment eroded from disturbed areas by mining operations were sampled. Sediment removal by ponds helps to meet regulatory effluent discharge limitations and to maintain the hydrological balance (Figure 3.1).

Temperature, pH and electrical conductivity were measured *in situ* using a WTW 3410 Set 2 multiparameter probe. Surface water was collected in each sampling point, stored in pre-cleaned, acid-washed polyethylene bottles and divided into four aliquots: one to determine the impact of the filtration cut-off on the E^{w}_{Cr} value calculation, a second one to determine the real E^{w}_{Cr} value according to the particle size range, a third one to measure the total Cr content and natural isotopic $^{53}Cr/^{52}Cr$ ratio in the bulk water, and the last one was filtered at 0.2 µm to determine the TOC and alkalinity levels.

3.2.2 Chemical analyses

Aliquots of each bulk water sample were evaporated on a hot plate to dryness and acid-digested with a mixture of distillated HF-HNO_3-HCl. The concentration of the major elements in both filtered water (pre-washed 0.2 µm filters) and the digested bulk water was determined using ICP-AES (ICAP 6200 Thermo Fisher), whereas HR-ICP-MS (Thermo Scientific Element II) was used for the trace elements analysis. The detection limits were typically between 0.6 and 74 ng L^{-1} and the standard deviation (1σ) associated with the measurements was smaller than 5%.

The concentration of the anions was determined by ion chromatography (ICS 1100 Thermo Fisher) with an Ionpac Thermo AS14 column and an Ionpac Thermo AG14 pre-column. The mobile phase was comprised of a mixture of 3.5 mmol Na_2CO_3 and 1 mmol $NaHCO_3$. The injection volume was 20 µL and the flow rate was 1.2 mL min^{-1}. The alkalinity was determined by titrating 100 mL of the water sample with H_2SO_4 to pH 4.5 and expressed as mg HCO_3^- per L.

The SPM concentration was determined after the filtration of the samples through 0.7 µm GF/F filters pre-combusted at 500°C for 2 h, pre-washed with Milli-Q (MQ) water, then dried and pre-weighed. The particulate organic carbon (POC) content was directly assessed from the GF/F filters. One eighth of each filter was weighed (± 0.001 mg DW) and analyzed in a ThermoScientific Flash 2000 organic elemental analyzer, after overnight (12 h) acidification under concentrated HCl (37%) acid vapor prior to the determination of the organic carbon. The internal reproducibility was 5%. The dissolved organic carbon (DOC) concentrations were measured in 0.2 µm filtrates using a Shimadzu total organic carbon TOC-VCSH analyzer. The detection limit was 0.24 mg C L^{-1} and the internal reproducibility was 2%.

The mineralogical composition of the SPM collected on the GF/F filters was determined using X-ray diffraction (XRD) analysis on a PANalytical diffractometer and using the Cu K_α radiation (at 45 kV–40 mA) in the grazing incidence angle in the 5°–70° 2θ range with a scan step of 0.013°. In addition, the surfaces of the filters were thin-coated with carbon and the filter observations were done with a Zeiss Auriga scanning electron microscope (SEM) equipped with a field emission electron gun (FEG) at 15 keV with a SE-Inlens detector.

3.2.3 Isotopic exchange technique

3.2.3.1 General considerations

Isotopic dilution techniques have been recognized as a useful tool to investigate a variety of processes related to the bioavailability and mobility of trace elements and contaminants, while determining the concentration of isotopically exchangeable elements (E value) (Collins et al., 2006; Collins and Waite, 2009; Gäbler et al., 2007; Hamon et al., 2008; Lombi et al., 2003; Marzouk et al., 2013; Rodríguez-González et al., 2005; Sivry et al., 2011). The spiking solution used for the present study was obtained by the dissolution of metal Cr (Euriso-top®, atomic abundance: 98.31%, 1.55%, 0.08% and 0.05% of ^{53}Cr, ^{52}Cr, ^{54}Cr and ^{50}Cr, respectively) in 6N HCl, then dilution with MQ water to obtain a 357 mg/L stock solution of $^{53}Cr(III)$ in 1.57 N HCl.

For elements with more than one oxidation state, the importance of evaluating speciation in the E value calculation has been highlighted. Johnson et al. (2002) and Collins and Waite (2009) demonstrated that the isotopic exchange between Fe(II) and Fe(III) hydroxide species occurred within only a few minutes, so that Fe speciation does not need to be considered when determining the E_{Fe} value. In contrast, Collins et al. (2006) found that SeO_3^{2-} and SeO_4^{2-} were not isotopically self-exchangeable during 24 h of isotope exchange, concluding that Se speciation must be considered in the determination of the E_{Se} value. The impact of Cr speciation on the determination of the E_{Cr} value has not yet been studied.

The redox kinetics of the Cr(III) and Cr(VI) species in aquatic media have been investigated by Wang et al. (2015) and Zink et al. (2010). These authors found that there is no significant isotopic exchange between Cr(VI) and Cr(III) species over a timescale of days to weeks in natural systems, while isotopic exchange inside the Cr(VI) pool is much faster (from 1 minute to 24 hours) (Garnier et al., 2009). This may be explained by the preferential formation of Cr(III) complexes as octahedrally coordinated hydroxide, whereas Cr(VI) form tetrahedrally coordinated ions with very strong Cr-O bonds. This marked difference in the binding environment of Cr species with different oxidation states, but especially the very strong oxygen bonds in dissolved Cr(VI) complexes, are evidently responsible for the lack of both

chromium and oxygen isotopic exchanges, of chromate and dichromate, with the prevailing surrounding environment. In addition, the isotopic exchange between Cr(VI) and Cr(III) requires three electron transfers, with the result that the rate of isotopic exchange is much lower (Apte et al., 2006; Wang et al., 2015b).

Based on the statements given above, it will be assumed in this study that after the addition of ^{53}Cr(III) from the spiking solution to natural water samples, it will redistribute itself within the solution and exchangeable pool similarly to the other Cr(III) isotopes (^{50}Cr(III), ^{52}Cr(III), and ^{54}Cr(III)). The information obtained will be related to the isotopically exchangeable pool of Cr(III) only. In the present study, the isotopic dilution was used to address two main issues: the impact of the cut-off on the determination of the E_{Cr} value in water (E^{W}_{Cr}) and the real E^{W}_{Cr} according to the range of particle sizes.

3.2.3.2 Spike experiment 1 (#E1): impact of size cut-off on the E^{W}_{Cr} estimation

In order to establish the impact of size cut-off on the determination of the E^{W}_{Cr} value, 500 mL of the bulk, i.e. non-filtered samples, was spiked with 10 µL of ^{53}Cr(III) spiking solution. The pH of the solution was measured before and after spiking and also before filtration in order to ensure that the pH variation was smaller than 5%. In order to ensure the equilibration of the spike with the sample, the first filtration was performed 72 hours after the spike was added (Hamon et al., 2008; Zelano et al., 2013). Cascade filtration was done through 0.7 µm (GF/F filter), 0.2 µm (cellulose acetate) with a filtration unit, and 500 kDa and 1 kDa (polyethersulfone) filters with an Amicon ultrafiltration stirred cell (Millipore).

3.2.3.3 Spike experiment 2 (#E2): E^{W}_{Cr} according to the range of particle sizes

The goal of this second experiment was to determine the E^{W}_{Cr} value for a specific range of particle sizes. For this purpose, 100 mL of each sample was independently filtrated at 0.7 µm, 0.2 µm, and 500 kDa. After equilibration for 72 h with 3 µL of ^{53}Cr(III) spiking solution, each filtrate was filtrated using 0.2 µm, 500 kDa and 1 kDa filters. This allows the calculation of the E^{W}_{Cr} value for three particle sizes: 0.2–0.7 µm, 500 kDa–0.2 µm and 1–500 kDa, respectively. Chromium associated with the colloidal fraction is typically included in the 500 kDa–0.2 µm and 1–500 kDa ranges, whereas the 0.2–0.7 µm range corresponds to the particulate fraction.

3.2.4 E^{W}_{Cr} determination

All of the filtrates from experiments #E1 and #E2, the un-spiked solutions of each sample, the standard solutions as well as the spike mother solution were analyzed using a High-Resolution ICP-MS (ThermoScientific Element II). All of the Cr isotopes were measured: ^{50}Cr, ^{52}Cr, ^{53}Cr and ^{54}Cr in medium resolution (R > 4000) in order to eliminate potential polyatomic

interferences, as well as ^{47}Ti, ^{51}V and ^{57}Fe to correct for possible isobaric interferences. The calculated $^{53}Cr/^{52}Cr$ isotopic ratio corresponds to the average of 20 runs with an analytical reproducibility better than 1% (2SD, n = 520). Samples were divided by blocks using bracketing with standard and natural un-spiked solutions in order to verify and correct, if necessary, drift in the signal and intensity.

The term E^W was introduced by Zelano et al. (2013) and is defined as the product of the concentration of suspended particulate matter (mg L^{-1}) and the isotopically exchangeable pool of metal E_{Me} (Sivry et al., 2011). On this basis, the amount of isotopically exchangeable chromium per liter of solution (E^W_{Cr}) was calculated as follows (1):

$$\boldsymbol{E^{w}_{Cr}} = Q\,.\,CSPM.\ \frac{M_{STD}}{M_s}.\frac{A_s}{A_{STD}}.\left[\frac{IR_{Spike}-IR_{Sample}}{IR_{Sample}-IR_{UN}}\right] \qquad \textbf{(3.1)}$$

where *Q* represents the amount of ^{53}Cr spike solution added (µg per kg of SPM), CSPM is the concentration of suspended particulate matter (kg of SPM per L of sample), M_{STD} and M_S represent the atomic mass of Cr in the standard and spike solutions (in g mol^{-1}), A_{STD} and A_S represent the abundance in percentage of ^{52}Cr in the standard and spike solutions, respectively; IR_{Spike}, IR_{Sample} and IR_{UN} represent the isotopic ratio $^{53}Cr/^{52}Cr$ in the spike solution, in the sample after spike addition and in the sample without spike addition, respectively. To assess the reproducibility of the method for experiments #E1 and #E2, the triplicates were analyzed for three cut-offs (0.7 µm, 0.2 µm and 500 kDa) and one particle size range (1–500 kDa), respectively. Three filtration blanks were also prepared to determine the filter and reagent contributions. The error propagation was used to calculate the uncertainty in the E^w_{Cr} values. The fractional uncertainties of the isotopic $^{53}Cr/^{52}Cr$ ratio in the spiked and un-spiked samples as well as in the spike solution were included in the error calculation. Each isotopic ratio results from the average of 20 runs of five scans each, with their associated standard deviation. The E^w_{Cr} values were calculated with their associated uncertainties as presented in Table 2.

3.3 RESULTS AND DISCUSSION

3.3.1 Water-rock interactions

Table 3.1 presents the concentrations of the dissolved (< 0.2 µm) major and trace elements, DOC and Cr concentration in the unfiltered bulk water samples, SPM content, POC, alkalinity and *in situ* sample parameters.

During water-rock interactions, serpentine mineral dissolution raises the pH to alkaline values, consistent with the values measured in the streams and ponds (between 7.4 and 8.3,

Table 3.1). In addition, the electrical conductivity ranges from 58 to 105.6 µS cm^{-1}. In Barro Alto, the water composition is the product of the interaction with the mafic-ultramafic layered intrusion composed mainly of interlayered dunite and hazburgite with rare interlayered pyroxenite for the ultramafic zone of the massif, and gabbronorite, anorthosite and banded clinopyroxene-garnet amphibolite for the mafic one (Ferreira Filho et al., 2010). The cation concentrations decrease in the order $Mg^{2+} > Ca^{2+} > Na^{+} > K^{+}$, and the Ca/Mg ratio for all of the water samples does not exceed 1, due to the low Ca concentration in ultramafic bedrocks, similar to findings for ultramafic water in the United States (Mcclain and Maher, 2016) and Greece (Kaprara et al., 2015).

Table 3.1 Major and trace cations, anions concentrations in dissolved fraction, i.e. after 0.2 µm filtration, suspended particulate matter concentration (SPM), dissolved organic carbon (DOC), particulate organic carbon (POC) content on filters, total Cr concentration of bulk unfiltered solution, conductivity, pH and alkalinity values and SPM mineralogy.

Parameter	Element	Pristine area		Mining area		
		Stream1	Stream2	Pond1	Pond2	Pond3
Dissolved metal concentrations (µg L^{-1})	Si	10506	7843	2963	6107	3530
	Fe	238	1.03	3.97	1.96	1.27
	Mn	85	6.258	1.597	0.371	1.052
	Al	0.77	0.95	1.27	1.14	1.18
	Cr	0.18	10.28	587.38	43.28	76.18
	Ni	38	77	14	10	8
Bulk concentration (µg L^{-1})	Cr	9	25	1031	459	378
SPM (mg L^{-1})		1.08	3.30	165.92	316.55	175.69
DOC (mg L^{-1})		1.78	1.66	2.03	2.31	5.48
POC (wt %)		3.65	1.60	1.18	0.64	1.13
Conductivity (µS cm^{-1})		96.2	60.0	58.0	105.6	62.6
pH		7.4	7.5	7.5	8.3	7.8
Alkalinity (mg HCO_3^- L^{-1})		30	29	15	37	15
SPM Mineralogy (XRD)		Hematite Serpentine Halite Sphalerite (traces)	Goethite Serpentine Chlorite Quartz Halite	Goethite Hematite Serpentine Quartz Chlorite or vermiculite	Goethite Serpentine Spinel Chlorite or vermiculite	Goethite Hematite Serpentine Quartz Chromite

The measured concentration of major ions in the water samples are plotted on a Piper diagram (Figure 3.2), which identifies the chemical composition of the streams and ponds as the Mg-HCO_3 type, indicating weathering (mainly silicates), ion exchange processes and water mixing. Margiotta et al. (2012) studied an ultramafic area located in the northern sector of the Pollino massif (Italy). They found Mg-HCO_3 type water produced through the interaction of meteoric waters with serpentines (ultramafic), and Ca-HCO_3 type waters produced through the interaction of meteoric waters with Ca-rich rocks (mafic).

In addition to major elements, trace metal abundances may also track the influence of water-rock interactions on the composition of the water, and provide insight into the Cr redox cycle. The Fe and Mn concentrations in stream 1 (238 and 85 µg L^{-1}, respectively), located in the

pristine area, are higher than in stream 2 and the ponds (Fe from 1.03 to 3.97 µg L^{-1} and Mn from 0.37 to 6.26 µg L^{-1}; mining area). The natural leaching of Ni was observed in the pristine area, due to the Ni concentration in solution (38 µg L^{-1}) in stream 1, however the level of Cr remains low (0.18 µg L^{-1}). In the mining area, stream 2 displays lower Fe and Mn concentrations than in the pristine area, but the Ni and Cr concentrations reached values of 77 and 10 µg L^{-1}, respectively. The Al concentrations always remained low with values between 0.77 and 1.27 µg L^{-1} for the pristine and mining areas, respectively. Typical regulatory limits in drinking water are 50 µg L^{-1} for dissolved total chromium and 10 µg L^{-1} for Cr(VI) (WHO, 2006).

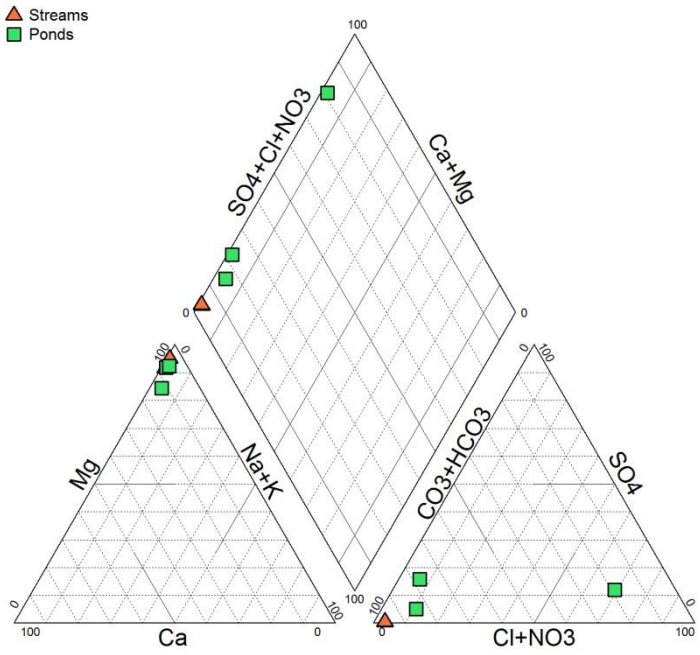

Figure 3.2 Piper diagram showing major cations and anions composition of surface water in streams and ponds in Barro Alto mine.

Streams in the mining area (stream 2) collect the runoff and flow into ponds, where eroded particles settle down and are stored. The suspended particulate matter concentration in the pristine area was 1.08 mg L^{-1} and roughly three times higher in stream 2 (3.30 mg L^{-1}). The settling effect of ponds was reflected in the SPM concentration with values of 165, 316 and 175 mg L^{-1} for ponds 1, 2 and 3, respectively. This accumulation of particles in the ponds has a direct effect on the total dissolved and bulk chromium concentrations which, in average, increased by more than 20 times compared to the pristine area. Nearly 2% of the total chromium was dissolved or colloidal in the pristine river water, while this value ranged between 57% and 9% in ponds 1 and 2 in the mining area.

On the other hand, a significant presence of total dissolved and colloidal organic carbon was found in the ponds with concentrations between 2.03 and 5.48 mg L^{-1}, while in the streams the average was 1.72 mg L^{-1}. In pond 1, 1.2% of the SPM was composed of carbon, whereas this value was 0.6% in pond 2 and 1.1% in pond 3. A similar proportion was observed in stream 2 (1.6%), while in stream 1 the value reached 3.65%. This result indicates that in both pristine and mining areas, organic matter was mainly represented by the colloidal fraction and, as expected, in the pristine area the POC was higher than in the eroded mining area. Natural organic matter (NOM) may constitute an important sink for chromium in the environment, due to the strong interaction with Cr(III), and its ability to reduce Cr(VI) to Cr(III) (Gustafsson et al., 2014). A positive correlation was observed between Cr and the DOC in the dissolved fraction (R^2 = 0.83), which could suggest that chromium was bound to low molecular weight organic ligands, as suggested by previous studies (Dominik and Gue, 2003; Ren et al., 2010).

In ultramafic areas, rock weathering, ion exchange and water mixing are the source of major elements and organic colloids in surface waters. In the impacted area, the presence of particulate matter and colloids in streams and ponds, mainly composed of inorganic compounds, is magnified due to the mining activities.

3.3.2 Chromium-bearing phases

The X-ray diffraction pattern highlights a different SPM mineralogy for streams and ponds (Table 3.1). In streams, the SPM contained Fe-(oxy)hydroxides (goethite and hematite), phyllosilicates (serpentine, chlorite and an undefined 2/1 mineral), quartz and halite. In the ponds, the X-ray patterns revealed a spinel contribution, both chromite and magnetite. Previously, Zelano et al. (2013) identified the same mineral phases in SPM from Barro Alto, i.e. chlorite (probably clinochlore), talc, serpentine and goethite. All of these minerals are known to be potential Cr-scavengers (Fendorf, 1995; Raous et al., 2013). Among the most relevant and abundant mineral phases found in the SPM from both streams and ponds were the iron (oxy)hydroxides, which are known to scavenge Cr(III) through absorption and adsorption (Richard and Bourg, 1991). Fe(III) (oxy)hydroxides provide a surface that may sequester Cr(III) coming from the weathering of Cr-bearing phases in serpentine and ultramafic rocks. In addition, Cr(III) sorbs onto surfaces of Fe(III)-containing oxides such as magnetite and hematite *via* inner-sphere complexation and form low-solubility precipitates at pH values higher than 4 (Oze et al., 2003).

Elemental analyses were performed by FEG-SEM-EDS on the 1 kDa and 500 kDa filters in order to monitor the occurrence of Cr in colloids, assuming that cascade filtration could be

used to retain colloidal particles only on the 1 kDa and 500 kDa filters, i.e. the fraction smaller than or equal to 500 kDa and 0.2 µm, respectively. The composition of these particles, in ponds and streams, included Fe, Si, Al and organic matter, the latter being predominant in the particles collected from the ponds. Figure 3.3 shows the presence of Cr-bearing colloids in streams 1 and 2, respectively, whereas no Cr was observed in the colloidal fraction from the ponds (Figure 3.3). Ji et al. (2016) classified metal-bearing colloids into three source groups: the geogenic group (barite, quartz, magnesite, Monazite and Fe oxy(hydroxides)), the anthropogenic group (magnetite, chromite) and the biogenic group (gypsum particles, cellular material, biological bone, biomass and kerogen). In accordance with this classification and the FEG-SEM-EDX performed on the filters, metal-bearing colloids in the study area belong to all the three groups, although the geogenic group is predominant, due to the enrichment on colloidal iron oxy(hydroxides) which, together with clay minerals and organic matter, are the primary controlling factor for the removal of trace metals in water.

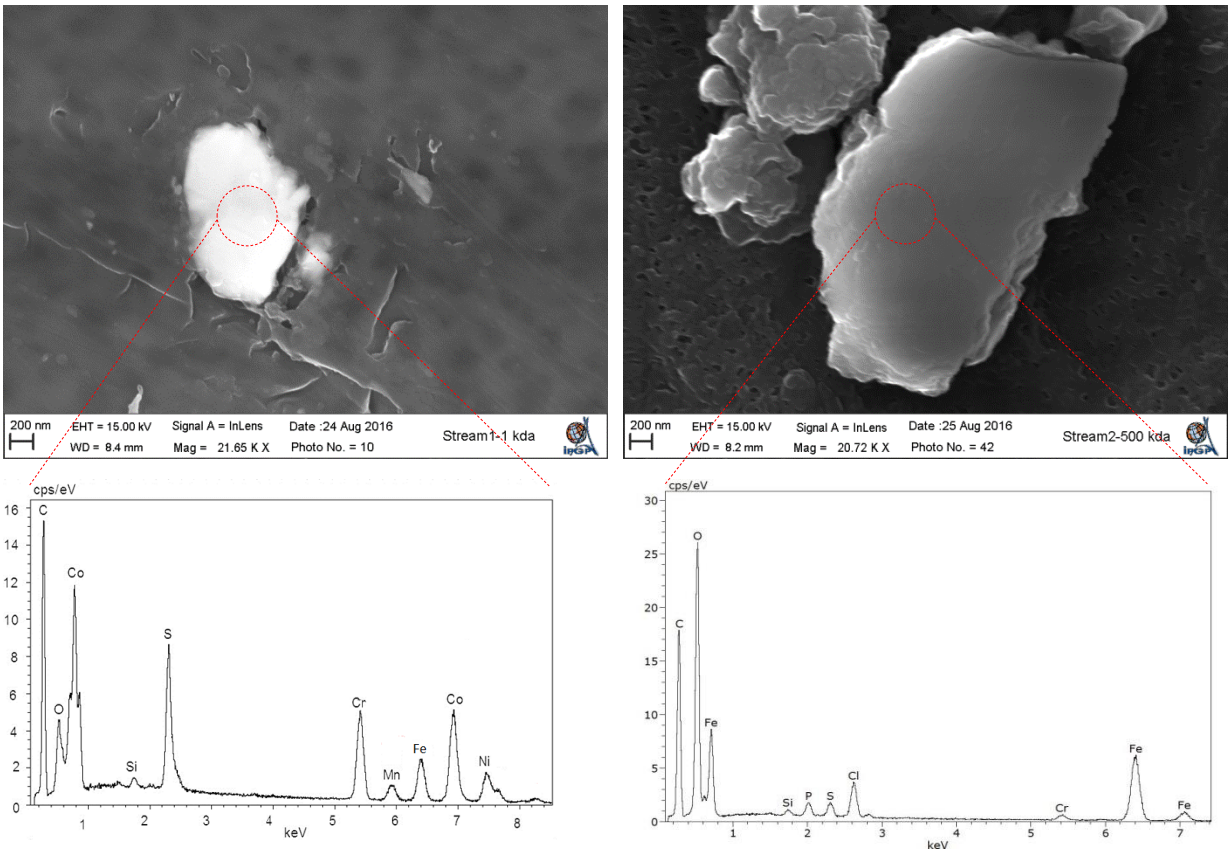

(a) (b)

Figure 3.3 Scanning electron microscope observation and its corresponding spectra of (a) 1 kDa and (b) 500 kDa filters in streams.

In streams and ponds, Cr-bearing phases are found in the SPM, where the presence of iron (oxy)hydroxides was highlighted. Colloids collected on the 1 and 500 kDa filters also contained Fe among other elements, including Si, Al, and Cr (Table 3.1). Chromium is only present in the colloids found in the streams. The abundance of Fe and its presence in particulate and colloidal form (especially in the mining area) in ultramafic areas plays an important role in Cr mobility.

3.3.3 Exchangeable pool of chromium

The isotopically exchangeable pool of chromium in the water samples (E^W_{Cr} value) was calculated for each sampling point, for different size cut-offs (0.7 µm, 0.2 µm, 500 kDa and 1 kDa) and for three particle size ranges (1–500 kDa, 500 kDa–0.2 µm, 0.2–0.7 µm and > 0.7 µm) as reported in Table 3.2 and Figure 3.4 and Figure 3.5.

Table 3.2 E^W_{Cr}-values (µg of Cr per L of solution) and E_{Cr}-values (mg of Cr per Kg of SPM for 0.7µm) for ponds and streams at different cut-offs and ranges of particle size and its corresponding uncertainty.

Sample	Cutoff	Cr un-spiked (µg L^{-1})	E^W_{cr} (µg L^{-1})	SD (µg L^{-1})	E_{cr} (mg kg^{-1})	SD (mg kg^{-1})	Range of size	E^W_{cr} (µg L^{-1})	SD (µg L^{-1})
Stream1	0.7 µm	0.21	0.41	0.02	380	25	0.7 µm	0.41	0.02
	0.2 µm	0.18	1.30	0.06			0.2 - 0.7 µm	0.34	0.01
	500 kDa	0.43	96.33	5.38			500 kDa - 0.2µm	1.38	0.05
	1 kDa		143.83	7.66			1-500 kDa	1.10	0.02
Stream2	0.7 µm	10.55	74	3	22500	961	0.7 µm	74.4	3.2
	0.2 µm	10.28	82	3			0.2 - 0.7 µm	25.9	0.3
	500 kDa	10.19	121	3			500 kDa - 0.2µm	14.8	0.2
	1 kDa		164	5			1-500 kDa	18.2	0.2
Pond1	0.7 µm	588.83	2350	67	14200	406	0.7 µm	2350	67
	0.2 µm	587.38	2225	56			0.2 - 0.7 µm	8946	155
	500 kDa	583.90	2170	60			500 kDa - 0.2µm	830	16
	1 kDa		2239	61			1-500 kDa	1344	24
Pond2	0.7 µm	44.09	893	30	2800	94	0.7 µm	893	30
	0.2 µm	43.28	874	29			0.2 - 0.7 µm	145	3
	500 kDa	42.90	839	26			500 kDa - 0.2µm	112	2
	1 kDa		883	28			1-500 kDa	57	1
Pond3	0.7 µm	118.02	387	32	2200	182	0.7 µm	387	32
	0.2 µm	76.18	368	10			0.2 - 0.7 µm	493	24
	500 kDa	86.22	366	10			500 kDa - 0.2µm	139	2
	1 kDa		372	10			1-500 kDa	159	3

The results of experiment 1 (#E1, filtration in cascade after spiking) highlight that E^w_{Cr} was affected by the filtration cut-off. In the pristine river water, increasing E^W_{Cr} values was calculated with decreasing filter cut-offs: from 0.41–1.30 µg L^{-1}, for the 0.2 and 0.7 µm cut-offs to 96 and 143 µg L^{-1}, for the 500 kDa and 1 kDa cut-offs, respectively (Figure 4). The same trend was observed for the water from stream 2, located in the mining area, but the range of variations was smaller, from 74.3 to 164 µg L^{-1} (Figure 3.4). The three pond water samples displayed a higher exchangeable pool of Cr than in the streams. In addition, there was no significant difference in the calculated E^W_{Cr} values according to the size cut-offs used: 2246 µg L^{-1}, 872 µg L^{-1} and 373 µg L^{-1} on average for ponds 1, 2 and 3, respectively.

Simultaneously, the second experiment (#E2) showed that the calculated E^{w}_{Cr} values were also highly different depending on the particle size range (1–500 kDa, 500 kDa–0.2 µm, 0.2–0.7 µm and > 0.7 µm). The E_{Cr} value could not be displayed in mg/kg for all of the particle size ranges as it was almost impossible to accurately weigh the mass of the particles retained on the smaller cut-off filters (0.2 µm, 500 kDa and 1 kDa); however, this was done for the particles larger than 0.7 µm. The results are displayed in Table 3.2.

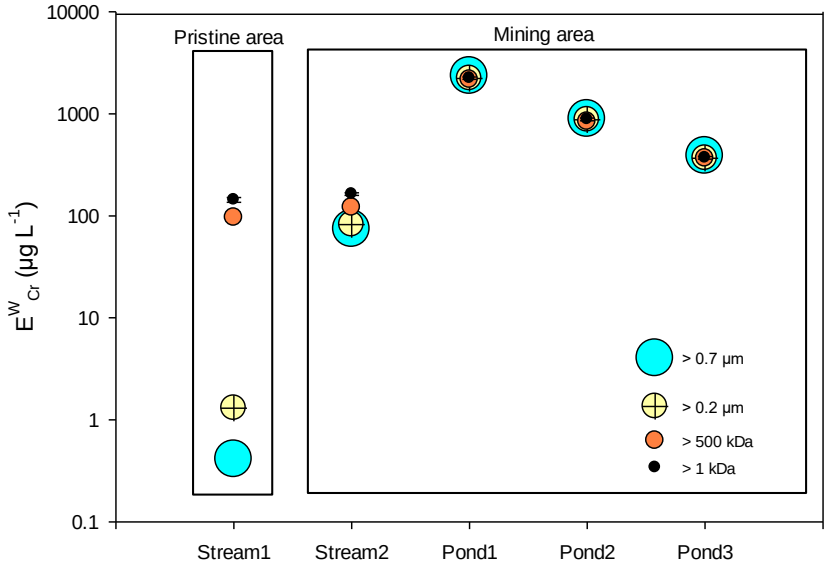

Figure 3.4 Isotopically exchangeable pool of Cr (E^{W}_{Cr}) for different cutoff.

In the pristine area, the particles larger than 0.7 µm and between 0.7 µm and 0.2 µm presented an E^{W}_{Cr} value of 0.41 and 0.34 µg L^{-1}, respectively, while for the colloidal fractions (1–500 kDa and 500 kDa–0.2 µm) the exchangeable pool of chromium was higher (1.38 and 1.10 µg L^{-1}, respectively). These results were consistent with the E^{W}_{Cr} values obtained in the first experiment (#E1). Again, the exchangeable pool of Cr was larger in the mining area than in the pristine area (Table 3.2). Unlike #E1, the E^{W}_{Cr} values obtained in #E2 also varied according to the range of particle sizes: the E^{W}_{Cr} value for the particulate fraction (> 0.2 µm) was higher than the one associated with the two colloidal fractions (1–500 kDa and 500 kDa–0.2 µm). In stream 2, the E^{W}_{Cr} value decreased from 74.4 µg L^{-1} for the particles larger than 0.7 µm to 25.9 µg L^{-1} in the 0.2–0.7 µm range and 16.5 µg L^{-1}, on average, for the colloidal fractions (Figure 3.5(a)). Among the water samples from the mining area, the ponds contained a higher exchangeable pool of chromium which was mainly associated with the particulate fraction (> 0.2 µm). For pond 1, the E^{W}_{Cr} value in the particulate fraction varied from 2350 to 8946 µg L^{-1}, which was higher than in pond 2 (145–893 µg L^{-1}) and pond 3 (387–493 µg L^{-1}).

Small particles are characterized by a larger specific surface area and are therefore able to sorb larger amounts of elements, including chromium, than large particles (Fendorf, 1995). The E^{W}_{Cr} values are expressed relatively to the volume of water and not to the mass of the particles, the high E^{W}_{Cr} values associated with large particles in the mining area may be related to the high SPM concentration. The positive correlation between the E^{W}_{Cr} values and SPM concentration indicates that the higher E^{W}_{Cr} value measured for bigger particles was clearly due to the higher mass of the particles (Figure 3.5(b)). As mentioned earlier, the normalization of the exchangeable Cr to the mass (E_{Cr} value) could only be done for the SPM (> 0.7 µm), which clearly highlights the challenge of working with exchangeable metal on colloids normalized to the volume (E^{w}_{Cr} value).

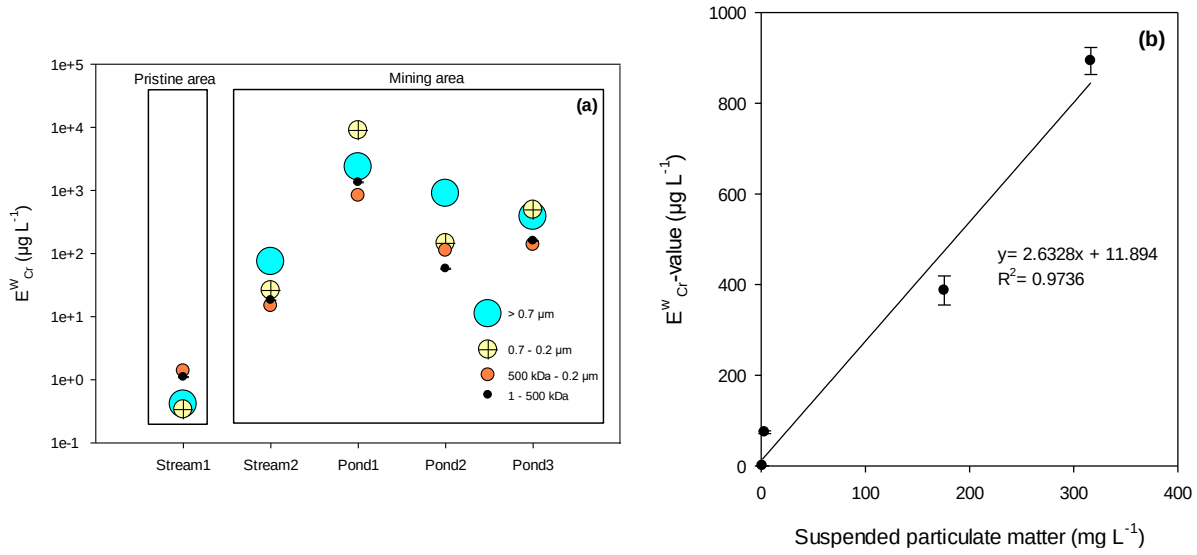

Figure 3.5 Isotopically exchangeable pool of Cr (E^{W}_{Cr}) for different ranges of particle size (a) and (b) the positive correlation between the E^{w}_{Cr}-*value* for > 0.7 µm and the SPM concentration after filtration at 0.7 µm.

The difference between the pristine and mining areas regarding the SPM content in exchangeable chromium could be explained by the water runoff that was enriched in particles eroded during the ore extraction, crushing and gridding operations. In addition, the presence of vegetation in the pristine area provides a soil support system (greater infiltration and less runoff) and slope stability which decrease the erosion rate.

In summary, in streams located in ultramafic areas there is a natural contribution of chromium that is leached from ultramafic rocks and lateritic profiles. In these systems, the isotopically exchangeable pool of Cr in the particles is partitioned according to size where small particles (1–500 kDa) contain a higher concentration of exchangeable chromium and larger particles (> 0.2 µm) contain less exchangeable chromium. On the other hand, anthropogenic sources such as mining activities increase the amount of larger particles

containing exchangeable chromium by increasing runoff together with the soluble chromium concentrations.

3.3.4 Impact of colloids on the determination of E^W_{Cr}

For both experiments #E1 and #E2, a significant bias was observed in the calculated isotopically exchangeable pool of chromium: for #E1, where the bulk samples were spiked, the E^W_{Cr} value should not display a higher value than the total chromium; and for #E2, the E^W_{Cr} value should not be higher than the total chromium concentration in the un-spiked solution of a given particle size range. Hence, the E^W_{Cr} values calculated for different cut-off sizes were compared to the total concentration of chromium in the bulk sample (Figure 3.6). In the pristine area (stream 1), the exchangeable pool of Cr for the 0.7 and 0.2 µm cut-offs represents nearly 4 and 14% of the total Cr present in the bulk, respectively. However, in the colloidal fractions (> 500 kDa and > 1 kDa), the E^W_{Cr} values are above the total Cr concentration in the bulk sample. In the mining area, stream 2 shows an overestimation of the exchangeable pool of Cr for all of the cut-off sizes; however, this discrepancy is higher for the colloidal fractions, as was the case for stream 1.

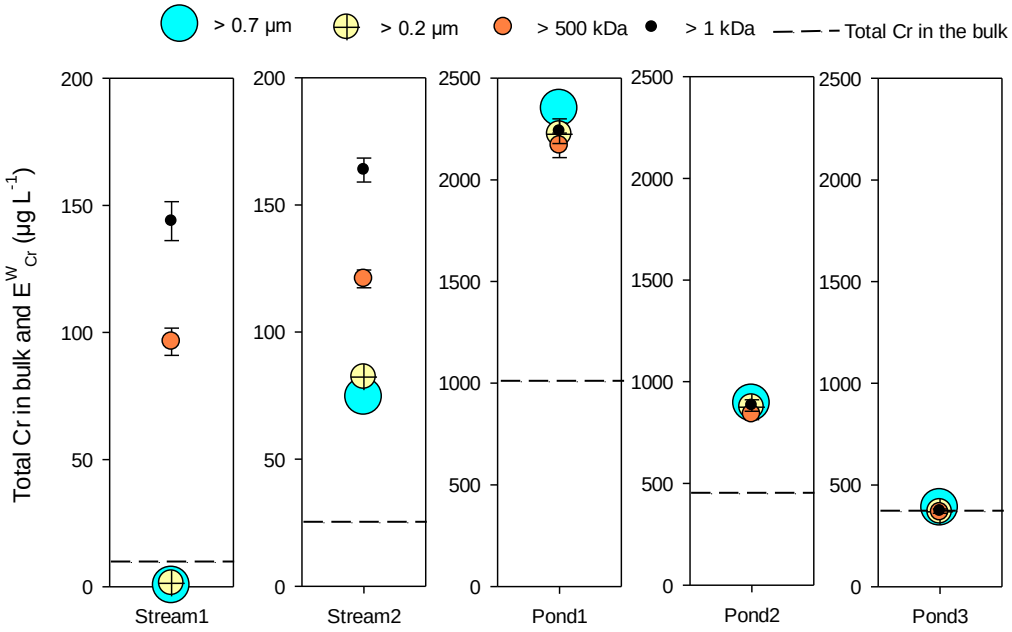

Figure 3.6 Total Cr in the bulk and E^W_{Cr} value for experiment 1 (#E1). An overestimation of the isotopically exchangeable pool of Cr is observed.

For ponds 1 and 2, the E^W_{Cr} value is almost twice the total Cr present in the bulk sample. In pond 3, 100% of the Cr present in the bulk sample seems to be exchangeable according to this calculation. Similarly, for #E2 the calculated E^W_{Cr} value is higher than the total chromium contained in the un-spiked solution of each particle size range. This difference is smaller in

the pristine area (up to 400%) compared to the mining area (higher than 1000%) and decreases with the particle size.

The presence of colloids could explain this overestimation of the exchangeable pool of chromium. The isotopic $^{53}Cr/^{52}Cr$ ratio is measured in the filtrates, where ^{53}Cr is the most abundant in the spike solution (98.3% and 9.5% for the spike and natural abundances, respectively) and ^{52}Cr is the most abundant in nature (83.8% and 1.6% natural abundance and abundance in the spike solution, respectively). Assuming that colloids passing through the filtration membranes have a high content of non-exchangeable colloidal chromium ($^{52}Cr_{nec}$), this can lead to an underestimation of the $^{53}Cr/^{52}Cr$ isotopic ratio and thus to an overestimation of the E^{W}_{Cr} values. Lombi et al. (2003) demonstrated the existence of non-isotopically exchangeable metal in suspended sub-micrometer colloidal particles (SCPs). They used Chelex 100 resin previously converted from the Na to Ca form as a sink for the exchangeable metals present in solution as free ions, soluble metal complexes and exchangeable metal adsorbed onto colloids. The E value in the solution eluted from the resin (E_r) was systematically lower than the E value in the sample (E) for Zn and Cu, concluding that the presence of colloids in the solution phase could lead to a significant overestimation of the E values. Other studies have shown that the differences between the E_r and E value for Pb, Zn and Cd are higher in soils with a large humus content and high pH (Marzouk et al., 2013). These results suggest that measuring the E value in a soil solution could lead to an overestimation in soils with a large organic matter and/or carbonate content.

In the present study, if the filtrate obtained after the spike addition includes colloids (1 kDa–0.2 µm) containing non-available Cr, the isotopic ratio in the filtrate can be expressed as follows:

$$\left(\frac{^{53}Cr}{^{52}Cr}\right)_m = \frac{^{53}Cr_d}{^{52}Cr_d + ^{52}Cr_{nec}} \quad \textbf{(3.2)}$$

where $(^{53}Cr/^{52}Cr)_m$ represents the isotopic ratio *measured* in the filtrate, $^{53}Cr_d$ and $^{52}Cr_d$ are the concentration of *dissolved* ^{53}Cr and ^{52}Cr, respectively and $^{52}Cr_{nec}$ represents the concentration of non-exchangeable colloidal Cr. To estimate the contribution of the colloidal $^{52}Cr_{nec}$ in the most unfavorable scenario, one can assume that 100% of the total Cr in the bulk (#E1) is exchangeable (E^{W}_{Cr}) and from equations (1) and (2), the corresponding theoretical isotopic ratio in the dissolved fraction $(^{53}Cr_d/^{52}Cr_d)_{Th\text{-}d}$ can be estimated (Equation 3, Table 3.3):

$$\left(\frac{^{53}Cr_d}{^{52}Cr_d}\right)_{Th-d} = \frac{IR_{Spike} + \frac{E_{Cr}^{w} \,.\, v \,.\, M_s \,.\, A_{STD}}{Q \,.\, M_{STD} \,.\, A_s} \,.\, IR_{UN}}{\frac{E_{Cr}^{w} \,.\, v \,.\, M_s \,.\, A_{STD}}{Q \,.\, M_{STD} \,.\, A_s} + 1} \quad \textbf{(3.3)}$$

The theoretical isotopic ratio in the filtrate is higher than the measured one, because the ^{52}Cr that corresponds to the truly dissolved and exchangeable chromium concentration is smaller than in the measured sample, which includes the colloidal fraction in addition to the truly dissolved fraction. For the cut-off at 0.7 µm, stream 1 was the only sample where the estimated isotopic ratio was smaller than the measured one (Table 3.3). For this sample, no differences were observed between the total Cr concentration in the un-spiked samples at 0.7 µm (0.21 µg L^{-1}) and 0.2 µm (0.18 µg L^{-1}), probably because in stream 1 the amount of particles displaying a size higher than 0.2 µm is negligible (Table 3.2). The difference between the theoretical isotopic ratio ($(^{53}Cr/^{52}Cr)_{Th\text{-}d}$) and the measured ratio ($(^{53}Cr/^{52}Cr)_m$) in the filtrate could be defined as a Δ value by Equation (4):

$$\Delta = \left(\frac{^{53}Cr_d}{^{52}Cr_d}\right)_{Th-d} - \left(\frac{^{53}Cr}{^{52}Cr}\right)_m \quad \textbf{(3.4)}$$

Replacing $(^{53}Cr/^{52}Cr)_m$ from equation (4) in equation (2), the contribution of the non-exchangeable colloidal ^{52}Cr ($^{52}Cr_{nec}$) can be calculated with Equation (5):

$$^{52}Cr_{nec} = \left[\frac{1}{\left(\frac{^{53}Cr}{^{52}Cr}\right)_{th-d} - \Delta} - \frac{1}{\left(\frac{^{53}Cr}{^{52}Cr}\right)_{th-d}}\right] * \; ^{53}Cr_d \quad \textbf{(3.5)}$$

Considering that the isotopic ratio ($^{53}Cr/^{52}Cr$) is dimensionless, the units of the estimated contribution of the colloidal fraction in the samples (Figure 3.7) are defined by the $^{53}Cr_d$ units, which corresponds to the average of 20 measurements (Thermo Scientific Element II) in counts per second (CPS). It was possible to estimate the concentration through the use of the calibration curve.

In the pristine area, the contribution of colloidal Cr in the filtrate at 0.2 µm, 500 kDa and 1 kDa is within the same order of magnitude (1 µg L^{-1}). In contrast, for stream 2, located in the mining area, the contribution of non-exchangeable colloidal chromium in the filtrate at 1 and 500 kDa is three times higher than the one in the filtrate at 0.2 and 0.7 µm. With regards to the ponds, pond 1 shows the same contribution of colloidal Cr in all of the cut-offs meaning that Cr is mainly associated with small colloids that cross most of the cut-offs evaluated. In the case of ponds 2 and 3, the results are similar to stream 2 with a higher contribution of colloids in the smaller fractions and vice-versa.

Table 3.3 Measured $(^{53}Cr/^{52}Cr)_m$ and theoretical $(^{53}Cr/^{52}Cr)_{Th}$ isotopic ratio assuming that 100% of Cr in the bulk sample is exchangeable.

Sample	0.7 µm				0.2 µm				500 kDa				1 kDa			
	$(^{53}Cr/^{52}Cr)_m$	SD	$(^{53}Cr/^{52}Cr)_{Th}$	SD	$(^{53}Cr/^{52}Cr)_m$	SD	$(^{53}Cr/^{52}Cr)_{Th}$	SD	$(^{53}Cr/^{52}Cr)_m$	SD	$(^{53}Cr/^{52}Cr)_{Th}$	SD	$(^{53}Cr/^{52}Cr)_m$	SD	$(^{53}Cr/^{52}Cr)_{Th}$	SD
Stream1	20.5672	0.0898	1.465	0.088	8.3930	0.0567	27.520	1.614	0.2445	0.0023	30.655	1.379	0.2021	0.0008	17.488	0.684
Stream2	0.2823	0.0014	0.604	0.018	0.2665	0.0015	1.088	0.029	0.2189	0.0009	1.113	0.032	0.1921	0.0009	1.122	0.034
Pond1	0.1216	0.0006	0.127	0.004	0.1220	0.0002	0.133	0.004	0.1222	0.0005	0.133	0.004	0.1220	0.0004	0.133	0.004
Pond2	0.1301	0.0009	0.143	0.004	0.1302	0.0006	0.351	0.012	0.1309	0.0003	0.355	0.013	0.1302	0.0005	0.358	0.012
Pond3	0.1500	0.0006	0.149	0.004	0.1500	0.0007	0.204	0.009	0.1499	0.0005	0.252	0.007	0.1495	0.0007	0.236	0.007

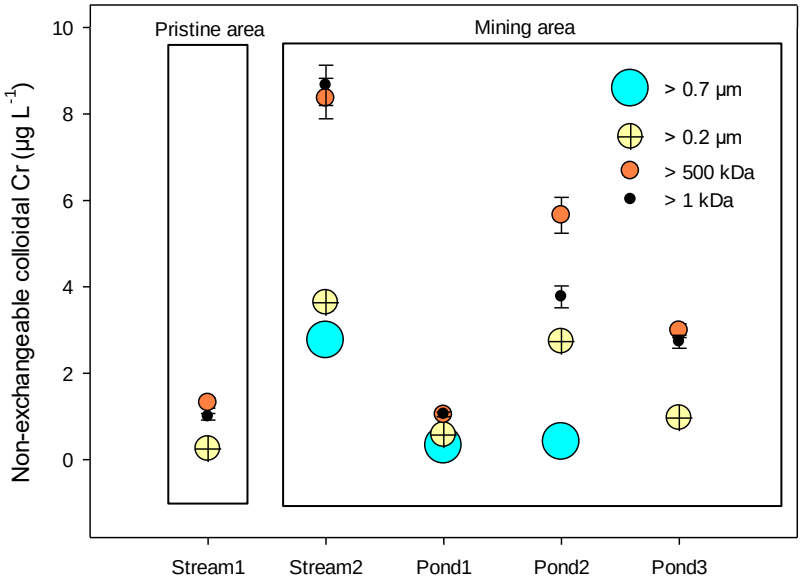

Figure 3.7 Theoretical concentration of the non-exchangeable colloidal chromium in the water samples at different cut-off.

Furthermore, in the mining area, chromium was mainly associated with small colloids (< 500 kDa) and to a smaller extent with large colloids (from 500 kDa to 0.2 µm). Ren et al. (2010) found that in the Yongdingxin River (China), Cr is strongly bound to very low molecular weight organic ligands and it cannot be complexed by larger size colloids (100 kDa to 0.22 µm) such as fulvic and/or humic acids, cell fragments or bacteria. Similarly, Pokrovsky and Schott (2002) showed that in organic and Fe-rich boreal rivers, Cr is associated with small-size (< 10 kDa) organic colloids or with Fe colloids (10 kDa–0.8 µm), which can contribute up to 50% of its dissolved fraction. Surprisingly, for stream 2, the contribution of colloidal Cr is higher compared to the ponds, where all of the particles coming from the stream area are stored. Pond 2 had the highest contribution of the colloidal fraction. The contribution of the small colloids is clearly higher in the mining area compared with the pristine area.

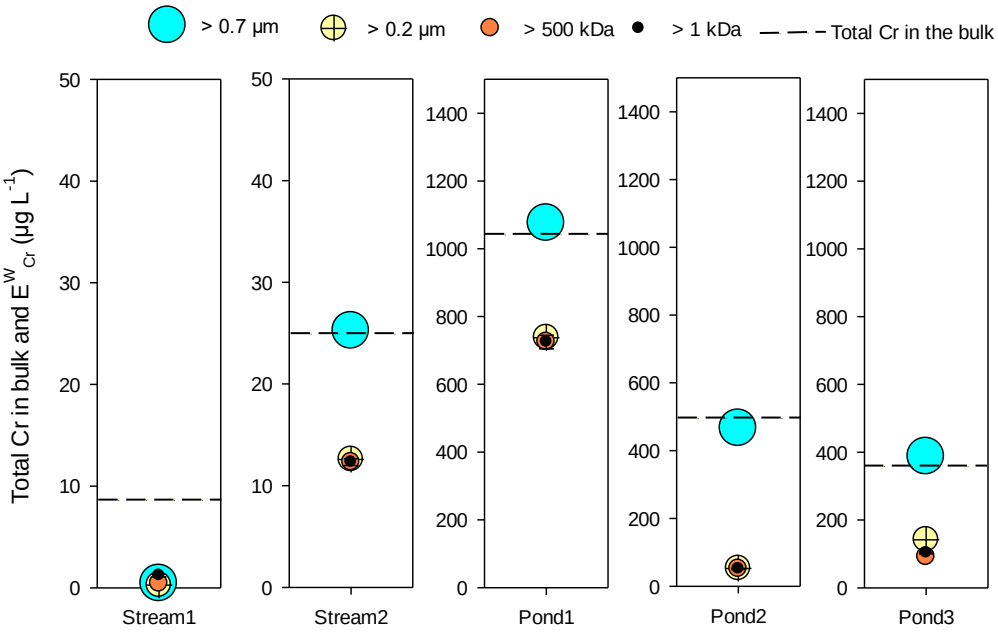

Figure 3.8 Total Chromium content in bulk un-spiked solution vs the corrected E^{W}_{Cr} value according to the estimated contribution of the colloidal Cr.

The contribution of the non-exchangeable colloidal chromium ($^{52}Cr_{nec}$) was then subtracted from the measured ^{52}Cr ($^{52}Cr_{Measured}$) to correct the ^{52}Cr considered in the determination of the isotopically exchangeable pool of Cr (Equation 6):

$$^{52}Cr_{Corrected} = {}^{52}Cr_{Measured} - {}^{52}Cr_{nec} \quad \textbf{(3.6)}$$

By applying this correction to each of the 15 ^{52}Cr measurements, a new $^{53}Cr/^{52}Cr$ isotopic ratio and the corresponding E^{W}_{Cr} were calculated (Figure 3.8). This estimation of the colloidal contribution to the E^{W}_{Cr} *value* was performed assuming that 100% of the Cr present in the

bulk is exchangeable. Hence, Figure 3.8 displays the most unfavorable scenario. In the pristine area (stream 1), once the contribution of the colloids was removed, there were no longer any differences observed between the cut-offs and the isotopically exchangeable pool of chromium, and this pool corresponded to 10% of the total chromium concentration present in the bulk (9 µg L^{-1}). In the mining area, pond 1 was the pond with the highest total chromium content in the bulk sample, in which 70% of the chromium is isotopically exchangeable in the > 0.2 µm, > 500 kDa and > 1 kDa fractions. In the same fractions, the E^{W}_{Cr} value corresponded to 49 and 11% for stream 2 and pond 2, respectively. The cut-off at 0.2 µm for pond 3 was slightly higher than the cut-offs at 500 and 1 kDa, representing 37 and 26% of the total Cr in the bulk, respectively.

3.4 CONCLUSIONS

- The evaluated impact of the cut-off in the E^{W}_{Cr} value calculation (#E1) showed differences between the cut-offs for the pristine area (stream 1). In the mining area, the differences were smaller for stream 2 than for stream 1, while in the ponds, where the isotopically exchangeable chromium concentration was higher, no differences between the cut-offs were observed.
- When the SPM was separated according to their specific size range (0.2–0.7 µm, 500 KDa–0.2 µm and 1–500 KDa) and then independently spiked (#E2), the ponds showed differences in the E^{W}_{Cr} values and the exchangeable chromium was mainly associated with the particulate fraction (> 0.2 µm), indicating that the exchangeable chromium was directly related with the number of particles.
- In the most unfavorable scenario, where 100% of Cr in the bulk is exchangeable, the isotopically exchangeable pool of chromium in the pristine area (stream 1) corresponded to 10% of the total chromium present in the bulk. In contrast, in the mining area, this went up to 70%.
- The presence of colloids in the pristine and mining areas led to an overestimation of the isotopically exchangeable pool of chromium (E^{W}_{Cr} value). The corrected E^{W}_{Cr} values in stream 1 showed that there are no differences in the available pool of chromium, meaning that the presence of different sizes of colloids artificially decreases the isotopic ratio and increases the estimated E^{W}_{Cr} value. In the mining area, the situation is similar for the 0.2 µm, 500 kDa and 1 kDa cut-offs, while in the biggest fraction (> 0.7 µm) the E^{W}_{Cr} value is less affected by the presence of colloids due to chromium bound to the particulate fraction.
- The occurrence of chromium associated with the colloidal fraction acts as a bias in isotopic exchange experiments, artificially decreasing the isotopic ratio in the filtrate with a consequent increase in the E^{W}_{Cr} value. This work reveals the importance of considering

the presence of non-exchangeable chromium in order to avoid overestimating the E^{W}_{Cr} value, and proposes a method to calculate a “worst case” scenario for the colloidal contribution. Future studies should systematically consider the presence of the non-exchangeable fraction of metals due to the colloidal contribution, while calculating both corrected and un-corrected E values, in order to assess the importance of the potential bias for a given sample.

3.5 BIBLIOGRAPHY

Apte, A.D., Tare, V., Bose, P., 2006. Extent of oxidation of Cr(III) to Cr(VI) under various conditions pertaining to natural environment. J. Hazard. Mater. 128, 164–174. doi:10.1016/j.jhazmat.2005.07.057

Collins, R.N., Tran, N.D., Bakkaus, E., Avoscan, L., Gouget, B., 2006. Assessment of isotope exchange methodology to determine the sorption coefficient and isotopically exchangeable concentration of selenium in soils and sediments. Environ. Sci. Technol. 40, 7778–7783.

Collins, R.N., Waite, T.D., 2009. Isotopically exchangeable concentrations of elements having multiple oxidation states: The case of Fe(II)/Fe(III) isotope self-exchange in coastal lowland acid sulfate soils. Environ. Sci. Technol. 43, 5365–5370.

Dominik, J., Gue, C., 2003. Partitioning of trace metals between particulate , colloidal and truly dissolved fractions in a polluted river : the Upper Vistula River (Poland). Appl. Geochemistry 18, 457–470.

Dupre, B., Dandurand, J., Polve, M., Benezeth, P., 2008. Major and trace elements associated with colloids in organic-rich river waters : ultrafiltration of natural and spiked solutions. Chem. Geol. 160, 63–80.

Fendorf, S.E., 1995. Surface reactions of chromium in soils and waters. Geoderma. doi:10.1016/0016-7061(94)00062-F

Ferreira Filho, C.F., Pimentel, M.M., de Araujo, S.M., Laux, J.H., 2010. Layered intrusions and volcanic sequences in Central Brazil: Geological and geochronological constraints for Mesoproterozoic (1.25Ga) and Neoproterozoic (0.79Ga) igneous associations. Precambrian Res. 183, 617–634. doi:10.1016/j.precamres.2010.06.008

Gäbler, H.E., Bahr, A., Heidkamp, A., Utermann, J., 2007. Enriched stable isotopes for determining the isotopically exchangeable element content in soils. Eur. J. Soil Sci. 58, 746–757. doi:10.1111/j.1365-2389.2006.00863.x

Gaillardet, J., Vier, J., Dupré, B., 2014. Trace Elements in River Waters, in: Treatise on Geochemistry (Second Edition). pp. 195–234. doi:10.1016/B978-0-08-095975-7.00507-6

Gallego-urrea, A., Hassello, M., Hammes, J., 2013. Geographically distributed classification

of surface water chemical parameters influencing fate and behavior of nanoparticles and colloid facilitated contaminant transport. Water Res. 47, 5350–5361. doi:10.1016/j.watres.2013.06.015

Garnier, J., Quantin, C., Echevarria, G., Becquer, T., 2009. Assessing chromate availability in tropical ultramafic soils using isotopic exchange kinetics. J. Soils Sediments 9, 468–475. doi:10.1007/s11368-009-0062-4

Gustafsson, J.P., Persson, I., Oromieh, A.G., Schaik, J.W.J. Van, Sjo, C., Kleja, D.B., 2014. Chromium(III) Complexation to Natural Organic Matter: Mechanisms and Modeling. Environ. Sci. Technol. 48, 1753–1761.

Hamon, R.E., Parker, D.R., Lombi, E., Donald, L.S., 2008. Chapter 6 Advances in Isotopic Dilution Techniques in Trace Element Research: A Review of Methodologies, Benefits, and Limitations. Adv. Agron. Volume 99, 289–343. doi:10.1016/s0065-2113(08)00406-9

Ji, H., Ding, H., Tang, L., Li, C., Gao, Y., Briki, M., 2016. Chemical composition and transportation characteristic of trace metals in suspended particulate matter collected upstream of a metropolitan drinking water source , Beijing. J. Geochemical Explor. 169, 123–136. doi:10.1016/j.gexplo.2016.07.018

Johnson, C.M., Skulan, J.L., Beard, B.L., Sun, H., Nealson, K.H., Braterman, P.S., 2002. Isotopic fractionation between Fe(III) and Fe(II) in aqueous solutions. Earth Planet. Sci. Lett. 195, 141–153. doi:10.1016/S0012-821X(01)00581-7

Kaprara, E., Kazakis, N., Simeonidis, K., Coles, S., Zouboulis, A.I., Samaras, P., Mitrakas, M., 2015. Occurrence of Cr (VI) in drinking water of Greece and relation to the geological background. J. Hazard. Mater. 281, 2–11. doi:10.1016/j.jhazmat.2014.06.084

Lombi, E., Hamon, R.E., Mcgrath, S.P., Mclaughlin, M.J., 2003. Lability of Cd , Cu , and Zn in Polluted Soils Treated with Lime , Beringite , and Red Mud and Identification of a Non-Labile Colloidal Fraction of Metals Using Isotopic Techniques. Environ. Sci. Technol. 37, 979–984.

Margiotta, S., Mongelli, G., Summa, V., Paternoster, M., Fiore, S., 2012. Trace element distribution and Cr (VI) speciation in Ca-HCO 3 and Mg-HCO 3 spring waters from the northern sector of the Pollino massif , southern Italy. J. Geochemical Explor. 115, 1–12. doi:10.1016/j.gexplo.2012.01.006

Marzouk, E.R., Chenery, S.R., Young, S.D., 2013. Measuring reactive metal in soil : a comparison of multi-element isotopic dilution and chemical extraction. Eur. J. Soil Sci. 64, 526–536. doi:10.1111/ejss.12043

Mcclain, C.N., Maher, K., 2016. Chromium fl uxes and speciation in ultrama fi c catchments and global rivers. Chem. Geol. 426, 135–157. doi:10.1016/j.chemgeo.2016.01.021

Mishra, H., Sahu, H.B., 2013. Environmental Scenario of Chromite Mining at Sukinda Valley – A Review. Int. J. Environ. Eng. Manag. 4, 287–292.

Osaki, S., 1983. The effect of organic matter and colloidal particles on the determination of chromium (VI) in natural waters. Talanta 30, 523–526.

Oze, C.J., Laforce, M.J., Wentworth, C.M., Hanson, R.T., Bird, D.K., Coleman, R.G., Bird, K., Coleman, R.G., 2003. Chromium geochemistry of serpentinous sediment in the Willow core , Santa Clara County , CA. U.S. Department of the interior, U.S. geological survey, Open-File Report 03-251.

Pokrovsky, O.S., Schott, J., 2002. Iron colloids / organic matter associated transport of major and trace elements in small boreal rivers and their estuaries (NW Russia). Chem. Geol. 190, 141–179.

Raous, S., Echevarria, G., Sterckeman, T., Hanna, K., Thomas, F., Martins, E.S., Becquer, T., 2013. Potentially toxic metals in ultramafic mining materials: Identification of the main bearing and reactive phases. Geoderma 192, 111–119. doi:10.1016/j.geoderma.2012.08.017

Ren, H., Liu, H., Qu, J., Berg, M., Qi, W., Xu, W., 2010. Chemosphere The influence of colloids on the geochemical behavior of metals in polluted water using as an example Yongdingxin River , Tianjin , China. Chemosphere 78, 360–367. doi:10.1016/j.chemosphere.2009.11.018

Richard, F.C., Bourg, A.C.M., 1991. Aqueous geochemistry of chromium: A review. Water Res. 25, 807–816. doi:10.1016/0043-1354(91)90160-R

Rodríguez-González, P., Marchante-Gayón, J.M., García Alonso, J.I., Sanz-Medel, A., 2005. Isotope dilution analysis for elemental speciation: A tutorial review. Spectrochim. Acta - Part B At. Spectrosc. 60, 151–207. doi:10.1016/j.sab.2005.01.005

Schäfer, A.I., Schwicker, U., Fischer, M.M., Fane, A.G., Waite, T.D., 2000. Microfiltration of colloids and natural organic matter. J. Memb. Sci. 171, 151–172.

Sivry, Y., Riotte, J., Munoz, M., Redon, P., Denaix, L., Dupr, B., Laboratoire, M., 2011. Multielementary (Cd , Cu , Pb , Zn , Ni) Stable Isotopic Exchange Kinetic (SIEK) Method To Characterize Polymetallic Contaminations. Environ. Sci. Technol. 45, 6247–6253.

Taylor, S.R., McClennan, S.M., 1985. The continental crust: its composition and evolution. Blackwell. Malden, pp. 312.

Viers, J., Dupré, B., Gaillardet, J., 2008. Chemical composition of suspended sediments in World Rivers : New insights from a new database. Sci. Total Environ. 407, 853–868. doi:10.1016/j.scitotenv.2008.09.053

Wang, X., Johnson, T.M., Ellis, A.S., 2015a. Equilibrium isotopic fractionation and isotopic exchange kinetics between Cr(III) and Cr(VI). Geochim. Cosmochim. Acta 153, 72–90. doi:10.1016/j.gca.2015.01.003

Wang, X., Johnson, T.M., Ellis, A.S., 2015b. Equilibrium isotopic fractionation and isotopic

exchange kinetics between Cr(III) and Cr(VI). Geochim. Cosmochim. Acta 153, 72–90. doi:10.1016/j.gca.2015.01.003

WHO, 2006. Guidelines for Drinking-water Quality.

Zelano, I., Sivry, Y., Quantin, C., Gélabert, a., Tharaud, M., Jouvin, D., Montarges-Pelletier, E., Garnier, J., Pichon, R., Nowak, S., Miska, S., Abollino, O., Benedetti, M.F., 2013. Colloids and suspended particulate matters influence on Ni availability in surface waters of impacted ultramafic systems in Brazil. Colloids Surfaces A Physicochem. Eng. Asp. 435, 36–47. doi:10.1016/j.colsurfa.2013.02.051

Zhang, C., Yu, Z., Zeng, G., Jiang, M., Yang, Z., Cui, F., Zhu, M., Shen, L., Hu, L., 2014. Effects of sediment geochemical properties on heavy metal bioavailability. Environ. Int. 73, 270–281. doi:10.1016/j.envint.2014.08.010

Zink, S., Schoenberg, R., Staubwasser, M., 2010. Isotopic fractionation and reaction kinetics between Cr(III) and Cr(VI) in aqueous media. Geochim. Cosmochim. Acta 74, 5729–5745. doi:10.1016/j.gca.2010.07.015

CHAPTER 4

Availability and mobility of chromium in ultramafic areas affected by mining activities: An isotopic study

CHAPTER 4

4.1 INTRODUCTION

Rock weathering together with anthropogenic discharges (chemicals, tailings, slag and scrap) are the main Cr sources in rivers with a contribution of, respectively, 5×10^8 mol year^{-1} and 2×10^9 mol year^{-1} (Mcclain and Maher, 2016). Specifically ultramafic rocks and soils developed from them are highly enriched in chromium, containing concentrations exceeding 1.8 and 15 g kg^{-1}, respectively (Oze et al., 2004). When the ultramafic bedrock enters in contact with water, weathering takes place during the wet season. Si and Mg are leached from the bedrock and laterite is formed and enriched in the most insoluble ions, such as Fe and Al, but also Cr (Ent et al., 2018). This process occurs in three phases: i) hydratation of the ultramafic parent rock, ii) leaching of Mg and Si by unsaturated descending meteoritic waters and iii) relative enrichment of weathering resisting chrome spinels, Fe and Al hydroxides (Raous et al., 2010). Trivalent chromium (Cr(III)) is the predominant species in ultramafic rocks and their weathering product (Crowe et al., 2013; Frei and Polat, 2013).

Chemical speciation of chromium is a key factor to understand chromium mobility and availability in the environment (Oze et al., 2004; Choppala et al., 2013). Cr(III) is considered strongly hydrolyzed in aqueous solutions and is prevalent under reducing conditions and acidic pH (pH<4). At pH>4, Cr(III) forms low solubility compounds and strongly adsorbs on mineral surfaces and organic matter (Fendorf, 1995; Oze et al., 2004). On the other hand, Cr(VI) exists as chromate (CrO_4^{2-}) and/or dichromate anions ($Cr_2O_4^{2-}$), which are highly soluble. Due to its anionic nature, Cr(VI) is not retained appreciably on negatively charged colloids of soils and sediments, whereas it has an affinity for Al and Fe oxides and their net positive charge through the formation of outer-sphere complexes (Fendorf, 1995). In addition, Cr(VI) is highly toxic for humans, animals and plants what makes it an important focus of study (Choppala et al., 2013; Shahid et al., 2017).

Changes in the Cr speciation, controlled by redox reactions, are known to rule the variation of the Cr isotopic composition ($\delta^{53}Cr$) in natural environments (Ellis, 2002; Schauble et al., 2004; Wang et al., 2015a; Qin and Wang, 2017). Chromium has four stables isotopes: ^{50}Cr (abundance 4.31%), ^{52}Cr (abundance 83.76%), ^{53}Cr (abundance 9.55%) and ^{54}Cr (abundance 2.38%). During reduction of Cr(VI) to Cr(III), controlled by organic material,

sulfides, and ferrous species (Fendorf, 1995), ^{52}Cr exhibit faster reactions rates, due to its higher vibrational frequencies. There is thus an enrichment in the produced Cr(III) (Schauble et al., 2004; Qin and Wang, 2017). Similarly, Cr(III) can be hydrolyzed from isomorphically substituted Cr to $Cr(OH)_3$, which can be slowly oxidized to the toxic and mobile hexavalent chromium (Cr(VI)) by the reduction of easily reducible Mn oxides (Leita et al., 2009). This process also induces chromium isotopic fractionation, and leaves a residual Cr(III) depleted in ^{53}Cr and Cr(VI) isotopically heavy and mobile, which is removed by run-off (Crowe et al., 2013). Even if the natural oxidation of solid Cr(III) is expected to be small (Johnson and Bullen, 2004; Novak et al., 2017) due to a “rind effect”, which limits the isotope fractionation, isotopic exchange involving Cr(III) oxy(hydr)oxide may be rapid enough to cause significant effects over a time scale of months (Wang et al., 2015b).

Hexavalent chromium enriched in ^{53}Cr ($\delta^{53}Cr(VI)_{aq}$ = 3.9‰) (Novak et al., 2014) produced during weathering of ultramafic rocks leaches and reaches surface and groundwater. In this sense, weathering of Cr-rich ultramafic rocks causes natural Cr contamination in soils, surface and groundwater (Izbicki et al., 2008; Trebien et al., 2011). Chromium can also be released from anthropogenic sources, such as electroplating, tanning and chemical industry, where there is a significantly higher fractionation (5.8‰) compared with Cr released naturally (Novak et al., 2014). In groundwater polluted by Cr-electroplating, the high $\delta^{53}Cr$ (2.9‰) is associated with Cr(VI) reduction (Novak et al., 2017). The differences in chromium isotopic composition between natural and industrial contamination sources can be potentially used to distinguish these two sources (Ellis, 2002; Izbicki et al., 2012; Novak et al., 2014; Wang et al., 2015). In the work of Novak et al., (2014) and Novak et al. (2017), the sources of pollution are industrial, and Cr is introduced in the environment in its hexavalent form. Mining activities are also important anthropogenic sources of chromium to the environment, not only in its hexavalent form but also in its trivalent form which can be potentially oxidized to toxic Cr(VI). One of the most extensive mining activities consists of the removal of the ground cover in order to gain access to the ore deposit. This causes the exposure of the material removed by rain and wind, which end up in the streams and ponds of the mine. This process is comparable to an accelerated erosion, which together with the rain falls, temperature, topography, and soil age are known to control weathering rates (White and Blum, 1995) and potentially affect chromium isotopic composition.

In ultramafic soils, chromate availability has been studied in Brazil (Garnier et al., 2009b, 2008, 2006) and New Caledonia (Becquer et al., 2010, 2006, 2003). Also Raous et al. (2013) determined the parameters controlling the release of Cr from ores and spoils of a nickel mining site, and the fate of Cr influenced by hydrological conditions (Raous et al., 2010).

However, no isotopic studies dealing with ultramafic mining environments have yet been done. Therefore, we collected solid samples including ores, soils, bedrock and sediments, as well as surface and groundwater in an ultramafic mining area. Our aim was to assess the impact of mining activities in the chromium isotopic composition of the material extracted in the mine and its relation with the chromium mobility and availability in ultramafic areas. A stratigraphy profile was reconstructed and the degree of alteration and its correlation with chromium fate and isotopic composition was established. In addition, the impact of mining activities was assessed. The Cr isotopic signature of the material extracted in the mine, as well as the potential use of Cr isotopes as a tracer for mining areas was evaluated.

4.2 MATERIALS ANS METHODS

4.2.1 Study site

The Barro Alto, Niquelândia and Caña Brava complexes are part of the 350 km long belt located in the north of Goiás state, of Brazil. The Barro Alto complex is bounded by metamorphic volcanic-sedimentary sequences (Ferreirafilho et al., 1992) and is a major mafic-ultramafic layered intrusion that was subjected to granulite facies metamorphism. It is composed mainly of gabbronorite, with minor dunite, peridotite, norite, gabbro, anorthosite and banded clinopyroxene-garnet amphibolite (Moraes and Fuck, 2000). In the complexes of Niquelandia and Barro Alto, lateritic weathering has formed important reserves of extractable Ni ore, representing around 2 million tons of metallic Ni (Raous et al., 2010). Ultramafic areas are characterized by a natural enrichment in heavy metals. In the case of the Barro Alto complex, this enrichment is mainly in Ni, however the Cr content has been reported as high as 6030 mg kg^{-1} (Ratié et al., 2015) and 46800 mg kg^{-1} (Raous et al., 2010), which is not high enough to be extracted, but potentially harmful for the environment. Mineral phases containing Cr include Cr-rich magnetite ($Fe^{2+}(Fe^{3+}, Cr)_2O_4$), chromite ($FeCr_2O_4$), talc ($Mg_3Si_4O_{10}(OH)_2$) chlorite ($(Mg, Fe)_5$ $Al[(OH)_8$ $AlSi_3O_{10}]$) and spinels (Oze et al., 2004).

The Barro alto mine (Figure 4.1) is located in the Barro Alto complex and extends for 35 km in an arc from southwest to northeast. The mineral resource is primarily saprolite, overlain by laterites and is composed of a sequential serpentinised dunites and pyroxenes, enveloped by gabros. The Barro Alto mine consists of an open pit mine and a ferronickel plant which has been mined since 2011 by Anglo American's Codemin (Raous et al., 2010). No blasting is required to access the laterite and saprolite ore, which is loaded with excavators. The ore is transported by trucks to the ore preparation yard at the plant site for a later beneficiation process which includes crushing, calcination, smelting and refining (Moore, 2012).

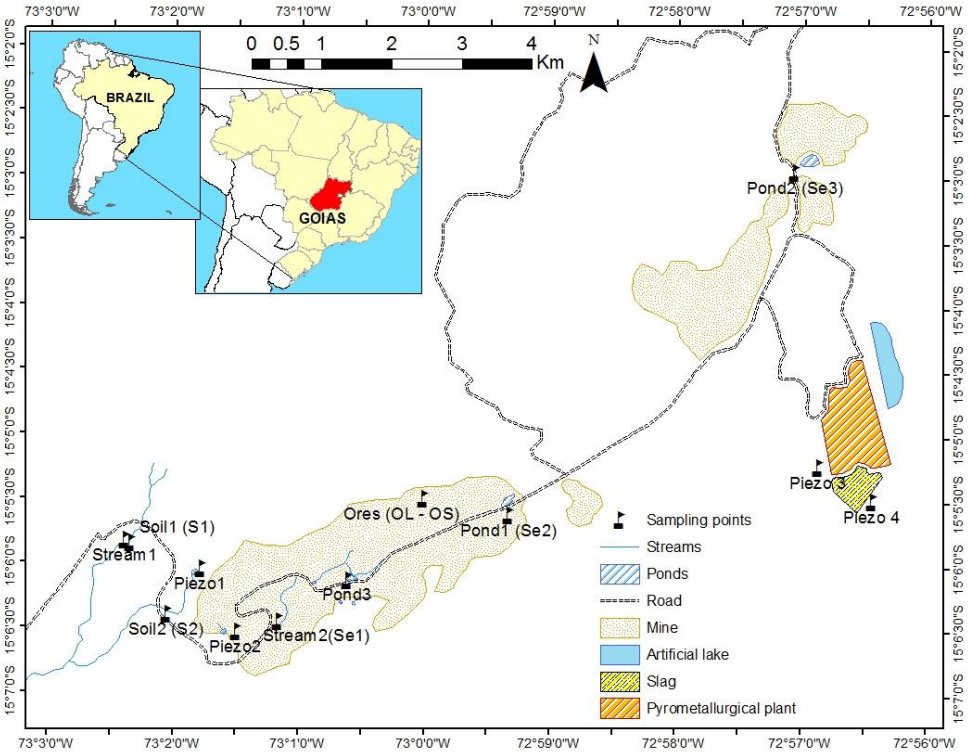

Figure 4.1 Map of the study area in Barro Alto mine and location of the sampling sites. Names in parenthesis are the ones used for the solid samples.

The Barro Alto, Niquelândia and Caña Brava complexes have been recently subject to many studies of nickel isotopic fractionation associated to tropical weathering (Ratié et al., 2015), smelting and refining processes (Ratié et al., 2016), the influence of colloids and suspended particulate matter on Ni availability (Zelano et al., 2013), the determination of the Ni exchangeable pool of Ni (Zelano et al., 2015) and the mobility of nickel in spoil materials (Raous et al., 2010). Also, reactive phases for Ni and other trace elements (Cu, Cr and Mn) have been identified in ultramafic mining materials (Raous et al., 2013) and leaching tests have been performed with slags and fly ash (Ettler et al., 2015). While most of the studies have focused on Ni, there are few studies dealing with chromium speciation and availability (Garnier et al., 2013, 2009a, 2006; Raous et al., 2010). No studies addressing the issue of chromium isotopic fractionation in this area have been reported. However, all those studies participate to a better understanding of the Cr fate and behavior of ultramafic environments affected by mining activities.

4.2.2 Samples

We collected nine water samples from streams, ponds and groundwater in June 2015 in the Barro Alto mine (Goiás State, Brazil). Stream 1 was located in the ultramafic area but out of the mine and it was used as a reference, while stream 2 was located inside the mine. The three sediment ponds are inside the mine and are used to store runoff water. The

groundwater was collected in four piezometers, before (Piezo 1) and after (Piezo 2) the mine and before (Piezo 3) and after (Piezo 4) the smelter area (Figure 4.1). For each sample, approximately one litter of water was collected and stored in acid-cleaned polyethylene bottles. *In situ* parameters including temperature, pH and electrical conductivity were measured directly on the field using a WTW 3410 Set 2 multiparameter. Within 24 h after sampling, one part of the samples was filtered through pre-cleaned 0.7 µm Whatman™ glass microfiber filters grade GF/F for suspended particulate analysis. The other part was filtered through a 0.22 µm syringe PES (Polyethersulfone) filter and acidified with ultrapure concentrated HNO_3 for total major and traces. One part of the filtered sample was stored in amber glass bottles and acidified with H_3PO_4 for dissolved organic carbon (DOC) and the other part was stored without acidification for anion determination. The filtered acidified and non-acidified samples were stored at 4°C. There was no rainfall prior to the sampling event.

We also sampled solids such as soils, ores, sediments and bedrocks in June 2015. Two soil profiles were collected: soil 1 profile (S1) had three layers between 0-10cm, 10-40cm and 80-100cm and soil 2 profile (S2) had two layers between 0-15cm and 15-40cm. Eight lateritic (OL1 – OL8) and three saprolitic (OS1 – OS3) ores were collected in the mine exploitation area. The bottom sediment samples were collected in stream 2 (Se1), pond 1 (Se2) and pond 2 (Se3) (Figure 4.1). The bedrock B1 is a serpentinite collected in the area, while B2 and B3 were provided by the Anglo American mining company and come from two cores that were drilled through the lateritic regolith at 27m and 28m depths, respectively, and correspond to the samples C1 and C2 of Ratié et al. (2015). Solid samples were dried down at atmospheric temperature, sieved to <2 mm and stored in polypropylene plastic bags. The dry samples were powdered with a marble mortar and stored for further analysis.

4.2.3 Analytical methods

Soils, ores and sediments were crushed, powdered and homogenized in a marble mortar, while rocks were crushed in a ceramic jaw crusher and powdered with an agate mill. Total metal concentration in the solid samples was determined by X-ray fluorescence (XRF), using a Panalytical X fluorescence spectrometer equipped with Energy Dispersive Minipal 4 (Rh X Ray tube-30kV-9W), at a resolution of 150 eV (Mn Kα). Measurements were performed according to the thin-layer hypothesis. Considering the importance of the characterization of the main metal bearing phases to predict their mobility in ultramafic materials (Tina et al., 2006), the mineralogical composition was determined using X-ray diffraction (XRD) analysis on a PANalytical diffractometer and using the Cu Kα radiation (at 45kV – 40 mA) in grazing incidence in the 5°-70° 2θ range with a scan step of 0.013°.

About 0.05 g of soils, ores, sediments and rocks powders were dissolved in 2 mL concentrated ultrapure distilled HNO_3 and 1 mL HF on a hotplate at 100 °C for 48 h. Samples were then dried and flushed with aqua regia (HCl and HNO_3 in a ratio 3:1) to dissolve fluorides. After that, samples were dried and dissolved in 1 mL of 6N HCl. If black residues were still remaining (characteristic of samples containing minerals as chromite), the dissolved fraction was extracted and 100 µL of $HClO_4$ was added to the black residue and it was placed in a hot plate at 120 °C for 24 h. After dissolution, the $HClO_4$ was evaporated in an evapoclean and the residue was dissolved in 6N HCl and mixed with the original dissolved fraction for trace elements and isotope analysis. River, ponds and groundwater samples were evaporated and then redissolved in 1 mL 6N HCl. The suspended particulate matter was removed from the filters and dissolved with the same procedure as the solid samples.

Anions (F^-, Cl^-, NO_3^-, SO_4^{2-}) were measured by ion chromatography (ICS 1100, Thermo Fisher) equipped with a column Ionpac Thermo AS14 and a pre-column Ionpac Thermo AG14. The mobile phase consisted of a mixture of Na_2CO_3 and $NaHCO_3$. The injection volume was 20 µL and the flow rate was 1.2 mL min^{-1}. Dissolved organic carbon (DOC) analyses were performed with Shimadzu total organic carbon TOC-VCSH analyzer. Trace (Fe, Mn, Al, Cr, Ni) and major element concentrations (Na, K, Mg, Ca, Si) for all samples diluted in 2% ultrapure HNO_3 were measured on a ICAP 6200 (Thermo Fisher) or High-Resolution ICP-MS (Element II, ThermoScientific) for concentrations under 10 µg L^{-1} using multi-element standard solutions. Detection limits for the ICP-AES were typically between 10 and 200 µg L^{-1} and for the ICP-MS between 0.006 and 0.074 µg L^{-1}. The standard deviation (1σ) associated to the measurements was smaller than 5%. Based on measured concentrations, aliquots of acid digested samples were used for chromium purification following the cation exchange resin method (Birck and Allegre, 1988; Trinquier et al., 2008). Two successive elutions in 1N HCl were performed in Biorad AG 50WX8 cation exchanger. Samples were dissolved in 0.1N HCl and passed through the resin. Chromium was collected immediately after loading and an additional 5 mL 1N HCl was used to completely elute any remaining Cr. After that, 2 mL of 6N HCl were added to the resin and the fraction was collected and passed again through the resin as it was previously described. The two elutions were mixed and evaporated. Subsequently, 60 µL of 16 N HNO_3 were added to dissolve the residue, followed by 2 mL of Milli-Q water and the mixture was heated at 100°C for 24 h. Once the sample cooled down, the sample was passed through the resin. This load was discarded. Additional 5 mL of 0.5N HF and 22 mL of 1N HCl were used to eliminate residual Ti, Na and Al. Finally, chromium was eluted with 10 mL of 2N HCl. Between the elutions, columns were washed with 15 mL 6N HCl. The samples were evaporated until

dryness in order to eliminate the HCl and the concentration was adjusted to 100 ppb or 50 ppb of Cr with 0.6% HNO_3.

Chromium isotopic compositions were measured on a Multicollector ICP-MS (Neptune, Thermo Scientific) housed at the Institut de physique du globe de Paris (IPGP). Purified Cr samples were dissolved in 0.5% HNO_3 with concentrations of 100 ppb or 50 ppb for solid and water samples, respectively. Dilute samples were introduced in the plasma with a PFA µFlow nebulizer (100 µL/min) coupled with an Apex IR desolvation introduction system (Elemental scientific) without additional gas or membrane desolvation. With a jet sample cone and H skimmer cone and under high-resolution mode, the obtained sensitivity was 2.8 – 4.9 V ^{52}Cr per 100 ppb Cr. All ion beams were measured on Faraday detectors connected to 10^{11} Ω amplifiers. The isotopes ^{49}Ti, ^{51}V and ^{56}Fe were measured and monitored to correct for isobaric interferences of ^{50}Ti, ^{50}V and ^{54}Fe. The unprocessed NIST SRM 979 standard was analyzed after every three samples to monitor potential drift, which was < 0.1% within each analytical session. On-peak blanks were measured before and after every sample/standard. The analytical accuracy and precision were assessed by repeatedly processing and measuring USGS reference material BHVO-2 standard (-0.11 ± 0.02‰, 2SD, n=3).

The $^{53}Cr/^{52}Cr$ ratio was expressed using the δ notation, which is a per mil deviation from the standard reference material NIST SRM 979, as it was done for previous Cr isotopes studies (equation (4.1)). The analytical results are expressed in the conventional δ notation in part per mil (‰).

$$\delta^{53}Cr(‰) = \left[\left(\frac{^{53}Cr/^{52}Cr_{sample}}{^{53}Cr/^{52}Cr_{SRM\ 979}}\right) - 1\right] * 1000 \quad \textbf{(4.1)}$$

4.2.4 Chromium mobility

4.2.4.1 Isotopic exchange

The isotopically exchangeable pool of Cr(VI), $E_{Cr(VI)}$-Spike, was determined through the addition of Cr(VI) with a totally modified isotopic signature compared with the natural one. The ^{50}Cr(VI) (natural abundance 4.345%) spike solution with a certified isotopic abundance of 96.5% in ^{50}Cr was purchased from ISOFLEX USA in its oxide form. The chromium oxide was dissolved in 6N HCl and evaporated for later addition of $HClO_4$. The solution was heated at 190°C for two days. After evaporation in the evapoclean, the spike was redissolved again in 16N HNO_3 and diluted with Milli-Q water to give a stock solution of 100 mg L^{-1}.

The soil suspensions consisted in a mix of 1 g of sample (< 2 mm) with 10 mL of Milli-Q water and 10 µL of 24.8 mg L^{-1} NaN_3, which were placed in an end-over shaker for 48 h. After

that, 10 µL of the spike solution was added to the suspensions and the samples were shaken for a further day, followed by filtration at 0.22 µm PES (Polyethersulfone) filter. Considering the low pH of the spike solution, the amount of spike added for each sample was restricted to 10 µL to avoid chemical equilibrium alteration. The filtrate was acidified to a final concentration of 2% HNO_3. No significant isotopic exchange occurs between Cr species over a time scale of days to weeks in natural systems (Zink et al., 2010; Wang et al., 2015), while isotopic exchange between Cr(VI) species occurs in less than 24 hours (Garnier et al., 2009b). It means that the isotopic equilibrium is reached through the exchange of the $^{50}Cr(VI)$ added with the labile Cr(VI) species of the solid samples. As a result, the isotopic signature measured in the filtrate after 48 hours, gave the information of the isotopically exchangeable pool of Cr(VI).

Isotopic abundances of ^{50}Cr, ^{52}Cr, ^{53}Cr and ^{54}Cr were determined in the filtrates, the spike solution and the unspiked sample by High-Resolution ICP-MS (Element II, ThermoScientific). Other isotopes including ^{47}Ti, ^{51}V and ^{57}Fe were analyzed to correct isobaric interferences with ^{50}Cr and ^{54}Cr. The isotopic ratio corresponds to the average of 20 runs with an analytical reproducibility higher than 1% (2SD, n=520). Samples were divided by blocks using bracketing with standard and un-spiked solutions in order to verify and correct, if necessary, the drifts in signal and intensity.

The isotopically exchangeable pool of Cr ($E_{Cr(V}$ - spike) was determined from the ratio $^{50}Cr/^{52}Cr$, which are the most abundant isotopes in the suspension. E_{Cr} – spike (mg kg^{-1}) was calculated from Eq. (4.2) (Zelano et al., 2013).

$$E_{Cr(VI)} - spike = Q * \frac{M_{STD}}{M_S} * \frac{A_S}{A_{STD}} * \left[\frac{(I.R.)_{Spike} - (I.R.)_{Sample}}{(I.R.)_{Sample} - (I.R.)_{UN}}\right] \quad \textbf{(4.2)}$$

where Q represents the added amount of spike (µg of spike per kg of sample), M_{STD} and M_S represent the atomic masses of Cr (g mol^{-1}) in the standard and the spike solutions, respectively, and A_{STD} and A_S represent the abundance percentage of ^{52}Cr in the standard and spike solutions, respectively. Isotopic abundances were determined in un-spiked solutions ($(I.R.)_{UN}$) and in the sample ($(I.R.)_{Sample}$). In the sequence of analysis, triplicate samples were bracket with their correspondent un-spiked solution and spikes and blanks were analyzed in order to monitor the signal, isotopes abundances and possible pollution between samples.

4.2.4.2 Chemical exchange

The principle of this technique is based on the fact that even if chromate ions are tightly bound compared with other anions (chloride, nitrate, sulfate), they can be desorbed by reactions of the soil with other specifically desorbed anions, such as phosphates (PO_4^{3-}) and sulfates (Adriano, 2001). In the case of trivalent species, the exchange is done with the potassium ion. Based on this fact the exchangeable pool of Cr(VI), label as $E_{Cr(VI)}$-KH_2PO_4, and Cr(III), labeled as $E_{Cr(III)}$-KCl, were extracted with 0.1 M KH_2PO_4 and 1 M KCl, respectively. A suspension of 1 g of soil was agitated with 25 mL of the reactant for 1 h (Garnier et al., 2006). The supernatant was separated by centrifuging for 15 min at 2500 rpm followed by filtration with 0.22 µm PES filter. Finally, the total Cr concentration was determined with ICP-AES and High-Resolution ICP-MS when the concentration was below 10 µg L^{-1}.

In each sample, Cr speciation was analyzed by an anion exchange column (Thermo Scientific, chrome FAST CF-KIT-Cr36) coupled to the High Resolution ICP-MS, so as to verify the selective extraction of Cr(VI) with the solution of KH_2PO_4. This is an on-line method which allows the determination of the Cr(VI) and Cr(III) content at a single run and within one analytical unit. The speciation column is added to an existing SC-DX-FAST system for separation of Cr species by isocratic elution anion exchange chromatography. The HPLC separation of chromium species is performed with a mobile phase, at pH 2, constituted by 68% HNO_3, 25% NH_3 and 10 ppm Tm. The flow rate through the column was between 170 and 180 µL min^{-1} (10 RPM on the peristaltic pump). Prior to using the column, the mobile phase was allowed to flow through the column for 30 minutes in order to condition the column with the ion-pair reagent. After use, the column was rinsed with MQ water and stored wet to prevent drying out. The detection limit for Cr(VI) is 4 ng L^{-1} and for Cr(III) is 3 ng L^{-1}. Chromium standards, ranging from 10 ppt to 10 ppb, were prepared from 1000 mg L^{-1} stock solution of Cr(III) (PerkinElmer, $Cr(NO_3)_3.9H_2O$) and Cr(VI) (Merk, CrO_4^{2-}). The calibration curve for Cr(III) and Cr(VI) was done considering the area below the curve, which was estimated with a curve integration program ("Integlec", Microsoft Visual Basic environment, R. Losno, personal communication) using trapeze integration method with a user defined baseline and a graphical front-end. The noise reduction was calculated with a Hamming filter. To estimate the Cr(III) and Cr(VI) concentrations in the samples, the area down the curve was calculated for each sample and using the calibration curve, the concentration was estimated.

4.3 RESULTS

4.3.1 Soils, ores, sediments and rocks characterization

Al, Cr, Fe, Mg, Mn and Ni content and mineralogy in bedrock, ores, soils and sediments are presented in Table 4.1. The bedrock B1 is basically serpentine with some traces of chromite, while B2 and B3 besides serpentine have chlorite and olivine. In B1, B2 and B3, Mg is the most concentrated element with concentrations from 184 to 202 g kg^{-1}, and in second place iron which ranged between 86 and 103 g kg^{-1}. Al, Cr and Mn were below 1 g kg^{-1} in the bedrock.

Most of the ores are enriched in Fe with content varying from 85 to 536 g kg^{-1}, which is consistent with the range of variation reported by Ratié et al. (2015) in Barro Alto mine (56 – 446 g kg^{-1}). However, in saprolitic ores OS2 and OS3, the Mg content is higher than for Fe, with values up to 156 and 146 g kg^{-1}, respectively. Al is the third most abundant element in the lateritic ores, with concentrations ranging from 14 to 70 g kg^{-1} and is less variable in the saprolitic ores with concentrations of 18 g kg^{-1} for OS1, 16 g kg^{-1} for OS2 and 14 g kg^{-1} for OS3. Iron mineral phases in the lateritic (OL1-OL8) and saprolitic (OS1-OS3) ores include hematite and goethite, while in the saprolitic ores Mg might be related with the occurrence of serpentine. This finding agrees with the one of Ratié et al. (2015). In concordance, Raous et al. (2013) describe the presence of two different types of materials in Niquelândia and Barro Alto (Goiás State, Brazil): garnierite and limonite. Garnierite is enriched in Si, representative of saprolitic ore consisting of a mixture of phyllosilicates including smectite and willemseite. On the other hand, limonite is representative of lateritic horizon enriched in Fe with goethite, hematite and chromiferous spinel as the main mineral phases. The mineralogy of the saprolitic samples is consistent with the typical weathering of ultramafic rocks that are commonly dominated by phyllosilicates, including minerals of the serpentine group, as well as clay minerals (smectite and chlorite).

Ni concentrations are particularly high in the saprolite (22 g kg^{-1} to 32 g kg^{-1}), while the concentration in the laterite is lower, except for ores OL2, OL4 and OL6, with Ni content of 22, 22 and 21 g kg^{-1}, respectively. In the lateritic and saprolitic ores, the Cr content ranges from 3 to 19 g kg^{-1}. The higher Cr content is found in the lateritic ores, probably due to the presence of Cr-bearing phases in the first stage of ultramafic rock weathering (Raous et al., 2013), while in the saprolitic ores the Cr concentration is lower, with values of 3, 4 and 4 g kg^{-1} for ores OL3, OL2 and OL1, respectively. In the lateritic ores smectite and other clay minerals may represent significant Ni and Cr concentrations.

In the profiles soil1 (S1) and soil2 (S2), the Fe content ranges from 250 to 281 g kg^{-1} and from 272 to 330 g kg^{-1}, respectively. The Cr content varies between 10 to 12 g kg^{-1} S1, while in S2 the range is between 16 to 12 g kg^{-1}. In S1 and S2 soil profiles, both Fe and Cr are more concentrated in the first layer (0-15 cm) of the profile. Apart from Fe(III) oxides and Fe(III) (oxy)hydroxides (i.e. hematite), other mineral phases found are chlorite and quartz. Also chromite and magnetite is present in the S2 soil profile. Contrary to Fe and Cr, the Al concentration is slightly higher in the deeper soils (80-100 cm) of S1(79 g kg^{-1}) compare to the superficial soils (74 g kg^{-1}), while it remains higher in the surface (0-15 cm) in S2 with a content of 77 g kg^{-1}. In S1 neither Ni nor Mn display any variation along the soil profile with an average content of 6 g kg^{-1} and 4 g kg^{-1}, respectively. In S2 Ni (9 g kg^{-1}) and Mn (11 g kg^{-1}) are higher in the surface, compared with S1.

In the sediment ponds, Fe is the most concentrated element (201.81 - 331.93 g kg^{-1}), followed by Mg (66 – 86 g kg^{-1}), Al (11 – 44 g kg^{-1}), Ni (9 – 17 g kg^{-1}), Cr (3 – 9 g kg^{-1}) and Mn (3 – 4 g kg^{-1}). The mineralogy in the sediments is dominated by iron oxides (goethite and hematite), serpentine, clinochlore and quartz, which basically corresponds to the mineralogy of the ore and overburden (soil) deposits in Barro Alto mine.

4.3.2 Exchangeable pool of chromium

The chemically extracted Cr(VI) and Cr(III) for ores, soils and sediments is presented in Table 4.2. The chemically extracted Cr(VI) was always higher than the chemically extracted Cr(III). It means that for ores, sediments and soils, Cr is mainly under the toxic and mobile oxyanionic Cr(VI) form (i.e. $Cr_2O_7^{2-}$ or CrO_4^{2-}) which can form labile complexes displaced by phosphates as reported by Garnier et al. (2006). In the Barro Alto ores there is an important variability in the $E_{Cr(VI)}$-KH_2PO_4 pool, with values ranging from 1.3 to 104 mg kg^{-1} (Figure 4.2), while the concentration for Cr(III) extracted is smaller (0.2 to 10 mg kg^{-1}).

The exchangeable Cr(VI) and Cr(III) show differences between stream 2 (Se1) and sediment ponds (Se2 and Se3). In stream 2 (Se1), located inside the mine, the $E_{Cr(VI)}$-KH_2PO_4 reported a concentration of 1.2 mg kg^{-1}, while higher values of 10 and 2.4 mg kg^{-1} were found for pond 1 (Se2) and 2 (Se3), respectively.

Table 4.1 Total content of elements, δ^{53}Cr value and mineralogical composition of the solids collected in Barro Alto (soils, ores, bedrock and sediments). Sm: smectite; Srp: serpentine; Chl: chlorite; talc, Oli: olivine; Hem: hematite; Goe: goethite; Spi: Spinel and Qz: quartz. ∆Cr represent the enrichment or depletion of Cr respect to the bedrock. UMIA is the Ultramafic Index of Alteration (Aiglsperger et al., 2016).

Sample type	Sample code	∆Cr	UMIA	δ^{53}Cr(‰)	±2σ	Concentration (g kg^{-1})						Mineralogy									
						Al	Cr	Fe	Mg	Mn	Ni	Sm	Srp	Chl	Talc	Oli	Hem	Goe	Spi	Qz	Others
Soils	S1(0-10 cm)	542	50	-0.28	0.01	76.97	12.23	280.71	34.51	4.04	6.68			+			+			+	
	S1(10-40 cm)	478	47	-0.10	0.04	74.29	11.01	250.13	38.16	3.75	6.45			+			+			+	
	S1(80-100)	437	48	-0.05	0.04	79.47	10.24	271.35	35.96	3.02	6.12			+	+		+				
	S2(0-15 cm)	701	62	-0.26	0.01	76.62	15.26	330.05	15.96	10.69	8.75			+	+		+	+		+	Magnetite
	S2(15-40 cm)	496	51	-0.28	0.06	62.44	11.37	272.25	11.67	9.98	6.47						+	+		+	Chromite
Lateritic ores	OL1	476	74	-0.24	0.02	48.43	10.97	331.82	10.92	3.92	8.08							+	+	+	
	OL2	633	50	-0.55	0.03	30.56	13.98	369.02	32.74	5.85	21.73	+	+					+			
	OL3	729	80	-0.76	0.07	42.13	15.80	536.17	9.14	6.92	3.90			+			+	+	+	+	
	OL4	627	60	-0.52	0.09	69.72	13.85	424.30	21.54	6.27	22.19							+			
	OL5	774	80	-0.16	0.05	66.91	16.65	465.59	15.59	7.05	12.23							+			
	OL6	720	61	-0.50	0.07	57.97	15.64	403.85	24.52	6.22	21.10		+					+			
	OL7	418	65	-0.43	0.02	42.02	9.88	297.78	13.80	4.66	10.05	+						+			
	OL8	883	69	-0.51	0.06	63.13	18.75	451.98	24.80	6.49	15.35							+	+		
Saprolitic ores	OS1	125	13	1.05	0.12	17.89	4.28	109.58	105.95	2.47	31.51		+								Verliculite
	OS2	140	12	0.93	0.05	15.78	4.58	133.78	156.44	2.40	22.16	+	+								
	OS3	66	8	0.97	0.08	13.84	3.16	84.93	146.54	1.03	21.56	+	+								
Bedrock	B1	-	10	-0.17	0.01	0.60	0.27	103.34	202.23	0.20	1.00		+								Chromite
	B2	-	11	0.18	0.08	0.74	0.20	92.27	196.66	0.30	1.11		+	+		+					Amphibole
	B3	-	11	0.10	0.04	0.37	0.08	86.50	184.98	0.28	1.15		+	+		+				+	
Sediments	Se1	-	28	-0.77	0.05	20.50	3.81	264.19	65.87	3.30	16.84		+	+				+		+	
	Se2	-	41	-0.50	0.04	43.65	9.05	331.93	48.54	3.79	8.85			+					+	+	
	Se3	-	21	-0.23	0.04	11.43	3.40	201.81	86.14	2.82	12.97		+	+			+				

In the soil profiles, $E_{Cr(VI)}$-KH_2PO_4 and $E_{Cr(III)}$-KCl is always lower in surface horizons than in the deeper ones. $E_{Cr(VI)}$-KH_2PO_4 increase almost 30 times from the first 10 cm (0.7 mg kg^{-1}) until 100 cm (21 mg kg^{-1}) and $E_{Cr(III)}$-KCl change from 0.39 mg kg^{-1} in the layer 10-40 cm to 3.7 mg kg^{-1} in the deeper soil layer (80 – 100 cm). Figure 4S.1(a) shows the speciation of a standard containing Cr(VI) and Cr(III). Figure 4S.2(b) and (c) present typical chromatograms obtained for leachates obtained with either KCl or KH_2PO_4 extraction, respectively. These results evidence the selective extraction of Cr(VI) with KH_2PO_4 and Cr(III) with KCl.

Table 4.2 Exchangeable pool of Cr(VI) ($E_{Cr(VI)}$-KH_2PO_4) and Cr(III) ($E_{Cr(III)}$-KCl) in the solid samples.

Sample type	Sample code	$E_{Cr(VI)}$-KH_2PO_4 (mg kg^{-1})	SD	$E_{Cr(III)}$-KCl (mg kg^{-1})	SD
Soils	S1(0-10 cm)	0.74	0.06	<LoD	-
	S1(10-40 cm)	4.43	0.34	0.39	0.02
	S1(80-100 cm)	21.14	2.17	3.69	0.54
	S2(0-15 cm)	4.06	0.30	0.34	0.03
	S2(15-40 cm)	5.39	1.05	0.43	0.01
Saprolitic ores	OL1	29.65	2.64	7.49	0.43
	OL2	5.84	0.68	0.57	0.05
	OL3	89.79	1.82	7.30	0.30
	OL4	2.04	0.25	0.25	0.02
	OL5	65.44	5.96	10.46	0.38
	OL6	1.68	0.16	0.20	0.03
	OL7	12.53	0.59	1.15	0.15
	OL8	104.09	7.70	6.56	0.68
	OS1	1.31	0.09	0.39	0.02
	OS2	2.46	0.18	0.72	0.08
	OS3	1.27	0.15	0.44	0.13
Sediments	Se1	1.57	0.03	20.89	5.50
	Se2	10.06	1.60	0.62	0.17
	Se3	2.37	1.84	1.49	0.71

*Limit of detection (LoD) Cr = 0.1 mg kg^{-1}

The Figure 4.3 shows the comparison between the chemically ($E_{Cr(VI)}$-KH_2PO_4) and isotopically exchangeable pool of Cr ($E_{Cr(VI)}$-spike). $E_{Cr(VI)}$-KH_2PO_4 and $E_{Cr(VI)}$-spike are positively correlated for ores, sediments and soils. Marzouk et al., (2013) compared multi-element isotopic dilution and chemical extraction for Zn, Cd and Pb. According to the authors, stable isotope dilution provides an accurate and reproducible measurement of the reactive metal in soils that is more meaningful than a single extraction procedure.

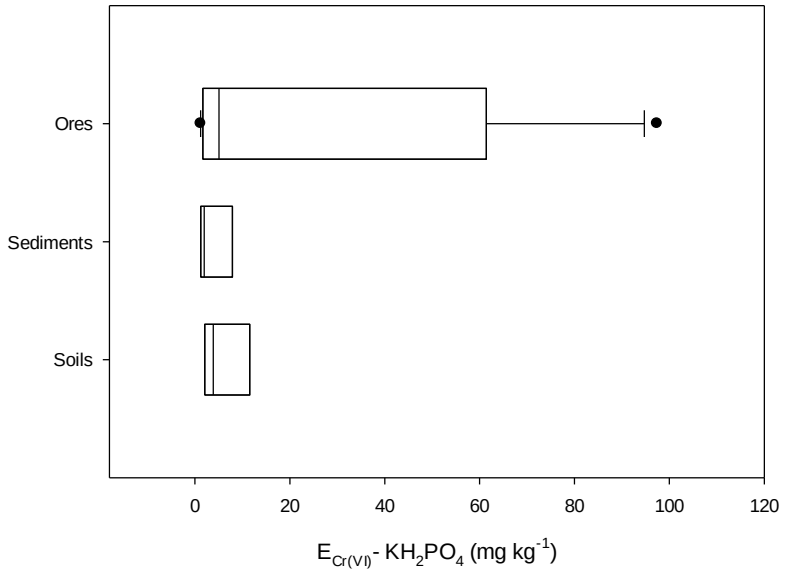

Figure 4.2 Distribution of the chemically exchangeable pool of Cr(VI) ($E_{Cr(VI)}$-KH_2PO_4). Ores present a higher range of variation compared with sediments and soils.

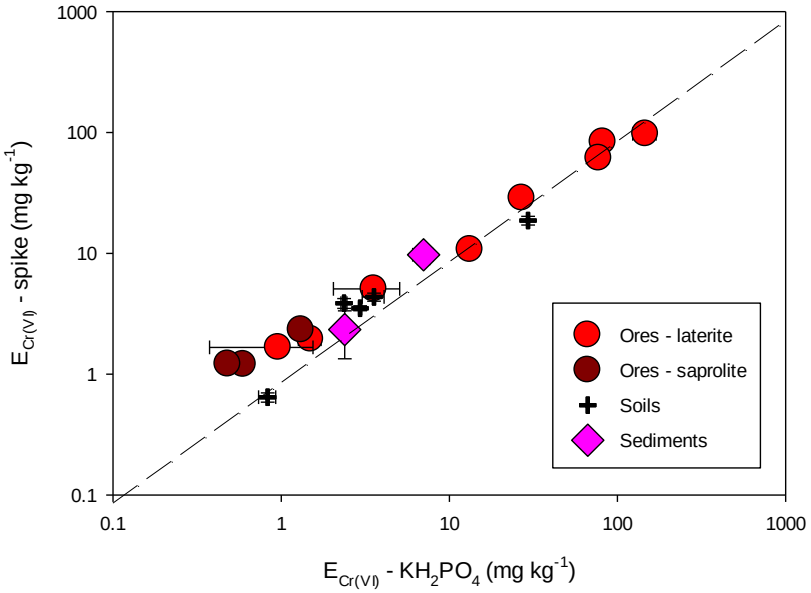

Figure 4.3 Positive correlation between isotopically and chemically exchangeable pool of Cr(VI) in solid samples of Barro Alto.

Based on this statement, in the saprolitic ores and the soil 1 (S1) between 10 and 40 cm, the $E_{Cr(VI)}$-KH_2PO_4 is under-estimated. However, in the case of saprolite ores the deviation of the $E_{Cr(VI)}$-KH_2PO_4 pool with respect to the one-one line could also be explained by the presence of sub-micrometer colloidal particles (SCPs) (Bolaños-Benítez et al., 2018; Lombi et al., 2003; Marzouk et al., 2013), which contain non-isotopically exchangeable metal and may induce an over-estimation of the $E_{Cr(VI)}$-spike. Whereas the exchangeable pool of Cr(VI) represents less than 1% of the total Cr, the remaining 99% represent a reservoir of Cr(III)

which is not mobile, according to KCl extractions but can potentially be oxidized and mobilized to the fresh water.

4.3.3 Water chemistry

In situ parameters (temperature, pH, electrical conductivity) measured in streams, ponds and groundwater, alkalinity, concentration of dissolved cations, traces and major elements, suspended particulate matter concentrations (SPM), dissolved organic carbon (DOC) and particulate organic carbon (POC) are presented in Table 4.3. The water composition evolves upon interaction with a layered mafic-ultramafic intrusion resulting in an alkaline (pH 7.3 – 9.2) Mg and HCO_3^- enriched water, due to minerals dissolution (Mcclain and Maher, 2016).

The groundwater in the piezometers before the mine (Piezo 1) and the smelter (Piezo 3) present the higher electrical conductivity with values of 167 µS cm^{-1} and 292 µS cm^{-1}, respectively. In the piezometers after the mine (Piezo 2) and the smelter (Piezo 4), the electrical conductivity in the groundwater decreases to 155 µS cm^{-1} and 48 µS cm^{-1}, respectively. This result is accompanied by the 90% of calcium and magnesium loss, together with the decreases of alkalinity from 79 to 11 mg L^{-1} and the neutralization capacity loss (pH from 6.6 to 5.7) through the smelter area. Other elements including K, Na and Si, also decreased in the groundwater of the piezometers of the smelter, exhibiting a concentration drop of 61, 64 and 78%, respectively.

The concentration of major elements in waters in contact with ultramafic soils naturally tends to be high. For instance, in the stream 1, major elements concentrations reach 10696 µg L^{-1} for Mg^{2+}, 2288 µg L^{-1} for Ca^{2+} and 10506 µg L^{-1} for Si. However, contact water tends to have even higher concentrations of major elements, especially in the pond where there is an accumulation of the materials coming from the streams. In pond 2, Mg^{2+} reaches concentrations up to 11008 µg L^{-1}, Na^+ up to 1680 µg L^{-1} and Ca^{2+} up to 4320 µg L^{-1}, while Si is lower in the impacted area compared with the pristine area, with a maximum concentration of 7843 µg L^{-1} in stream 2. In general, cation concentrations decrease in the order Mg^{2+}>Ca^{2+}> Na^+>K^+ and anion concentrations decrease in the order NO_3^- or SO_4^{2-}> Cl^-> F^-, which is in agreement with other studied ultramafic areas (Mcclain and Maher, 2016).

In ultramafic regions, Mg^{2+} and Ca^{2+} in surface waters are primarily derived from rock weathering, while K^+ and Na^+ have a significant contribution from rain (Schopka et al., 2011). In addition, the Ca/Mg ratio never exceeded 1, due to the low Ca concentration in the bedrock, except in the piezometers of the mine (piezometers 1 and 2), as it has been shown for other ultramafic areas in the United States (Mcclain and Maher, 2016) and Greece

(Kaprara et al., 2015). In the surface water, ponds and groundwater (except in the piezometer of the mine) the alkalinity and the Mg^{2+} concentration are positively correlated (R^2=0.829), indicating that there is a gradient in the extent of water-rock interaction in the watershed.

In addition to major elements, trace element abundances may also track the influence of ultramafic rocks in the water composition (Mcclain and Maher, 2016). While Ni is the metal extracted in the Barro Alto mine, it is enriched together with Cr which is a characteristic of ultramafic rocks and derived soils and consequently in water in contact with them (Table 4.3). Fe and Mn are also abundant in water bodies, and are known to control Cr reduction and oxidation, respectively. Cr is concentrated in the ponds with values of 737, 56 and 88 µg L^{-1} for pond 1, 2 and 3, respectively. In the stream 2 (12 µg L^{-1}), the Cr concentration is 30 times higher than in the stream 1 (0.38 µg L^{-1}), displaying the Cr contribution from the mine disposal materials. In the groundwater (2.33 µg L^{-1}) and the smelter (1.27 µg L^{-1}), there are insignificant differences in the Cr concentration and Cr precipitates along the mine and the smelter with a final concentration of 0.34 and 0.38 µg L^{-1}, respectively.

In Barro Alto mine, settling ponds are used as impoundments for sediment laden water running off excavated lands. For this reason, the ponds presented the highest suspended particulate matter (SPM) concentrations ranging from 165.92 to 316.55 mg L^{-1}, which are up to 30 times higher than the concentrations found in fresh and groundwater (Table 4.3).

The dissolved organic carbon is slightly higher in the groundwater of the mining area (3.74 mg L^{-1} for piezometer 1 and 4.65 mg L^{-1} for piezometer 2), probably due to the contribution of colloidal organic matter coming from the overburden (soils) stored in the mine, which is exposed to the environment. In contrast, the particulate carbon is higher in the groundwater of the smelter, with concentrations of 6.51 and 9.63% before and after the smelter area, respectively, compared to 5.84% in average groundwater in the mine. In fresh water, particulate carbon ranged from 0.64 to 3.65% (Table 4.3).

Table 4.3 Major and trace cations and anions in dissolved fraction, suspended particulate matter (SPM), alkalinity, dissolved organic carbon (DOC), carbon (C) content in filters, conductivity, temperature and pH values.

Element		Mining area								Pristine area
		Stream2	Pond1	Pond2	Pond3	Piezo 1 (before mine)	Piezo 2 (after mine)	Piezo 3 (before smelter)	Piezo 4 (after smelter)	Stream1
Dissolved metal concentrations (µg L^{-1})	K	48	139	227	313	210	168	3106	1211	21
	Mg	7038	5774	11008	6453	21772	19482	16053	1205	10696
	Ca	805	1171	4320	1072	532	1728	30068	3203	2288
	Na	248	318	1680	444	198	211	11045	4028	550
	Si	7843	2963	6107	3530	10755	1034	28008	6141	10506
	Fe	1.04	3.97	1.96	1.27	1.13	0.7	1.11	1.31	238*
	Mn	6.26	1.60	0.37	1.05	1.01	0.32	1.55	81.69	85*
	Al	0.95	1.27	1.14	1.18	4.15	5.84	17.33	0.69	0.77
	Cr	12*	737*	56*	88*	2.33	0.34	1.27	0.38	0.20
	Ni	77*	14*	10*	8*	13*	0.96	2.00	12*	38*
Dissolved fraction	δ^{53}Cr(‰)	2.10	2.62	3.66	-	-	-	2.18	2.19	2.60
	±2σ	0.14	0.01	0.04	-	-	-	0.08	0.16	0.04
Particulate fraction	δ^{53}Cr(‰)	0.94	-0.38	-0.18	-0.89	0.65	0.93	-0.54	-0.34	0.01
	±2σ	0.09	0.08	0.07	0.01	0.09	0.08	0.06	0.05	0.09
Dissolved anion concentrations (µg L^{-1})	F^-	< LoD	32	61	44	99	60	254	53	< LoD
	Cl^-	330	436	1604	18916	447	393	820	2990	359
	NO_3^-	726	3352	353	65338	5042	24	419	4007	260
	SO_4^{2-}	97	1884	1385	5988	729	2441	2986	168	55
DOC (mg L^{-1})		1.66	2.03	2.31	5.48	3.74	4.65	2.94	2.28	1.78
Alkalinity (mg L^{-1})		28.79	15.13	37.09	15.37	49.78	54.41	78.62	10.98	29.77
SPM (mg L^{-1})		3.3	165.92	316.55	175.69	4.6	8.07	7.92	18.15	1.08
Particulate Organic Carbon (wt %)		1.6	1.18	0.64	1.13	5.86	5.01	6.51	9.63	3.65
Temperature (°C)		23.3	22.2	26.5	26.1	27.8	25.8	25.3	27.2	24.4
Conductivity (µS cm^{-1})		60	58	105.6	62.6	166.7	155	292	48.3	96.2
pH		7.5	7.5	8.3	7.8	7.4	9.2	6.6	5.7	7.4

* Limit of detection (LoD) F^- = 20 µg L^{-1}; NO_3^-= 20 µg L^{-1}

4.3.4 Chromium isotopic composition

δ^{53}Cr values were determined in solid and liquid samples in the ultramafic area, inside and outside the mine, in order to identify the natural and anthropogenic processes which control isotopic fractionation. Figure 4.4 displays the δ^{53}Cr values measured for all the samples collected.

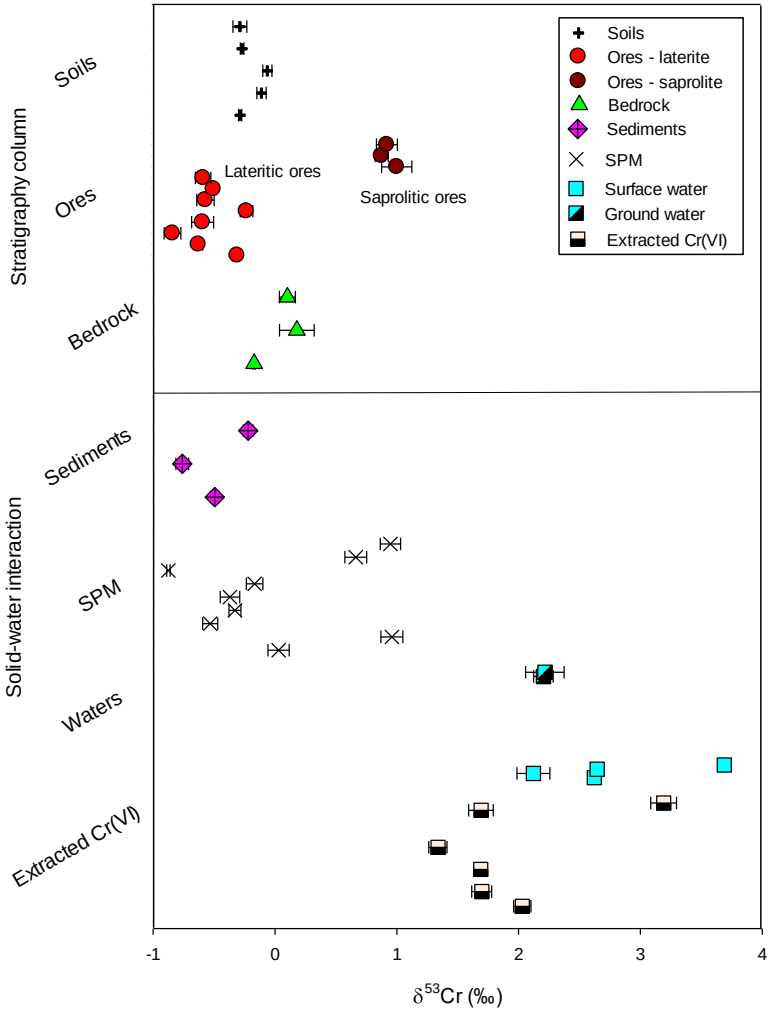

Figure 4.4 Cr isotopic composition (in ‰) of the samples from this study, including solid samples (soils, ores, bedrock and sediments), Cr(VI) extracted with KH_2PO_4 and liquid samples (surface and ground water).

A negative δ^{53}Cr was found for some solid samples like lateritic ores (-0.76 ± 0.068‰ to -0.24 ± 0.02‰), soils (-0.28 ± 0.06‰ to -0.10 ± 0.04‰), sediments (-0.77 ± 0.05‰ to -0.22 ± 0.04‰) and part of the suspended particulate matter-SPM (-0.89 ± 0.01‰ to -0.18 ± 0.07‰), which can be associated to a Cr loss (Qin and Wang, 2017; Frei and Polat, 2013; Berger and Frei, 2014). The bedrock B1 also displays a negative δ^{53}Cr of -0.17 ± 0.01‰, whereas it is positive for B2 and B3 with +0.18 ± 0.08‰ and +0.10 ± 0.04‰, respectively. Saprolitic ores have positive δ^{53}Cr values ranging from +0.93 ± 0.05‰ to

+1.05 ± 0.12‰. The highest $\delta^{53}Cr$ measured in the suspended particulate matter corresponds to stream 2 (+0.94 ± 0.09 ‰), as well as the piezometer before (Piezo 1) (+0.65 ± 0.09 ‰) and after (Piezo 2) (+0.93 ± 0.08‰) the mine (Table 4.3).

In water samples, heavy $\delta^{53}Cr$ values were found, from +2.10 ± 0.13‰ to +3.66 ± 0.04‰, which is within the same range of variation as the isotopic signatures found in the Cr(VI) extracted with KH_2PO_4 (+1.34 ± 0.07‰ to +4.37 ± 0.06) (Table 4.3).

4.4 DISCUSSION

4.4.1 Weathering in ultramafic environments

During weathering of ultramafic rocks, silica and magnesia are leached, leaving the most insoluble elements such as iron hydroxide as a residue. This process starts with the hydratation of the ultramafic parent rock, followed by the leaching of Mg and Si by unsaturated descending meteoritic waters. As a consequence, relative enrichment of weathering resistant chrome spinels, as well as Fe and Al hydroxides occurs (Raous et al., 2010). Based on this pattern and considering the silica (SiO_2), magnesia (MgO) iron and aluminium oxides (Fe_2O_3/FeO and Al_2O_3) content, it is possible to determine the degree of alteration of the samples collected in the Barro Alto mine. The mining activity in Barro Alto may have substantially disturbed the natural stratigraphic column. Hence, all the surface samples collected may have a different original position in that column. Assuming that this position is directly related to the extent of alteration, an index of alteration can be calculated for bedrocks, ores, soils and sediments, in order to reconstruct a theoretical stratigraphic column. A variety of weathering indices are available in the literature, comprising a valuable tool for estimating the engineering behavior of rocks (Rigopoulos et al., 2015). The silica-to-alumina mole ratio (R) and index of lateritization (IOL) are based on silica-loss during weathering (Yang et al., 2016). Other indices focus on the mobility of major elements (Na, Ca, K and Mg), like the weathering index of Parker (WIP), which is more suitable for *in situ* weathering profiles developed in heterogeneous metamorphic parent rocks. Another group of indexes (CIA, CIW, PIA, CPA and CIX) is based on the weathering of feldspars as they represent the most abundant mobile components of the upper continental crust and their conversion to secondary clay minerals therefore dominates the chemical weathering processes at the Earth's surface (Nesbitt and Young, 1982).

The multiple-element weathering index (Δ4Si%, $R^{3+}/(R^{3+}+R^{2+}+M^{+})$ and MIA) utilizes major oxides to acquire more complete scenarios for chemical modifications during weathering processes. The Mafic Index of Alteration (MIA) extends the equation of Chemical Index of Alteration (CIA) to include Mg and Fe as major elements (Babechuk et al., 2014). Table 4.1

presents the UMIA values calculated for each solid sample. In oxidative weathering environments, Fe is retained by the formation of insoluble ferric iron [Fe^{3+}] oxides and oxy(hydr)oxides and thus enriched along with Al (Babechuk et al., 2014). Under this scenario, Fe and Al are seen as immobile elements. Specifically for ultramafic systems, Aiglsperger et al. (2016) developed the ultramafic index of alteration (UMIA), based on previous work done by Babechuk et al. (2014). The authors considered the dominance of MgO and SiO_2 compared to the negligible content of CaO, Na_2O, K_2O in ultramafic rocks, as well as the depletion of MgO and Si_2O with concomitant enrichment of Fe_2O_3 and Al_2O_3 towards the surface in most Ni laterites (Aiglsperger et al., 2016). The ultramafic index of alteration (UMIA) is presented in the following equation:

$$UMIA = \frac{Al_2O_3 + Fe_2O_3}{Al_2O_3 + Fe_2O_3 + MgO + SiO_2} * 100 \quad \textbf{(4.3)}$$

The UMIA evaluates the degree of mineralogical weathering, i.e. the transformation ratio of a primary mineral into its equivalent alteration mineral. UMIA yields values between 0 and 100, and reflects incipient (UMIA<20), intermediate (UMIA= 20-60) or intense to extreme (UMIA> 60) mineralogical transformations.

The UMIA of the lateritic ores is higher than 60 (82 – 98), except for OL2 (Table 4.1), which reflects an intense mineralogical transformation, leading to the enrichment of chromium mainly as Cr(III). One of the main mechanisms which promotes trivalent chromium enrichment is the sorption of Cr(III) on surfaces of Fe(III) - containing oxides such as magnetite and hematite via inner-sphere complexation. As a results low - solubility precipitates are formed at pH values greater than 4 (Oze, 2003). Besides Fe oxides (goethite and hematite), serpentine and talc are present in minor proportion in lateritic ores (Ratié et al., 2015). In concordance, Raous et al. (2013) describe the presence of limonite which is representative of a lateritic horizon enriched in Fe with goethite, hematite and chromiferous spinel as the main mineral phases. In contrast, for the saprolitic ores and the bedrock, the UMIA reflects the incipient degree of alteration with values between 8 and 13. Saprolitic ores, described as garnerite by Raous et al. (2013) are enriched in Si, consisting in a mixture of phyllosilicates including smectite and willemite.

The UMIA calculated for the soils (47-62) displays values between the saprolitic and the lateritic ores. In spite of a comparable chemical composition between lateritic ores and soils, these latter show a different mineralogy with the occurrence of other mineral phases including hematite, chlorite and quartz. Hematite, goethite, maghemite, and amorphous Fe

(oxy)hydroxides are soil-forming phases in serpentine soils (Coleman and Jove, 1993). Quartz may be present in soils because they can be formed as a secondary mineral in lateritic regoliths over ultramafic rock (Vojcu and Bardoux, 1997). Finally, for the sediments the UMIA indicated intermediate mineralogical alteration. However, as it was mentioned before this result is associated with the fact that sediments are a mixture of particles coming from different sources, so one might think that it represents an average of UMIA in soils and ores. As an example, pond 1 (Figure 4.1) is located next to the area where ores (saprolitic and lateritic) are extracted, but there is also soil around. If one considers that all the lateritic and saprolitic ores and soils are mixed in the same proportion, an average UMIA will be close to 50 indicating intermediate alteration which is the same classification for the sediment collected in pond 1 (Se2).

Even though the UMIA gives an indication of the degree of alteration, local formation of mineral phases can act as a *bias*. Aiglsperger et al. (2016) proposed as an example the local occurrence of amorphous silica within highly altered limonite, which resulted in a low UMIA value. To avoid this misinterpretation, the UMIA is combined with an Al-Fe-Si-Mg molar ternary plot which illustrates the weathering trend of mafic and ultramafic minerals, mainly serpentine. Figure 4.5 shows a defined trend of weathering, starting from the bedrock as the less altered samples to the lateritic-ores as the most altered one. The last one is depleted on Mg and Si, and enriched in Fe due to the formation of secondary oxides(s).

Lateritic ores (OL1-OL8) are enriched in Fe (298 - 536 g kg^{-1}) and Al (42 – 70 g kg^{-1}) due to the presence of Fe oxides (goethite and in minor proportion hematite), while Mg remained low (9 – 33 g kg^{-1}) compared to saprolitic ores. Saprolitic ores (OS1, OS2 and OS3) present incipient mineralogical transformations. They are characterized by a low content of Al (14 – 18 g kg^{-1}) and Fe (85 – 134 g kg^{-1}) and enrichment in Mg (106 – 156 g kg^{-1}). In addition, the main mineral phases are serpentine and smectite (Table 4.1). The enrichment in Mg could be explained by the fact that Mg-bearing alteration minerals like serpentine and talc can be formed in ultramafic rocks, despite chlorite is the main Mg-mineral phase in saprolite (Vojcu and Bardoux, 1997).

The bedrocks (B1, B2 and B3) exhibit a low degree of alteration (Table 4.1). The large amount of Mg (185 – 202 g kg^{-1}) and extremely low content of Al (0.4 – 0.7 g kg^{-1}), Cr (0.1 – 0.3 g kg^{-1}), Mn (0.2 – 0.3 g kg^{-1}) and Ni (1.0 – 1.1 g kg^{-1}) is characteristic of this kind of samples where soluble elements, such as Mg, are still present because they have not been weathered. The mineralogy assemblage consists of serpentine and chlorite with traces of chromite and amphibole, as well as olivine. The soils are located close to the group of

lateritic ores as their element content decreases in the order Fe> Al > Mg, while in sediments the Mg content surpassed the Al content and Fe remained dominant (Table 4.1).

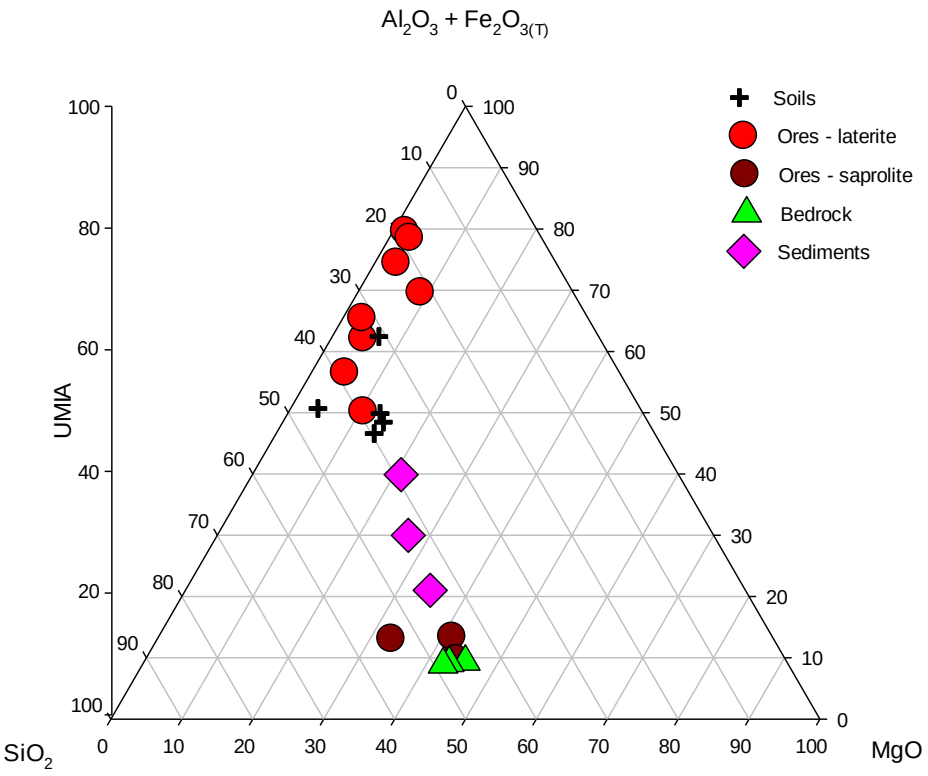

Figure 4.5 Ternary plot in the Al-Fe-Mg-Si space and its relationship with the ultramafic index of alteration (UMIA).

4.4.2 Chromium behavior during weathering

So far, in this study, the behavior of the most susceptible elements (Fe, Al, Mg and Si) in ultramafic weathering has been described. Among those elements iron and aluminum play an important role in the mobility and availability of chromium. In the case of iron, Fe(II) contributes to the reduction of Cr(VI) and the consequent formation of a solid Cr(III) phase. Adsorption and reduction can occur in the presence of Fe(II)-bearing minerals such as magnetite (Døssing et al., 2011). In addition, hydrous oxides of Al and Fe present a net positive charge and have therefore a potential affinity for Cr(VI) oxyanions (Fendorf, 1995).

The Figure 4.6(a) shows the total chromium content in the samples as a function of the ultramafic index of alteration (UMIA). The bedrock samples are the less altered material and contain the lower chromium content (0.1 – 0.3 g kg^{-1}). This parent material is subject to weathering which produces the formation of lateritic and saprolitic ores and soils. In those weathering products, owing to their insolubility especially when chromite is present,

chromium is concentrated according to the degree of alteration. Among the most chromium rich and altered materials are the lateritic ores, with chromium concentrations between 10 and 19 g kg^{-1}. The Cr enrichment in altered materials is associated with its insolubility, compared with elements such as Si and Mg which are leached from the bedrock. Cr enrichment is also observed in soils (10 – 15 g kg^{-1}), while in the saprolite the content of chromium reaches an average of only 4 g kg^{-1}. Sediments are a mixture of soils and ores (Cr between 3 and 9 g kg^{-1}), and are possibly more altered material due to its permanent contact with water. The content of chromium in the sediments of the pond 1 (Se2) is 9 g kg^{-1}. This high value is linked with the collection of runoff water from the ore extraction area to pond 1 (Figure 4.1). In concordance with the present study, a weathering profile performed in OMC-chromite mine (Sukinda valley, India) by Paulukat et al. (2015) presented total Cr concentrations between 24 and 60 g kg^{-1} in the laterite, 33 g kg^{-1} in the saprolite and a drastic drop to 7 g kg^{-1} (in average) in the serpentine.

The Figure 4.6 (b) displays the relation between the exchangeable pool of Cr(VI) and the UMIA. The most weathered material contains the higher concentration of exchangeable Cr(VI). This happens as a response of the oxidative weathering of rocks where Cr(III) is oxidized to Cr(VI), which at the circumneutral pH of most meteoritic and ground water is highly soluble and mobile as a chromate oxyanion (CrO_4^{2-}) (Oze et al., 2007; Frei and Polat, 2013). The Cr oxidation is promoted by the presence of compounds with high redox activities, such as elemental oxygen and manganese oxides and hydroxides (Trebien et al., 2011). The co-precipitation and substitution of metals in Mn oxides is expected to occur, especially when soil experiences alternate wetting and drying cycles, creating the opportunity to associate with freshly precipitated Mn oxides (Essington, 2005 in Trebien et al., 2011). The repetition of wet and dry season is essential for the formation of laterite, thus it can be expected that Mn oxides play an important role in the oxidation of chromium in ultramafic areas such as Barro Alto. A significant positive correlation between manganese and total chromium content (R^2=0.9) and UMIA (R^2=0.8) was established. Soil 2 (S2) is out of the correlations possibly because of the presence of magnetite and chromite, which are not present in the rest of the solid samples. The same correlation is observed between the extracted Cr(VI) and the total content of Mn. This correlation suggests the role of Mn in the oxidation of Cr(III) and the consequent production of the toxic hexavalent Cr. However, it is necessary to highlight that the extent of Cr(III) oxidation depends on the concentration of easily reducible Mn oxides and not on the total Mn concentration (Trebien et al., 2011).

Iron oxides can be also responsible for the adsorption of Cr(VI) because they carry high point of zero net charge (PZNC), and it can effectively adsorb oxyanions such as Cr(VI) in the pH

range of 2 to 7 (Zachara et al., 1989). Chromate adsorption in material enriched in kaolinite and crystalline iron oxide has shown to be greater at low pH (Zachara et al., 1989). The mechanism suggests the formation of outer-sphere complexes of Cr(VI) on the oxides surfaces (Fendorf, 1995). The chromium oxidation through outer-sphere complexes occurs when at least one water molecule of the hydration sphere is retained upon sorption (Borda and Sparks, 2008). Fe and Cr are positively correlated in bedrock, saprolitic ores, lateritic ores, soils and sediments (R^2= 0.84). Among the lateritic ores, OL1, OL3, OL5, OL7 and OL8, which are mainly composed of Fe oxides, present the higher content of exchangeable Cr(VI) (12 – 104 mg kg^{-1}) (Table 4.2). For the rest of the samples the range of variation of the exchangeable pool of Cr(VI) is smaller compared to the ores described earlier (0.7 – 21 mg kg^{-1}).

The equation [4] was adapted from Frei and Polat (2013) to determine the enrichment or depletion of chromium compared to the bedrock.

$$\Delta Cr = \frac{Cr_{sample} - Cr_{Bedrock}}{Cr_{Bedrock}} * 100 \quad \textbf{(4.4)}$$

where ∆Cr represents the change in concentration compared to the bedrock, and Cr_{Sample} and $Cr_{Bedrocks}$ the concentration of total Cr in g kg^{-1} in the samples and bedrock, respectively. Average gains (+∆) and losses (-∆) in Cr concentration relative to the bedrock are contained in Table 4.1. All the samples display an enrichment of Cr content compared to the bedrock. Previous studies have shown that enrichment or losses of chromium due to oxido-reduction processes can induce isotopic fractionation (Crowe et al., 2013; Frei and Polat, 2013; Wang et al., 2015a). Figure 4.6(c) displays the evolution of δ^{53}Cr according to the UMIA. Two end members are present, for one side the lateritic ores with enrichment in lighter ^{52}Cr isotopes and high index of alteration, and from the other side the saprolitic ores with incipient alteration and Cr enrichment in heavy ^{53}Cr. The enrichment of the lateritic ore in lighter isotopes can be explained by the removal of heavy and exchangeable Cr, leaving Cr negatively fractionated. On the contrary, the positive δ^{53}Cr in the saprolitic ores can be explained by re-deposition of mobilized isotopically heavy Cr (Crowe et al., 2013; Frei and Polat, 2013; Berger and Frei, 2014).

The weathered rocks are the only geological reservoir possessing negative δ^{53}Cr (Qin and Wang, 2017). This is observed in the samples collected, however the saprolitic ores are enriched in heavy isotopes. Farkaš et al. (2013) reported high δ^{53}Cr in serpentinites (up to +1.22 ‰) as a response of serpentinization processes that could shift altered peridotites to

isotopically high $\delta^{53}Cr$, which was interpreted as a result of reduction of isotopically heavier Cr(VI) in serpentinizing fluids. Wang et al. (2016) found that altered peridotite with lower Cr content had higher $\delta^{53}Cr$ values. They proposed two possibilities: a) light Cr isotopes are lost to fluids during serpentinization as a result of kinetic fractionation, leaving isotopically heavy Cr behind; or b) Cr was initially lost to fluids without isotopic fractionation, then isotopically heavy Cr was accumulated during later-stage sulfate reduction. The re-deposition of mobilized isotopically heavy Cr coupled with Cr enrichment can also explain this result (Crowe et al., 2013; Frei and Polat, 2013; Berger and Frei, 2014). Farkaš et al. (2013) have found weathered ultramafic rocks enriched in ^{53}Cr, which was attributed to reductive sequestration of ^{53}Cr-enriched Cr(VI) from the weathering fluid.

To better understand this, Figure 4.6(d) shows the balance between the isotopic signature of the total chromium and the corresponding extracted Cr(VI) (extraction performed with KH_2PO_4). For the saprolitic ores, the $\delta^{53}Cr$ for the total chromium (+0.97 ± 0.08‰) and the extracted Cr(VI) (+1.34 ± 0.07‰) is positive and there is a small difference between both values, indicating that the losses of heavy Cr(VI) in the saprolitic ores are negligible. This statement is in agreement with the incipient degree of alteration of the saprolitic ores. In contrast, for the lateritic ores the fractionation of total Cr (-0.76 ± 0.07‰) and Cr(VI) (+4.37 ± 0.06‰) is considerably higher. This occurs as a consequence of the loose of Cr(VI) enriched in heavy isotopes during weathering. This result agrees with Frei and Polat (2013) and Crowe et al. (2013), who affirm that the presence of oxygen in the atmosphere leads to oxidative weathering of Cr, where the ^{53}Cr-enriched Cr(VI) pool is removed by runoff and the residual soil remains depleted in ^{53}Cr.

4.4.3 Water rock interaction during natural weathering

Soils derived from serpentinite usually contain 90% solid Cr(III) oxy(hydr)oxides, with 10% adsorbed Cr(VI), and runoff at pH > 7 is dominated by dissolved Cr(VI) (Mcclain and Maher, 2016; Novak et al., 2017). In the stream 1 (out of the mining area), the total dissolved chromium concentration is 0.2 µg L^{-1}, while the total chromium concentration in the bulk sample is 8.67 µg L^{-1}, indicating that 97% of Cr present in the stream is associated to the suspended particulate matter. Gueguen et al. (2016) affirmed that several Cr species can be present in the suspended Cr, including adsorbed Cr(VI), adsorbed ligand-bound Cr(III) and colloidal Cr(III) and clay-bound Cr(III). The proportion of each pool listed above determines the Cr isotopic composition in suspended particulate matter.

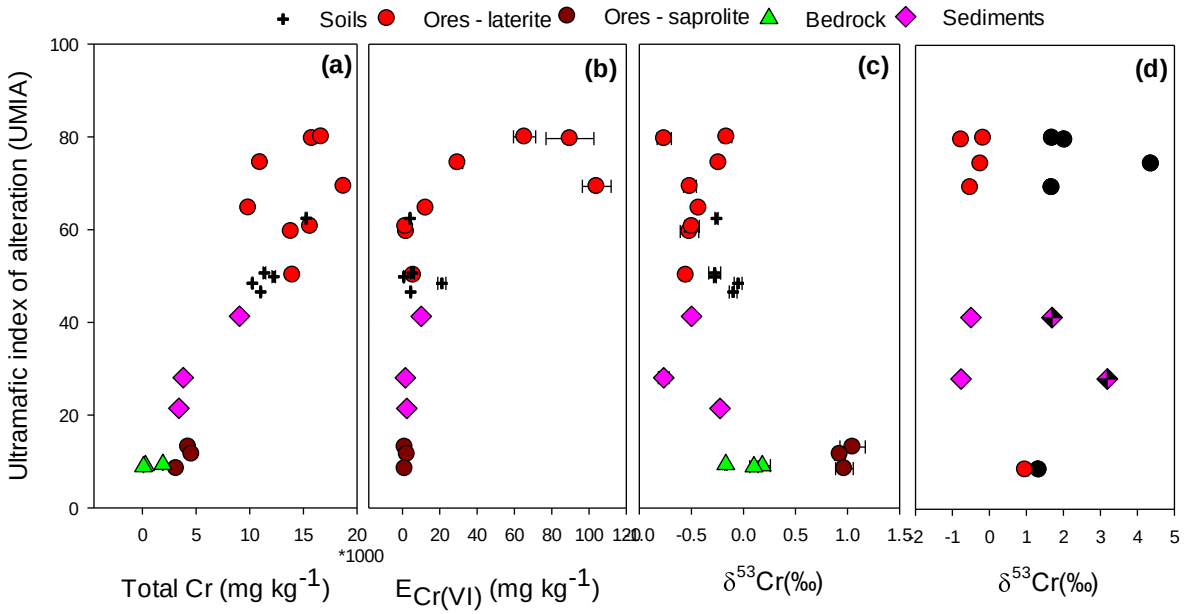

Figure 4.6 Evolution, according to the ultramafic index of alteration of a) the total Cr content, b) the exchangeable pool of Cr, c) the Cr isotopic composition of the bulk samples and d) the Cr isotopic composition of both bulk samples and corresponding extracted Cr(VI) (KH_2PO_4).

Suspended particulate matter is characterized to have positive δ^{53}Cr values, as was shown by Wu et al. (2017) in the Connecticut river (United States), which catchment is dominated by basalts. However, the Cr isotopic fractionation is negligible for the presence of potentially detrital Cr directly associated with the catchment lithology. Lithology is thought to be a dominant factor controlling weathering rates in watersheds, with mineral weatherability decreasing in the order from carbonate> mafic silicates> feldespars> quartz (White and Blum, 1995). The lithology of the area could explain the δ^{53}Cr composition (0.015 ± 0.09 ‰) of the SPM collected in stream 1, along with the inheritance of the high δ^{53}Cr from the dissolved Cr(VI) (+2.60 ± 0.04 ‰). The δ^{53}Cr values obtained in the present work cannot be compared with other ultramafic environments, due to the lack of studies related to the chromium isotopes fractionation associated to SPM in those areas.

Regarding the dissolved fraction, D'Arcy et al. (2016) interpreted positive δ^{53}Cr in the dissolved fraction can be interpreted from two aspects. First, it can be a direct expression of the Cr isotopic fractionation processes in an ultramafic profile. Second, it can be a result of additional processes during riverine transport such as redox fractionation processes, adsorption and/or mixing from riverine water with different δ^{53}Cr (D'Arcy et al., 2016). Another option is related to the Cr(VI) on Cr(III)-bearing oxy(hydr)oxides, where δ^{53}Cr decreases in the solid phase while residual aqueous Cr(VI) reaches streams and rivers (Wang et al.,

2015b). However, Cr fractionation does not exceed 0.3‰ and requires long-term contact between Cr(VI) and Cr(III) oxy(hydr)oxides (D'Arcy et al., 2016). If in the stream 1 the positive δ^{53}Cr is explained by the oxidation of Cr(III) to Cr(VI), one should consider that the large activation energy required for this transformation will not show a high fractionation (Zink et al., 2010). Wang et al. (2015) affirm that the fractionation of solid Cr(III) is expected to be small due to a "rind effect". Each micro-layer of the Cr(III) oxy(hydr)oxide particles is essentially completely oxidized leading to limited isotopic fractionation. The high content of Fe in stream 1, besides the large Cr fractionation observed, could suggest, the reduction of Cr(VI) to Cr(III), as one of the dominant processes leaving behind Cr(VI) enriched in ^{53}Cr. The release of Cr(III) during weathering, which may decrease the overall balance of the δ^{53}Cr in the dissolved fraction has also to be considered (D'Arcy et al., 2016).

4.4.4 Accelerated weathering due to mining activities

During the ore exploitation in mines, there is an appreciable quantity of material removed and transported, which can be compared with extensive physical erosion. White and Blum (1995) describe physical erosion as one of the factors controlling weathering rates. The concentration of suspended particulate matter in the water bodies inside the mine (3.3 – 316 mg L^{-1}) is higher compared to stream 1, localized in a similar but non affected system (1.1 mg L^{-1}). This evidences the particle contribution due to extraction, transport and stockpiling of the residues produced during mining processes. SPM in the water bodies inside the mine was enriched in Cr with concentrations between 24 and 1064 µg L^{-1}. The Cr enrichment was even reflected in the dissolved fraction with concentration up to 737 µg L^{-1}. Wu et al. (2017) observed that oxide loads did not have a significant influence on the δ^{53}Cr of suspended Cr, as adsorption would inherit dissolved Cr(VI) δ^{53}Cr and this should have made the suspended Cr isotopically heavy. This result agrees with the δ^{53}Cr of particulate Cr of stream 2 (+0.94 ± 0.09‰), which reflects enrichment in isotopically heavy Cr. In contrast, particulate Cr in stream 1 remains unfractionated.

The eroded material coming from the overburden, waste rock, and extracted ores are stored in the ponds and therefore its sediments represents a mixture. Lateritic ores (-0.76 ± 0.07‰ to -0.16 ± 0.05‰) and soils (-0.05 ± 0.04‰ to -0.28 ± 0.06‰) are enriched in light isotopes, which explain negative δ^{53}Cr found in sediments (Figure 4.6(c)). In pond 1, particulate Cr (-0.38 ± 0.08‰) and Cr in the sediments (-0.50 ± 0.04‰) are negatively fractionated, the second one is slightly higher probably due to the oxidation of Cr(III) and the release of Cr(VI) enriched in heavy isotopes. This hypothesis suggests that sediments in the ponds represent a source of isotopically heavy Cr(VI) for the water column.

The total dissolved chromium in the groundwater before and after the smelter area, is enriched in ^{53}Cr with $\delta^{53}Cr$ values of +2.18 ± 0.08‰ and 2.19 ± 0.16‰, respectively (Figure 4.4). Those values are within the $\delta^{53}Cr$ range (0.7 to 5.1‰) reported in 32 uncontaminated wells studied by Izbicki et al. (2008) and native groundwaters (1.1 to 5.8‰) reported by Coplen et al. (2002). The significant fractionation obtained in the samples may occur either on the surface of the mineral grains or it may occur in solution as dissolved oxygen concentrations decline and Cr is removed from solution as Cr(III) (Izbicki et al., 2008). In the particulate fraction, the depletion in ^{53}Cr is higher before (-0.55 ± 0.06 ‰) than after the smelter area (-0.34 ± 0.05‰) (Figure 4.4). This result indicates the liberation of Cr(III) is favored as a results of the reductive smelting process of the ore for the production of Fe-nickel (smelting at 1600°C) (Economou-Eliopoulos et al., 2016). The depletion of oxygen in the groundwater also can favor the reduction of Cr(VI) to Cr(III) and the consequent decrease of the $\delta^{53}Cr$ value.

In order to verify the contribution of the Cr(VI) from the solid residues and ores to the water bodies, the isotopic signature of the Cr(VI) extracted with KH_2PO_4 was analyzed for some samples. Figure 4.7 shows the distribution of the $\delta^{53}Cr$ for solids, the Cr(VI) extracted and the surface waters. The range of variation for the surface waters is within the range of the extracted Cr(VI).

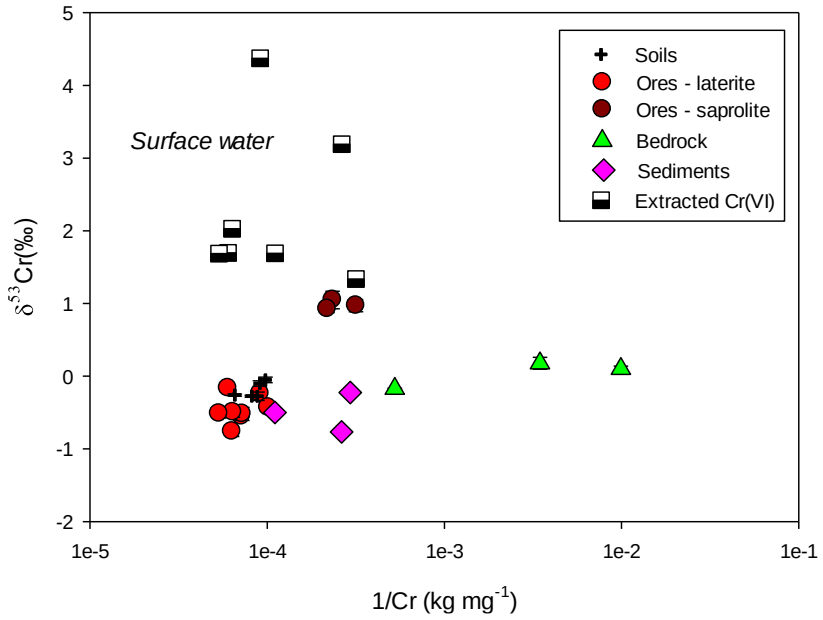

Figure 4.7 Total chromium concentration in solid samples and its correspondent $\delta^{53}Cr$. The blue band represents the $\delta^{53}Cr$ range of variation in surface water, which is within the range found for Cr(VI) extracted with KH_2PO_4.

It indicates that the enrichment of ^{53}Cr in the surface and even in the groundwater is associated to the release of Cr(VI) from the Cr(III) oxidation in the solid phases. Part of the contribution is related to natural weathering, where we observed an increase in the concentration of Cr(VI) in more altered materials and the correspondent depletion of ^{53}Cr in the remaining solid. But there is also an important contribution directly linked with erosion promoted by the mining processes, accelerating the natural weathering. In the pristine area, stream 1, the total chromium concentration is lower (0.20 µg L^{-1}) compared with the rest of surface waters evaluated. However, the $\delta^{53}Cr$ remains within the range of variation of the Cr(VI) extracted (Figure 4S.2).

4.5 CONCLUSIONS

This study contributed to the understanding of the behavior of Cr isotopes in ultramafic environments and more specifically in mining areas. The reconstruction of the stratigraphy column indicated the presence of material with different degree of alteration (ultramafic index of alteration - UMIA). The results of the UMIA reflected an intense mineralogical transformation of the lateritic ores and soils. In contrast, the less altered material was the saprolitic ores and the bedrock which are composed mainly by Mg and Si. Sediments have an intermediary degree of alteration, located between lateritic and saprolitic ores.

The most altered materials were enriched in Cr (10 – 18 g kg^{-1}) and Fe (85 – 536 g kg^{-1}) as a result of Cr(III) complexation and Cr(VI) adsorption on Fe oxides and hydroxides. The exchangeable pool of Cr(VI) ($E_{Cr(VI)}$) also increased with the degree of alteration. Mineral phases, in particular Fe oxides, control the release of Cr(VI). A significant positive correlation of total manganese with total chromium content (R^2=0.9) and UMIA (R^2=0.8) suggests Mn oxides play a role in Cr(III) oxidation.

For the saprolitic ores, the $\delta^{53}Cr$ for the total chromium (+0.97 ± 0.08‰) and the extracted Cr(VI) (+1.34 ± 0.07‰) is positive and there is a small difference between both values, indicating that the losses of heavy Cr(VI) in the saprolitic ores are negligible. The positive $\delta^{53}Cr$ in the saprolitic ores can be explained by re-depositioning of mobilized isotopically heavy Cr. In contrast, for the lateritic ores the difference between the fractionation of total Cr (-0.76 ± 0.07‰) and the extracted Cr(VI) (+4.37 ± 0.06‰) is considerably higher. This occurs as a consequence of the loss of isotopically heavy and exchangeable Cr(VI) during weathering, leaving Cr negatively fractionated.

The range of variation of $\delta^{53}Cr$ for the surface waters (+ 2.10 ± 0.04 to + 3.66 ± 0.04 ‰) is within the range of the extracted Cr(VI) (+ 1.34 ± 0.07 to + 4.37 ± 0.06 ‰). It indicates that

the enrichment of ^{53}Cr in the surface and even in the groundwater is associated to the release of Cr(VI) from the Cr(III) oxidation in the solid phases. Part of the contribution is related to natural weathering, but there is also an important contribution directly link with erosion promoted by the mining processes, accelerating the natural weathering. In the pristine area (stream 1) the total chromium concentration is lower (0.20 µg L^{-1}) compared with the rest of surface waters evaluated. However, the $\delta^{53}Cr$ remains within the range of variation of the Cr(VI) extracted. This suggests that $\delta^{53}Cr$ can potentially be used as a tracer of sources in the dissolved fraction. However, its interpretation must be accompanied with other parameters like total chromium concentration in the dissolved fraction together with Fe, Mn, organic carbon and chromium speciation.

4.6 BIBLIOGRAPHY

Aiglsperger, T., Proenza, J.A., Lewis, J.F., Labrador, M., Svojtka, M., Rojas-purón, A., Longo, F., Jana, Ď., 2016. Critical metals (REE, Sc, PGE) in Ni laterites from Cuba and the Dominican Republic 73, 127–147. doi:10.1016/j.oregeorev.2015.10.010

Babechuk, M.G., Widdowson, M., Kamber, B.S., 2014. Quantifying chemical weathering intensity and trace element release from two contrasting basalt pro fi les , Deccan Traps , India 363, 56–75.

Becquer, T., Quantin, C., Boudot, J.P., 2010. Toxic levels of metals in Ferralsols under natural vegetation and crops in New Caledonia. Eur. J. Soil Sci. 61, 994–1004.

Becquer, T., Quantin, C., Rotte-Capet, S., Ghanbaja, J., Mustin, C., Herbillon, A.J., 2006. Sources of trace metals in Ferralsols in New Caledonia. Eur. J. Soil Sci. 57, 200–213.

Becquer, T., Quantin, C., Sicot, M., Boudot, J.P., 2003. Chromium availability in ultramafic soils from New Caledonia. Sci. Total Environ. 301, 251–261. doi:10.1016/S0048-9697(02)00298-X

Berger, A., Frei, R., 2014. The fate of chromium during tropical weathering: A laterite profile from central madagascar. Geoderma 213, 521–532. doi:10.1016/j.geoderma.2013.09.004

Birck, J.L., Allegre, C.J., 1988. Manganese-chromium isotope systematics and the development of the early Solar System. Nature 331, 579–584.

Bolaños-Benítez, V., van Hullebusch, E.D., Garnier, J., Quantin, C., Tharaud, M., Lens, P.N.L., Sivry, Y., 2018. Assessing chromium mobility in natural surface waters: Colloidal contribution to the isotopically exchangeable pool of chromium (EwCrvalue). Appl. Geochemistry 92, 19–29. doi:10.1016/j.apgeochem.2018.02.007

Choppala, G., Bolan, N., Park, J.H., 2013. Chromium Contamination and Its Risk Management in Complex Environmental Settings, Advances in Agronomy. Elsevier. doi:10.1016/B978-0-12-407686-0.00002-6

Coleman, R.G., Jove, C., 1993. Geological origin of serpentinites, in: The Vegetation of Ultramafic (Serpentine) Soils. Andover, NH, pp. 1–17.

Coplen, T.B., Hopple, J. a, Böhlke, J.K., Peiser, H.S., Rieder, S.E., Krouse, H.R., Rosman, K.J.R., Ding, T., Vocke, R.D.J., Révész, K.M., Lamberty, A., Taylor, P., Bièvre, P. De, 2002. Compilation of minimum and maximum isotope ratios of selected elements in naturally occurring terrestrial materials and reagents, U.S. Geol. Surv. Water Resour. Invest. Rep.

Crowe, S.A., Døssing, L.N., Beukes, N.J., Bau, M., Kruger, S.J., Frei, R., Canfield, D.E., 2013. Atmospheric oxygenation three billion years ago. Nature 501, 535–538. doi:10.1038/nature12426

D'Arcy, J., Babechuk, M.G., Døssing, L.N., Gaucher, C., Frei, R., 2016. Processes controlling the chromium isotopic composition of river water: Constrains from basaltic river catchments. Geochim. Cosmochim. Acta 186, 296–315. doi:10.1016/j.gca.2016.04.027

Døssing, L.N., Dideriksen, K., Stipp, S.L.S., Frei, R., 2011. Reduction of hexavalent chromium by ferrous iron: A process of chromium isotope fractionation and its relevance to natural environments. Chem. Geol. 285, 157–166. doi:10.1016/j.chemgeo.2011.04.005

Economou-Eliopoulos, M., Frei, R., Megremi, I., 2016. Potential leaching of Cr (VI) from laterite mines and residues of metallurgical products (red mud and slag): An integrated approach. J. Geochemical Explor. 162, 40–49. doi:10.1016/j.gexplo.2015.12.007

Ellis, A.S., Johnson, T.M., Bullen, T.D., 2002. Chromium Isotopes and the Fate of Hexavalent Chromium in the Environment. Science. 295, 2060–2062. doi:10.1126/science.1068368

Ent, A. Van Der, Cardace, D., Tibbett, M., Echevarria, G., 2018. Catena Ecological implications of pedogenesis and geochemistry of ultrama fi c soils in Kinabalu Park (Malaysia). Catena 160, 154–169. doi:10.1016/j.catena.2017.08.015

Ettler, V., Kvapil, J., Šebek, O., Johan, Z., Mihaljevič, M., Ratié, G., Garnier, J., Quantin, C., 2015. Leaching behaviour of slag and fly ash from laterite nickel ore smelting (Niquelândia, Brazil). Appl. Geochemistry 64, 118–127. doi:10.1016/j.apgeochem.2015.09.019

Farkaš, J., Chrastný, V., Novák, M., Čadkova, E., Pašava, J., Chakrabarti, R., Jacobsen, S.B., Ackerman, L., Bullen, T.D., 2013. Chromium isotope variations ($\delta^{53/52}$Cr) in mantle-derived sources and their weathering products: Implications for environmental studies and the evolution of $\delta^{53/52}$Cr in the Earth's mantle over geologic time. Geochim. Cosmochim. Acta 123, 74–92. doi:10.1016/j.gca.2013.08.016

Fendorf, S.E., 1995. Surface reactions of chromium in soils and waters. Geoderma 67, 55–

71. doi:10.1016/0016-7061(94)00062-F

Ferreirafilho, C., Nilson, a, Naldrett, a, 1992. The Niquelândia Mafic-Ultramafic Complex, Goias, Brazil: a contribution to the ophiolite X stratiform controversy based on new geological and structural data. Precambrian Res. 59, 125–143. doi:10.1016/0301-9268(92)90054-R

Frei, R., Polat, A., 2013. Chromium isotope fractionation during oxidative weathering — Implications from the study of a Paleoproterozoic (ca. 1.9 Ga) paleosol, Schreiber Beach, Ontario, Canada. Precambrian Res. 224, 434–453. doi:10.1016/j.precamres.2012.10.008

Garnier, J., Quantin, C., Echevarria, G., Becquer, T., 2009a. Assessing chromate availability in tropical ultramafic soils using isotopic exchange kinetics. J. Soils Sediments 9, 468–475. doi:10.1007/s11368-009-0062-4

Garnier, J., Quantin, C., Guimaraes, E., Becquer, T., 2008. Can chromite weathering be a source of Cr in soils? Mineral. Mag. 72, 49–53.

Garnier, J., Quantin, C., Guimarães, E., Garg, V.K., Martins, E.S., Becquer, T., 2009b. Understanding the genesis of ultramafic soils and catena dynamics in Niquelândia, Brazil. Geoderma 151, 204–214. doi:10.1016/j.geoderma.2009.04.020

Garnier, J., Quantin, C., Guimarães, E.M., Vantelon, D., Montargès-Pelletier, E., Becquer, T., 2013. Cr(VI) genesis and dynamics in Ferralsols developed from ultramafic rocks: The case of Niquelândia, Brazil. Geoderma 193–194, 256–264. doi:10.1016/j.geoderma.2012.08.031

Garnier, J., Quantin, C., Martins, E.S., Becquer, T., 2006. Solid speciation and availability of chromium in ultramafic soils from Niquelândia, Brazil. J. Geochemical Explor. 88, 206–209. doi:10.1016/j.gexplo.2005.08.040

Gueguen, B., Reinhard, C.T., Algeo, T.J., Peterson, L.C., Nielsen, S.G., Wang, X., Rowe, H., Planavsky, N.J., 2016. The chromium isotope composition of reducing and oxic marine sediments. Geochim. Cosmochim. Acta 184, 1–19. doi:10.1016/j.gca.2016.04.004

Izbicki, J.A., Bullen, T.D., Martin, P., Schroth, B., 2012. Delta Chromium-53/52 isotopic composition of native and contaminated groundwater, Mojave Desert, USA. Appl. Geochemistry 27, 841–853. doi:10.1016/j.apgeochem.2011.12.019

Izbicki, J. a., Ball, J.W., Bullen, T.D., Sutley, S.J., 2008. Chromium, chromium isotopes and selected trace elements, western Mojave Desert, USA. Appl. Geochemistry 23, 1325–1352. doi:10.1016/j.apgeochem.2007.11.015

Johnson, T.M., Bullen, T.D., 2004. Mass-Dependent Fractionation of Selenium and Chromium Isotopes in Low-Temperature Environments. Rev. Mineral. Geochemistry 55, 289–317. doi:10.2138/gsrmg.55.1.289

Kaprara, E., Kazakis, N., Simeonidis, K., Coles, S., Zouboulis, A.I., Samaras, P., Mitrakas,

M., 2015. Occurrence of Cr (VI) in drinking water of Greece and relation to the geological background. J. Hazard. Mater. 281, 2–11. doi:10.1016/j.jhazmat.2014.06.084

Leita, L., Margon, A., Pastrello, A., Arčon, I., Contin, M., Mosetti, D., 2009. Soil humic acids may favour the persistence of hexavalent chromium in soil. Environ. Pollut. 157, 1862–1866. doi:10.1016/j.envpol.2009.01.020

Lombi, E., Hamon, R.E., Mcgrath, S.P., Mclaughlin, M.J., 2003. Lability of Cd, Cu, and Zn in Polluted Soils Treated with Lime, Beringite, and Red Mud and Identification of a Non-Labile Colloidal Fraction of Metals Using Isotopic Techniques. Environ. Sci. Technol. 37, 979–984.

Marzouk, E.R., Chenery, S.R., Young, S.D., 2013. Measuring reactive metal in soil : a comparison of multi-element isotopic dilution and chemical extraction. Eur. J. Soil Sci. 64, 526–536. doi:10.1111/ejss.12043

Mcclain, C.N., Maher, K., 2016. Chromium fluxes and speciation in ultramafic catchments and global rivers. Chem. Geol. 426, 135–157. doi:10.1016/j.chemgeo.2016.01.021

Moore, P., 2012. Anglo's new nickel. Int. Min. 20–24.

Moraes, R., Fuck, R.A., 2000. Ultra-high-temperature metamorphism in Central Brazil: The Barro Alto complex. J. Metamorph. Geol. 18, 345–358. doi:10.1046/j.1525-1314.2000.00262.x

Nesbitt, H.W., Young, G.M., 1982. Early proterozoic climates and plate motions inferred from major element chemistry of lutites. Nature 299, 715–717.

Novak, M., Chrastny, V., Cadkova, E., Farkas, J., Bullen, T.D., Tylcer, J., Szurmanova, Z., Cron, M., Prechova, E., Curik, J., Stepanova, M., Pasava, J., Erbanova, L., Houskova, M., Puncochar, K., Hellerich, L.A., 2014. Common occurrence of a positive $\delta^{53}Cr$ shift in central european waters contaminated by geogenic/industrial chromium relative to source values. Environ. Sci. Technol. 48, 6089–6096. doi:10.1021/es405615h

Novak, M., Chrastny, V., Sebek, O., Martinkova, E., Prechova, E., Curik, J., Veselovsky, F., Stepanova, M., Dousova, B., Buzek, F., Farkas, J., Andronikov, A., Cimova, N., Houskova, M., 2017. Chromium isotope fractionations resulting from electroplating, chromating and anodizing: Implications for groundwater pollution studies. Appl. Geochemistry 80, 134–142. doi:10.1016/j.apgeochem.2017.03.009

Oze, C., Bird, D.K., Fendorf, S., 2007. Genesis of hexavalent chromium from natural sources in soil and groundwater. Proc. Natl. Acad. Sci. 104, 6544–6549. doi:10.1073/pnas.0701085104

Oze, C., Fendorf, S., Bird, D.K., Coleman, R.G., 2004. Chromium Geochemistry of Serpentine Soils. Int. Geol. Rev. 46, 97–126. doi:10.2747/0020-6814.46.2.97

Oze, C.J., 2003. Chromium geochemistry of serpentines and serpentine soils, PhD thesis. Submitted to Stanford University, Stanford, USA. 198 p.

Paulukat, C., Døssing, L.N., Mondal, S.K., Voegelin, A.R., Frei, R., 2015. Oxidative release of chromium from Archean ultramafic rocks, its transport and environmental impact – A Cr isotope perspective on the Sukinda valley ore district (Orissa, India). Appl. Geochemistry 59, 125–138. doi:10.1016/j.apgeochem.2015.04.016

Qin, L., Wang, X., 2017. Chromium Isotope Geochemistry. Rev. Mineral. Geochemistry 82, 379–414.

Raous, S., Becquer, T., Garnier, J., Martins, É.D.S., Echevarria, G., Sterckeman, T., 2010. Mobility of metals in nickel mine spoil materials. Appl. Geochemistry 25, 1746–1755. doi:10.1016/j.apgeochem.2010.09.001

Raous, S., Echevarria, G., Sterckeman, T., Hanna, K., Thomas, F., Martins, E.S., Becquer, T., 2013. Potentially toxic metals in ultramafic mining materials: Identification of the main bearing and reactive phases. Geoderma 192, 111–119. doi:10.1016/j.geoderma.2012.08.017

Ratié, G., Jouvin, D., Garnier, J., Rouxel, O., Miska, S., Guimarães, E., Vieira, L.C., Sivry, Y., Zelano, I., Pelletier, E.M., Thil, F., Quantin, C., 2015. Nickel isotope fractionation during tropical weathering of ultramafic rocks. Chem. Geol. 402, 68–76. doi:10.1016/j.chemgeo.2015.02.039

Ratié, G., Quantin, C., Jouvin, D., Calmels, D., Ettler, V., Sivry, Y., Vieira, L.C., Ponzevera, E., Garnier, J., 2016. Nickel isotope fractionation during laterite Ni ore smelting and refining: Implications for tracing the sources of Ni in smelter-affected soils. Appl. Geochemistry 64, 136–145. doi:10.1016/j.apgeochem.2015.09.005

Rigopoulos, I., Tsikouras, B., Pomonis, P., Hatzipanagiotou, K., 2015. Assessment of the engineering behavior of ultramafic and mafic rocks using chemical indices. Eng. Geol. 196, 222–237. doi:10.1016/j.enggeo.2015.07.019

Schauble, E., Rossman, G.R., Taylor, H.P., 2004. Theoretical estimates of equilibrium chromium-isotope fractionations. Chem. Geol. 205, 99–114. doi:10.1016/j.chemgeo.2003.12.015

Schopka, H.H., Derry, L.A., Arcilla, C.A., 2011. Chemical weathering , river geochemistry and atmospheric carbon fluxes from volcanic and ultramafic regions on Luzon Island , the Philippines. Geochim. Cosmochim. Acta 75, 978–1002. doi:10.1016/j.gca.2010.11.014

Shahid, M., Shamshad, S., Rafiq, M., Khalid, S., Bibi, I., Niazi, N.K., Dumat, C., Rashid, M.I., 2017. Chromium speciation, bioavailability, uptake, toxicity and detoxification in soil-plant system: A review. Chemosphere 178, 513–533. doi:10.1016/j.chemosphere.2017.03.074

Tina, S., Echevarria, G., Becquer, T., Ghanbaja, J., Leclerc-cessac, E., Morel, J., 2006. Control of nickel availability by nickel bearing minerals in natural and anthropogenic soils. Geoderma 136, 28–37. doi:10.1016/j.geoderma.2006.01.008

Trebien, D.O.P., Bortolon, L., Tedesco, M.J., Bissani, C.A., Camargo, F.A.O., 2011. Environmental Factors Affecting Chromium-Manganese Oxidation-Reduction Reactions in Soil ∗ 1 21, 84–89.

Trinquier, A., Birck, J.-L., Allègre, C.J., 2008. High-precision analysis of chromium isotopes in terrestrial and meteorite samples by thermal ionization mass spectrometry. J. Anal. At. Spectrom. 23, 1565. doi:10.1039/b809755k

Vojcu, G., Bardoux, M., 1997. Mineralogical norm calculations applied tropical weathering profiles. Mineral. Mag. 61, 185–196.

Wang, X., Johnson, T.M., Ellis, A.S., 2015a. Equilibrium isotopic fractionation and isotopic exchange kinetics between Cr(III) and Cr(VI). Geochim. Cosmochim. Acta 153, 72–90. doi:10.1016/j.gca.2015.01.003

Wang, X., Johnson, T.M., Ellis, A.S., 2015b. Equilibrium isotopic fractionation and isotopic exchange kinetics between Cr(III) and Cr(VI). Geochim. Cosmochim. Acta 153, 72–90. doi:10.1016/j.gca.2015.01.003

Wang, X., Planavsky, N.J., Reinhard, C.T., Zou, H., Ague, J.J., Wu, Y., Gill, B.C., Schwarzenbach, E.M., Peucker-Ehrenbrink, B., 2016. Chromium isotope fractionation during subduction-related metamorphism, black shale weathering, and hydrothermal alteration. Chem. Geol. 423, 19–33. doi:10.1016/j.chemgeo.2016.01.003

White, A.F., Blum, A.E., 1995. Effects of climate on chemical weathering in watersheds. Geochim. Cosmochim. Acta 59, 1729–1747. doi:10.1016/0016-7037(95)00078-E

Wu, W., Wang, X., Reinhard, C.T., Planavsky, N.J., 2017. Chromium isotope systematics in the Connecticut River. Chem. Geol. 456, 98–111. doi:10.1016/j.chemgeo.2017.03.009

Yang, J., Cawood, P.A., Du, Y., Li, W., Yan, J., 2016. Reconstructing Early Permian tropical climates from chemical weathering indices 739–751. doi:10.1130/B31371.1

Zachara, J.M., Ainsworth, C.C., Cowan, C.E., Resch, C.T., 1989. Adsorption of Chromate by Subsurface Soil Horizons. Soil Sci. Soc. Am. J. 53, 418–428. doi:10.2136/sssaj1989.03615995005300020018x

Zelano, I., Sivry, Y., Quantin, C., Gélabert, A., Tharaud, M., Nowak, S., Garnier, J., Malandrino, M., Benedetti, M.F., 2015. Study of Ni exchangeable pool speciation in ultramafic and mining environments with isotopic exchange kinetic data and models. Appl. Geochemistry 64, 146–156. doi:10.1016/j.apgeochem.2015.09.021

Zelano, I., Sivry, Y., Quantin, C., Gélabert, a., Tharaud, M., Jouvin, D., Montarges-Pelletier, E., Garnier, J., Pichon, R., Nowak, S., Miska, S., Abollino, O., Benedetti, M.F., 2013. Colloids and suspended particulate matters influence on Ni availability in surface waters of impacted ultramafic systems in Brazil. Colloids Surfaces A Physicochem. Eng. Asp. 435, 36–47. doi:10.1016/j.colsurfa.2013.02.051

Zink, S., Schoenberg, R., Staubwasser, M., 2010. Isotopic fractionation and reaction kinetics

between Cr(III) and Cr(VI) in aqueous media. Geochim. Cosmochim. Acta 74, 5729–5745. doi:10.1016/j.gca.2010.07.015

4.7 SUPPLEMENTARY DATA

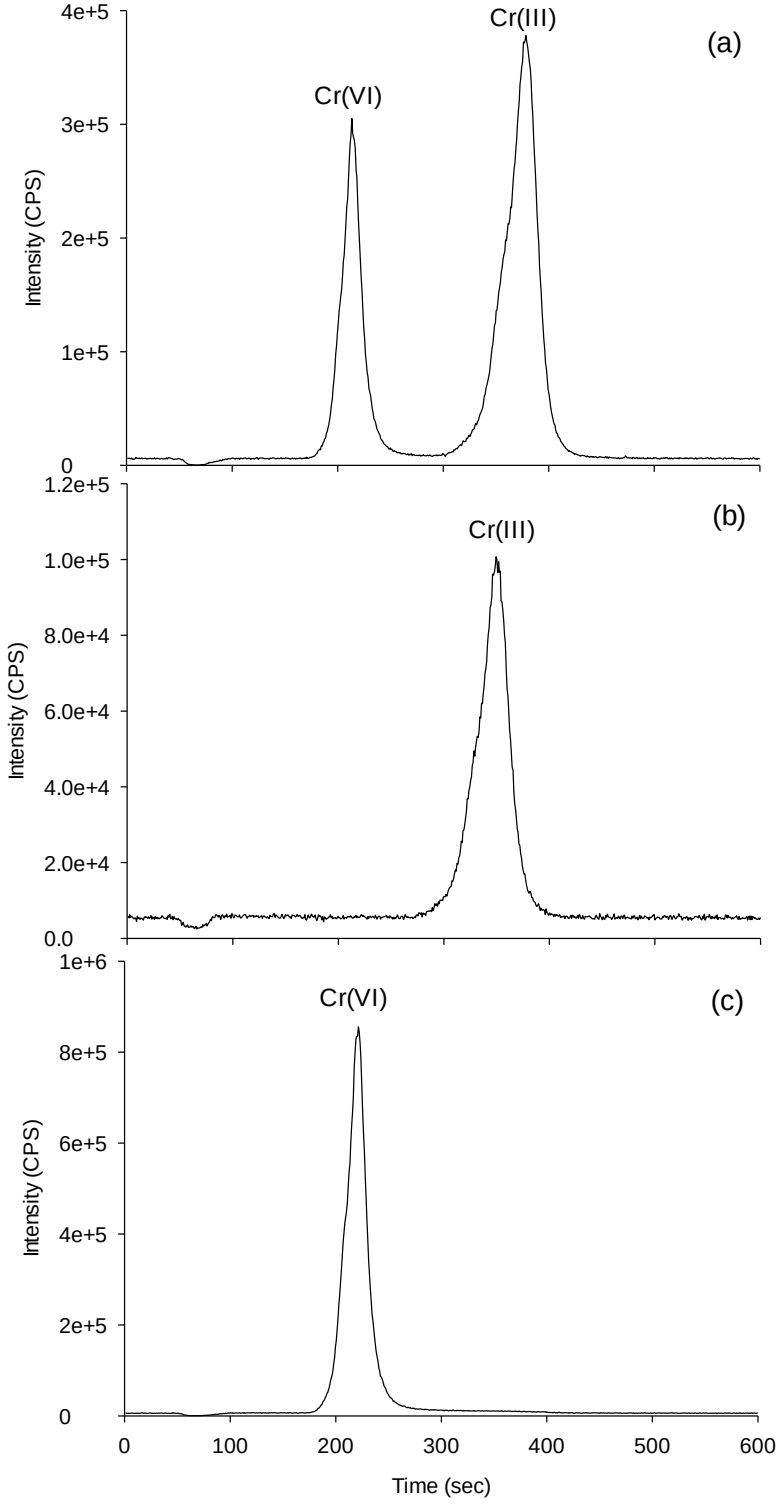

Figure S4.1. Typical Cr speciation obtained with LC-ICP-MS, for (a) standard with 2.3 ppb of Cr(VI) and 5.0 ppb of Cr(III); (b) Cr(III) extracted with 1M KCl for ore OL1 and (c) Cr(VI) extracted with 0.1M KH_2PO_4 for OL1.

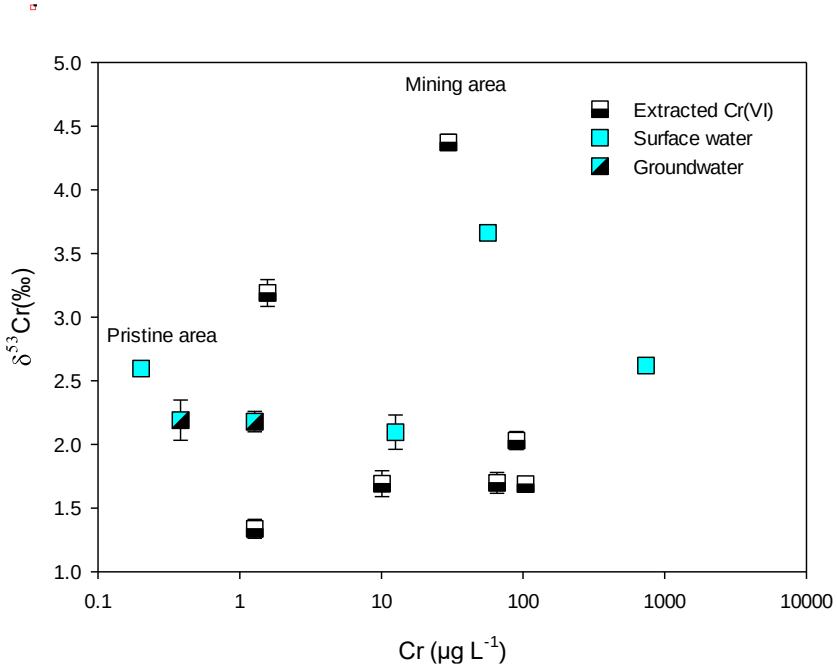

Figure S4.2 Total dissolved chromium concentration vs δ^{53}Cr in the dissolved fraction for surface and groundwater. In the pristine area, stream 1 represents the surface water and the piezometer before the smelter the groundwater.

CHAPTER 5

Chromium availability and mobility in soils affected by mineral extraction

CHAPTER 5

5.1 INTRODUCTION

The presence of heavy metals in soils is a current concern for the environment. The presence of metals and metalloids in soils is not only related to anthropogenic sources, but also they can be geogenic origin (Mpouras et al., 2017). Geogenic chromium (Cr) can be highly concentrated in soils derived from ultramafic rocks. Compared with heavy metals of anthropogenic origin, those of lithogenic origin are less mobile in soils. However, increased bioavailability of Cr is a potential environmental hazard in serpentine soils (Becquer et al., 2003; Garnier et al., 2006). Due to this natural enrichment, ultramafic areas are mined for mineral extraction, such as chromite ($FeCr_2O_4$), which is the main Cr bearing mineral phase. Mining activities involve mineral extraction and processing, which can contaminate soils, surface and groundwater bodies in the vicinity. Godgul and Sahu (1995) studied the pollution produced by chromite mine in Sukinda valley and showed that despite the chromite is resistant to alteration, its oxidation represents a significant source of Cr dispersion to the environment. Regardless the closure of mining activities, soil remains polluted as it was shown by Krishna et al. (2013) who found soils around abandoned chromite mine with Cr, Ni and Co enrichment factors higher than the soil quality guideline (SQGL). Similarly, Kien et al. (2010) observed high enrichment on Cr (5750 mg kg^{-1}), Co (375 mg kg^{-1}) and Ni (5590 mg kg^{-1}) on paddy fields around the largest chromite mine in Vietnam. Solgi and Parmah (2015) observed that soil contamination, by Cr and Ni, increases with distance from the mining area, demonstrating how pollutants can be transported to long distances from the source.

To study Cr mobility and availability in the environment, it is necessary to understand the bearing phases which can be involved in Cr adsorption and release in ultramafic areas. Several studies on lateritic regolith developed on ultramafic rocks such as ones in New Caledonia, have shown several Cr bearing phases including Cr(III)-bearing goethite, Cr-bearing lizardite and Cr-bearing enstatite (Becquer et al., 2003; Fandeur et al., 2009; Garnier et al., 2009). In those soils, the main source of exchangeable Cr(VI) are the Fe-oxides with lower concentrations of exchangeable Cr(VI) in the surface horizons than in the deeper ones. In Niquelândia Ferralsols (Goiás, Brazil), Garnier et al. (2009b) have shown a large Cr availability under the hexavalent form, mainly controlled by amorphous Fe oxides.

Besides the role of Cr mineral phases, chromium oxidation-reduction reactions also determine the immobilization and release of Cr(VI) to the environment. In natural waters, sediments and soils, the significant redox couples include (reducing agents/ oxidation agents): H_2O/O_2 (aq), Mn(II)/Mn(IV), NO_2^-/NO_3^-, Fe(II)/Fe(III), S_2^-/SO_4^{2-} and CH_4/CO_2. Manganese can act as a transporter of electrons between oxygen and Cr(III) and therefore Mn indirectly oxidizes Cr(III) to Cr(VI) (Choppala et al., 2013). The oxidation rate increases as pH decreases and the surface area to solution volume increases (Stanin, 2004). Cr(VI) can also be naturally reduced to Cr(III), process that is called by James and Bartlett (1988) and Kotaś and Stasicka (2000) “dechromification”. Cr(VI) reduction, can be catalyzed by reducers such as Fe(II) or S^{2-}. Cr oxidation-reduction processes have been shown to induce isotopic fractionation, which depends on the difference between their bonding environments. At isotopic equilibrium, heaver isotopes (e.g. ^{53}Cr) are enriched in species with stronger bonds (e.g. CrO_4^{2-}), whereas lighter isotopes (e.g. ^{52}Cr) are enriched in species with weaker bonds (e.g. $Cr(H_2O)_6^{3+}$) (Qin and Wang, 2017; Schauble et al., 2004). During reduction, the lighter isotopes are preferentially reduced, resulting in an enrichment of ^{53}Cr relative to ^{52}Cr values in the remaining Cr(VI) pools (Economou-Eliopoulos et al., 2014). This enrichment is measured as the change in the ratio of $^{53}Cr/^{52}Cr$ and is expressed as $\delta^{53}Cr$ values in units per mil (‰) relative to the standard (Ellis et al., 2002). In spite of, Cr(III) enrichment in lighter isotopes, some studies have shown that Cr(III) can be enriched in heavy isotopes after a re-deposition and subsequently reduction of heavy Cr(VI) (Crowe et al., 2013; Frei and Polat, 2013; Berger and Frei, 2014).

The oxidation of Cr(III) with the consequent production of Cr(VI), and its release to the environment end up in surface and groundwater pollution. The study of Dhakate et al. (2008) evidenced the presence of hexavalent Cr in the seepages of chromite mines and the Damsala Nala river. Sediments of Damsala nala river and creeks carrying mine discharges have also shown high degree of contamination with Cr(VI) (Equeenuddin and Pattnaik, 2017). Most of studies carried out so far, focused on current mineral extraction, but the long term impact of chromite extraction has not been evaluated yet, which is important specially for Cr(VI) production due to its mobility and toxicity (Choppala et al., 2013; Fendorf, 1995; Oze et al., 2004). In addition Cr contamination studies in ultramafic areas (Garnier et al., 2013, 2009, 2008, Raous et al., 2013, 2010) do not include isotopic measurements to understand processes controlling Cr fate.

Considering the lack of information about long term impact of antique mineral extraction in Cr in soil, the toxicity of Cr(VI) in the environment, its redox sensitivity and the changes in the isotopic composition, this work focuses in the understanding of the Cr comportment in soils

affected by antique mining activities. Cromínia, an antique chromite exploitation area was selected as study area because it is a small mine which facilitated the identification of chromite extraction and the non-affected area. Other advantage is that mining activities have stopped few decades earlier, thus no artifacts regarding recent activities are present. In addition, two creeks cross the area, which allows establishing the connection between the potential release of Cr from the solid compartment and its presence in the liquid phase. All those benefits enable a better understanding of Cr dynamics, which can be extrapolated to a bigger scale.

5.2 MATERIAL AND METHODS

5.2.1 Study site

This study was carried out in Cromínia, (Mairipotaba, Goiás state, Brazil) on soils derived from meta-ultramafic rocks associated to an ophiolitic mixture (Angeli et al., 2010). Cromínia takes part of the Araxa Group which comprises mostly micaschists, quartzites and carbonate-bearing schists. Locally, the most abundant rock type are lenticular bodies aligned E-W, composed of rock with cumulate texture and harzburgitic to dunitic compositions. According to Angeli et al. (2010), the chromitites exhibit massive to breccioid structure and pull-apart texture, with chromite crystals around 0.5 mm in size dispersed in the matrix, essentially composed of serpentine and subordinately of chlorite and talc. Climate is characterized by average annual precipitation of 1384 mm, with a wet season occurring from November to February and an average annual temperature of 23.6°C.

In Cromínia-Mairipotaba, chromite has been extracted intermittently, mainly in the chromitite levels where chromite reached 70 to 85% by volume of the rock. Chromite deposits are predominantly of a high-refractory-grade that can be used without further processing. In Cromínia, chromite exploitation was carried out through open cast mining with the terrace mining method. The terrace mining method is a multi-benched sideways-moving method, where the whole mine moves over the ore reserve from one end to other, but not necessarily in a single bench.

5.2.2 Samples

Considering that the chromite exploitation in Cromínia is a small area, it was accessible to distinguish the zone where the mineral was extracted. In June 2015, solid samples were collected in different areas based on the degree of affectation by antique mining activities. Three areas were defined: non-affected area, directly affected area and indirectly affected area. The non-affected area is located in the top of the hill and around of the upper terrace, where sampling point T1, T2 and T3 are located. The directly affected area, corresponds

basically to the area of exploitation in the concavity of the terraces where a soil profile S1 was collected. And finally the indirectly affected area corresponds to the areas where material produced by exploitation activities have been crushed, or to area downhill where the material extracted have deposited after being washed down by runoff. For this area, superficial soils (S2 and T4) and one sediment sample (Sed) were collected (Figure 5.1).

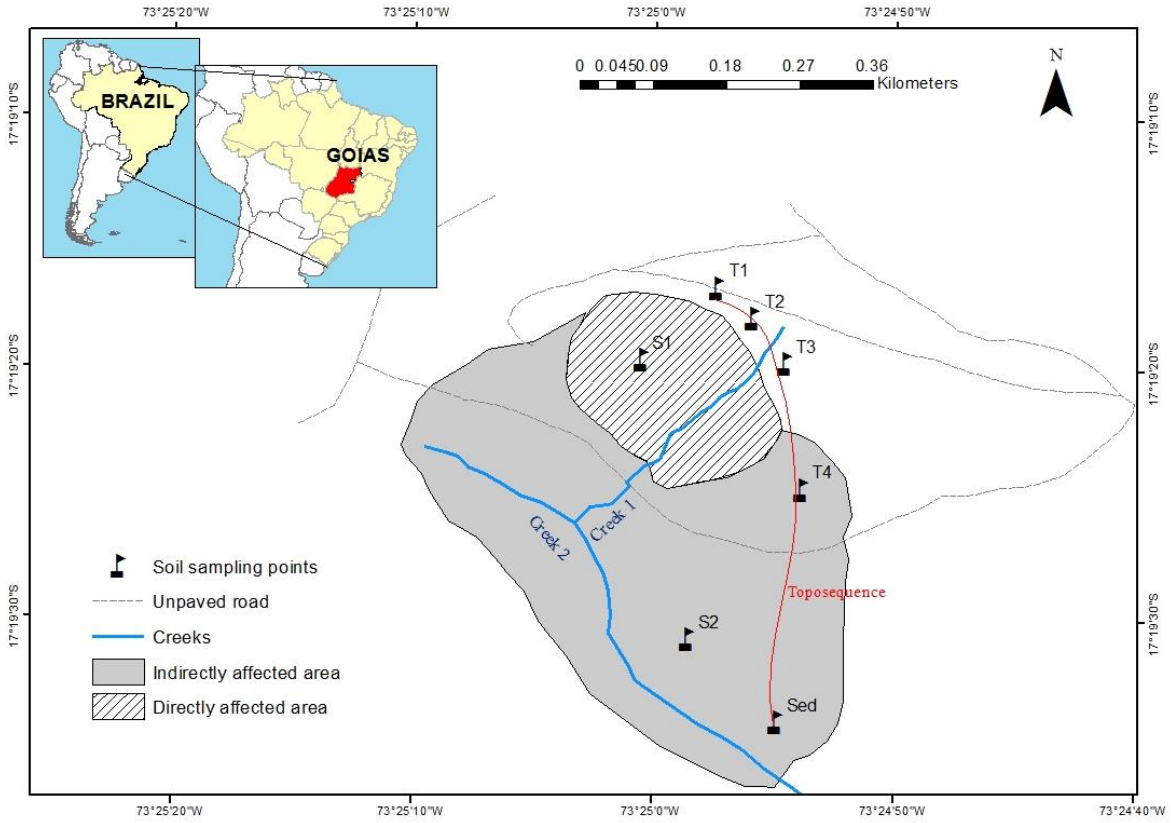

Figure 5.1 Cromínia (Goiás state, Brazil) antique chromite exploitation area. The directed impacted area is where the chromite exploitation took place. The indirectly area is affected for transport of mining residues. The toposequence (T1, T2, T3, T4 and Sed) studied is also displayed in the figure.

The toposequence grouping soils T1, T2, T3, T4 and Sed) included non-affected and indirectly affected soils and sediments. The toposequence coved altitudes between 763 and 711 meters above sea level and there is a total distance of 300 meters between the pedon T1 located in the upper part of the hill and Sed which is sediment of creek 2. From the sampling point mentioned previously, two soil profiles representing non-affected (T3) and affected soils (S1) were studied. The soil profile in T3 was 140 cm depth and between 70 and 110 cm, according to color variation, 4 subsamples were collected, which later were associated with contrasting mineralogical and chemical composition. The soil profile in S1 was 150 cm depth, and 5 subsamples through the profile were collected. Solid samples were

dried down at atmospheric temperature, sieved to <2 mm and stored in polypropylene plastic bags. The dry samples were powdered with a marble mortar and stored for further analysis.
We also sampled water of two creeks, named creek 1 and creek 2, which cross the area. For each sample, approximately one litter of water was collected and stored in acid-cleaned polyethylene bottles. *In situ* parameters including temperature, pH and electrical conductivity were measured directly on the field using a WTW 3410 Set 2 multiparameter. Within 24 h after sampling, one part of the samples was filtered through pre-cleaned 0.7 µm Whatman™ glass microfiber filters grade GF/F for suspended particulate analysis. Other part was filtered through 0.22 µm syringe PES (Polyethersulfone) filters, and acidified with ultrapure concentrated HNO_3 for major and traces. One part of the filtered sample was stored in amber glass bottles and acidified with H_3PO_4 for dissolved organic carbon (DOC) and other part was stored without acidification for anions. The filtered acidified and non-acidified samples were stored at 4°C. There was no rainfall prior to the sampling event.

5.2.3 Analytical methods

Soils and sediments were crushed, powdered and homogenized in a marble mortar. Total analysis of the major elements in solid samples were done with a wavelength-dispersive X-ray fluorescence (XRF), using a Panalytical X fluorescence spectrometer equipped with Energy Dispersive Minipal 4 (Rh X Ray tube-30kV-9W), at a resolution of 150 eV (Mn Kα). Measurements were performed according to the thin-layer hypothesis. To establish the mineralogical composition X-ray diffraction (XRD) analysis were performed with a Panalytical diffractometer and using the Cu Kα radiation (at 45kV – 40 mA), in grazing incidence angle in the 5°-70° 2θ range with a scan step of 0.013°. Total carbon content in soils was measured by a dry combustion method with Shimadzu total organic carbon TOC-VCSH analyzer. Organic carbon was measured after elimination of inorganic carbon with concentrated phosphoric acid. Inorganic carbon was calculated as the difference between total carbon and organic carbon.

Extractions of exchangeable Cr(VI) and Cr(III) in solid samples were performed with 1 M KCl and 0.1 M KH_2PO_4, respectively. Suspension of 1 g of soil was agitated with 25 mL of the reactant for 1 h (Becquer et al., 2003; Garnier et al., 2006). The supernatant was separated by centrifuging for 15 min at 2500 rpm followed by filtration with 0.22 µm syringe PES filter. In each sample, Cr speciation was analyzed by a anion exchange column (Thermo Scientific, chrome FAST CF-KIT-Cr36) coupled to the High Resolution ICP-MS, so as to verify the selective extraction of Cr(VI) with the solution of KH_2PO_4. This is an on-line method which allows the determination of Cr(VI) and Cr(III) content at a single run and within one analytical unit. The speciation column is added to an existing SC-DX-FAST system for separation of Cr

species by isocratic elution anion exchange chromatography. The HPLC separation of chromium species is performed with a mobile phase, at pH 2, constituted by 68% HNO_3, 25% NH_3 and 10 ppm Tm. The flow rate through the column was between 170 and 180 µL min^{-1} (10 RPM on the peristaltic pump). Prior to using the column, mobile phase was allowed to flow through the column for 30 minutes in order to condition the column with the ion-pair reagent. After use column was rinsed with MQ water and was stored wet to prevent drying out. The detection limit for Cr(VI) is 4 ng L^{-1} and for Cr(III) is 3 ng L^{-1}. Chromium standards, ranging from 10 ppt to 10 ppb, were prepared from 1000 mg L^{-1} stock solution of Cr(III) (PerkinElmer, $Cr(NO_3)_3.9H_2O$) and Cr(VI) (Merk, CrO_4^{2-}). The calibration curve for Cr(III) and Cr(VI) was done considering the area down the curve, which was estimated with a curve integration program ("Integlec", Microsoft Visual Basic environment, R. Losno, personal communication) using trapeze integration method with a user defined baseline and a graphical front-end. The noise reduction was calculated with a Hamming filter. To estimate the Cr(III) and Cr(VI) concentrations in the samples, the area down the curve was calculated for each sample and using the calibration curve, the concentration was estimated.

About 0.05 g of soils and sediments were dissolved in 2 mL concentrated ultrapure distilled HNO_3 and 1 mL HF on a hotplate at 100 °C for 48 h. Samples were then dried and flushed with aqua regia (HCl and HNO_3 in a ratio 3:1) to dissolve fluorides. After that samples were dried and dissolved in 1 mL of 6N HCl. If black residues were still remaining (characteristic of samples containing minerals as chromite), the dissolved fraction was extracted and 100 µL of $HClO_4$ was added to the black residue and it was placed in a hot plate at 120 °C for 24 h. After dissolution, the $HClO_4$ was evaporated in an evapoclean and the residue was dissolved in 6N HCl and mixed with the original dissolved fraction for trace elements and isotope analysis. Creek samples were evaporated and then redissolved in 1 mL 6N HCl.

Anions (F^-, Cl^-, NO_3^-, SO_4^{2-}) were measured by ion chromatography (ICS 1100, Thermo Fisher) equipped with a column Ionpac Thermo AS14 and a pre-column Ionpac Thermo AG14. The mobile phase consisted of a mixture of Na_2CO_3 and $NaHCO_3$. The injection volume was 20 µL and the flow rate was 1.2 mL min^{-1}. Dissolved organic carbon (DOC) analyses were performed with Shimadzu total organic carbon TOC-VCSH analyzer. Trace (Fe, Mn, Al, Cr, Ni) and major elements concentration (Na, K, Mg, Ca, Si) for solids and waters samples, and Cr(VI) and Cr(III) chemically extracted (total Cr) diluted in 2% ultrapure HNO_3 were measured on a (ICAP 6200, Thermo Fisher) or High-Resolution ICP-MS (Element II, ThermoScientific) for concentrations under 10 µg L^{-1} using multi-element standard solutions. Detection limits for the ICP-AES were typically between 10 and 200 µg L^{-1} and for the ICP-MS between 0.006 and 0.074 µg L^{-1}. The standard deviation (1σ)

associated to the measurements was smaller than 5%. Based on measured concentrations, aliquots of acid digested samples were used for chromium purification following the cation exchange resin method (Birck and Allegre, 1988; Trinquier et al., 2008). Two successive elutions in 1N HCl were performed in Biorad AG 50WX8 cation exchanger. Samples were dissolved in 0.1N HCl and passed through the resin. Chromium was collected immediately after loading and an additional 5 mL 1N HCl was used to completely elute any remaining Cr. After that 2 mL of 6N HCl were added to the resin and the fraction was collected and passed again through the resin as it was previously described. The two elutions were mixed and evaporated. Subsequently, 60 µL of 16 N HNO_3 were added to dissolve the residue, followed by 2 mL of Milli-Q water and the mixture was heated at 100°C for 24 h. Once the sample cooled down, the sample was passed through the resin. This load was discarded. Additional 5 mL of 0.5N HF and 22 mL of 1N HCl were used to eliminate residual Ti, Na and Al. Finally chromium was eluted with 10 mL of 2N HCl. Between elutions, columns were washed with 15 mL 6N HCl. The samples were evaporated until dryness in order to eliminate the HCl and the concentration was adjusted to 100 ppb or 50 ppb of Cr with 0.6% HNO_3.

Chromium isotopic compositions were measured on a Multicollector ICP-MS (Neptune, Thermo Scientific) housed at the Institut de physique du globe de Paris (IPGP). Purified Cr samples were dissolved in 0.5% HNO_3 with concentrations of 100 ppb or 50 ppb for solid and water samples, respectively. Dilute samples were introduced to the plasma with a PFA µFlow nebulizer (100 µL min^{-1}) coupled with an Apex IR desolvation introduction system (Elemental scientific) without additional gas or membrane desolvation. With a jet sample cone and H skimmer cone and under high-resolution mode, the obtained sensitivity was 2.8 – 4.9 V ^{52}Cr per 100 ppb Cr. All ion beams were measured on Faraday detectors connected to 10^{11} Ω amplifiers. The isotopes ^{49}Ti, ^{51}V and ^{56}Fe were measured and monitor to correct for isobaric interferences of ^{50}Ti, ^{50}V and ^{54}Fe. The unprocessed NIST SRM 979 standard was analyzed after every three samples to monitor potential drift, which was < 0.1% within each analytical session. On-peak blanks were measured before and after every sample/standard. The analytical accuracy and precision were assessed by repeatedly processing and measuring USGS reference material BHVO-2 standard (-0.11 ± 0.02‰, 2SD, n=3).

The $^{53}Cr/^{52}Cr$ ratio was expressed using the δ notation, which is a per mil deviation from the standard reference material NIST SRM 979, as it was done for previous Cr isotopes studies (equation 5.1). The analytical results are expressed in the conventional δ notation in part per mil (‰).

$$\delta^{53}Cr(‰) = \left[\left(\frac{^{53}Cr/^{52}Cr_{sample}}{^{53}Cr/^{52}Cr_{SRM\ 979}}\right) - 1\right] * 1000 \quad \textbf{(5.1)}$$

5.3 RESULTS AND DISCUSSION

5.3.1 Antique chromite extraction impact on soils: directly affected vs non-affected soil profile

Al, Cr, Fe, Mg, Mn and Ni content, mineralogy, chromium isotopic composition and organic carbon content in soils and sediments are presented in Table 5.1. The mineralogy of the soil profiles is dominated by the presence of serpentine (lizardite and/or orthochrysotile), quartz, hematite and spinel (chromite and/or magnetite). Oze (2003) observed that the enrichment and range of Cr concentrations in serpentine soils are directly related to the presence of Cr-spinels, specifically chromite and Cr-magnetite. Serpentine and clinochlore have been identified in previous studies in ultramafic areas as potential Cr-bearing phases (Equeenuddin and Pattnaik, 2017). Both in the non-affected (T3) and affected (S1) soil profile the main Cr bearing phases are serpentine, hematite and spinels (chromite and/or magnetite). Chlorite was found in the non-affected soils profile (T3) with higher content in T3W, while in the affected soil profile it was not present.

In the non-affected soil profile (T3), between 70 and 110 cm, a heterogeneous composition of the subsamples is observed. While quartz, chlorite, serpentine, hematite and spinel are present in all the subsamples of this layer (70-110 cm), soils T3W and T3Y contain talc 2M and T3R contains micas. Despite that micas and talc 2M are not known as Cr bearing phases, in the heterogeneous layer Cr content varies from 1 to 5 g kg^{-1}. In the soil profile T3, Cr is enriched in the first 20 cm (4 g kg^{-1}), which is dominated by the presence of quartz, micas, chlorite, serpentine, talc 2M, hematite and spinel. The presence of spinel is clearly associated with chromite and/or magnetite, which could explain the Cr enrichment. However, in the horizon composed of various materials, between 70 and 110 cm, the subsamples T3Y and T3O present larger Cr content (5 g kg^{-1} in average) respectively to the other subsamples, which may be related to the amount of chromite and/or magnetite. Superficial soils T1 and T2 also located in the non-affected area present the same mineralogy than soil T3. Soil T1 is highly enriched in spinels and Cr content (25 g kg^{-1}). When comparing soils profiles in Cromínia, a significant geochemical variability is observed. The chromite deposits in Goiás state fall in the podiform type that occurs in alpine-type peridotite and mafic complexes (Neves de Figueiredo, 1977). In podiform deposits, Dickey (1975) demonstrated that chromites exhibit chemical variations caused by fractional crystallization of primitive magmas buffered by residual, mafic silicates. This geological variability partially explains the differences between soil profiles of this study area.

Table 5.1 Total content of elements, organic carbon (C), δ^{53}Cr (‰) and mineralogical composition of the soils and sediments collected in Crominía. Qz: Quartz, micas, Clino: Clinochlore, Srp: Serpentine, talc 2M, Hem: Hematite and Spi: Spinel.

Sample type		Sample code	Depth (cm)	δ^{53}Cr (‰)	±2σ	C	Concentration (g kg^{-1})						Mineralogy						
						(%)	Al	Cr	Fe	Mg	Mn	Ni	Qz	Micas	Chl	Srp*	Talc 2M	Hem	Spi*
Soil	Non-affected area	T1	0	-0.10	0.07	1.3	31.57	25.48	272.25	81.38	3.67	6.46	+		+	+	+	+	+
		T2	0	-0.26	0.03	3.3	24.90	3.61	184.43	144.47	2.36	4.66	+			+		+	+
		T3	0-20	-0.70	0.01	1.3	30.38	3.64	142.99		1.38	3.67	+	+	+	+	+	+	+
		T3	20 -70	-0.53	0.05	1.1	96.84	2.74	123.85	27.05	1.47	2.29	+	+	+	+	+	+	+
		T3W	70 - 110	-0.16	0.03	0.2	10.38	1.83	47.41	128.60	2.66	2.00	+		+	+	+	+	+
		T3Y	70 - 110	0.07	0.04	0.2	80.65	5.28	180.93	32.53	0.95	1.12	+		+	+	+	+	+
		T3R	70 - 110	-0.01	0.03	0.3	111.60	0.99	99.08	23.99	1.11	1.05	+	+	+	+		+	+
		T3O	70 - 110	-0.44	0.07	0.4	56.74	5.05	259.29	29.49	3.89	0.95	+		+	+		+	+
		T3	130 - 160	0.21	0.02	0.2	92.49	0.34	61.24	13.20	0.24	0.39	+	+	+	+		+	+
	Directly affected area	S1	0 – 30	3.88	0.10	1.2	28.92	2.22	82.42	11.65	0.77	1.02	+	+		+	+	+	+
		S1	30 – 40	2.29	0.02	0.9	97.08	5.19	135.40	9.09	1.35	1.34	+	+		+	+	+	+
		S1	40 – 100	-0.32	0.04	0.3	102.60	0.61	85.05	7.45	1.20	0.56	+	+		+		+	+
		S1	100 – 150	0.15	0.03	0.5	93.15	1.67	96.79	7.10	0.81	0.78	+	+		+		+	+
		S1	> 150	2.81	0.04	0.2	46.20	0.33	50.92	1.79	0.45	0.32	+	+		+		+	+
	Indirectly affected area	T4	0	-0.67	0.07	2.5	51.73	14.47	428.21	13.69	5.51	5.50	+			+		+	+
		S2	0	-0.33	0.04	0.4	56.17	13.75	267.58	61.85	3.63	4.18	+	+	+	+		+	+
Sediment		Sed	0	-0.50	0.06	1.2	50.79	6.58	159.45	10.81	1.55	3.02	+		+	+		+	+

* Srp (orthocrysotile and/or lizardite); Spi (chromite and/or magnetite).

Cr(III) derived from primary chromite and pyroxene may be isomorphically substituted into the Fe(III) site of magnetite due to size and charge similarities (Oze, 2003). In addition, Cr(III) readily sorbs on surfaces of Fe(III)-containing oxides such as magnetite and hematite via inner-sphere complexation and forms low-solubility precipitates at pH greater than 4 (Charlet and Manceau, 1992; Oze, 2003). The fact that Fe oxides are an important Cr-bearing phase, explains that in the subsamples enriched in Cr, T3Y and T3O, the Fe content is higher (220 g kg^{-1} in average) than in other samples of the same layer. Oze et al. (2004) already noted that in serpentine soil profiles, Cr concentration decreases with depth toward the protolith. Without considering those two atypical values on the soil profile, total Cr is tenfold higher in the surface compared with the deeper soils (0.3 g kg^{-1}) while for Fe the difference is only two fold (143 g kg^{-1} in the surface and 61 g kg^{-1} in the deeper layer).

Ni content decreases with the depth showing concentrations of 4 g kg^{-1} in the surface and 0.4 g kg^{-1} between the 130 and 160 cm. There is six fold more Mn in the surface (4 g kg^{-1}) than in the deep soil (0.2 g kg^{-1}), however in the heterogeneous layer between 70 and 110 cm, there are two maximum values (3 and 4 g kg^{-1}) in samples T3W and T3O, respectively. Mg is also enriched (129 g kg^{-1}) in the sample T3W which is characterized by the presence of talc 2M, while in the rest of the profile Mg content ranges between 13 and 32 g kg^{-1}. Organic carbon varies between 0.2 and 1.2 % (w/w) and is higher in the surface. Oze et al. (2003) found in serpentine sediments a positive correlation of Cr with Fe, Mg, Mn and Ni suggesting that Cr may be related to oxy(hydr)oxides, spinels, Fe-Mg smectite and Fe-Mg vermiculites, which are common minerals in serpentine soils. In the present study, Cr, Fe, Mn, Mg, Ni and organic carbon have the same tendency, decreasing from the top of the profile to the bottom, however only for Fe and Cr concentrations the correlation (R^2= 0.76) is significant. This result could highlight the important role of Fe oxides in the retention of both Cr(VI) and Cr(III), and their incidence on the fate of chromium (Choppala et al., 2013). In addition, redox reactions, controlled by the presence of Fe but also Mn and organic matter, will determine the chromium oxidation state and therefore its mobility and toxicity (Fendorf, 1995).

Erosion and eolian transport of the material produced by mining activities in both the non-affected area, and the directly affected area, is reflected in the soil S2 and sediment Sed. Both S2 and Sed present an important quantity of spinel and chlorite. Other mineral phases included quartz, serpentine and hematite. The occurrence of spinel in S2 together with the Cr content (14 g kg^{-1}) indicates the presence of chromite. Mineral phases in the directly affected soil profile S1 include quartz, micas, serpentine, hematite and spinel. In S1, chlorite is not present. In addition, the first 40 cm of the soil profile contains talc 2M. The chemical

composition of the directly affected soil profile (S1) shows lower Fe content compared with the non-affected soil profile (T3) (51 – 135 g kg^{-1} and 259 g kg^{-1}, respectively) associated with the presence of hematite and/or magnetite. The lower abundance of hematite in the directly affected soil profile (S1) starting from the 40 cm, compared to the non-affected soil profile (T3) could explain this discrepancy. Despite of the lower Fe content in the affected soil profile, a significant positive correlation (R^2= 0.81) with Cr content is still visible. Nevertheless, the range of Cr content for both profiles remains the same (0.3 – 5.0 g kg^{-1}) with a tendency to decrease with depth. Similarly, Ni is positively correlated with Cr (R^2= 0.90) and concentrations vary between 0.3 and 1 g kg^{-1}, being lower in comparison with the non-affected soil profile (0.9 – 4 g kg^{-1}). In addition, the S1 soil profile systematically presents high content of Fe, Cr and Ni between 30 and 40 cm and between 100 and 150 cm. No differences of organic carbon content are observed between affected (S1) and non-affected soil profile (T3), indeed in both cases, it decreases with depth (0.2 – 1.3%). This tendency was already reported in previous studies in ultramafic soils (Mills et al., 2011).

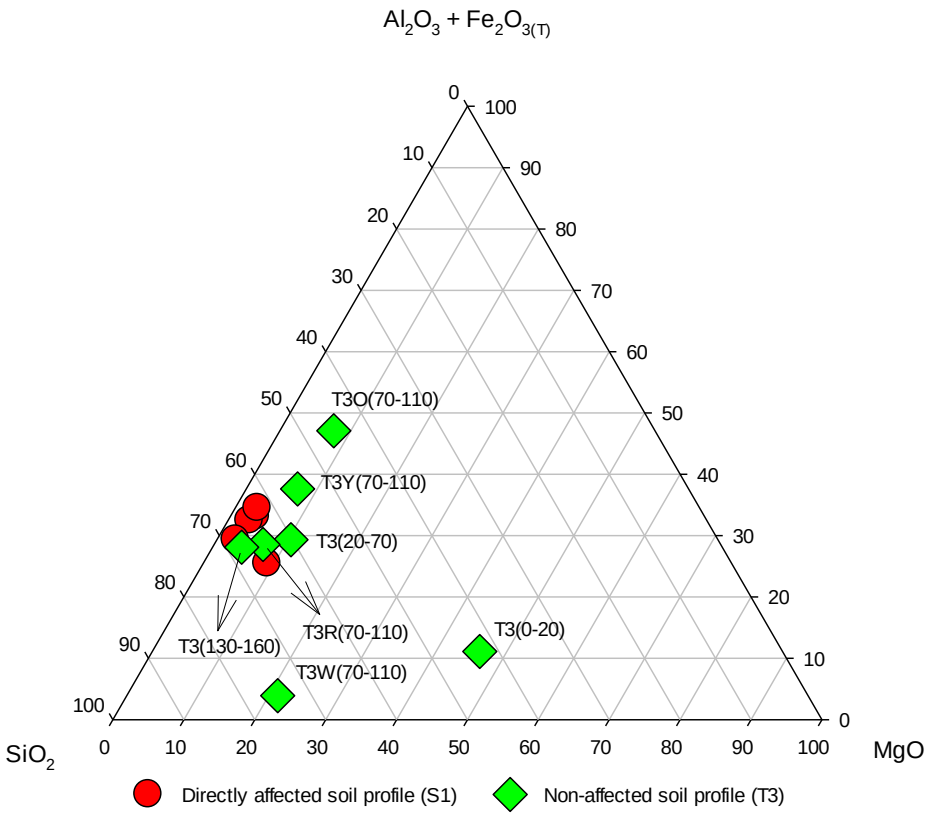

Figure 5.2 Ternary plot in the Al-Fe-Mg-Si space of the soils profiles S1 in the directly affected area (red) and T3 in the non-affected area (green).

In order to assess the degree of alteration of the samples collected in both soil profiles, a ternary plot was built (Figure 5.2). The non-affected soil profile T3 (green) has a wider distribution on the plot compared with the directly affected soil profile S1 (red), however it

does not follow a specific tendency. Indeed superficial soil (0-20 cm) in the non-affected profile T3, has a higher content of Mg and Si oxides, with concentrations of 17 and 23%, compared with the rest of the soil profile. Something similar occurs in the heterogeneous layer of the soil profileT3, between 70 and 110 cm, where subsamples T3W, T3R and T3Y are enriched in micas and talc 2M. Aiglsperger et al. (2016) plotted the trend of weathering in ultramafic rocks in a ternary plot. They showed that continuous weathering of pyroxenes and olivine leads to a loss of Mg and Si, whereas redox dependent elements such as Fe are constantly enriched by formation of secondary oxide(s). Hematite is more abundant in the non-affected soil profile (T3) compared to the directly affected soil profile (S1), reason why in the ternary plot, all the points of S1 are grouped in the first third of the graph.

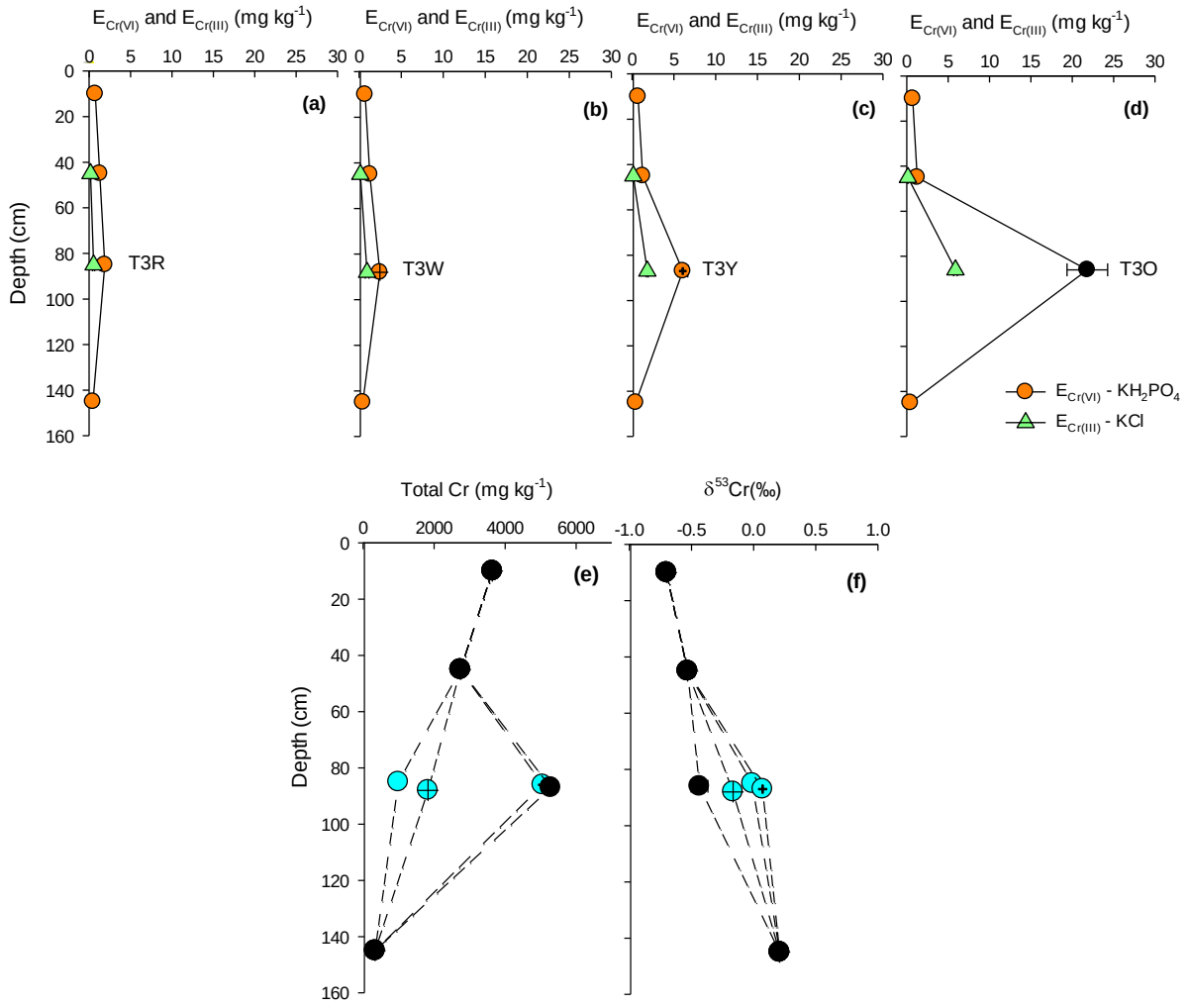

Figure 5.3 Chemically exchangeable pool of Cr(VI) ($E_{Cr(VI)}$) and Cr(III) ($E_{Cr(III)}$) in the non-affected soil profile, T3. The heterogeneous layer between 70 and 110 cm is shown in separates profiles: with ○-T3R (a), with ⊕-T3W (b), with ⊙-T3Y (c) and with ●-T3O (d). Total chromium content (e) and δ^{53}Cr value (f) of soil profile T3 are also displayed.

5.3.2 Changes on Cr exchangeability in soil profiles

To evaluate the impact of antique chromite extraction on Cr exchangeability and mobility in soil profiles, chemical extraction of Cr(VI) and Cr(III) with KH_2PO_4 and KCl, respectively was performed. For all the samples, exchangeable Cr is mainly under the toxic and mobile anionic Cr(VI) form, which can form labile complexes displaced by phosphates as it has been reported by Garnier et al. (2006).

Figure 5.3 shows the non-affected soil profile (T3) divided according to the composition of the heterogeneous layer between 70 and 110 cm, where there are two high values of exchangeable Cr(VI) and Cr(III), as well as total Cr in samples T3Y and T3O. In this layer (70 – 110 cm), the $E_{Cr(III)}$-KCl varies between 0.5 and 5.9 mg kg^{-1} and the $E_{Cr(VI)}$-KH_2PO_4 is dominant with a range of variation of 1.9 to 23.3 mg kg^{-1}. Oze et al. (2003) found that in serpentine soils, Fe(III) oxides and Fe(III) oxy(hydr)oxides provide a host of structural and surface sites to sequester Cr(III) bearing minerals during soil forming processes. In addition, the presence of Cr(III) silicates will lead to a Cr(VI) production rate (Oze et al., 2007). The oxidation of Cr(III) is not the only source of Cr(VI), Cr(VI) oxyanions can also be adsorbed in the surface of Fe and Al oxides, which are positively charged. Sandy material has also a great preponderance of positively charged surfaces over a range of pH from 5 to 7.5, resulting in a great affinity for CrO_4^- (Stanin, 2004). In the present study, the presence of hematite and magnetite associated to a high Fe content (259 g kg^{-1}) could explain the higher extracted Cr(VI) and Cr(III), such is the case for sample 3TO.

Among the Cr bearing phases found in the studied soils, hematite is known to adsorb Cr(VI). Hematite has a capacity of chromate adsorption, and is capable of mediating the reduction of surface-bound chromate to chromium (III) (Johnston and Chrysochoou, 2015). Adsorption of Cr(VI) onto hematite takes place through the formation of inner-sphere chromate complexes on hematite (Rai et al., 1989). The formation of bidentate complexes, similar to the oxyanion-iron oxide systems is also possible (Johnston and Chrysochoou, 2015; Manceau et al., 1992). Despite goethite was not detected with the XRD measurements in the samples studied, its presence in low concentration is not discarded. Goethite can adsorb chromate via electrostatic and/or outer-sphere complexes (Abdel-Samad and Watson, 1997; Garnier et al., 2009). Abdel-Samad and Watson (1997) also observed that initially a small amount of Cr(III) adsorbs via a redox reaction, which could explain in our study the presence of exchangeable Cr(III) in the samples containing goethite. Regardless of the presence of Cr(III), the majority remains as exchangeable Cr(VI). In samples 3TY and 3TO, iron oxides might bound Cr(VI) and Cr(III), controlling their exchangeability. Nevertheless, total Cr content is probably controlled by the occurrence of chromite. Even if chromite and Cr-magnetite have been

proposed by Garnier et al., (2008) as a source of Cr in ultramafic soils, supported with XANES evidences for oxidation of Cr(III) to Cr(VI) by Mn-oxides in a lateritic regolith (Fandeur et al., 2009; Garnier et al., 2008), the r-spinel are resistant to alteration. Thus, chromite is not expected to be a source of the Cr(VI) and/or Cr(III) extracted with KH_2PO_4 and KCl, respectively.

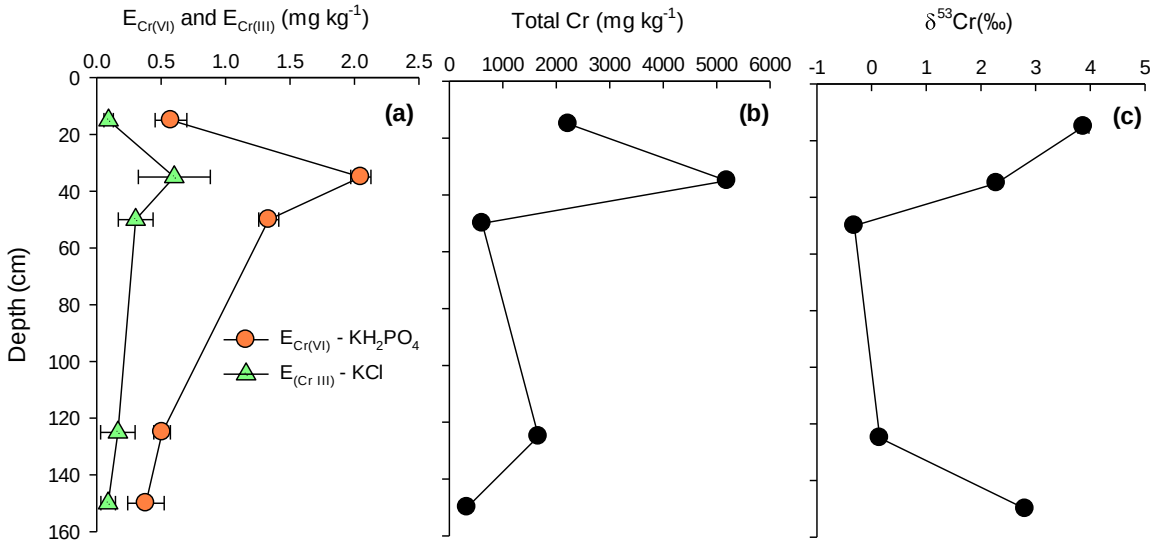

Figure 5.4 Chemically exchangeable pool of Cr (VI) and Cr(III) (a), total chromium content (b) and δ^{53}Cr (c) in the directly affected soil profile S1.

If the heterogeneous layer between 70 and 110 cm is excluded from the non-affected soil profile (T3), and comparing the top and the bottom soil, a tendency of $E_{Cr(VI)}$-KH_2PO_4 to decrease with the depth was observed, with a reduction of 50% between the surface and the deep soil. Garnier et al. (2009) and Mills et al. (2011) have shown the opposite tendency in tropical ultramafic soils were the pool of exchangeable chromium increases with depth. However, in Niquelândia Garnier et al. (2009) reported $E_{Cr(VI)}$-KH_2PO_4 values ranging between 64 and 1,014 mg kg^{-1}, while in the present study the maximum $E_{Cr(VI)}$-KH_2PO_4 is 23.3 mg kg^{-1}, which is 45 folds lower than the values of Garnier et al. (2009). Conversely, in Sacramento valley the $E_{Cr(VI)}$-KH_2PO_4 reported by Mills et al. (2011) was only 0.03 mg kg^{-1}, which is about 750 lower than the maximum value in Cromínia. Garnier et al. (2009) and Mills et al. (2011) affirmed that the presence of positive charges in deeper horizons are the main reason to explain the increase of Cr(VI) with depth (Garnier et al., 2006; Parfitt, 1981).

In the directly affected soil profile (S1), exchangeable Cr(VI), Cr(III) and total chromium decrease with depth. Between 30 and 40 cm, it displays its highest values with 2.08 mg kg^{-1}, 0.6 g kg^{-1} and 5 g kg^{-1}, respectively. Despite the Cr content in the directly affected (0.33 – 5.19 mg kg^{-1}) and non-affected soil profile (0.34 – 5.28 mg kg^{-1}) has the same range of

variability, the exchangeable pool of Cr(III) and Cr(VI) are lower in the directly affected soil profile (Figure 5.4).

5.3.3 Changes on Cr isotopic composition in soil profiles

In order to better understand the processes controlling Cr mobility and availability in soils affected by mining activities, the chromium isotopic ratio was analyzed on the solid samples (Figure 5.3 and Figure 5.4). In the non-affected soil profile (T3) the δ^{53}Cr increased with depth from -0.70 to 0.20 ‰. The heterogeneity on the mineralogical and elemental composition of the layer between the 70 and 110 cm is reflected by the δ^{53}Cr values. The sample with the highest exchangeable pool of Cr(VI) (T3O), has the lowest δ^{53}Cr value (-0.44 ‰). The enrichment of soils in lighter chromium isotopes, evidences the removal of positively fractionated Cr, leaving the sample negatively fractionated. The Cr removed corresponds to the ^{53}Cr-enriched Cr(VI) pool removed by runoff, leaving the remaining soil depleted in ^{53}Cr (Berger and Frei, 2014; Crowe et al., 2013; Frei and Polat, 2013).

In the directly affected soil profile (S1), there is not a defined tendency in the first 100 cm. The δ^{53}Cr decreases from 3.88 to -0.32 ‰, and then it increases up to 2.81 ‰. Comparing the positive δ^{53}Cr values obtained in the directly affected soil profile (S1) (from +0.15 ± 0.03 to +3.88 ± 0.10), and the ones reported in previous studies (from +0.23 to +1.22), a considerable gap is observed. Two mechanisms could explain the positive δ^{53}Cr obtained in the directly affected soil profile S1: hydrothermalism or surface processes such as desorption/ adsorption and weathering. In first place, regarding hydrothermalism, relatively large positive δ^{53}Cr signatures (up to 1.2 ‰) have been documented (Crowe et al., 2013; Frei and Polat, 2013; Berger and Frei, 2014). Farkaš et al. (2013) reported high δ^{53}Cr in serpentinites (up to +1.22 ‰) as a response of serpentinization processes that could shift altered peridotites to isotopically high δ^{53}Cr. Farkaš et al. (2013) suggested that the isotopically heavy Cr was the result of reduction of isotopically heavier Cr(VI) in serpentinizing fluids. In altered peridotites, Wang et al. (2016) found that high δ^{53}Cr values are related to low Cr content. They proposed two possibilities: a) light Cr isotopes are lost to fluids during serpentinization as a result of kinetic fractionation, leaving Cr isotopically heavy behind; or b) Cr was initially lost to fluids without isotopic fractionation, then isotopically heavy Cr was accumulated during later-stage sulfate reduction. Similarly, Schoenberg et al. (2008) found that heavy Cr isotopic composition of natural crocoites are most likely the result of isotope fractionation during hydrothermal Cr cycling involving repeated redox processes.

After studying chromite from many localities, Fisher (1929) concluded that much of the chromite is of primary crystallization and that it is to both early and late magmatic origin.

Besides, the author affirmed that there is evidence of dissolution and re-deposition of this chromite by hydrothermal processes. Fisher (1929) also observed the chromite grains of hydrothermally altered rocks are predominantly anhedral. Despite that, neither in Cromínia nor in the Araxa group, studies have evidenced hydrothermalism processes, in the present work the presence of isotopically heavy Cr(III) in Cromínia could indicate hydrothermalism or the presence of isotopically heavy Cr(III) which is not hydrothermal chromite.

The Cr isotopic signature of chromite from the western Bushveld Complex (South Africa) and from the Great Dyke Zimbabwe measured by Schoenberg et al. (2008) had a range of variation between -0.02 and -0.02‰ with an average $\delta^{53}Cr$ value of -0.08±0.06‰. Irvine (1977) explained that massive chromitite layers formed when new ultramafic melt is injected into a magma chamber containing evolved, fractionated melt, driving the composition of the mixed, hybrid magma into the stability field of chromite. The crystallized chromite reflects the isotopic composition of the injected ultramafic melt, since evolved magma is depleted in chromium. Consequently chromites are indistinguishable in $\delta^{53/52}Cr_{SRM\ 979}$ values from those mantle xenoliths and ultramafic rocks and cumulates (Schoenberg et al., 2008). Cr enriched in light ^{52}Cr has been also reported in a protolith of metamorphic rocks by Shen et al. (2015) in the following order: chromite-free peridotite (-0.21‰ to -0.11‰) < chromite-bearing peridotite (-0.07‰) < chromite (- 0.06‰). Those finding imply potential mantle heterogeneity as a result of the partial melting or fractional crystallization associated with chromite. Chromite enriched in isotopically heavy Cr has never been reported, however there are evidences of the existence of hydrothermal chromite which could be potentially enriched in ^{53}Cr. Arai and Akizawa (2014) suggested that chromite could precipitate from a hydrothermal solution rich in carbonate, sulfate and chloride components. This also implies that Cr could be mobile within the mantle wedge via the action of hydrous fluids released from the slab. Taguchi et al. (2012) observed textural and compositional evidences associated to chemical changes of the primary chromite with increasing metamorphic grade. According to the author, it is the result of primary hydrothermal alteration that ended up in serpentinization and carbonation of the ultramafic protolith. If hydrothermal processes took place in Cromínia, it can be a reason that partially explains the Cr enrichment on heavy ^{53}Cr in the soils samples of the directly affected soil profile S1. This adding to the total Cr enrichment and low exchangeable Cr(VI) and Cr(III) could suggest the presence of hydrothermal chromite, with dominant ^{53}Cr.

The second mechanisms that could explain the presence of Cr enriched in heavy isotopes are surface processes such as weathering and adsorption/desorption. Frei et al. (2014) found chromium enrichment, coupled with positively fractionated $\delta^{53}Cr$ values (+0.23 ± 0.04),

in weathering profiles basalt. They found that the $\delta^{53}Cr$ enrichment occurred because of reduction and adsorptive immobilization of positively fractionated Cr liberated from elsewhere in the profile. The re-deposition of Cr(VI) occurs via Fe-oxide trapping during oxide precipitation (Wang et al., 2015). This mechanism, can be expected in this study, in the directly affected soil profile (S1) due to a significant positive correlation between Fe and Cr (R^2= 0.811). Frei and Polat (2013) have found re-deposition of heavy Cr at lower levels of the weathering profile, which is typically associated with enrichment of iron (presence of hematite) and other redox sensitive elements such as U, Ce and V. Also, clays such as kaolinite and illite can participate to the Cr(VI) reduction (Kwak et al., 2018). In the present study high content of organic matter (OM) is correlated with positively fractionated Cr enrichment (R^2=0.998) and with total Cr (R^2=0.975), because OM is an effective Cr-trap in surface water runoff (Frei et al., 2014). Both Fe and OM are known to play a role in Cr(VI) reduction, which is a step needed to immobilize the re-deposited heavy Cr(VI) (Frei and Polat, 2013).

We believe that both, hydrothermalism and surface processes might explain the enrichment in heavy ^{53}Cr isotopes observed in the soil profile (S1). However, given the differences between the ^{53}Cr values of the non-affected soil profile (T3) and the directly affected soil profile (S1), we suspect that antique exploitation activities could have any impact on the Cr mobility and therefore, it is an additional factor affecting the Cr isotopic signature. Mining activities imply the movement of large amount of material, exposing some mineral phases to open air. In this context, the exposed material is more susceptible to be weathered, with a consequent release of heavy metals including Cr. Nevertheless, the weathering or alteration of the exposed material occurs at higher rates than in non-affected environments, such as soil profile T3. Mineral extraction is also comparable with accelerated erosion, which takes place once the plant cover is removed to gain access to the mineral deposit. If weathering rates are higher in mining environments, mobilized Cr is also higher, which could to a certain extent, explain the Cr isotopes fractionation values observed. Taking into consideration the following reduction step of heavy Cr(VI) to heavy Cr(III) in the affected soil profile, the positively fractionated $\delta^{53}Cr$ values does not imply the presence of mobile Cr(VI), which is consistent with the low exchangeable pool of Cr(VI) extracted (Figure 5.4). Cr(VI) could have been previously released from the upper layers, which were removed during the period of chromite exploitation.

5.3.4 Cr transport along the toposequence

Despite the low exchangeable pool of chromium in the non-affected (T3) (Figure 5.3) but especially in the directly affected soil profile (S1) (Figure 5.4), Cr(VI) can be released

reaching surface and ground waters. To address this question, a toposequence, from the convex shoulder (pedon T1) to the foot-slope (pedon Sed), comprising non-affected (T1, T2 and T3) and indirectly affected superficial soil (T4 and Sed) was studied. In the toposequence total Cr tended to decrease from pedon T1 to pedon T3, with concentrations starting from 25 g kg^{-1} to 4 g kg^{-1} and then it increases again until 14 and 6 g kg^{-1} in the foot-slope, pedon T4 and Sed, respectively. The Cr content increases in the sediments (Sed) which is related to the abundant presence of chromite and/or magnetite, detected by XRD. The exchangeable pool of hexavalent chromium ($E_{Cr(VI)}$ KH_2PO_4) also increases along the toposequence with a range of concentration of 0.6 to 1.3 mg kg^{-1} while Cr(III) is above the detection limit only in T1 (0.06 mg kg^{-1}) and T4 (0.3 mg kg^{-1}) (Figure 5.5).

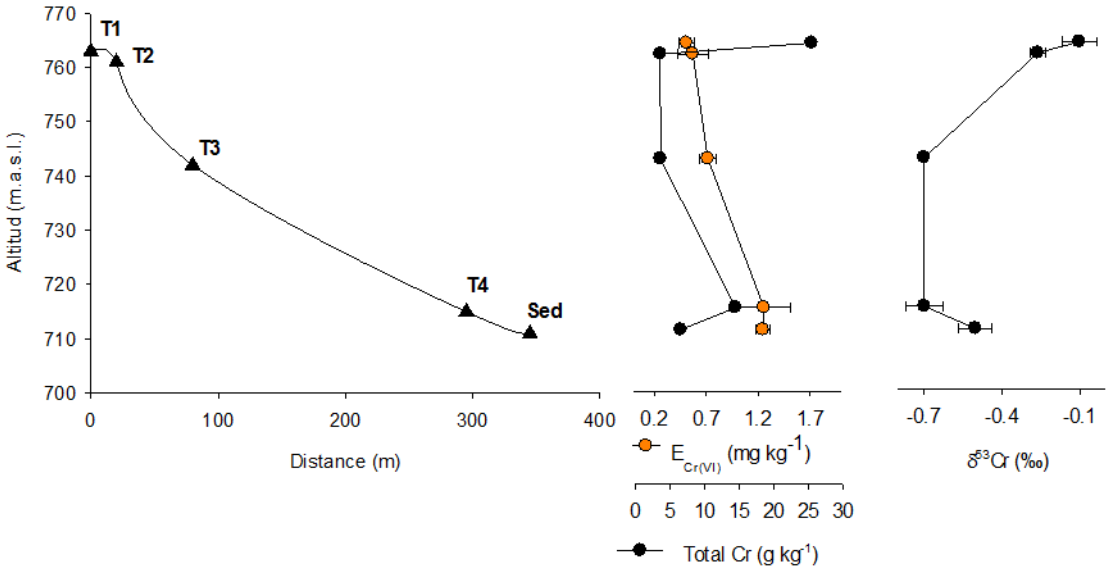

Figure 5.5 Total Cr, Cr(VI) and δ^{53}Cr along the superficial soil of the toposequence including non-affected soil (T1, T2 and T3) and indirectly affected soil (T4) and sediment (Sed).

In addition, the positive correlation between Cr and Ni (R^2= 0.711) may indicate that both elements have been leached from the shoulder to the foot-slope of the toposequence. Fe has also the same tendency than Cr and Ni, however at the foot-slope (pedon T4) it is 1.5 fold higher (428 g kg^{-1}) than in pedon T1 (272 g kg^{-1}). The increase of $E_{Cr(VI)}$-KH_2PO_4 may occurs due to erosion, deposition and lateral flow along the toposequence. Because finer sediments are more easily eroded, coarser materials were left behind on the shoulder and back slope (Cheng et al., 2011). The foot-slope received run-off water containing solutes and suspended particles from upslope, and were potentially more leached. Sediment (Sed) is rich in Cr, and has larger exchangeable Cr content, which can be related to the deposition of sediments on the foot-slope. Cheng et al. (2011) studied the pedogenetic processes

controlling the geochemical fraction of the metals. They observed that the degree of soil development increased along the toposequence (Entisol, Inceptisol and Alfisol) together with the availability of metals including Cr. Besides the increase on the Cr exchangeable fraction, total Cr increase could also be related with erosion of the topsoil containing Cr, mostly present in the residual fraction (refractory phases) (Salvador-Blanes et al., 2006).

The increase of exchangeable Cr along the toposequence, is reflected in the Cr isotopic signature, which decreases from -0.10 in the convex shoulder (T1) to -0.67 ‰ in the T4. This result suggests that part of Cr, mainly as Cr(VI) enriched in ^{53}Cr has been leached leaving behind soil depleted in heavy isotopes. As Cr is leached from the convex shoulder to the foot-slope, Cr(III) accumulates, but at the same time Cr(VI) is released to surface and groundwaters. The index of alteration (UMIA) also supports this hypothesis, because an increase of degree of alteration along the toposequence occurs (Figure 5.6). Once in the sediments, Cr isotopic signature increases again up to -0.50‰ which can be related to the active oxidation reduction because of the fluctuating seasonal water table, which enhances the Cr mobility (Cooper, 2002).

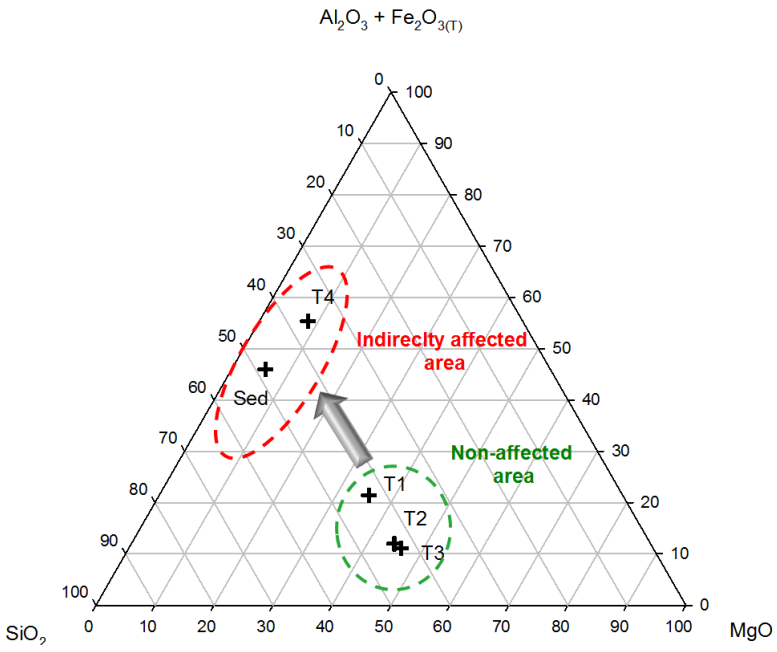

Figure 5.6 Ternary plot in the Al-Fe-Mg-Si space of the superficial soil along the toposequence between soil, T1 and Sediment, Sed.

The chemical composition of the two creeks sampled in the vicinity of the toposequence is displayed in Table 5.2. In both creeks the dissolved Cr concentration is close to 0.5 µg L^{-1}, which is under the typical regulatory limit for drinking water according to the World Health Organization. Ni presents concentrations of 3.9 and 5.9 µg L^{-1}, Fe of 33.6 and 61.8 µg L^{-1} and Mn of 1.8 and 22.6 µg L^{-1} for creek 1 and 2, respectively.

The suspended particulate matter (SPM) is 0.003 mg L^{-1}, in average for both creeks, and is highly concentrated on chromium and organic carbon. Viers et al. (2008) reported an average Cr concentration in suspended sediments of world rivers of 0.1 mg kg^{-1}. The high Cr content in the SPM in Cromínia is associated with the presence of chromite and probably other Cr bearing phases.

Table 5.2 Major and trace cations and anions in dissolved fraction, suspended particulate matter (SPM), alkalinity, dissolved organic carbon (DOC), Particulate organic carbon (POC) content in filters, conductivity, temperature and pH values.

Element		Creek 1	Creek 2
Dissolved metal concentrations (µg L^{-1})	K	948	629
	Mg	3620	3228
	Ca	1699	1596
	Na	2255	1058
	Si	7518	4788
	Fe	33.56	61.8
	Mn	1.823	22.6
	Al	21.46	5.79
	Cr	0.531	0.591
	Ni	3.888	5.885
Dissolved anion concentrations (µg L^{-1})	F^-	73	<LoD
	Cl^-	200	799
	NO_3^-	<LoD	446
	SO_4^-	76	30
DOC (mg L^{-1})		2.93	2.28
Alkalinity (mg L^{-1})		15.13	15.13
SPM (mg L^{-1})		0.01	0.01
POC (wt %)		2.15	2.5
Temperature (°C)		25.1	21.7
Conductivity (µS cm^{-1})		61.3	41.4
pH		7.7	7.3

* Limit of detection (LoD) F^- = 20 µg L^{-1}; NO_3^-= 20 µg L^{-1}

The SPM Cr enrichment is accompanied by a positively fractionated δ^{53}Cr values (+2.78 and +2.36 ‰), which corresponds to the Cr(III) leach from weathering profiles. In average the SPM has a similar isotopic composition than the surface of the affected soil profile (+3.08 ‰) which is located in the vicinity of the creek 1. The δ^{53}Cr in the dissolved fraction of creek 1 is +0.121 ‰. D'Arcy et al. (2016) evidenced that the contribution from Cr(III) in the dissolved fraction of river water, associated to the presence of Cr(III)-organic complexes, is expected to lower the overall Cr isotopic composition. Nevertheless, in the creeks evaluated the content of dissolved organic carbon is low (2.6 mg L^{-1}) which represents a limiting factor for the formation of Cr(III) organic complexes. Moreover, if Cr(III) is enriched in heavy δ^{53}Cr, it cannot lower the Cr isotopic signature of the dissolved fraction. As it was shown with the chemical extraction, Cr(VI) is released from the directly affected and non-affected area, reaching the nearby creeks. Even if the speciation of the samples collected was not established because of the low chromium concentration, the positive δ^{53}Cr is associated with

the presence of hexavalent chromium, as it has been shown in previous studies (Crowe et al., 2013; Ellis et al., 2002; Schauble et al., 2004).

5.4 CONCLUSIONS

In summary, by comparing the non-affected (T3) and affected soil profile (S1), this study reveals that there is no enrichment of total chromium in the profile neither higher pool of exchangeable Cr(VI) and Cr(III). Mineralogical and geochemical differences were observed between the directly affected (S1) and non-affected soil profile (T3). Two main factors explain those discrepancies. In first place, the geological variability probably associated to the chromites chemical variation caused by fractional crystallization of primitive magma. In second place, the antique chromite extraction activities, where the material extracted are exposed to open air, being more susceptible to weathering. Chromium isotopic fractionation was particularly high in the affected soil profile (up to 3.87‰) in comparison with the non-affected area, which cannot be explained only with the reasons just mentioned. Hydrothermalism processes seem to had occurred in Cromínia, being a third factor which affect Cr isotopic composition. While several studies have shown that chromite is enriched in light isotopes (-0.082±0.058‰, according to Schoenberg et al. (2008)), if hydrothermal processes took place in Cromínia, hydrothermal chromite would be enriched in ^{53}Cr. The presence of Cr(III) isotopically heavy is explained by the release of Cr(VI) during weathering processes, with a consequent re-deposition of Cr(VI) (via Fe-oxide trapping) which later was reduced to isotopically heavy Cr(III). This process can occur naturally, however the δ^{53}Cr values reported are never higher than +1‰. We hypothesis that exploitation mining activities, which implies mobilization and transport of a relevant amount of material, increase the heavy Cr(VI) mobilized and re-deposited as Cr(III) which can partially explain the high δ^{53}Cr values observed in the affected soil profile (>+3 ‰).

Hexavalent chromium can be released from both affected and non-affected soil profiles, which can be transported from the shoulder to the foot-slope of the toposequence and it can reach the nearby creeks. The SPM in the creeks present a similar, but slightly lower δ^{53}Cr value than the one on the top of the affected-soil profile (+2.78 - +2.36 ‰ and +3.08 ‰, respectively) due to dilution effect in the transport from the affected area to the creek. While in the dissolved fraction δ^{53}Cr value was simply associated to the presence of the mobile hexavalent chromium.

5.5 BIBLIOGRAPHY

Abdel-Samad, H., Watson, P.R., 1997. An XPS study of the adsorption of chromate on goethite (α-FeOOH). Appl. Surf. Sci. 108, 371–377. doi:10.1016/S0169-4332(96)00609-

5

Aiglsperger, T., Proenza, J.A., Lewis, J.F., Labrador, M., Svojtka, M., Rojas-purón, A., Longo, F., Jana, Ď., 2016. Critical metals (REE ,Sc ,PGE) in Ni laterites from Cuba and the Dominican Republic 73, 127–147. doi:10.1016/j.oregeorev.2015.10.010

Angeli, N., Rafael, G., Navarro, B., 2010. Caracterização Química de Cromitas nos Maciços de Cromínia e. Geol. série Cient. USP 10, 87–99.

Arai, S., Akizawa, N., 2014. Precipitation and dissolution of chromite by hydrothermal solutions in the Oman ophiolite: New behavior of Cr and chromite. Am. Mineral. 99, 28–34. doi:10.2138/am.2014.4473

Becquer, T., Quantin, C., Sicot, M., Boudot, J.P., 2003. Chromium availability in ultramafic soils from New Caledonia. Sci. Total Environ. 301, 251–261. doi:10.1016/S00489697(02)00298-X

Berger, A., Frei, R., 2014. The fate of chromium during tropical weathering: A laterite profile from central madagascar. Geoderma 213, 521–532. doi:10.1016/j.geoderma.2013.09.004

Birck, J.L., Allegre, C.J., 1988. Manganese-chromium isotope systematics and the development of the early Solar System. Nature.

Charlet, L., Manceau, A., 1992. X-Ray Absorption Spectroscopic Study of the Sorption of Cr (lll) at the Oxide-Water Interface. J. Colloid Interface Sci. 148, 443–458.

Cheng, C., Jien, S.-H., Lizuka, Y., Tsai, H., Chang, Y.-H., Hseu, Z.-Y., 2011. Pedogenic Chromium and Nickel Partitioning in Serpentine Soils along a Toposequence. Pedology 75, 659–668. doi:10.2136/sssaj2010.0007

Choppala, G., Bolan, N., Park, J.H., 2013. Chromium Contamination and Its Risk Management in Complex Environmental Settings, Advances in Agronomy. Elsevier. doi:10.1016/B978-0-12-407686-0.00002-6

Cooper, G.R.C., 2002. Oxidation and toxicity of chromium in ultramafic soils in Zimbabwe. Appl. Geochemistry 17, 981–986. doi:10.1016/S0883-2927(02)00014-8

Crowe, S.A., Døssing, L.N., Beukes, N.J., Bau, M., Kruger, S.J., Frei, R., Canfield, D.E., 2013. Atmospheric oxygenation three billion years ago. Nature 501, 535–538. doi:10.1038/nature12426

D'Arcy, J., Babechuk, M.G., Døssing, L.N., Gaucher, C., Frei, R., 2016. Processes controlling the chromium isotopic composition of river water: Constrains from basaltic river catchments. Geochim. Cosmochim. Acta 186, 296–315. doi:10.1016/j.gca. 2016.04.027

Dhakate, R., Singh, V.S., Hodlur, G.K., 2008. Impact assessment of chromite mining on groundwater through simulation modeling study in Sukinda chromite mining area, Orissa, India. J. Hazard. Mater. 160, 535–547. doi:10.1016/j.jhazmat.2008.03.053

Dickey, J.S., 1975. A hypothesis of origin for podifom chromite deposits. Geochim. Cosmochim. Acta 39, 1061–1074.

Economou-Eliopoulos, M., Frei, R., Atsarou, C., 2014. Application of chromium stable isotopes to the evaluation of Cr(VI) contamination in groundwater and rock leachates from central Euboea and the Assopos basin (Greece). Catena 122, 216–228. doi:10.1016/j.catena.2014.06.013

Ellis, A.S., Johnson, T.M., Bullen, T.D., 2002. Chromium Isotopes and the Fate of Hexavalent Chromium in the Environment. Science. 295, 2060–2062. doi:10.1126/science.1068368

Equeenuddin, S.M., Pattnaik, B.K., 2017. Assessment of heavy metal contamination in sediment at Sukinda ultramafic complex using HAADF-STEM analysis. Chemosphere 185, 309–320. doi:10.1016/j.chemosphere.2017.06.131

Fandeur, D., Juillot, F., Morin, G., Livi, L., Cognigni, A., Webb, S.M., Ambrosi, J.P., Fritsch, E., Guyot, F., Brown, G.E., 2009. XANES evidence for oxidation of Cr(III) to Cr(VI) by Mn-oxides in a lateritic regolith developed on serpentinized ultramafic rocks of New Caledonia. Environ. Sci. Technol. 43, 7384–7390. doi:10.1021/es900498r

Farkaš, J., Chrastný, V., Novák, M., Čadkova, E., Pašava, J., Chakrabarti, R., Jacobsen, S.B., Ackerman, L., Bullen, T.D., 2013. Chromium isotope variations (δ53/52Cr) in mantle-derived sources and their weathering products: Implications for environmental studies and the evolution of δ53/52Cr in the Earth's mantle over geologic time. Geochim. Cosmochim. Acta 123, 74–92. doi:10.1016/j.gca.2013.08.016

Fendorf, S.E., 1995. Surface reactions of chromium in soils and waters. Geoderma 67, 55–71. doi:10.1016/0016-7061(94)00062-F

Fisher, L., 1929. Origin of chromite deposits. Econ. Geol. 24, 691–721.

Frei, R., Poiré, D., Frei, K.M., 2014. Weathering on land and transport of chromium to the ocean in a subtropical region (Misiones, NW Argentina): A chromium stable isotope perspective. Chem. Geol. 381, 110–124. doi:10.1016/j.chemgeo.2014.05.015

Frei, R., Polat, A., 2013. Chromium isotope fractionation during oxidative weathering — Implications from the study of a Paleoproterozoic (ca. 1.9 Ga) paleosol , Schreiber Beach ,. Precambrian Res. 224, 434–453. doi:10.1016/j.precamres.2012.10.008

Garnier, J., Quantin, C., Echevarria, G., Becquer, T., 2009. Assessing chromate availability in tropical ultramafic soils using isotopic exchange kinetics. J. Soils Sediments 9, 468–475. doi:10.1007/s11368-009-0062-4

Garnier, J., Quantin, C., Guimaraes, E., Becquer, T., 2008. Can chromite weathering be a source of Cr in soils? Mineral. Mag. 72, 49–53.

Garnier, J., Quantin, C., Guimarães, E.M., Vantelon, D., Montargès-Pelletier, E., Becquer, T., 2013. Cr(VI) genesis and dynamics in Ferralsols developed from ultramafic rocks: The

case of Niquelândia, Brazil. Geoderma 193–194, 256–264. doi:10.1016/j.geoderma.2012.08.031

Garnier, J., Quantin, C., Martins, E.S., Becquer, T., 2006. Solid speciation and availability of chromium in ultramafic soils from Niquelândia, Brazil. J. Geochemical Explor. 88, 206–209. doi:10.1016/j.gexplo.2005.08.040

Godgul, G., Sahu, K.C., 1995. Chromium Contamination from Chromite Mine. Environ. Geol. 25, 251–257. doi:10.1007/BF00766754

Irvine, T.N., 1977. Origin of the chromitite layers in the Muskoz intrusion and other stratiform intrusion: A new interpretation. Geology 5, 273–277. doi:10.1130/0091-7613(1977)5<273:OOCLIT>2.0.CO;2

Johnston, C.P., Chrysochoou, M., 2015. Mechanisms of chromate adsorption on boehmite. J. Hazard. Mater. 281, 56–63. doi:10.1016/j.jhazmat.2014.05.067

Kien, C.N., Noi, N. V., Son, L.T., Ngoc, H.M., Tanaka, S., Nishina, T., IWasaki, K., 2010. Heavy metal contamination of agricultural soils around a chromite mine in Vietnam. Soil Sci. Plant Nutr. 56, 344–356. doi:10.1111/j.1747-0765.2010.00451.x

Kotaś, J., Stasicka, Z., 2000. Chromium occurrence in the environment and methods of its speciation. Environ. Pollut. 107, 263–283. doi:10.1016/S0269-7491(99)00168-2

Krishna, A.K., Mohan, K.R., Murthy, N.N., Periasamy, V., Bipinkumar, G., Manohar, K., Rao, S.S., 2013. Assessment of heavy metal contamination in soils around chromite mining areas, Nuggihalli, Karnataka, India. Environ. Earth Sci. 70, 699–708. doi:10.1007/s12665-012-2153-6

Kwak, S., Yoo, J.C., Moon, D.H., Baek, K., 2018. Role of clay minerals on reduction of Cr(VI). Geoderma 312, 1–5. doi:10.1016/j.geoderma.2017.10.001

Manceau, A., Charlet, L., Boisset, M.C., Didier, B., Spadini, L., 1992. Sorption and speciation of heavy metals on hydrous Fe and Mn oxides. From microscopic to macroscopic. Appl. Clay Sci. 7, 201–223. doi:10.1016/0169-1317(92)90040-T

Mills, C.T., Morrison, J.M., Goldhaber, M.B., Ellefsen, K.J., 2011. Applied Geochemistry Chromium (VI) generation in vadose zone soils and alluvial sediments of the southwestern Sacramento Valley , California : A potential source of geogenic Cr(VI) to groundwater. Appl. Geochemistry 26, 1488–1501. doi:10.1016/j.apgeochem.2011.05.023

Mpouras, T., Chrysochoou, M., Dermatas, D., 2017. Investigation of hexavalent chromium sorption in serpentine sediments. J. Contam. Hydrol. 197, 29–38. doi:10.1016/j.jconhyd.2016.12.009

Neves de Figueiredo, A., 1977. Depósitos de cromita de Goiás e campo formoso (BA) - Diagnose e análise comparativa. Rev. Bras. Geociencias 7, 73–83.

Oze, C., Bird, D.K., Fendorf, S., 2007. Genesis of hexavalent chromium from natural sources

in soil and groundwater. Proc. Natl. Acad. Sci. 104, 6544–6549. doi:10.1073/pnas.0701085104

Oze, C., Fendorf, S., Bird, D.K., Coleman, R.G., 2004. Chromium Geochemistry of Serpentine Soils. Int. Geol. Rev. 46, 97–126. doi:10.2747/0020-6814.46.2.97

Oze, C.J., 2003. Chromium geochemistry of serpentines and serpentine soils, PhD thesis. Submitted to the Department of Geological & Environmental Sciences of Stanford University. Stanford, USA, 215 p.

Oze, C.J., Laforce, M.J., Wentworth, C.M., Hanson, R.T., Bird, D.K., Coleman, R.G., Bird, K., Coleman, R.G., 2003. Chromium geochemistry of serpentinous sediment in the Willow core , Santa Clara County , CA.

Parfitt, R.L., 1981. Chemical properties of variable charge soils, in: Soils with Variable Charge. pp. 167–195.

Qin, L., Wang, X., 2017. Chromium Isotope Geochemistry. Rev. Mineral. Geochemistry 82, 379–414.

Rai, D., Eary, L.E., Zachara, J.M., 1989. Environmental chemistry of chromium. Sci. Total Environ. 86, 15–23.

Raous, S., Becquer, T., Garnier, J., Martins, É.D.S., Echevarria, G., Sterckeman, T., 2010. Mobility of metals in nickel mine spoil materials. Appl. Geochemistry 25, 1746–1755. doi:10.1016/j.apgeochem.2010.09.001

Raous, S., Echevarria, G., Sterckeman, T., Hanna, K., Thomas, F., Martins, E.S., Becquer, T., 2013. Potentially toxic metals in ultramafic mining materials: Identification of the main bearing and reactive phases. Geoderma 192, 111–119. doi:10.1016/j.geoderma.2012.08.017

Salvador-Blanes, S., Cornu, S., Bourennane, H., King, D., 2006. Controls of the spatial variability of Cr concentration in topsoils of a central French landscape. Geoderma 132, 143–157. doi:10.1016/j.geoderma.2005.05.003

Schauble, E., Rossman, G.R., Taylor, H.P., 2004. Theoretical estimates of equilibrium chromium-isotope fractionations. Chem. Geol. 205, 99–114. doi:10.1016/j.chemgeo.2003.12.015

Schoenberg, R., Zink, S., Staubwasser, M., von Blanckenburg, F., 2008. The stable Cr isotope inventory of solid Earth reservoirs determined by double spike MC-ICP-MS. Chem. Geol. 249, 294–306. doi:10.1016/j.chemgeo.2008.01.009

Shen, J., Liu, J., Qin, L., Wang, S.-J., Li, S., Xia, J., Ke, S., Yang, J., 2015. Chromium isotope signature during continental crust subduction recorded in metamorphic rocks. Geochemistry, Geophys. Geosystems 16, 3840–3854. doi:10.1002/2015GC005944

Solgi, E., Parmah, J., 2015. Analysis and assessment of nickel and chromium pollution in soils around Baghejar Chromite Mine of Sabzevar Ophiolite Belt, Northeastern Iran.

Trans. Nonferrous Met. Soc. China (English Ed. 25, 2380–2387. doi:10.1016/S1003-6326(15)63853-5

Stanin, F., 2004. The transport and fate of Cr(VI) in the Environment, in: Chromium (VI) Handbook. pp. 161–204. doi:10.1007/978-94-007-4375-5

Taguchi, T., Satish-Kumar, M., Hokada, T., Jayananda, M., 2012. Petrogenesis of Cr-rich calc-silicate rocks from the bandihalli supracrustal belt, Archean Dharwar Craton, India. Can. Mineral. 50, 705–718. doi:10.3749/canmin.50.3.705

Trinquier, A., Birck, J.-L., Allègre, C.J., 2008. High-precision analysis of chromium isotopes in terrestrial and meteorite samples by thermal ionization mass spectrometry. J. Anal. At. Spectrom. 23, 1565. doi:10.1039/b809755k

Viers, J., Dupré, B., Gaillardet, J., 2008. Chemical composition of suspended sediments in World Rivers : New insights from a new database. Sci. Total Environ. 407, 853–868. doi:10.1016/j.scitotenv.2008.09.053

Wang, X., Johnson, T.M., Ellis, A.S., 2015. Equilibrium isotopic fractionation and isotopic exchange kinetics between Cr(III) and Cr(VI). Geochim. Cosmochim. Acta 153, 72–90. doi:10.1016/j.gca.2015.01.003

Wang, X., Planavsky, N.J., Reinhard, C.T., Zou, H., Ague, J.J., Wu, Y., Gill, B.C., Schwarzenbach, E.M., Peucker-Ehrenbrink, B., 2016. Chromium isotope fractionation during subduction-related metamorphism, black shale weathering, and hydrothermal alteration. Chem. Geol. 423, 19–33. doi:10.1016/j.chemgeo.2016.01.003

CHAPTER 6

Saprolitic and lateritic ores alteration in mining environments

CHAPTER 6

6.1 INTRODUCTION

Soil, surface and groundwater contamination by hexavalent chromium (Cr(VI)) is a big world's concern. Cr(VI) is highly mobile and toxic by inhalation, ingestion, dermal exposure and is carcinogenic. It affects also the growth and development of plants (Choppala et al., 2013). Anthropogenic activities including mining (smelting), tanning, electroplating and industrial waste disposal are the main sources of Cr, in which Cr is directly release to the environment mainly as toxic Cr(VI) species. Mining exploitation activities are also important anthropogenic sources of chromium to the environment, not only in its hexavalent form, but also in its trivalent form which can be potentially oxidize to the toxic Cr(VI). One of the most extensive mining activities consists on the removal of the ground cover, in order to gain access to the ore deposit. This causes the exposure of the material removed to the rain and wind, which end up in the water streams and ponds of the mine. This process is comparable to an accelerate erosion, which together with the precipitation, temperature, topography, and soil age are known to control weathering rates (White and Blum, 1995).

It is well documented that a substantial quantity of siderophile elements including Cr, Ni and Co are exceptionally high in serpentinites (hydrothermally altered ultramafic rocks) compared to the Earth's crust (Tashakor et al., 2017). Chemical weathering of ultramafic rocks is one of the most important sources of geogenic Cr(VI) in soils and aquatic ecosystems. Not only natural rocks are affected by weathering, but also mining residues or altered rocks, resulting from mining activities. These materials are exposed to open air and rainfall, and consequently some metals can be dissolved. Several studies performed in soil profiles (Berger and Frei, 2014; Crowe et al., 2013; Frei and Polat, 2013; Paulukat et al., 2015) demonstrated that oxidative rock weathering is accompanied by isotopic shifts, where the mobilized Cr(VI) released to runoff is enriched in isotopically heavy Cr, leaving behind an isotopically light Cr(III) pool in the soil (Paulukat et al., 2015).

To understand the Cr(VI) release associated to weathering processes in ultramafic areas, leaching experiments associated with mineralogical studies of the source have been developed as a promising tool. Raous et al. (2013) studied the potential toxic metals, including Cr, in ultramafic mining materials. They found that in garneritic and limonitic typical samples and their corresponding spoil material, Ni and Cr are the main secondary metals. In

garnerite, Cr displayed a very low leachability, which can be linked to its sequestration in chromiferous spinels but also as constitutive element of octahedral sheet in the smectite structure. However, 0.7% of total Cr was extracted as a Cr(VI) which corresponds to Cr complexed on the silanol and aluminol peripheral groups of smectite. In limonite, the presence of goethite explained the presence of Cr(VI). Raous et al. (2013) concluded that Cr concentrations in waters lixiviating from soil heaps can be expected to exceed the World Health Organization (WHO) guideline concentration for drinking water (0.05 mg L^{-1} for total Cr). In Niquelândia (Brazil), a Ferro-nickel mine, Raous et al. (2010) performed leaching experiments on limonite and revealed Cr concentration, in waters exceeding 0.05 mg L^{-1}, mainly Cr(VI) (CrO_4^{2-} or $HCrO_4^-$).

Only one study of Fe-Ni laterite ores leaching is reported by Economou-Eliopoulos et al. (2016). These authors performed leaching experiments in batch reactors using natural fresh water and sea water with Fe-Ni laterite sample. The $\delta^{53}Cr$ values measured in natural water leachates ranged between 1.01 ± 0.05 ‰ and -0.21 ± 0.08 ‰. Despite the absence of a clear correlation between Cr(VI) content and $\delta^{53}Cr$ values in the diverse leachates, there is an indication that the laterite leachates with high Cr(VI) concentrations yielded less positively fractionated $\delta^{53}Cr$ values, compared to the laterite leachates where Cr(VI) concentrations are low and exhibit a strongly positively fractionated $\delta^{53}Cr$ value. In order to reconstruct the process that led to soils with a slightly lighter Cr isotopic composition relative to the parent tonalitic bedrock, Berger and Frei (2014) performed leaching experiments under neutral, acidic and alkaline conditions in a laterite profile. They obtained positive fractionation in the leaching experiments with pure water (+0.21 ± 0.05‰) and with alkaline conditions (+0.48 ± 0.03‰), however under acidic condition a negative Cr fractionation was obtained (-0.12 ± 0.02‰). Negatives $\delta^{53}Cr$ values were associated with dissolution of primary sulfides, while in the leachates with small solubilized Cr fractions derived from silicates toward heavier isotopic composition of the mobilized Cr. Larger Cr fractionation is expected to occur in batch experiments, because isotopic fractionation might depend on the kinetic of Cr reduction, as it was found by Døssing et al. (2011) during $Cr(VI)_{aq}$ reduction experiments by $Fe(II)_{aq}$. However, isotopic fractionation also depends on the mechanism of Cr(VI) reduction. Ellis et al. (2002) reported considerable Cr fractionation during Cr(VI) reduction by magnetite over a couple of days. The $^{53}Cr/^{52}Cr$ ratio of the product was 3.4 ± 0.1 ‰ less than that of the reactant.

Given the fact that most of the studies focus on Cr mobility from mining waste materials and that there is a lack of information regarding laterite mines in tropical regions, the main scope of this work is to establish the potential leaching of geogenic chromium in ores of ultramafic

areas and to determine the Cr isotopic composition of the Cr potentially released. Five lateritic and saprolitic ores were selected to perform batch leaching experiments and several physical and chemical parameters were monitored to understand its role in chromium fate. Fe and Cr speciation was analyzed as well as the Cr isotopic signature of the leachate.

6.2 MATERIAL AND METHODS

6.2.1 Study site

Barro Alto, Goiás state (Brazil) is an opencast mine and ferronickel plant located in the Barro Alto complex which came into production by the Angloamerican company in 2011 (Raous et al., 2013). The company is exploiting two main types of ores: Saprolitic and limonitic ore. Saprolitic ore is enriched in phyllosilicates near the ultramafic bedrock and lateritic ore is enriched in iron oxides and is located in the upper layers of the regolith (Colin et al., 1990). The mineral resources in Barro Alto mine is primarily saprolite, overlain by laterites and extends for 35 km in an arc from southwest to northeast. Five different type of ores including lateritic (OL) and saprolitic (OS) (identified as OL1, OL3, OL5, OL8 and OS3) were sampled in June 2015 in Barro Alto mine (S 76°56'26.8'' W 43°32'29.5'').

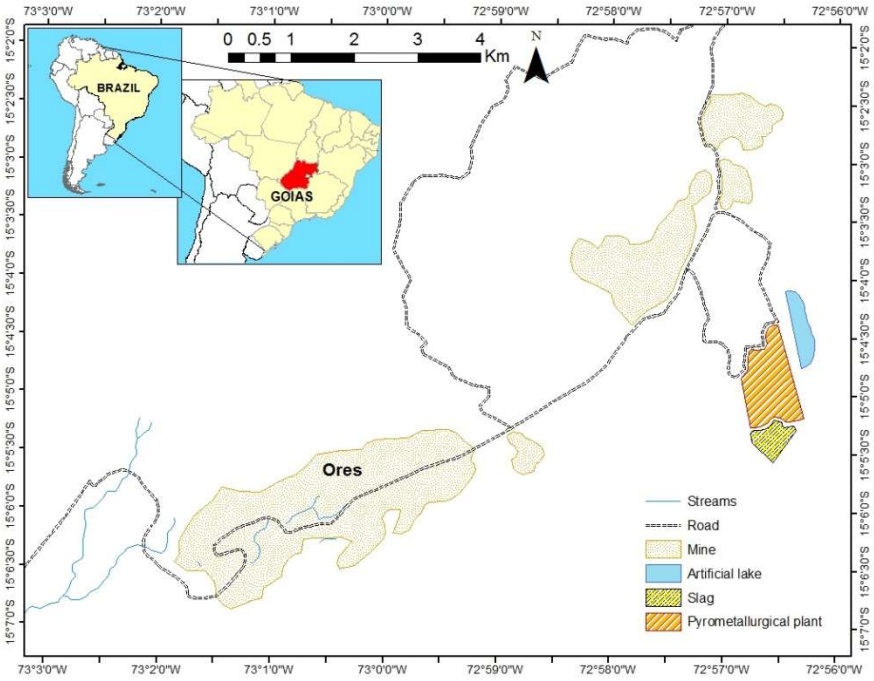

Figure 6.1 Study area in Barro Alto mine.

6.2.2 Selection of saprolitic and lateritic ore samples

The five ores selected for the leaching experiments are part of a group of 11 ores collected in Barro Alto mine in June 2015. The selection criteria for the leaching experiments included the pool of exchangeable Cr(VI) and Cr(III) and the degree of alteration.

The exchangeable pool of Cr(VI) ($E_{Cr(VI)}$-KH_2PO_4) and Cr(III) ($E_{Cr(III)}$-KCl) was determined using the protocol of Bartlett and James (1996). The principle of this protocol is based on the fact that Cr(VI) is mainly present in the anionic form, which can form labile complexes with Fe oxides surfaces and can be displaced by phosphates (Bartlett and James, 1996). Similarly, trivalent chromium species can be extracted trough exchange with potassium.

For the extraction, to one gram of sample without crush was added 25 mL of 0.1 M KH_2PO_4 for Cr(VI) extraction, while for Cr(III) extraction were performed with 25 mL 1 M KCl. The mix was placed in a horizontal shaker for 1hour at 20°C. After that, the sample was centrifuged to separate the solid from the liquid phase, and the supernatant was extracted and filtered with a 0.22 µm syringe PES (Polyethersulfone) filter to measure total Cr concentration. Extractions were performed in triplicate and average is reported with its correspondent standard deviation.

The results of chemical extraction of Cr(III) and Cr(VI) are presented in Figure 6.2. The selected ores, were the one with the highest exchangeable pool of Cr(VI). The concentration of Cr(VI) ranged between 28 and 97 mg kg^{-1}, while extracted Cr(III) ranged between 6 to 10 mg kg^{-1} and represented between 0.46 and 0.05% of total Cr, respectively.

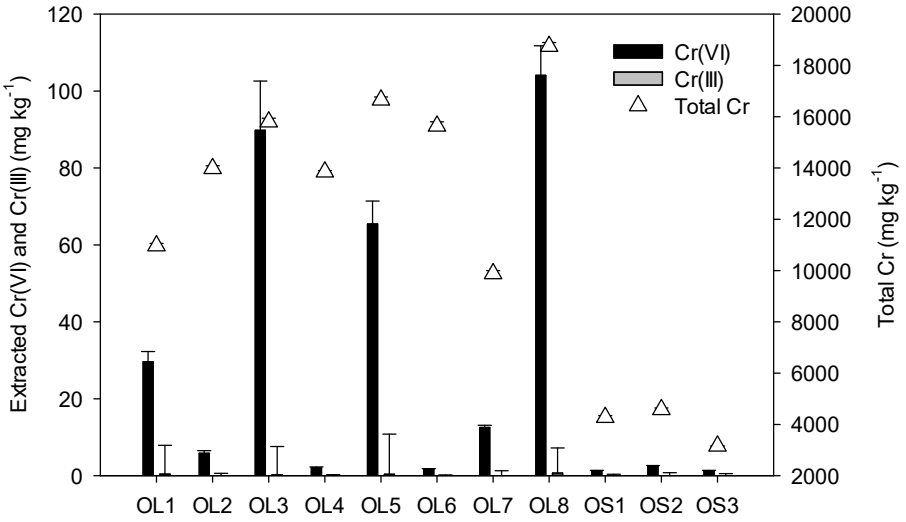

Figure 6.2 Extractable concentrations of Cr(VI), Cr(III) and total Cr content in the lateritic and saprolitic ore samples.

In order to evaluate the degree of mineralogical weathering i.e. the transformation ratio of a primary mineral into its equivalent alteration mineral, the ultramafic index of alteration (UMIA) was calculated using the following equation:

$$UMIA = \frac{Al_2O_3 + Fe_2O_3}{Al_2O_3 + Fe_2O_3 + MgO + SiO_2} * 100 \quad \textbf{(6.1)}$$

The UMIA yields values between 0 and 100, and reflects incipient (UMIA<20), intermediate (UMIA= 20-60) and intense to extreme (UMIA> 60) mineralogical transformations. Lateritic ores (OL) which had the highest exchangeable pool of Cr(VI) are the most altered samples, with and UMIA between 69 and 80, while for the saprolitic ore (OS) the UMIA was only 8.

6.2.3 Batch leaching experiments

About 15 g of the sample previously sieved through a 2.0 mm mesh, were mixed with 300 mL of the electrolyte, 10^{-3}M $NaNO_3$. This corresponds to a solid-liquid ratio of 20:1, used in previous works (Liu et al., 2013) and closely related to the field land conditions. Sodium azide (NaN_3 0.02% w/v), an antimicrobial agent, was added to prevent biological activity in the system. The mixture was shaked with a magnetic bar at a speed of 120 rpm for 11 days. In order to establish the leaching kinetic in the studied mineral phase, several subsamples were collected: 1h, 4h, 7h, 11h, 1d, 2d, 3d, 4d, 5d, 7d, 9d and 11d. *In situ* parameters such as pH, dissolved oxygen, temperature and electrical conductivity was permanently monitored. Subsamples of 30 mL were collected in the middle of the water level with a plastic tube that was installed on the side of the batch reactor. To avoid the collection of particles and the consequent modification of the solid liquid ratio, the shaker was stopped about 30 minutes before the sample collection. In addition, the volume sampled was immediately replaced by an equivalent volume of the leaching solution (10^{-3}M $NaNO_3$) to keep the same solid-liquid ratio.

Samples were filtered using 0.22 µm syringe PES (Polyethersulfone) filters, and acidified with ultrapure concentrated HNO_3 for major (Na, Ca, K, Mg, Si) and traces (Fe, Mn, Al, Cr, Ni) analyses. Aliquots of the filtered sample was stored in amber glass bottles and acidified with H_3PO_4 for dissolved organic carbon (DOC) analyses. Aliquot of the filtrated non acidified sample was used for anions (F^-, Cl^-, NO_3^-, SO_4^{2-}) and Fe speciation.

6.2.4 Analytical methods

6.2.4.1 Mineralogy characterization

Ores were crushed, powdered and homogenized in a marble mortar. Total metal concentration in the solid samples was determined by X-ray fluorescence (XRF), using a Panalytical X fluorescence spectrometer equipped with Energy Dispersive Minipal 4 (Rh X Ray tube-30kV-9W), at a resolution of 150 eV (Mn Kα). Measurements were performed according to the thin-layer hypothesis. Considering the importance of the characterization of the main bearing phases metals to predict their mobility in ultramafic materials (Tina et al., 2006), the mineralogical composition was determined using X-ray diffraction (XRD) analysis on a PANalytical diffractometer and using the Cu Kα radiation (at 45kV – 40 mA), in grazing incidence in the 5°-70° 2θ range with a scan step of 0.013°.

6.2.4.2 Major and traces measurements

About 0.05 g of ores were dissolved in 2 mL concentrated ultrapure distilled HNO_3 and 1 mL HF on a hotplate at 100 °C for 48 h. Samples were then dried and flushed with aqua regia (HCl and HNO_3 in a ratio 3:1) to dissolve fluorides. After that samples were dried and dissolved in 1 mL of 6N HCl. If black residues were still remaining (characteristic of samples containing minerals as chromite), the dissolved fraction was extracted and 100 µL of $HClO_4$ was added to the black residue and it was placed in a hot plate at 120 °C for 24 h. After dissolution, the $HClO_4$ was evaporated in an evapoclean and the residue was dissolved in 6N HCl and mixed with the original dissolved fraction for trace elements and isotope analyses. Dilutions of the samples, were done with 2% ultrapure HNO_3. Analyses of major (Na, K, Mg, Ca, Si) and trace elements (Fe, Mn, Al, Cr, Ni) of the acid digested solid samples and the leachate, were performed with ICP-AES (ICAP 6200, Thermo Fisher) or High-Resolution ICP-MS (Element II, ThermoScientific) for concentrations under 10 µg L^{-1} using multi-element standard solutions. Detection limits for the ICP-AES were typically between 10 and 200 µg L^{-1} and for the ICP-MS between 0.006 and 0.074 µg L^{-1}. The standard deviation (1σ) associated to the measurements was smaller than 5%. Fe speciation in the leachate was determined with the ferrozine method (Viollier et al., 2000).

6.2.4.3 Anions and dissolved carbon measurements in the leachate

Anions (F^-, Cl^-, NO_3^-, SO_4^{2-}) in the leachate were measured by ion chromatography (ICS 1100, Thermo Fisher) equipped with a column Ionpac thermos AS14 and a pre-column Ionpac thermos AG14. The mobile phase consisted of a mixture of Na_2CO_3 and $NaHCO_3$. The injection volume was 20 µL and the flow rate was 1.2 mL min^{-1}. Dissolved organic carbon (DOC) analyses in the leachate were performed with Shimadzu total organic carbon TOC-VCSH analyzer.

6.2.4.4 Chromium speciation

In each leachate, Cr speciation was analyzed by a anion exchange column (Thermo Scientific, chrome FAST CF-KIT-Cr36) coupled to the High Resolution ICP-MS. This is an on-line method which allows the determination of Cr(VI) and Cr(III) content at a single run and within one analytical unit. The speciation column was added to an existing SC-DX-FAST system for separation of Cr species by isocratic elution anion exchange chromatography. The HPLC separation of chromium species was performed with a mobile phase, at pH 2, constituted by 68% HNO_3, 25% NH_3 and 10 ppm Tm. The flow rate through the column was between 170 and 180 µL min^{-1} (10 rpm on the peristaltic pump). Prior to using the column, mobile phase was allowed to flow through the column for 30 minutes in order to condition the column with the ion-pair reagent. After use column was rinsed with MQ water and was stored wet to prevent drying out. The detection limit for Cr(VI) is 4 ng L^{-1} and for Cr(III) is 3 ng L^{-1}. Chromium standards, ranging from 10 ppt to 10 ppb, were prepared from 1000 mg L^{-1} stock solution of Cr(III) (PerkinElmer, $Cr(NO_3)_3.9H_2O$) and Cr(VI) (Merck, CrO_4^{2-}). The calibration curve for Cr(III) and Cr(VI) was done considering the area down the curve, which was estimated with a curve integration program ("Integlec", Microsoft Visual Basic environment, R. Losno, personal communication) using trapeze integration method with a user defined baseline and a graphical front-end. The noise reduction was calculated with a Hamming filter. To estimate the Cr(III) and Cr(VI) concentrations in the samples, the area down the curve was calculated for each sample the concentration was estimated using the calibration curve.

6.2.4.5 Chromium isotopic measurements

Based on measured concentrations in the leachate, aliquots were used for chromium purification following the cation exchange resin method (Birck and Allegre, 1988; Trinquier et al., 2008). Two successive elutions in 1N HCl were performed in Biorad AG 50WX8 cation exchanger. Samples were dissolved in 0.1N HCl and passed through the resin. Chromium was collected immediately after loading and an additional 5 mL 1N HCl was used to completely elute any remaining Cr. After that 2 mL of 6N HCl were added to the resin and the fraction was collected and passed again through the resin as it was previously described. The two elutions were mixed and evaporated. Subsequently, 60 µL of 16 N HNO_3 were added to dissolve the residue, followed by 2 mL of Milli-Q water and the mixture was heated at 100°C for 24 h. Once the sample cooled down, the sample was passed through the resin. This load was discarded. Additional 5 mL of 0.5N HF and 22 mL of 1 N HCl were used to eliminate residual Ti, Na and Al. Finally chromium was eluted with 10 mL of 2 N HCl. Between elutions, columns were washed with 15 mL 6 N HCl. The samples were evaporated until dryness in order to eliminate the HCl and the concentration was adjusted to 100 ppb or 50 ppb of Cr with 0.6% HNO_3.

Chromium isotopic compositions were measured on a Multicollector ICP-MS (Neptune or Neptune plus, Thermo Scientific) housed at the IPGP. Purified Cr samples were dissolved in 0.5% HNO_3 with concentrations of 100 ppb or 50 ppb for solid and water samples, respectively. Dilute samples were introduced in the plasma with a PFA µFlow nebulizer (100 µL min^{-1}) coupled with an Apex IR desolvation introduction system (Elemental scientific) without additional gas or membrane desolvation. With a jet sample cone and H skimmer cone and under high-resolution mode, the obtained sensitivity was 2.8 – 4.9 V ^{52}Cr per 100 ppb Cr. All ion beams were measured on Faraday detectors connected to 10^{11} Ω amplifiers. The isotopes ^{49}Ti, ^{51}V and ^{56}Fe were measured and monitor to correct for isobaric interferences of ^{50}Ti, ^{50}V and ^{54}Fe. The unprocessed NIST SRM 979 standard was analyzed after every three samples to monitor potential drift, which was < 0.1% within each analytical session. On-peak blanks were measured before and after every sample/standard. The analytical accuracy and precision were assessed by repeatedly processing and measuring USGS reference material BHVO-2 standard (-0.11 ± 0.02‰, 2SD, n=3).

The $^{53}Cr/^{52}Cr$ ratio was expressed using the δ notation, which is a per mil deviation from the standard reference material NIST SRM 979, as it was done for previous Cr isotopes studies (equation (6.2)). The analytical results are expressed in the conventional δ notation in part per mil (‰).

$$\delta^{53}Cr(‰) = \left[\left(\frac{^{53}Cr/^{52}Cr_{sample}}{^{53}Cr/^{52}Cr_{SRM\ 979}}\right) - 1\right] * 1000 \quad \textbf{(6.2)}$$

6.2.5 Statistical data processing information

The chemical equilibrium code Visual MINTEQ v3.0 was used to calculate the saturation index and to identify possible phases controlling solubility. The total elemental concentrations as well as Cr(VI) and Fe(II) measured from the different bio-leaching and chemical leaching, were input into the model.

Linear regression analyses were carried out with the software SigmaPlot version 12.0 from Systat Software, INC., San Jose California USA, which yielded regression slopes, coefficients of determination (R^2), P values, and standard errors of the regression (S.E.).

6.3 RESULTS AND DISCUSSION

6.3.1 Chromium hosts

Al, Cr, Fe, Mg, Mn and Ni content, mineralogy in Barro Alto ores and the ultramafic index of alteration (UMIA) are presented in Table 6.1. While iron is the most abundant element in lateritic ores with concentrations ranging from 332 to 536 g kg^{-1}, in the saprolitic ore OS3 the

magnesium content is higher than for Fe, with values up to 146 g kg^{-1}. Iron mineral phases in the ores include hematite and goethite and the possible presence of amorphous iron oxides, which are not detected by the XRD. In the saprolitic ore OS3, non crystalized Fe phases explain the presence of Fe, while Mg might be related with the occurrence of serpentine. Al is the third most abundant element in the lateritic ores, with concentrations ranging from 42 to 67 g kg^{-1}, and is less abundant in the saprolitic ores: OS3 (14 g kg^{-1}). Ratié et al. (2015) reported Fe concentration in Barro Alto mine ores ranging from 140 to 440 g kg^{-1} for the lateritic ores. Saprolitic ores are enriched in Mg (56 – 177 g kg^{-1}), while in the lateritic ore the Mg concentration is lower (5 – 81 g kg^{-1}). The mineralogy of the saprolitic samples is consistent with the typical weathering features of ultramafic rocks that are commonly dominated by phyllosilicates, including minerals of the serpentine group, as well as clay minerals (smectite, chlorite). The mineralogy of the lateritic samples is dominated by Fe oxides (goethite and hematite) and in minor proportion serpentine and talc (Ratié et al., 2015). In concordance, Raous et al. (2013) described the presence of two different type of materials in Niquelândia and Barro Alto (Goiás State, Brazil): garnierite and limonite. Garnierite is enriched in Si, representative of saprolitic ore consisting in a mixture of phyllosilicates including smectite and willemseite. On the other hand, limonite is representative of lateritic horizon enriched in Fe with goethite, hematite and chromiferous spinel as the main mineral phases.

Table 6.1 Total content of elements and mineralogical composition of the ores. Sm: smectite; Srp: serpentine; Chl: chlorite; Hem: hematite; Goe: goethite; Spi: Spinel and Qz: quartz. UMIA is the ultramafic index of alteration.

Ore type	Sample code	UMIA	Concentration (g kg^{-1})*						Mineralogy						
			Al	Cr	Fe	Mg	Mn	Ni	Sm	Srp	Chl	Hem	Goe	Spi	Qz
Lateritic	OL1	74	48	11	332	11	4	8					+	+	+
	OL3	80	42	16	536	9	7	4			+	+	+	+	+
	OL5	80	67	16	466	16	7	12					+		
	OL8	69	63	19	452	25	6	15					+	+	
Saprolitic	OS3	8	14	3	85	146	1	22	+	+					

*The relative standard deviation varied between 0.5 and 0.9%.

Ni concentrations are particularly high in the saprolite (22 g kg^{-1}), while the concentration in the laterite is lower. Cr content ranges from 3 to 19 g kg^{-1}. The higher Cr content is found in the lateritic ores, probably due to the presence of Cr-bearing phases in the first stage of ultramafic rock weathering (Raous et al., 2013), while in the saprolitic ore the Cr concentration is lower (3 g kg^{-1}). In the lateritic ores smectite and other clay minerals may contain significant amount of Ni and Cr.

The differences in the mineralogical and bulk geochemical composition of the primary laterite ores may affect the leachability and mobilization of Cr from these materials. Cr and Mn content is higher in the lateritic ores compared to the saprolitic ore, in which the Cr leachability was low (< 6 µg L^{-1}). Similar result was obtained in leaching experiments

performed with Fe-Ni laterites from Greece. In addition, abundant Cr-rich hydrous Fe-oxides were present in samples with higher Cr leachability (Economou-Eliopoulos et al., 2016). Mobilization of Cr(VI) may be driven by Mn-oxide phase such birnessite. Cooper (2002) identified lower Mn oxides such as hausmannite (Mn_3O_4) and manganite (MnOOH) as capable of oxidizing Cr(III), because the reduction of these oxides provides the most free energy for Cr(III) oxidation.

6.3.2 Understanding of the chromium behavior in the leachate

6.3.2.1 Physico-chemical parameters

The pH tends to increase slightly for ores OL5, OL8 and OS3 with average values of 6.9, 5.9 and 6.8, respectively (Figure 6.3(a)).This result is in agreement with Raous et al. (2010) who performed leaching experiments in columns with spoil material of garnerite (saprolitic ore) and limonite (lateritic ore) from Niquelândia ultramafic complex (Goiás State, Brazil). They observed pH in a range of 6.2 to 7.3 units, which increased over time. Slightly acidic pH has been already reported in other studies in ultramafic areas. Mcclain and Maher (2016) reported raising pH, Mg^{2+} and HCO_3^- concentrations as a result of serpentinite dissolution due to rock-water interaction in ultramafic catchments. The pH increase promotes the deprotonation of functional groups of the solid phase surface. And, due to the decrease of protons amounts, the competition between protons and cations is lower and therefore the repulsion decreases. Thus, the solubility of cations (e.g. Ba^{2+}, Co^{2+}, Ni^{2+}, Zn^{2+}) decreases with increasing pH. Hydroxyl Cr(III) species such as $Cr(OH)^{2+}$, $Cr(OH)_3$ and $Cr(OH)^{4+}$ can also precipitate, however the solubility of Cr(VI) hydrolyzes such as $HCrO_4^-$, CrO_4^{2-} and $Cr_2O_7^{2-}$ increases when increasing pH (Supplementary data Table S6.1- S6.5).

The electrical conductivity (Figure 6.3(b)) increases slightly overtime in all ores samples. The lateritic ores presented the highest range of variation: for OL1 was between 101 and 150 µS cm^{-1}, for OL5 between 125 and 187 µS cm^{-1}, and for OL8 between 113 and 182 µS cm^{-1}. The highest variation was observed for ore OL3 where the electrical conductivity at the end of the leaching period doubled compared to the initial value (219 µS cm^{-1} and 111 µS cm^{-1}, respectively). Mineral dissolution affects electrical conductivity, in this sense this parameter is an indicator of weathering as it has been proposed by Casarotto de Oliveira and Valentin (2017) for basaltic lithotypes.

Finally, dissolved oxygen does not vary significantly for ores OL1, OL3, OL8 and OS3 with average values of 8.6 ± 0.15, 7.5 ± 0.7, 8.9 ± 0.4 and 8.87 ± 0.7 mg L^{-1}, respectively (Figure 6.3(c)). For the leaching experiments with ore OL3, a significant decrease of dissolved

oxygen was observed (8.40 to 3.87 mg L^{-1}). This decrease probably reveals the occurrence of an intense oxidation reaction in the system, which could use O_2 as oxidative agent.

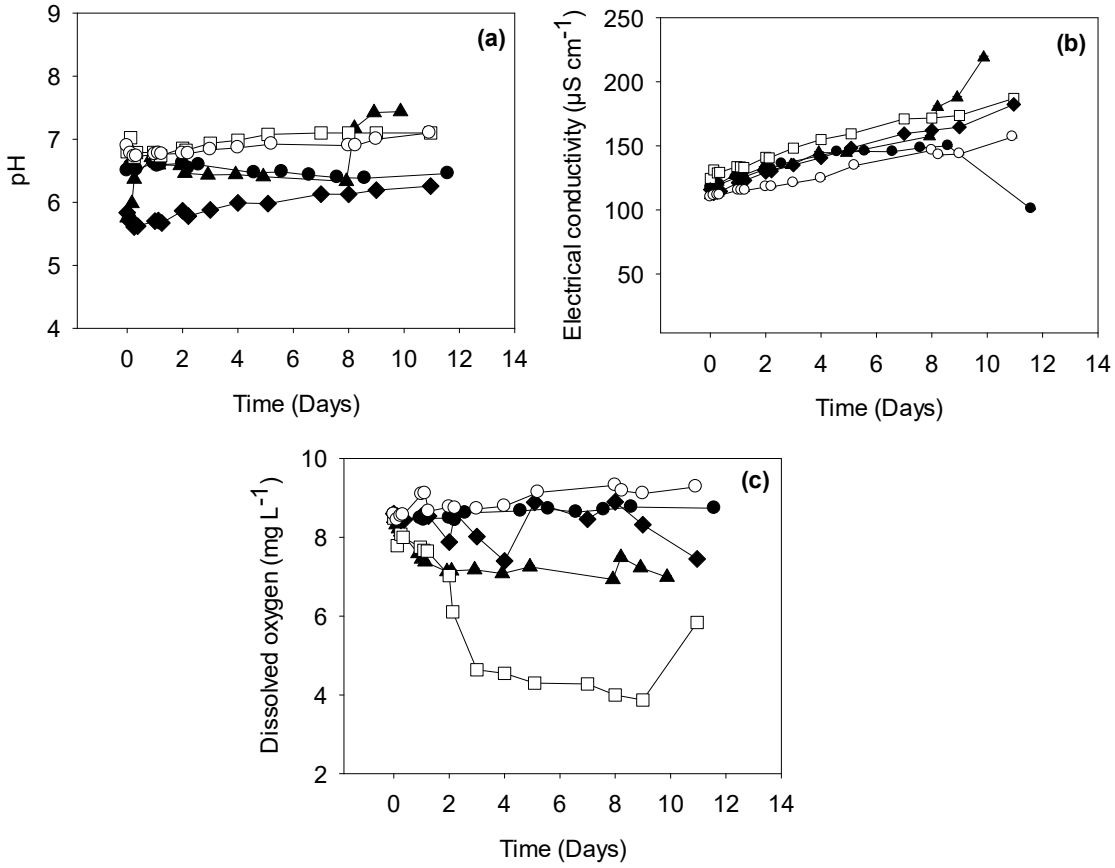

Figure 6.3 Variation of (a) pH, (b) electrical conductivity and (c) dissolved oxygen as a function of time for leaching of ores (—●—) OL1, (—▲—) OL3, (—□—) OL5, (—◆—) OL8 and (—○—) OS3.

6.3.2.2 Fate of chromium and other metals

As shown in Figure 6.4 after 10 to 12 days of leaching Ni have the greatest leachability from the ores as well as Cr (Figure 6.7), followed by Ba and Zn, and Co displayed the lowest one. Raous et al. (2013) investigated the mobilization of metals from garnierite and limonite and they found Ni and Cr as the main trace elements mobilized by water. Despite the low content of Ba in ultramafic rocks, its release is stable overtime and is higher for ore OL1 (35 to 47 µg L^{-1}) than for other samples (0.3 to 4.1 µg L^{-1}). The quartz content (30wt% of the bulk sample) of ore OL1 is higher compared with the other samples, which could explain the higher concentration of Ba in solution (Supplementary data Table S6.1). The concentration of Zn (35 to 50 µg L^{-1} for OL1 and 0.1 to 10 µg L^{-1} for the other samples) in the leachate is within the same order of magnitude of Ba.

Co levels in the leachate are even lower than Ba with a maximum concentration of 2.5 µg L^{-1}. Contrary to Ba, Co content in ultramafic rocks reaches110 mg kg^{-1} (Stueber and Goles,

1967), however its leachability is 200, 5, 10, 2 and 12 fold (in average) lower for ore samples OL1, OL3, OL5, OL8 and OS3, respectively (Figure 6.4(b)). Co together with Mn and Cr are relatively immobile, and their concentrations may not be affected by any serpentinizing solution, which could explain his low concentration in the leachate. However, Marker et al. (1991) found that relatively unstable minerals such as olivine, pyroxene or serpentine can release elements like Mn, Co, Ni and Cr from lateritic covers above ultramafic complexes. In the leaching experiment with the ore OL8, Co concentration slightly decreases overtime. Co can be initially adsorbed by negatively charged Mn^{4+} colloids and later incorporated into Mn oxides (Marker et al., 1991).

Ni presented the highest leachability from ores especially from ores OL8 followed by OS3 (Supplementary data Table S6.4 and S6.5). Nevertheless it is only 0.08 and 0.03% of the total Ni present in the ore samples for ore OL8 and OS3, respectively. Smectite present in ore OS3 could represent an important source of Ni, because this element desorbs through ion exchange from smectite surface sites (Raous et al., 2010). Other important Ni bearing phase is goethite, where Ni can adsorb on the surface or can be introduced into the structure thanks to the presence of silica (Becquer et al., 2006). In leaching experiments performed in column by Raous et al. (2013) with limonitic ore, the leachability of both Ni and Cr integrated in the goethite lattice was low under oxic conditions. On the contrary, Becquer et al. (2006) identified Ni-rich needle-shaped goethite as one of the most soluble phases in ferralsols in New Caledonia, which control the potential mobility of trace metals. The positive correlation (R^2= 0.95) for ore OS3 between dissolved Fe and Ni in the present study, suggest the Ni mobilization from iron oxides (Figure 6.4(d)). Together with Ni, Cr was one of the most concentrated elements in the leachate, in addition every ore behaves differently. For ore OL3, the significant positive correlation between Ni and Mn (R^2= 0.99) and Co (R^2= 0.99), suggests that all those elements are dissolved from the same mineral phase. Figure 6.4(c) present a compilation of Cr concentration overtime in the leachate for all the ore samples.

In ultramafic environments, the bedrock is enriched in light elements such as Si and Mg, and depleted in heavy ones like Fe, Cr, Al and Ni. During weathering, light elements are leached which induce the leaving of the more insoluble ions, predominantly Fe and Al (Fagoyinbo and Adeola, 2017). The saprolitic ore OS3, which is the one the less altered in comparison with all the other ores, is characterized by the highest concentration of Mg in the leachate, with a range of variation between 3231 µg L^{-1} and 3434 µg L^{-1} comparatively to the Mg lateritic ores (233 µg L^{-1}, 15 µg L^{-1}, 450 µg L^{-1} and 1200 µg L^{-1} in ores OL1, OL3, OL5 and OL8, respectively). This is consistent with the idea that clay minerals are the most reactive phases during the leaching of ore OS3.

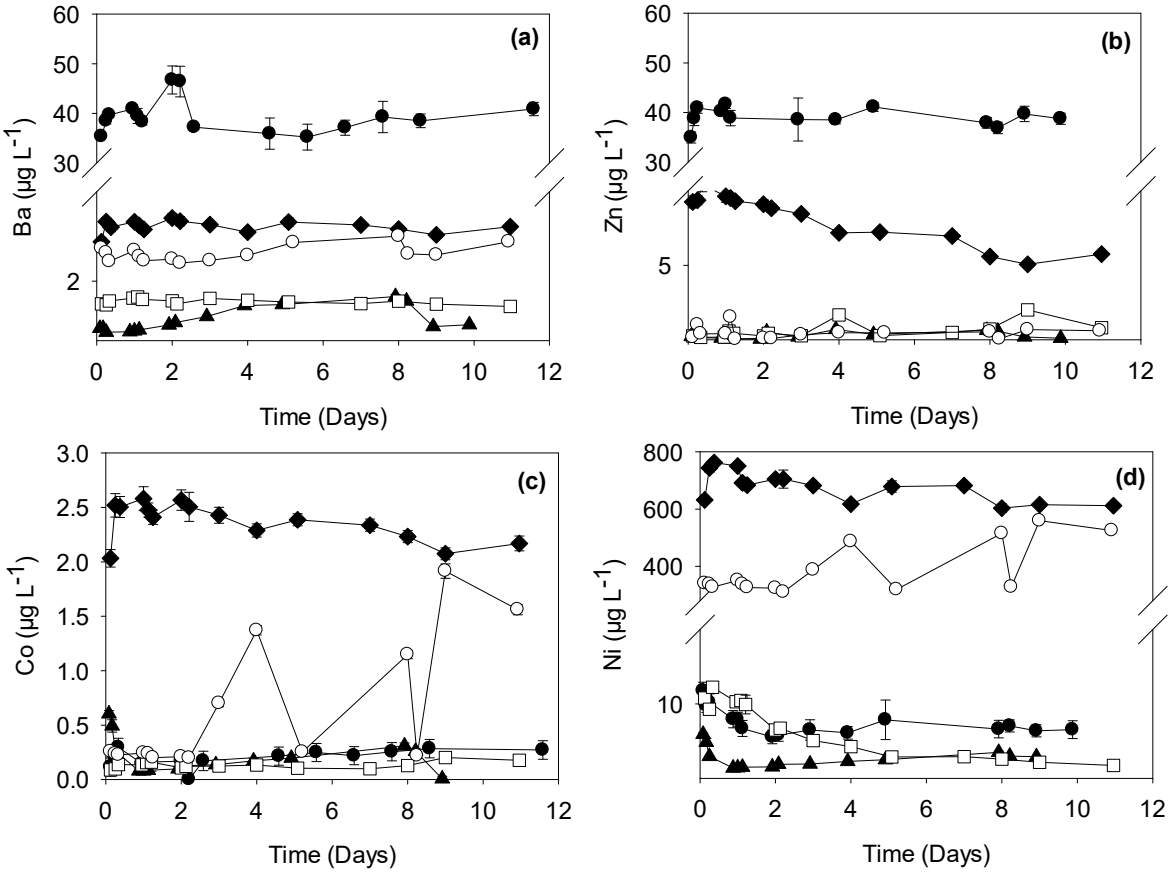

Figure 6.4 Concentration of (a) Ba, (b) Zn, (c) Co and (d) Ni as a function of time for ores (—●—) OL1, (—▲—) OL3, (—□—) OL5, (—◆—) OL8 and (—○—) OS3.

6.3.2.3 Chromium fate

Chromium behaved differently to Ni and other metal cations. During leaching experiment with ore OL1 (Figure 6.7(a)), total dissolved chromium varies between 5.08 and 7.64 µg L^{-1}. In the first 24 hours total dissolved Cr increases in the leachate until the equilibrium is reached, and in the following hours Cr changes are not significant with an average value of 6.65 µg L^{-1}. The initial mass ratio Ni:Cr in ore OL1 was 0.73 while in the first leachate collected was 2.03, and Ni was consequently more mobile than Cr. Ni in ultramafic rock and soils is present in serpentine minerals (lizardite, antigorite and chrysotile) and is more easily weathered compared to Cr, which primarily resides in highly refractory chromite (Morrison et al., 2015). However the mass ratio Ni:Cr decreases in the leachate over time. This result indicates that the phases containing chromium in ore OL1 were not significantly dissolved all along the experiment, and were different from the one containing Ni.

In spite of being detected as major constitutive element of ore OL1, the total dissolved concentrations of Al and Fe were unexpectedly low (<0.006 µg L^{-1}). Thereby, Al and Fe mainly remain in the solid phase. In natural waters exposed to open air atmosphere (O_2), the

most common species of ferric iron is ferric hydroxide, $Fe(OH)_3$ which is mainly in the solid state due to its low solubility in the pH range from 5 to 8. Iron (oxy)hydroxides such like goethite can complex soluble Cr(VI) on their surface and Cr(VI) is also known to be reduced to solid Cr(III) by the presence of iron oxide and organic matter (Fendorf, 1995). Those processes could explain the low concentration of total dissolved Cr in solution (Figure 6.7 (a)).

In ore OL3 (Figure 6.7 (b)), the concentration of Cr is increasing from 6.71 µg L^{-1} to 72.74 µg L^{-1} during the first 24 hours and then decreases to 21.82 µg L^{-1} until the end of the experiment (9 days) (Supplementary data Table S6.2). Fast kinetic leaching of Cr(VI) with Cr(VI) concentrations up to 2.1 µg L^{-1} have been reported by Lilli et al. (2015) in Asopos basin (Greece). While both dissolution of ore OL3 mineralogical phases and precipitation of secondary phases probably occur simultaneously, one can assume that during the first 24 hours, the dissolution of phases containing Cr is the predominant process, whereas after 24 hours the precipitation is predominant. The fluoride F^- anion presents the same behavior than Cr(VI) species, which means that both are simultaneously release and precipitated. The significant positive correlation (R^2=0.83) between total Cr concentration and pH suggests that ionic strength controls the release of Cr(III) species through cation exchange mechanism (Butler, 2009). The fluoride anion, F^-, seems to be associated with the comportment of Cr(VI). Figure 6.6 (a) and (b) show the correlation between Cr and Ni in ores OL3 and OL5, respectively. A negative correlation between the total dissolved Cr concentration and Ni is observed.

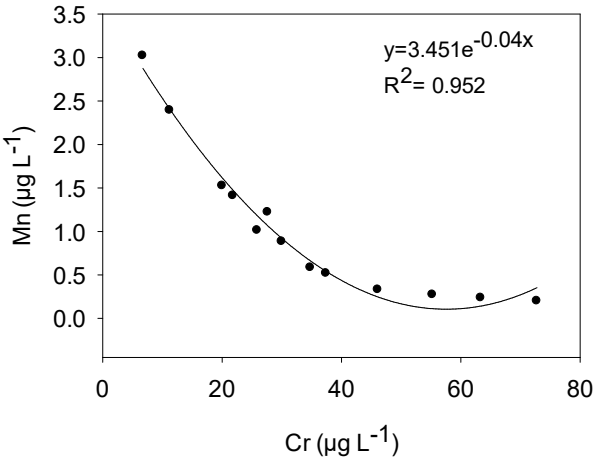

Figure 6.5 Correlation between Cr and Mn in ore OL3.

In addition, in ore OL3 there is a strong interaction between Cr and Mn represented by a significant negative correlation (R^2= -0.87) (Figure 6.5). During the leaching experiment the

pH of the ore OL3 increases from 5.7 to 7.4 units. By increasing pH, oversaturation increases and Mn can precipitates through the formation of secondary phases. A thermodynamic calculation performed with the Visual MinteQ model allowed to predict an over saturation of manganese relatively to Bixbyite (Mn_2O_3, SI = +23) after 24h of interaction, which corresponds to the highest dissolved chromium concentration (Figure 6.7 (b)). Thus, the decrease displayed by dissolved Cr concentration is probably explained by a co-precipitation with manganese oxides.

For ore OL5 and OL8 (Figure 6.7 (c) and (d), resp.), the concentration of total dissolved Cr constantly increases from 94.5 µg L^{-1} to 220.3 µg L^{-1} and from 4.0 to 28.0 µg L^{-1}, respectively. Both ores have in common the presence of goethite, which could contain labile Cr. The significant negative correlation of dissolved oxygen with total dissolved Cr (R^2= 0.80) suggests that Cr is mainly released when dissolved oxygen concentrations are lower. The decrease of oxygen promotes the appearance of Cr(III) species, because the environment is more reducer, however Cr(VI) remains dominant.

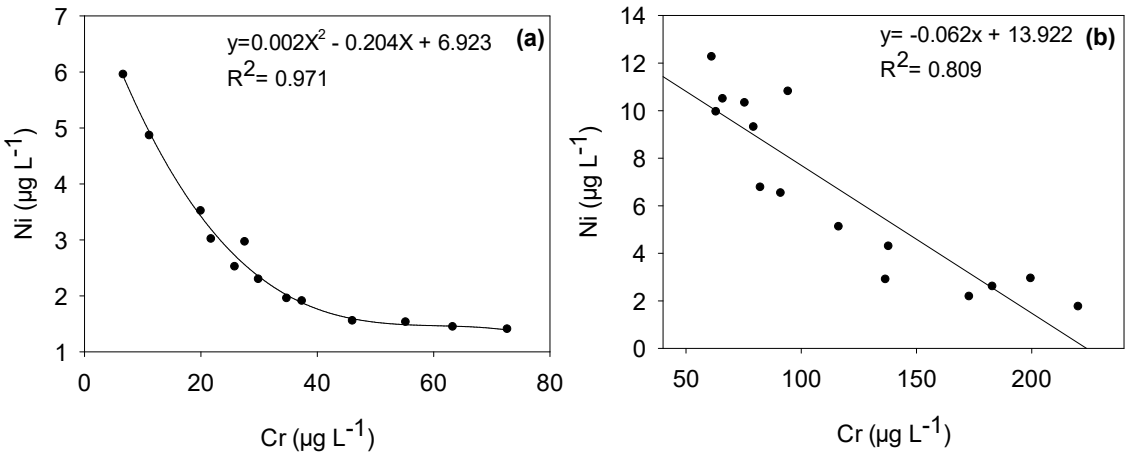

Figure 6.6 Correlation between Cr and Ni in ores (a) OL3 and (b) OL5.

Compared with the lateritic ores, ore OS3 exhibits the lower leachability with Cr concentration between 1.9 and 8.3 µg L^{-1}. This result is associated with the low degree of alteration of the sample. Economou-eliopoulos et al. (2016) found Cr(VI) concentrations in the leachate of laterite 120 times higher than in the saprolite. Several studies have shown that weathering processes promote the oxidation of Cr(III) to Cr(VI). Compounds such as Mn oxides and hydroxides and oxygen can oxidize significant amounts of Cr(III) to Cr(VI) during their reduction (Leita et al., 2009).

Contrary to lateritic ores, the correlation between Cr and Ni is positive in the saprolitic ore OS3 (R^2= 0.88). XRD mineralogical result shows that smectite (clay) and serpentine are the dominant phases in ore OS3. Clay minerals may represent significant Ni and Cr-bearing phases in the first stage of ultramafic rock weathering (Raous et al., 2013).

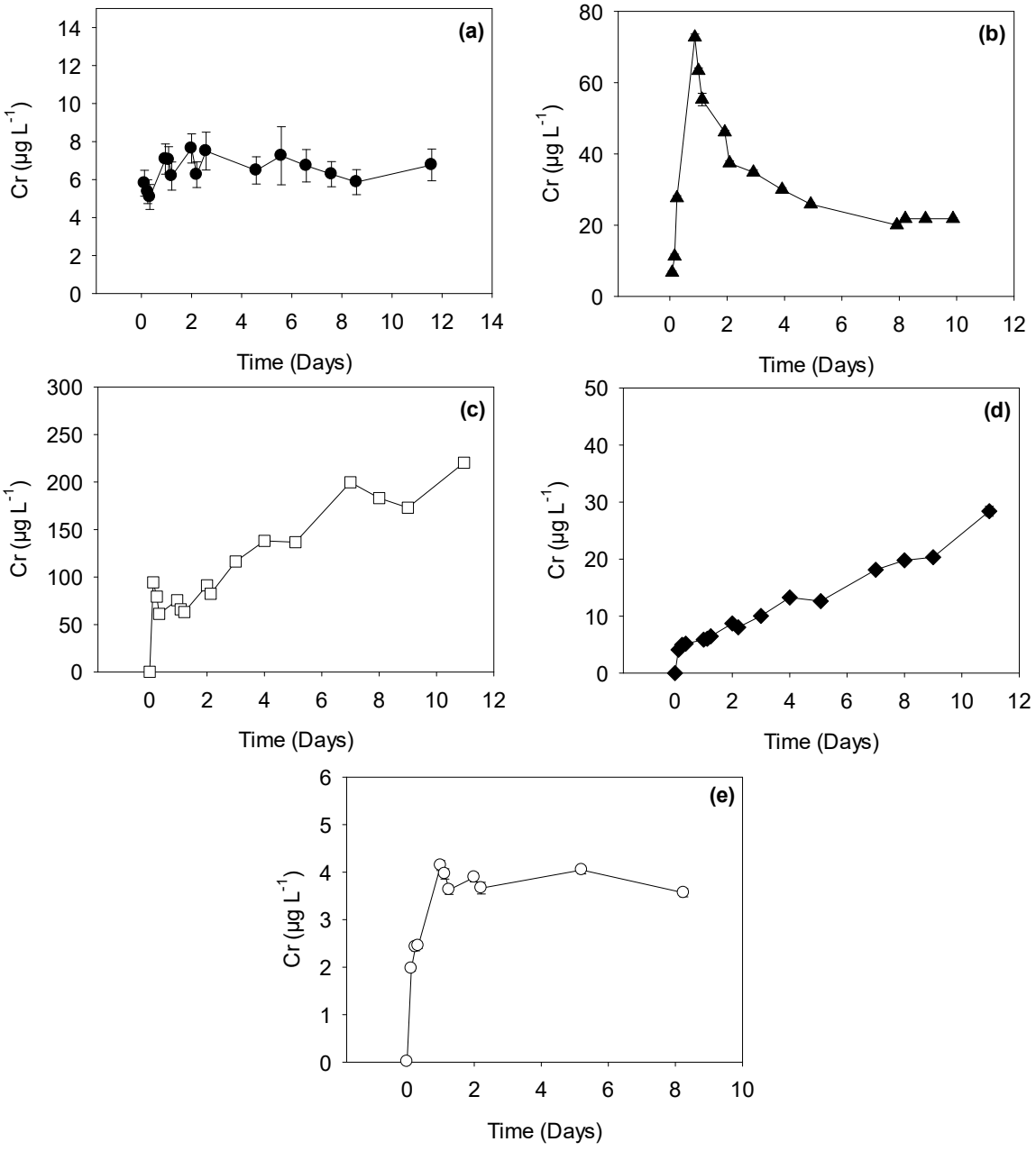

Figure 6.7 Total dissolved Cr concentration as function of time in ores (a) OL1, (b) OL3, (c) OL5, (d) OL8 and (e) OS3.

Ore OS3 displays a positive correlation (R^2=0.89) between total dissolved Cr and Mn concentration. Manganese oxides are known to oxidize Cr(III) to Cr(VI), and manganese dioxides (MnO_2) are the most common oxidant. First, the Cr(III) is sorbed onto MnO_2 surface sites. Then, the Cr(III) is oxidized to Cr(VI) by Mn(IV) on the surface sites, however, all the

Mn(IV) reaction sites are probably not accessible to Cr(III). Finally, the reaction products, Cr(VI) and Mn(II), would be desorbed (Trebien et al., 2011), inducing an increase of both elements in the dissolved fraction.

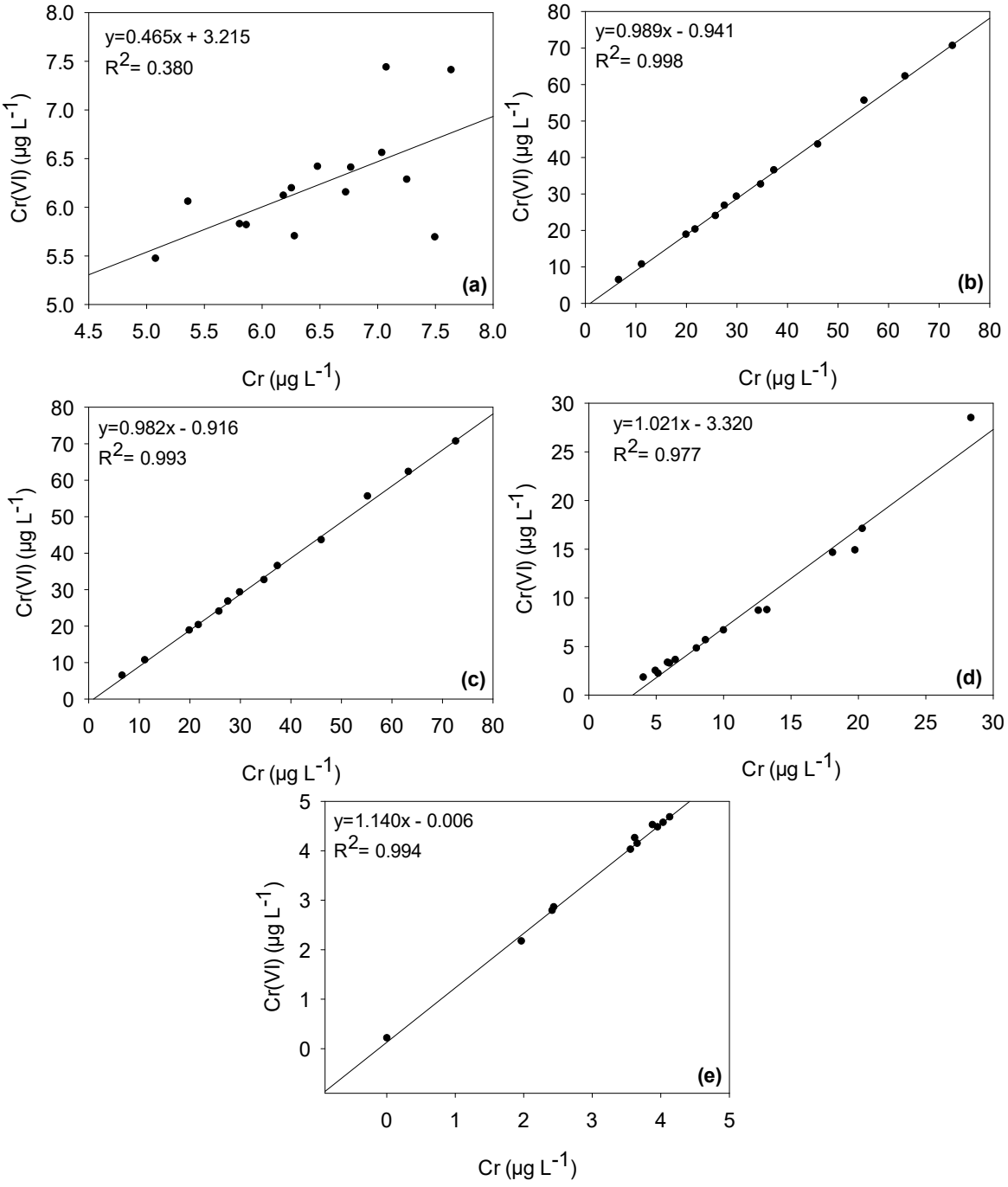

Figure 6.8 Correlation between total dissolved Cr and Cr(VI) concentration as function of time in ores (a) OL1, (b) OL3, (c) OL5, (d) OL8 and (e) OS3.

One of the biggest concerns associated with Cr release from ultramafic environments is its speciation, because hexavalent Cr is known to be highly mobile and toxic (Choppala et al., 2013). Under this consideration, Cr speciation in the leachate was evaluated with HPLC

coupled to an HR-ICP-MS. A positive correlation between total Cr and Cr(VI) was observed in the leachate for all the ores (Figure 6.8). As a result, the total dissolved Cr in the leachates of all the experiments is mainly present as Cr(VI), the most toxic and mobile form. Economou-eliopoulos et al. (2016) performed leaching experiments of Fe-Ni laterites of two locations in Greece (Lokris and Kastoria). Only about 2 μg L^{-1} of Cr(VI) were leached from the Fe-Ni laterites of Lokris, while Kastoria Cr(VI) concentrations reached values as high as 1300 μg L^{-1}. The red mud samples presented Cr(VI) concentrations in the leached as high as 2100 μg L^{-1}. The higher Cr(VI) concentrations in the leachate were associated with the Cr and Mn content which is higher in the lateritic ores compared to the saprolitic one, in which the Cr leachability was low (< 6 μg L^{-1}). Similar result was obtained in leaching experiments performed with Fe-Ni laterites from Greece. In addition, abundant Cr-rich hydrous Fe-oxides were present in samples with higher Cr leachability (Economou-Eliopoulos et al., 2016). Mobilization of Cr(VI) may be driven by Mn-oxide phase such as birnessite. Cooper (2002) identified lower Mn oxides such as hausmannite (Mn_3O_4) and manganite (MnOOH) as capable of oxidizing Cr(III), because the reduction of these oxides provides the most free energy for Cr(III) oxidation according to equations (6.3 and 6.4).

$$\frac{1}{2}Mn_3O_4 + 4H^+ + e^- = \frac{3}{2}Mn^{2+} + 2H_2O \quad \text{Log K} = +30.7 \qquad \textbf{(6.3)}$$

$$MnOOH + 3H^+ + e^- = Mn^{2+} + 2H_2O \quad \text{Log K} = +26.1 \qquad \textbf{(6.4)}$$

6.3.3 Chromium stable isotope values in the leachate

The δ^{53}Cr values measured in the leachate of saprolitic and lateritic ores range between +1.70±0.01‰ and +4.84±0.06‰. The highest Cr isotopes fractionation in the leachate compared with the rest of ore samples was obtained in the lateritic ore OL1 after 12 days of leaching (+4.84±0.06‰). For ore OL1, the total Cr concentration in the leachate was low which limited the δ^{53}Cr measurement during the first 11 days. For the ore OL3, the δ^{53}Cr values did not changed significantly over time with a range of variation between +2.10±0.01‰ and +2.17±0.01‰, however there are statistically distinguishable, showing a release of Cr enriched in heavy ^{53}Cr. For ore OL5 (composed mainly by goethite) the difference of δ^{53}Cr over time is higher than for ore OL3. During the first day δ^{53}Cr is +1.93±0.02‰, +2.04±0.01‰ during the second day and +2.07±0.02‰ after seven days of leaching experiment. The increase of δ^{53}Cr is accompanied with an increase in total and Cr(VI) concentration (R^2=0.60). In spite of Cr concentration increasing over time in both ores, OL5 and OL8, in ore OL8 δ^{53}Cr values did not followed a specific pattern. The δ^{53}Cr increases from +1.72±0.01‰ during the third day of leaching experiment to +1.99±0.01‰ and then decreases again to +1.70±0.01‰ at the end of the experiment. In the saprolitic ore OS3, which is composed by smectite and serpentine, the δ^{53}Cr was within the range of

variation for the lateritic ores. Due to the low total Cr concentration in the leachate, only one δ^{53}Cr value was measured at the end of the experiment (+1.71±0.02‰).

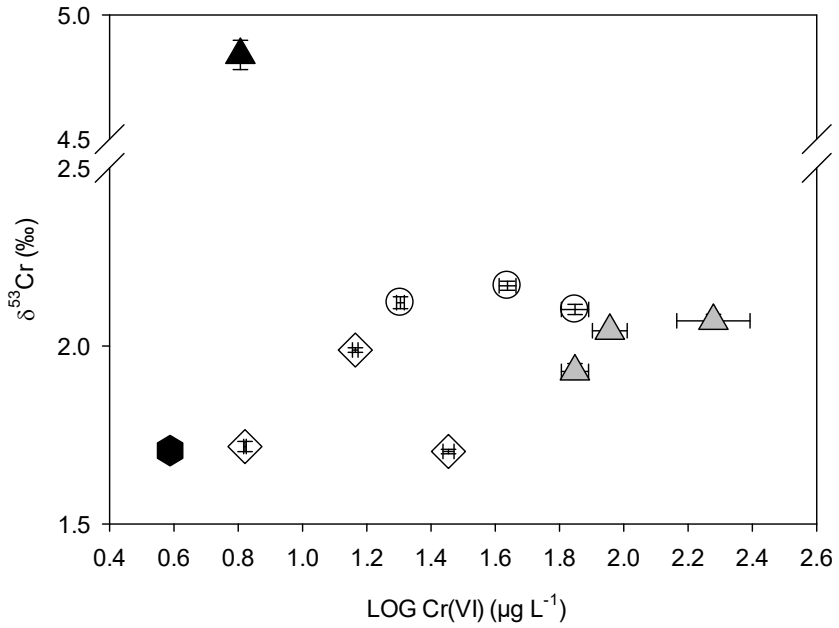

Figure 6.9 Diagram of δ^{53}Cr values in leachate of Fe-Ni laterite from ores OL1 (▲), OL3 (○), OL5(△), OL8(◇) and OS3(⬢).

Given the composition of ore OL3, where only goethite was observed, it can be assumed that Cr(VI) enriched in ^{53}Cr was constantly released from goethite. Two mechanisms could explain this result. In first place, Cr(III) enriched in ^{52}Cr forming inner-sphere complexes onto goethite (Charlet and Manceau, 1992) could be oxidized to Cr(VI) enriched in ^{53}Cr and later mobilized in solution. The second mechanism, includes the direct release of Cr(VI) which was previously sorbed onto goethite. In relation with the first mechanism, Zink et al. (2010) found small (< 1.3 ‰) Cr isotopic fractionation during Cr(III) oxidation experiments under alkaline medium using H_2O_2. Cr isotopic fractionation during Cr(III) oxidation to Cr(VI) has not been extensively studied, compared to Cr(VI) reduction. Thus, probably some pathways producing higher Cr isotopic fractionation during Cr(III) oxidation has not been explored yet. On the other hand, redox processes have been shown to produce significant Cr isotope fractionation whereby the lighter isotopes are preferentially reduced. This results in an enrichment of ^{53}Cr relatively to ^{52}Cr values in the remaining Cr(VI) pools (Ellis et al., 2002). Nevertheless, the reduction of Cr(VI) to Cr(III) with the consequent Cr enrichment in ^{53}Cr in the dissolved fraction, can only be expected to occur in the ore OL3 and less probably in OS3, where total Cr concentration and Cr(VI) decreased after the first day.

Economou-Eliopoulos et al. (2016) performed leaching experiments in batch reactors using natural fresh water and sea water with Fe-Ni laterite sample. The δ^{53}Cr values measured in

natural water leachates ranged between 1.01 ± 0.05 ‰ and -0.21 ± 0.08 ‰. Despite the absence of a clear correlation between Cr(VI) content and δ^{53}Cr values in the diverse leachates, there was an indication that high Cr(VI) concentrations in the laterite leachates yielded to less positively fractionated δ^{53}Cr values. On the contrary, the laterite leachates where Cr(VI) concentrations were low, exhibiting a strongly positively fractionated δ^{53}Cr value. On the opposite, not significant correlation between the δ^{53}Cr value and the Cr(VI) concentration in the leachate were found in the present study, but there is an indication that higher Cr(VI) concentration is more enriched in heavy Cr.

Other study with soils derived from tonalitic bedrock was performed by Berger and Frei (2014). They did leaching experiments under neutral, acidic and alkaline conditions and obtained positive fractionation in the leaching experiments with pure water (+0.21 ± 0.05‰) and with alkaline conditions (+0.48 ± 0.03‰), however under acidic conditions a negative Cr fractionation was obtained (-0.12 ± 0.02‰). Negatives δ^{53}Cr values were associated with dissolution of primary sulfides, while the leachates with small solubilized isotopically heavy Cr was derived from silicates. In the present study, no negative values were obtained in none of the lateritic nor saprolitic ore leachates, which is consistent with the findings of Berger and Frei (2014) and with the speciation of Cr in the leachate (Cr(VI)). Nevertheless, in the present study the sources of Cr(VI) are mainly iron oxides and in minor proportion chlorite, smectite and serpentine.

6.4 CONCLUSIONS

The saprolitic ore was dominated by phyllosilicates, including minerals of the serpentine group, as well as clay minerals (smectite, chlorite). In contrast, Fe oxides (goethite and hematite) were dominant in lateritic ores which presented a higher degree of alteration (UMIA) compared with the saprolitic ore. The exchangeable pool of Cr was significantly higher in lateritic than saprolitic ores, and it was mainly represented by the toxic Cr(VI). This result is associated with the presence of Fe oxides, which serve as a host for exchangeable Cr(VI).

Among the heavy metals released from ores, Cr and Ni are prevalent. Leaching experiments show that Cr(VI) is the dominant Cr species for all the ores, and there are three different Cr comportments overtime. In the leaching experiment with the ore OL1 (quartz, spinel and goethite) chromium remains stable over time. OL1 reported the highest (+4.84±0.06‰) Cr isotopic fractionation (at the end of the experiment) compared with the rest of the ores. In ore OL3 (mainly hematite and chlorite) Cr fate is controlled by manganese oxides which promote a first oxidation from Cr(III) to Cr(VI) followed by co-precipitation. In ores OL5 (goethite) and

OL8 (goethite and spinel) Cr increases overtime as well as the $\delta^{53}Cr$ value, with a maximum concentration for OL8, which presents the highest exchangeable pool of Cr(VI) according to chemical extraction with KH_2PO_4. In the lateritic ore OL5, dissolved oxygen controls Cr speciation because it promotes the presence of Cr(III), however Cr(VI) remains dominant. Finally, in agreement with the exchangeable pool of Cr(VI) and the degree of alteration the saprolitic ore OS3 presented the lowest Cr concentration in the leachate (< 6 μg L^{-1}). However the $\delta^{53}Cr$ value (+1.71±0.02‰) was within the range of variation of the lateritic ores.

Despite weathering in ultramafic areas already being known as a natural source of Cr, mining activities acts as a “catalyst” of this process. This study reveals that although lateritic ores in ultramafic areas are used to extract Ni, significant amounts of Cr can be released, mainly as toxic Cr(VI), due to the exposure of that material to environmental factors such as rain and wind. In this process, pH, dissolved oxygen, manganese and iron oxides control Cr fate and speciation. Our results should encourage mining companies to focus on prevention and mitigation measures not only in Ni contamination, but also in other possible toxic metals such as Cr which can be released from ores to ponds, surface and groundwater.

6.5 BIBLIOGRAPHY

Bartlett, R., James, B., 1996. Chromium, in: Sparks DL, E. (Ed.), Methods of Soil Analysis, Part 3, Chemical Methods. Madison, WI, USA, pp. 683–701.

Becquer, T., Quantin, C., Rotte-Capet, S., Ghanbaja, J., Mustin, C., Herbillon, A.J., 2006. Sources of trace metals in Ferralsols in New Caledonia. Eur. J. Soil Sci. 57, 200–213.

Berger, A., Frei, R., 2014. The fate of chromium during tropical weathering: A laterite profile from central madagascar. Geoderma 213, 521–532. doi:10.1016/j.geoderma.2013.09.004

Birck, J.L., Allegre, C.J., 1988. Manganese-chromium isotope systematics and the development of the early Solar System. Nature 331, 579–584.

Butler, B.A., 2009. Effect of pH, ionic strength, dissolved organic carbon, time, and particle size on metals release from mine drainage impacted streambed sediments. Water Res. 43, 1392–1402. doi:10.1016/j.watres.2008.12.009

Casarotto de Oliveira, P., Valentin, L., 2017. Evaluation of weathering of basaltic lithotypes based on pH, electrical conductivity, and point-load strength tests. Civ. Eng. 70, 265–271.

Charlet, L., Manceau, A., 1992. X-Ray Absorption Spectroscopic Study of the Sorption of Cr (lll) at the Oxide-Water Interface. J. Colloid Interface Sci. 148, 443–458.

Choppala, G., Bolan, N., Park, J.H., 2013. Chromium Contamination and Its Risk Management in Complex Environmental Settings, Advances in Agronomy. Elsevier.

doi:10.1016/B978-0-12-407686-0.00002-6

Colin, F., Nahon, D., Trescases, J.J., Melfi, a. J., 1990. Lateritic weathering of pyroxenites at Niquelandia, Goias, Brazil: the supergene behavior of nickel. Econ. Geol. 85, 1010–1023. doi:10.2113/gsecongeo.85.5.1010

Cooper, G.R.C., 2002. Oxidation and toxicity of chromium in ultramafic soils in Zimbabwe. Appl. Geochemistry 17, 981–986. doi:10.1016/S0883-2927(02)00014-8

Crowe, S.A., Døssing, L.N., Beukes, N.J., Bau, M., Kruger, S.J., Frei, R., Canfield, D.E., 2013. Atmospheric oxygenation three billion years ago. Nature 501, 535–538. doi:10.1038/nature12426

Døssing, L.N., Dideriksen, K., Stipp, S.L.S., Frei, R., 2011. Reduction of hexavalent chromium by ferrous iron: A process of chromium isotope fractionation and its relevance to natural environments. Chem. Geol. 285, 157–166. doi:10.1016/j.chemgeo.2011.04.005

Economou-Eliopoulos, M., Frei, R., Megremi, I., 2016. Potential leaching of Cr (VI) from laterite mines and residues of metallurgical products (red mud and slag): An integrated approach. J. Geochemical Explor. 162, 40–49. doi:10.1016/j.gexplo.2015.12.007

Ellis, A.S., Johnson, T.M., Bullen, T.D., 2002. Chromium Isotopes and the Fate of Hexavalent Chromium in the Environment. Science. 295, 2060–2062. doi:10.1126/science.1068368

Fagoyinbo, C.V.O., Adeola, A.J., 2017. Relative Abundance of Minerals in Parent Rock and their Effects on Laterite Properties. J. Sci. Eng. Res. 4, 41–50.

Fendorf, S.E., 1995. Surface reactions of chromium in soils and waters. Geoderma 67, 55–71. doi:10.1016/0016-7061(94)00062-F

Frei, R., Polat, A., 2013. Chromium isotope fractionation during oxidative weathering — Implications from the study of a Paleoproterozoic (ca. 1.9 Ga) paleosol, Schreiber Beach, Ontario, Canada. Precambrian Res. 224, 434–453. doi:10.1016/j.precamres.2012.10.008

Leita, L., Margon, A., Pastrello, A., Arčon, I., Contin, M., Mosetti, D., 2009. Soil humic acids may favour the persistence of hexavalent chromium in soil. Environ. Pollut. 157, 1862–1866. doi:10.1016/j.envpol.2009.01.020

Lilli, M.A., Moraetis, D., Nikolaidis, N.P., Karatzas, G.P., Kalogerakis, N., 2015. Characterization and mobility of geogenic chromium in soils and river bed sediments of Asopos basin. J. Hazard. Mater. 281, 12–19. doi:10.1016/j.jhazmat.2014.07.037

Liu, S., Chen, L., Gao, Y., 2013. Hexavalent Chromium Leaching Influenced Factors in the Weathering Chrome Slag. Procedia Environ. Sci. 18, 783–787. doi:http://dx.doi.org/10.1016/j.proenv.2013.04.105

Marker, A., Friedrich, G., Carvalho, A., Melfi, A., 1991. Control of the distribution of Mn, Co,

Zn, Zr, Ti and REEs during the evolution of lateritic covers above ultramafic complexes. J. Geochemical Explor. 40, 361–383. doi:10.1016/0375-6742(91)90048-Y

Mcclain, C.N., Maher, K., 2016. Chromium fluxes and speciation in ultramafic catchments and global rivers. Chem. Geol. 426, 135–157. doi:10.1016/j.chemgeo.2016.01.021

Morrison, J.M., Goldhaber, M.B., Mills, C.T., Breit, G.N., Hooper, R.L., Holloway, J.A.M., Diehl, S.F., Ranville, J.F., 2015. Weathering and transport of chromium and nickel from serpentinite in the Coast Range ophiolite to the Sacramento Valley, California, USA. Appl. Geochemistry 61, 72–86. doi:10.1016/j.apgeochem.2015.05.018

Paulukat, C., Døssing, L.N., Mondal, S.K., Voegelin, A.R., Frei, R., 2015. Oxidative release of chromium from Archean ultramafic rocks, its transport and environmental impact – A Cr isotope perspective on the Sukinda valley ore district (Orissa, India). Appl. Geochemistry 59, 125–138. doi:10.1016/j.apgeochem.2015.04.016

Raous, S., Becquer, T., Garnier, J., Martins, É.D.S., Echevarria, G., Sterckeman, T., 2010. Mobility of metals in nickel mine spoil materials. Appl. Geochemistry 25, 1746–1755. doi:10.1016/j.apgeochem.2010.09.001

Raous, S., Echevarria, G., Sterckeman, T., Hanna, K., Thomas, F., Martins, E.S., Becquer, T., 2013. Potentially toxic metals in ultramafic mining materials: Identification of the main bearing and reactive phases. Geoderma 192, 111–119. doi:10.1016/j.geoderma.2012.08.017

Ratié, G., Jouvin, D., Garnier, J., Rouxel, O., Miska, S., Guimarães, E., Vieira, L.C., Sivry, Y., Zelano, I., Pelletier, E.M., Thil, F., Quantin, C., 2015. Nickel isotope fractionation during tropical weathering of ultramafic rocks. Chem. Geol. 402, 68–76. doi:10.1016/j.chemgeo.2015.02.039

Stueber, A.M., Goles, G.G., 1967. Abundances of Na, Mn, Cr, Sc and Co in ultramafic rocks. Geochim. Cosmochim. Acta 31, 75–93. doi:10.1016/0016-7037(67)90099-3

Tashakor, M., Hochwimmer, B., Brearley, F.Q., 2017. Geochemical assessment of metal transfer from rock and soil to water in serpentine areas of Sabah (Malaysia). Environ. Earth Sci. 76, 1–13. doi:10.1007/s12665-017-6585-x

Tina, S., Echevarria, G., Becquer, T., Ghanbaja, J., Leclerc-cessac, E., Morel, J., 2006. Control of nickel availability by nickel bearing minerals in natural and anthropogenic soils. Geoderma 136, 28–37. doi:10.1016/j.geoderma.2006.01.008

Trebien, D.O.P., Bortolon, L., Tedesco, M.J., Bissani, C.A., Camargo, F.A.O., 2011. Environmental Factors Affecting Chromium-Manganese Oxidation-Reduction Reactions in Soil. Pedosphere 21, 84–89. doi:10.1016/S1002-0160(10)60082-3

Trinquier, A., Birck, J.-L., Allègre, C.J., 2008. High-precision analysis of chromium isotopes in terrestrial and meteorite samples by thermal ionization mass spectrometry. J. Anal. At. Spectrom. 23, 1565. doi:10.1039/b809755k

Viollier, E., Inglett, P.W., Hunter, K., Roychoudhury, a. N., Van Cappellen, P., 2000. The ferrozine method revisited: Fe(II)/Fe(III) determination in natural waters. Appl. Geochemistry 15, 785–790. doi:10.1016/S0883-2927(99)00097-9

White, A.F., Blum, A.E., 1995. Effects of climate on chemical weathering in watersheds. Geochim. Cosmochim. Acta 59, 1729–1747. doi:10.1016/0016-7037(95)00078-E

Zink, S., Schoenberg, R., Staubwasser, M., 2010. Isotopic fractionation and reaction kinetics between Cr(III) and Cr(VI) in aqueous media. Geochim. Cosmochim. Acta 74, 5729–5745. doi:10.1016/j.gca.2010.07.015

6.6 SUPPLEMENTARY DATA

Table S6.1. Physicochemical characterization of the leachate of ore OL1 as a function of time.

	Ore OL1															
Time (hrs)	0	3	6	8	23	26	29	48	53	62	110	134	158	182	206	278
pH	6.5	6.6	6.5	6.5	6.6	6.6	6.6	6.6	6.5	6.6	6.5	6.5	6.4	6.4	6.4	6.5
Cond (µs cm^{-1})	117.7	118.8	119.7	120.0	125.4	125.5	125.7	132.0	131.9	136.0	145.3	145.7	145.5	148.5	150.1	100.8
OD (mg L^{-1})	8.6	8.5	8.5	8.5	8.5	8.4	8.5	8.5	8.4	8.6	8.7	8.7	8.6	8.7	8.8	8.7
T° (°C)	23.3	23.1	22.8	22.8	22.9	23.2	23.1	22.3	22.7	21.7	21.8	22.1	21.4	22	22.1	22.2
DOC (mg L^{-1})	0.53	2.85	3.21	2.35	4.84	7.29	4.20	4.53	4.35	4.27	2.97	2.95	2.73	2.51	3.11	4.92
Alkalinity (µM)	3.22	-	-	-	-	-	-	-	-	-	-	-	-	-	-	47.90
F^- (µg L^{-1})	< LoD	82.99	78.77	73.85	95.43	77.00	89.06	97.62	86.80	71.81	90.76	122.51	82.65	66.38	91.44	137.31
Cl^- (µg L^{-1})	313	2068	1975	1843	2310	2214	2124	2751	2702	3252	3347	3209	2780	2381	2333	3225
NO_3^- (µg L^{-1})	58370	54423	56039	56118	58541	59380	59928	62420	63023	67496	71160	74199	75633	75721	78365	92413
Al (µg L^{-1})	<LoD	<LoD	<LoD	<LoD	<LoD	0.37	<LoD	<LoD	0.01	<LoD	<LoD	<LoD	<LoD	<LoD	<LoD	<LoD
Ba (µg L^{-1})	<LoD	35.37	38.48	39.67	40.94	39.50	38.34	46.74	46.42	37.23	35.93	35.23	37.13	39.28	38.51	40.89
Ca (µg L^{-1})	49.72	68.03	58.95	51.76	57.31	43.11	45.67	40.54	42.01	44.05	37.96	41.46	41.07	49.04	48.10	92.94
Co (µg L^{-1})	<LoD	0.12	0.20	0.30	0.15	0.16	0.16	0.17	0.00	0.17	0.22	0.25	0.22	0.26	0.28	0.27
Total Cr(µg L^{-1})	<LoD	5.81	5.36	5.08	7.08	7.04	6.19	7.64	6.26	7.50	6.48	7.26	6.73	6.29	5.87	6.77
Cr(VI) (µg L^{-1})	< LoD	5.82	6.05	5.47	7.43	6.55	6.12	7.41	6.19	5.69	6.41	6.28	6.15	5.70	5.81	6.40
Cu (µg L^{-1})	<LoD	<LoD	<LoD	<LoD	<LoD	<LoD	<LoD	<LoD	<LoD	<LoD	<LoD	<LoD	<LoD	<LoD	<LoD	<LoD
Fe (µg L^{-1})	<LoD	<LoD	<LoD	<LoD	<LoD	<LoD	<LoD	<LoD	<LoD	<LoD	<LoD	<LoD	<LoD	<LoD	<LoD	<LoD
K (µg L^{-1})	21.09	1771	1663	1554	2034	1905	1877	2461	2418	2934	2083	2160	2647	2782	3091	3228
Mg (µg L^{-1})	2.90	266.99	257.90	244.56	241.45	220.49	208.79	212.78	204.64	234.72	196.88	201.73	223.49	240.68	263.16	285.79
Mn (µg L^{-1})	<LoD	1.12	1.33	1.36	1.54	1.38	1.33	1.56	1.79	1.44	2.23	3.11	3.09	3.53	3.61	3.79
Na (µg L^{-1})	21251	20843	20751	21006	21273	20826	21123	21654	21873	23276	25198	25087	25147	24044	24747	31912
Ni (µg L^{-1})	<LoD	11.79	9.80	10.26	7.97	7.95	6.72	5.58	5.79	6.52	6.12	7.87	6.63	7.06	6.40	6.56
P (µg L^{-1})	< LoD	<LoD	<LoD	<LoD	<LoD	<LoD	<LoD	<LoD	<LoD	<LoD	<LoD	<LoD	<LoD	<LoD	<LoD	<LoD
S (µg L^{-1})	< LoD	<LoD	<LoD	<LoD	<LoD	<LoD	<LoD	<LoD	<LoD	<LoD	<LoD	<LoD	<LoD	<LoD	<LoD	<LoD
Si (µg L^{-1})	5.25	1226	1224	1201	1242	1185	1158	1172	1164	1257	1181	1183	1208	1255	1324	1465
Zn (µg L^{-1})	< LoD	34.98	38.83	40.93	40.23	41.68	38.90	50.41	0.41	38.60	38.52	41.14	37.93	36.90	39.73	38.76

Table S6.2. Physicochemical characterization of the leachate of ore OL3 as a function of time.

	Ore OL3															
Time (hrs)	0	2	4	6	21	24	27	46	50	70	94	118	190	197	214	237
pH	5.8	5.8	6.0	6.4	6.7	6.7	6.6	6.6	6.5	6.4	6.4	6.4	6.3	7.2	7.4	7.4
Cond (µs cm^{-1})	111.4	111.6	115.1	119.8	127.3	126.5	126.5	133.3	130.6	135.1	144.8	144.6	157.4	180.4	187.7	219.0
OD (mg L^{-1})	8.5	8.3	8.2	8.1	7.6	7.5	7.4	7.1	7.2	7.2	7.1	7.3	6.9	7.5	7.2	7.0
T° (°C)	22.3	22.2	22.2	22.2	22.2	22.6	22.6	22.7	22.7	22.3	22.4	22.1	20.2	21.1	21.5	21.6
DOC (mg L^{-1})	0.94	1.97	2.17	2.06	2.27	2.47	2.49	2.90	2.62	2.61	5.00	2.81	3.17	5.52	2.90	3.61
Alkalinity (µM)	1.49	-	-	-	-	-	-	-	-	-	-	-	-	-	-	289.40
F^- (µg L^{-1})	103.51	108.35	168.50	274.21	149.88	158.01	143.24	107.81	102.96	126.32	160.34	156.36	200.01	176.99	245.80	218.70
Cl^- (µg L^{-1})	1587.51	407.83	254.40	436.41	100.34	136.99	131.28	6.44	339.54	53.24	47.39	0.53	308.81	105.17	482.83	360.92
NO_3^- (µg L^{-1})	61123	55972	58129	59790	63037	63602	64451	68013	68191	71929	76505	78626	92865	86787	92408	102177
Al (µg L^{-1})	< LoD	< LoD	< LoD	0.19	0.04	< LoD	< LoD	< LoD	< LoD	< LoD	< LoD	< LoD	< LoD	< LoD	0.79	0.88
Ba (µg L^{-1})	< LoD	0.42	0.42	0.29	0.30	0.33	0.36	0.53	0.61	0.81	1.18	1.22	1.48	1.34	0.47	0.54
Ca (µg L^{-1})	52.32	39.72	65.43	43.36	51.65	14.33	18.36	20.33	24.09	22.84	15.05	29.36	42.24	14.95	21.86	11.12
Co (µg L^{-1})	< LoD	0.60	0.49	0.26	0.08	0.08	0.09	0.10	0.13	0.14	0.17	0.20	0.31	0.26	0.01	< LoD
Total Cr(µg L^{-1})	< LoD	6.72	11.24	27.64	72.74	63.36	55.27	46.11	37.43	34.82	29.99	25.89	20.04	21.83	-	-
Cr(VI) (µg L^{-1})	<LoD	6.34	10.57	26.67	70.51	62.13	55.46	43.48	36.37	32.50	29.14	23.86	18.71	20.17	547.16	587.65
Cu (µg L^{-1})	0.04	0.01	< LoD	< LoD	< LoD	< LoD	< LoD	< LoD	0.35	< LoD	< LoD	< LoD	< LoD	< LoD	< LoD	< LoD
Fe (µg L^{-1})	< LoD	0.12	< LoD	0.13	< LoD	< LoD	< LoD	< LoD	< LoD	< LoD	0.20	< LoD	< LoD	< LoD	< LoD	< LoD
K (µg L^{-1})	28.49	687.39	1663.32	3081.92	4582.28	4223.93	3913.98	3731.04	3301.19	3105.93	2940.45	2779.46	2913.69	2560.18	-	-
Mg (µg L^{-1})	1.06	20.11	15.49	11.52	10.23	9.76	9.65	10.96	11.88	11.93	13.63	16.84	20.32	16.73	18.73	20.99
Mn (µg L^{-1})	< LoD	3.02	2.39	1.22	0.20	0.24	0.27	0.33	0.52	0.58	0.88	1.01	1.52	1.41	0.03	0.01
Na (µg L^{-1})	22800	20632	21639	21293	20740	21371	21159	23431	22854	24000	24409	25488	28642	27063	28105	29628
Ni (µg L^{-1})	< LoD	5.94	4.85	2.96	1.40	1.44	1.52	1.55	1.90	1.95	2.29	2.51	3.51	3.01	2.92	< LoD
P (µg L^{-1})	< LoD	< LoD	< LoD	< LoD	< LoD	< LoD	< LoD	< LoD	< LoD	< LoD	< LoD	< LoD	< LoD	< LoD	< LoD	< LoD
S (µg L^{-1})	< LoD	< LoD	< LoD	< LoD	< LoD	< LoD	< LoD	< LoD	< LoD	< LoD	< LoD	< LoD	< LoD	< LoD	< LoD	< LoD
Si (µg L^{-1})	11.24	1067.10	1103.93	1055.55	1022.72	1298.72	1002.11	1076.91	1041.43	1035.48	995.03	1007.05	1046.77	953.54	857.71	893.58
Zn (µg L^{-1})	1.09	0.23	0.20	0.15	0.12	0.05	0.09	0.05	0.54	0.20	0.70	0.38	0.64	0.58	0.20	0.11

Table S6.3. Physicochemical characterization of the leachate of ore OL5 as a function of time.

	Ore OL5															
Time (hrs)	0	3	6	8	23	26	29	48	51	72	96	122	168	192	216	263
pH	6.8	7.0	6.7	6.8	6.8	6.7	6.7	6.9	6.8	6.9	7.0	7.1	7.1	7.1	7.1	7.1
Cond (µs cm^{-1})	124.6	131.3	128.9	129.4	133.8	133.6	133.2	141.1	140.6	148.3	155.0	159.4	171.1	171.8	173.8	187.1
OD (mg L^{-1})	8.5	7.8	8.1	8.0	7.8	7.7	7.7	7.0	6.1	4.6	4.6	4.3	4.3	4.0	3.9	5.8
T° (°C)	22.7	22.3	22.4	22.2	22.0	22.3	22.4	22.0	22.4	21.9	22.2	22.6	22.1	22.2	22.0	22.4
DOC (mg L^{-1})	2.24	5.09	3.45	1.94	2.52	2.21	6.55	5.62	6.20	3.50	5.81	4.04	5.26	5.51	3.89	7.59
Alkalinity (µM)	1.49	-	-	-	-	-	-	-	-	-	-	-	-	-	-	168.37
F$^-$ (µg L^{-1})	67	133	142	154	144	138	292	157	167	167	357	182	196	257	181	93
Cl$^-$ (µg L^{-1})	59	33	212	64	171	361	533	386	348	359	719	381	66	403	99	110
NO_3^- (µg L^{-1})	65497	63841	64516	65570	68375	68909	70237	73547	74028	78701	84886	87046	94842	95282	96469	104997
Al (µg L^{-1})	0.05	0.11	-	-	0.07	0.05	0.05	0.11	0.15	0.20	0.38	0.34	0.28	0.30	0.36	0.49
Ba (µg L^{-1})	<LoD	1.24	1.20	1.33	1.43	1.47	1.39	1.34	1.24	1.42	1.36	1.30	1.25	1.33	1.23	1.15
Ca (µg L^{-1})	22.52	49.99	52.04	51.10	65.63	42.25	37.65	49.41	42.85	45.33	45.44	30.94	35.85	28.56	45.73	43.31
Co (µg L^{-1})	<LoD	0.09	0.10	0.14	0.13	0.16	0.16	0.11	0.12	0.12	0.13	0.10	0.10	0.13	0.20	0.18
Total Cr(µg L^{-1})	0.35	94.50	79.49	61.33	75.67	66.14	63.17	91.34	82.46	116.41	138.13	136.82	199.83	183.14	173.04	220.33
Cr(VI) (µg L^{-1})	<LoD	93.67	73.81	58.69	70.46	63.72	61.65	90.46	81.54	111.18	141.39	133.63	190.00	170.83	178.19	217.35
Cu (µg L^{-1})	<LoD	<LoD	<LoD	<LoD	<LoD	<LoD	<LoD	<LoD	<LoD	<LoD	0.01	<LoD	<LoD	<LoD	<LoD	<LoD
Fe (µg L^{-1})	9.29	<LoD	<LoD	<LoD	<LoD	<LoD	<LoD	<LoD	<LoD	<LoD	5.23	0.30	<LoD	<LoD	<LoD	<LoD
K (µg L^{-1})	17.71	5023.26	4312.73	3732.86	4393.74	4003.75	3740.25	4741.34	4308.41	5487.51	6316.42	6678.22	8041.24	7971.25	7498.17	8865.83
Mg (µg L^{-1})	0.47	583.63	512.23	536.73	521.46	497.78	452.66	455.43	430.76	431.05	423.40	390.38	414.43	379.95	337.92	352.69
Mn (µg L^{-1})	<LoD	0.23	0.34	0.41	0.38	0.49	0.60	0.43	0.48	0.58	0.79	0.85	0.56	0.92	1.39	1.27
Na (µg L^{-1})	21427	19957	19676	20105	20900	20841	20489	21807	22082	23347	24537	25288	27370	27319	26903	29574
Ni (µg L^{-1})	<LoD	10.79	9.29	12.24	10.30	10.48	9.93	6.51	6.75	5.09	4.27	2.88	2.92	2.59	2.16	1.74
P (µg L^{-1})	< LoD	< LoD	< LoD	< LoD	< LoD	< LoD	< LoD	< LoD	< LoD	< LoD	< LoD	< LoD	< LoD	< LoD	< LoD	< LoD
S (µg L^{-1})	< LoD	< LoD	< LoD	< LoD	< LoD	< LoD	< LoD	< LoD	< LoD	< LoD	< LoD	< LoD	< LoD	< LoD	< LoD	< LoD
Si (µg L^{-1})	0.73	1284	1266	1379	1516	1485	1415	1501	1456	1530	1528	1460	1572	1529	1389	1529
Zn (µg L^{-1})	0.14	0.26	0.24	0.17	0.19	0.59	0.44	0.26	0.43	0.28	1.68	0.28	0.50	0.73	2.01	0.82

Table S6.4. Physicochemical characterization of the leachate of ore OL8 as a function of time.

	Ore OL8															
Time (hours)	0	3	6	9	24	27	30	48	53	72	96	122	168	192	216	263
pH	5.8	5.7	5.6	5.6	5.7	5.7	5.7	5.9	5.8	5.9	6.0	6.0	6.1	6.1	6.2	6.3
Cond (µs cm^{-1})	115.9	112.7	113.8	114.6	121.3	122.1	123.1	129.3	130.4	135.0	140.8	148.4	159.6	162.1	164.7	182.4
OD (mg L^{-1})	8.6	8.5	8.4	8.5	8.5	8.6	8.5	7.9	8.6	8.0	7.4	8.9	8.5	8.9	8.3	7.5
T° (°C)	23.0	22.2	22.0	21.9	21.4	21.8	22.0	21.0	21.7	21.0	21.6	20.7	18.9	20.2	20.6	21.5
DOC (mg L^{-1})	4.1	8.4	8.1	6.8	4.0	3.8	5.0	16.0	15.5	13.0	6.7	17.7	6.0	9.3	7.7	21.3
Alkalinity (µM)	2.43	-	-	-	-	-	-	-	-	-	-	-	-	-	-	37.02
F$^-$ (µg L^{-1})	38.20	164.84	170.58	174.31	206.75	177.67	168.63	187.83	208.53	232.21	237.42	226.46	298.32	259.00	297.93	296.01
Cl$^-$ (µg L^{-1})	305.24	143.91	107.74	110.85	144.81	128.89	138.81	152.86	179.22	196.48	212.95	234.03	310.95	308.98	297.55	393.56
Al (µg L^{-1})	<LoD	0.69	0.24	0.24	0.47	0.25	0.19	0.12	0.20	0.26	0.30	0.66	0.54	0.49	0.72	1.70
Ba (µg L^{-1})	<LoD	3.32	4.00	3.81	3.99	3.87	3.74	4.12	4.01	3.90	3.65	3.99	3.89	3.75	3.56	3.83
Ca (µg L^{-1})	16.22	51.68	50.52	57.45	55.63	47.20	170.23	49.63	47.04	48.29	52.88	71.45	64.34	52.91	91.30	160.66
Co (µg L^{-1})	<LoD	2.03	2.52	2.50	2.58	2.48	2.41	2.57	2.51	2.43	2.29	2.39	2.34	2.23	2.07	2.17
Total Cr(µg L^{-1})	0.02	4.09	4.97	5.18	5.89	6.03	6.46	8.71	8.03	10.03	13.26	12.63	18.14	19.80	20.33	28.41
Cr(VI) (µg L^{-1})	<LoD	1.77	2.46	2.15	3.30	3.22	3.57	5.60	4.77	6.62	8.69	8.63	14.59	14.85	17.04	28.45
Cu (µg L^{-1})	<LoD	0.14	0.15	0.14	0.08	0.09	0.07	0.04	0.07	0.04	0.01	0.03	0.02	0.01	0.04	0.03
Fe (µg L^{-1})	1.42	0.41	0.12	0.12	0.34	0.18	0.23	<LoD	0.11	0.25	0.41	0.88	0.63	0.45	0.45	1.02
K (µg L^{-1})	10.88	221	198	264	622	580	669	1182	1176	1593	2134	2425	3582	3597	3996	5291
Mg (µg L^{-1})	1.27	1172	1362	1378	1384	1250	1261	1298	1296	1272	1160	1241	1308	1154	1184	1210
Mn (µg L^{-1})	<LoD	4.47	4.98	5.19	5.61	5.34	5.24	5.93	5.87	5.92	5.75	5.81	5.73	5.46	4.97	5.31
Na (µg L^{-1})	24113	19634	17761	19425	19852	19224	20582	21282	22006	23215	23734	25170	28115	27551	30392	32901
Ni (µg L^{-1})	0.29	632	744	763	750	692	684	705	705	682	617	679	682	603	616	612
P (µg L^{-1})	< LoD	< LoD	< LoD	< LoD	< LoD	< LoD	< LoD	< LoD	< LoD	< LoD	< LoD	< LoD	< LoD	< LoD	< LoD	< LoD
S (µg L^{-1})	< LoD	< LoD	< LoD	< LoD	< LoD	< LoD	< LoD	< LoD	< LoD	< LoD	< LoD	< LoD	< LoD	< LoD	< LoD	< LoD
Si (µg L^{-1})	1.41	1042	1287	1455	1577	1491	1510	1588	1610	1648	1582	1717	1727	1598	1665	1694
Zn (µg L^{-1})	0.22	9.26	9.38	10.42	9.64	9.52	9.31	9.11	8.84	8.46	7.18	7.23	6.97	5.59	5.07	5.76

Table S6.5. Physicochemical characterization of the leachate of ore OS3 as a function of time.

	Ore OS3															
Time (hrs)	0	3	6	8	24	27	30	48	53	72	96	125	192	198	216	262
pH	6.9	6.8	6.7	6.7	6.8	6.8	6.8	6.8	6.8	6.8	6.9	6.9	6.9	6.9	7.0	7.1
Cond (µs cm^{-1})	110.0	111.1	111.5	111.4	115.4	115.3	115.1	117.9	118.0	121.1	124.7	134.6	146.5	142.9	143.7	157.0
OD (mg L^{-1})	8.6	8.4	8.5	8.6	9.1	9.1	8.7	8.8	8.7	8.7	8.8	9.1	9.3	9.2	9.1	9.3
T° (°C)	23.4	23.2	23.4	23.3	23.1	23.1	23.1	22.4	22.6	22.2	22.2	21.1	20.5	20.9	21.0	20.6
DOC (mg L^{-1})	4.78	19.37	14.75	19.18	8.07	7.26	16.65	8.92	7.97	5.22	6.12	8.71	7.37	5.74	4.54	4.37
Alkalinity (µM)	2.43	-	-	-	-	-	-	-	-	-	-	-	-	-	-	121.08
F$^-$ (µg L^{-1})	37	126	140	141	170	176	142	168	154	153	138	145	125	109	106	148
Cl$^-$ (µg L^{-1})	107	287	273	255	282	262	612	243	220	230	269	262	390	277	262	295
Al (µg L^{-1})	0.20	2.16	2.78	2.85	4.67	4.47	4.25	4.51	4.14	4.63	4.60	4.56	5.26	4.01	3.68	3.87
Ba (µg L^{-1})	0.09	0.31	1.02	0.50	0.62	1.05	0.08	0.52	0.05	19.43	47.73	3.40	37.54	-	70.95	51.86
Ca (µg L^{-1})	<LoD	3.11	2.96	2.67	3.03	2.83	2.69	2.74	2.61	2.70	2.86	3.30	3.51	2.92	2.88	3.32
Co (µg L^{-1})	38	115	144	179	177	271	77	81	77	104	95	83	117	78	83	135
Total Cr(µg L^{-1})	<LoD	0.26	0.24	0.23	0.24	0.24	0.20	0.21	0.20	0.70	1.37	0.25	1.15	0.22	1.92	1.56
Cr(VI) (µg L^{-1})	0.01	1.97	2.42	2.45	4.14	3.96	3.63	3.89	3.66	5.51	6.99		7.15	-	8.36	7.73
Cu (µg L^{-1})	<LoD	0.03	0.12	0.03	0.04	0.05	<LoD	<LoD	<LoD	0.05	0.14	0.16	0.12	<LoD	0.22	0.15
Fe (µg L^{-1})	1.17	1.11	3.28	2.44	2.57	4.26	-	0.45	-	174.52	410.91	21.02	333.12	-	632.14	484.73
K (µg L^{-1})	32.94	646	576	595	677	698	640	814	770	882	988	1126	1763	1521	1545	4207
Mg (µg L^{-1})	3.05	3231	3097	2995	3153	2995	2876	2834	2681	2916	3155	2786	3718	2867	3248	3434
Mn (µg L^{-1})	<LoD	0.28	0.29	0.29	0.35	0.36	0.23	0.40	0.31	0.71	1.29	0.58	1.46	0.62	1.97	1.93
Na (µg L^{-1})	18839	13754	13631	14631	14704	15031	15418	16063	16281	16676	17562	18421	22387	21571	21498	23589
Ni (µg L^{-1})	1.58	340.58	337.24	327.68	351.26	337.69	326.60	323.92	310.16	387.96	487.13	319.62	515.53	328.65	559.76	525.30
P (µg L^{-1})	< LoD	< LoD	< LoD	< LoD	< LoD	< LoD	< LoD	< LoD	< LoD	< LoD	< LoD	< LoD	< LoD	< LoD	< LoD	< LoD
S (µg L^{-1})	< LoD	< LoD	< LoD	< LoD	< LoD	< LoD	< LoD	< LoD	< LoD	< LoD	< LoD	< LoD	< LoD	< LoD	< LoD	< LoD
Si (µg L^{-1})	1.42	3263	3906	4154	6216	6031	5814	6149	5752	6500	7151	6481	7647	5633	6509	6779
Zn (µg L^{-1})	0.19	0.18	1.02	0.41	0.41	1.54	0.05	0.11	0.09	0.35	0.48	0.47	0.53	0.07	0.69	0.62

CHAPTER 7

(Bio)leaching behavior of chromite tailings

This chapter has been published:

Bolaños-Benítez, V., van Hullebusch, E., Lens, P., Quantin, C., van de Vossenberg, J., Subramanian, S., Sivry, Y., 2018. (Bio)leaching Behavior of Chromite Tailings. Minerals 8, 261. https://doi.org/10.3390/min8060261

CHAPTER 7

7.1 INTRODUCTION

In India, there are 9900 mining leases, spread over an area of 7453 km^2, covering 55 minerals other than fuel. The Sukinda valley in Jajpur District, Orissa, known for its chromite ($FeCr_2O_4$) ores deposits, produces nearly 8% of the chromite ore in India (Dhakate et al., 2008). Chromite can be found in stratiform deposits, with concentrations up to 50%. Because of the high chromite content, no beneficiation process is required and the material can be directly extracted and used for metallurgical purposes. However, when the chromite concentration is lower than 33%, beneficiation with grinding and gravity methods is applied to concentrate the chromite ore (Murthy et al., 2011). Both in the mining and in the beneficiation process, a variety of waste residues are produced, including waste rock, overburden and tailings. The inconsistent feed quality during the beneficiation process results in a loss of efficiency and an increase of wastes, as is the case for tailings. Approximately 50% (by weight) of the total feed is discarded as tailings which still contain significant amounts of chromite (13-15%) (Murthy et al., 2011).

Several studies have been carried out in order to increase the chromite extraction yield and consequently decrease the tailings production (Raghu Kumar et al., 2009; Tripathy et al., 2013). A maximum of 83% recovery of chromite was reached with 23% Cr_2O_3 content. Despite the efforts that have been made to reduce chromite losses or reprocess stockpiled tailings, the ultrafine particle size makes chromite recovery and management difficult. Therefore, several tons of tailings per year are still produced and stored in open air conditions (Çiçek et al., 2008; Dwari et al., 2018; Özgen, 2012; Panda et al., 2014).

Chromium (Cr) has several oxidation states from -2 to 6, and the trivalent (Cr(III)) and hexavalent (Cr(VI)) states are primary oxidation states in nature. Hexavalent chromium is known to be highly mobile, soluble and toxic, while trivalent chromium is not toxic and largely immobile in the environment (Choppala et al., 2013). Nevertheless, Cr(III) can be mobilized by forming complexes with dissolved organic carbon (Sueker, 1964). Because of its toxicity, Cr(VI) has been shown to have several negative environmental impacts (Beukes et al., 2017; Schindler et al., 2018). In groundwater, the natural occurrence of Cr(VI) is linked to the hydrolysis of feldspar, some common mafic minerals such as Cr-bearing pyroxenes and chromite, together with calcite,

which causes alkaline groundwater conditions. This, coupled with the absence of natural reducing agents like Fe(II), organic matter or reducing organisms, may allow oxidation of Cr(III) to Cr(VI) (Beukes et al., 2017). In rocks, chromite grains are locked either within the iron ore minerals (goethite/hematite) and silicates or the chromite with inclusions of silicate (Dwari et al., 2018). Silicates are more susceptible to weathering than chromite, which represents a source of chromite nanoparticles (containing mainly Cr(III)), that after dissolution could be oxidized to Cr(VI) (Schindler et al., 2018, 2017). According to Beukes et al. (2017), Cr(VI) containing wastes generated by chromite mining are classified in three groups: i) recycled within the process, ii) re-purposed or re-used in other applications and iii) considered hazardous. Because tailings are not recycled or re-used and due to their potential to release Cr(VI), they belong to the third, hazardous, group of waste generated by chromite mining.

Consequently, all the efforts are focused on the understanding of Cr(VI) dynamics (Choppala et al., 2013; Kaprara et al., 2015; Mcclain and Maher, 2016; Osaki, 1983; Salem et al., 1989; Stanin, 2004; Thacher et al., 2015; Zachara et al., 1989) and the prevention or at least mitigation (Hamdan and El-Naas, 2014; Shahid et al., 2017; Tokunaga et al., 1999; Watts et al., 2015; Zaitseva et al., 2013) of the Cr(VI) production. Tiwary et al. (2005) studied the migration of metals leached from an overburden dump of chromite ore to groundwater. This study revealed that due to the poor permeability of the seepage, migration of metals occurs at a low rate and could only take place in the first layers down to 10 meters in 10 years. Godgul (1994) performed leaching experiments of chromite according to pH and highlighted that there is no relation between the total Cr in the solid sample and in the leached solution, because of the distribution of Cr in different mineral phases besides chromite. It was also observed that the maximum of Cr leached is obtained at pH 8 and all the elements (Cr, Fe, Al, Mn and Ni) are leached from the same mineral phase.

A great variety of microorganisms have been identified in mine waste, and microbial processes are usually responsible for the environmental hazard created by mine wastes. Microorganisms can, in principle, influence metals leaching from mine waste in several ways. However, they can also be used to retard the adverse impact of mine wastes on the environment (Ledin and Pedersen, 1996). Given the fact that some microorganisms contribute to metal immobilization, several studies have focused on the use of microorganisms such as bacteria for metal recovery or Cr(VI) reduction from mining residues. Das et al. (2014) studied the selection of Cr(VI) reducing bacteria from soils impacted by tailings. *Bacillus amyloliquefaciens* was isolated from

chromite mine soil and exhibited Cr(VI) tolerance and a Cr(VI) reduction rate of 2.2 mg Cr(VI) $L^{-1}h^{-1}$. Allegretti et al. (2006) investigated the presence of intermediary compounds, produced by *Acidithiobacillus* and *Thiobacillus*, that were responsible for Cr(VI) reduction. They identified several polythionates associated with sulfur particles between 0.45 and 3 µm. Wang et al. (2007) evaluated the leachability of Cr(VI) from tannery sludge with *A. thiooxidans*. After 5 days in a bubble column bioreactor at 30 °C, 99.7% of Cr was leached out from the tannery sludge. Naresh Kumar and Nagendran (2009) also observed efficient removal of metals, including Cr (95%), in soils through bioleaching with *A. thiooxidans*. Cr in the organic and residual fractions was unaltered during the course of the experiment, while the Fe-Mn oxide bound chromium was transformed to the exchangeable and carbonate fraction. Metal solubilization mechanisms by *A. thiooxidans* can be direct or indirect. In the direct mechanism, metal sulfides are oxidized to SO_4^{2-} directly by the bacteria, while in the indirect mechanism H_2SO_4, a strong leaching agent, is produced by *A. thiooxidans* (Nguyen et al., 2015). *Acidithiobacillus* species have also been used in both aerobic and anaerobic reductive dissolution of iron rich nickel laterite to remove target metals (Hallberg et al., 2011; Marrero et al., 2017) and in laterite tailings (Marrero et al., 2015) to recover heavy metals. Most of these studies target industrial applications. However, neither the leaching nor the bioleaching behavior of chromite tailings stockpiled in open air in the environment has been studied so far and the effect of bacteria on chromite tailings bioleaching has not yet been identified.

Given the increasing importance of chromite ores for the Cr world production and the huge amount of tailings produced (5×10^5 ton yr^{-1}- average production between 2016 and 2017 in all the chromite mines in Sukinda valley) (Indian Bureau of Mines, Ministry of Mines, 2017), it remains of key interest to fill the knowledge gap regarding the tailing discarded after the chromite beneficiation process. In the present study, the influence of pH on the bioleaching of chromite tailings was evaluated in batch experiments. Acidic and alkaline conditions were obtained through the incubation of tailings with *Acidithiobacillus thiooxidans* and *Pseudomonas putida*, respectively. The bacterial influence on tailings leachability was evaluated and the potential release of Cr(VI) from tailings was estimated. Fresh and old tailings were compared to estimate the potential risk of chromite tailings to the environment.

7.2 MATERIAL AND METHODS

7.2.1 Field settings

Superficial fresh chromite tailings and concentrate ore, as well as a core in the stockpiled old chromite tailings were collected in May 2017 from materials generated in a typical beneficiation plant of Sukinda valley, Jajpur district, Odisha, India (Figure 7.1). The Sukinda valley is located in the eastern part of the Indian peninsula, where the average annual precipitation is about 2400 mm. Most of the rain occurs during the monsoon season between May and October. It is primarily drained by the Damsala Nala River. The river flows westward through the central valley to meet the major river, Brahmani, which flows at a distance of 15 km downstream of the mining belt (Paulukat et al., 2015).

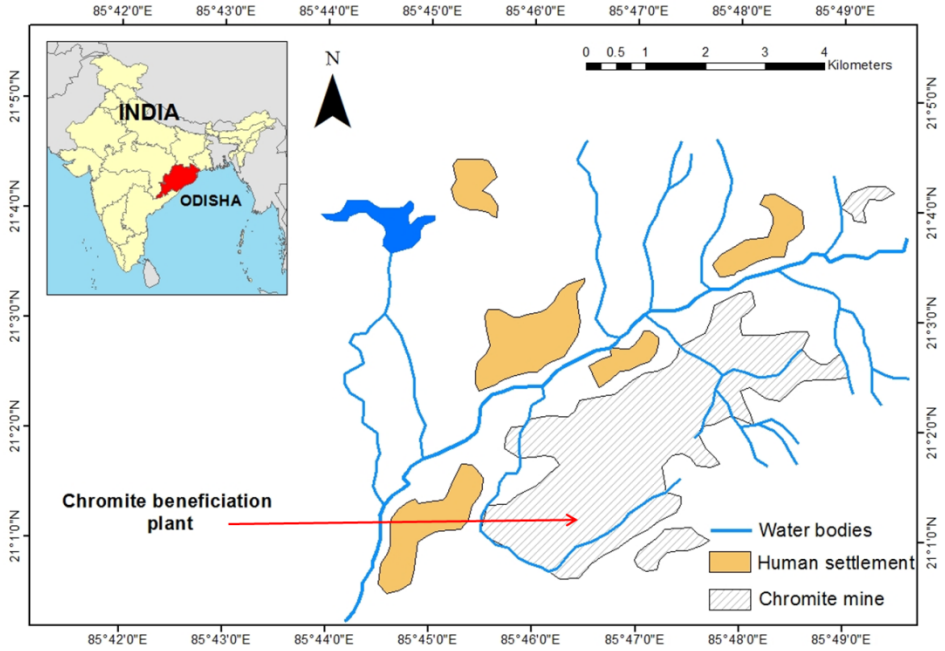

Figure 7.1 Chromite mine in Sukinda valley (Odisha, India).

Most of the mines are located in the central part of the valley and are operated by 12 different companies (BRGM, 1999). The Sukinda ultramafic complex is composed of alternate bands of chromite, dunite, peridotite and orthopyroxenite, which are extensively lateralized (Das et al., 2013; Equeenuddin and Pattnaik, 2017). The chromite bands in the Sukinda valley present various composition. When the Cr_2O_3 content is higher than 48%, the ore is “high grade” and is directly marketable, while between 32 and 45% of the ore is “medium grade” and finally lower than 30% is “low grade” (BRGM, 1999). For the last case, the presence of gangue minerals such as goethite, serpentine, olivine and talc has led to the utilization of lean ore after beneficiation.

The beneficiation process majorly consists in comminution to physically liberate the minerals followed by physical separation to generate the concentrate of the chromite ore (Raghu Kumar et al., 2009). During the comminution process, large quantities of fines are generated. The fines are commonly de-slimed using hydro-cyclone and cyclone underflow processed using gravity concentrators like spirals and tables. As a result, chromite concentrated ore is obtained, and roughly 50 to 70% of the chromite losses are in the fine fractions (tailings), where the fraction below 75 µm contains about 9-20% Cr_2O_3 (Dwari et al., 2018; Murthy et al., 2011).

7.2.2 Chemical and biological leaching experiments

The effect of bacterial bioleaching activity of fresh tailings was tested at three pulp densities of 5, 10 and 30 g L^{-1} in batch reactors. Batch reactors were selected in the present work, because they have been systematically used to study the kinetics of chromium transformations under typical environmental conditions (Salem et al., 1989), to establish the leachability of metals from laterite tailings (Coto et al., 2008) and to study the leaching characteristics of chromite ore processing residue (CORP) (Deakin et al., 2001; Tinjum et al., 2008; Weng et al., 1994). Also, batch experiments have been used to establish the microbial effect on chromium mobility (DeLeo and Ehrlich, 1994; Desjardin et al., 2002).

All the material was autoclaved at 121 °C for 20 minutes prior to use. The 500 mL reactors were closed using a cotton plug, both previously sterilized, and placed in an orbital shaker at 190 rpm and 30 °C. Samples were collected after 4 h, 1, 2, 5, 6, 8, 10, 12, 15 and 30 days. 20 mL of leachate were collected and replaced by fresh sterile medium to maintain the solid liquid ratio. In the samples collected, dissolved oxygen, pH and electrical conductivity were monitored using a WTW 3410 Set 2 multiparameter probe. In the case of bio-leaching with *P. putida*, approximately 5 mL of sample was frozen at -20 °C to determine protein content and siderophores concentration later. The rest of the sample was filtered through 0.45 µm pore size nitrocellulose syringe filters, for the determination of major and trace element concentrations in the leachate. Samples were acidified with 16 N HNO_3 and stored at 4 °C until their analysis. Biological and chemical leaching experiments were done in duplicate to verify reproducibility. For this reason the results presented in this work are an average of the duplicates with its associated standard deviation.

7.2.2.1 Bio-leaching with A. thiooxidans and P. putida

The bioleaching experiments of fresh tailings with *A. thiooxidans* and *P. putida* were performed in solutions containing the same components of the growth media where bacteria were pre-

grown (section 2.3.1. and 2.3.2). The initial pH of the growth media was set at 3.5 for *A. thiooxidans* and 7 for *P. putida*, with 1 N H_2SO_4 and 1 N NaOH, respectively. The batch reactors were inoculated with one percent (v v^{-1}) of pre-grown bacterial culture. The sterilized fresh tailing sample plus culture media were used as a control and distilled water plus sterilized tailing sample as a blank. In both cases sodium azide (NaN_3) was added to avoid bacterial growth.

7.2.2.1.1 Acidithiobacillus thiooxidans

The gram-negative bacterial strain *A. thiooxidans* (DSM 9463) was grown in a medium containing 2 g ammonium sulfate ($(NH_4)_2SO_4$), 0.25 g magnesium sulfate ($MgSO_4 \cdot 7H_2O$), 0.1 g dipotassium hydrogen phosphate (K_2HPO_4), and 0.1 g potassium chloride (KCl) per liter and 11% (wt v^{-1}) of elemental sulfur that was previously autoclaved at 121 °C for 20 minutes. The medium pH was adjusted to 3.5 before sterilization, and the sterilized sulfur was added subsequently together with the inoculum. The culture was maintained at 30 °C. The volume of the culture was increased gradually from 5 mL to 500 mL in separated Erlenmeyers.

7.2.2.1.2 Pseudomonas putida

The gram-negative bacterium *P. putida* (WCS 358) bacterial strain was kindly provided by Peter Bakker, University of Utrecht (The Netherlands). For siderophore production iron free succinate medium (SM) consisting (in g L^{-1}): K_2HPO_4 6.0, KH_2PO_4 3.0, $MgSO_4 \cdot 7H_2O$ 0.2, $(NH_4)_2SO_4$ 1.0 and succinic acid 4.0, pH 7.0 was used to inoculate *P. putida* at a concentration of 1% (v v^{-1}) inoculum.

7.2.2.2 Chemical leaching

In addition to the experiments done with *A. thiooxidans* and *P. putida*, chemical leaching of the fresh tailing sample with distilled water at pH 2 (adjusted with H_2SO_4) and distilled water at pH 9 (adjusted with NaOH) were carried out at a pulp density of 30 g L^{-1}. The leachability of chromite was also studied through the leaching of the concentrated ore coming from the beneficiation plant.

7.2.3 Chemical extraction

In order to determine the chemically exchangeable pool of Cr(VI) in the fresh and stockpiled old tailings and chromite ore chemical extraction was performed using distilled water and 0.1 M KH_2PO_4. The principle of the extraction with KH_2PO_4 is based on the fact that chromate ions can be desorbed by reactions of the soil with other specifically desorbed anions, such as phosphates (PO_4^{3-}) and sulfates. A suspension of 1 g of soil was agitated with 25 mL of the reactant (distilled

water or 0.1 M KH_2PO_4) for 1 h (Garnier et al., 2006). The supernatant was separated by centrifuging for 15 min at 2500 rpm followed by filtration with 0.22 µm pore size PES filter. Finally, the total Cr concentration in the supernatant was determined with ICP-AES. Cr(VI) was analyzed by colorimetric technique (diphenylcarbazide (DPC) method) (Onchoke and Sasu, 2016; Świetlik, 1998) and was measured with a Shimadzu UV-2550 spectrophotometer with a 1 cm quartz cell at λ of 540 nm.

7.2.4 Analytical methods

7.2.4.1 Chromite tailings characterization

The mineralogical composition of the fresh tailing sample and the concentrated ore was determined using X-ray diffraction (XRD) analysis on a PANalytical diffractometer and using the Cu Kα radiation (at 45 kV – 40 mA) in the grazing incidence angle in the 5°-70° 2θ range with a scan step of 0.013°. In addition, total metal concentration was determined by X-ray fluorescence (XRF), using an X fluorescence PANalytical spectrometer equipped with Energy Dispersive Minipal 4 (Rh X Ray tube-30kV - 9W) at a resolution of 150 eV (Mn Kα). The fresh tailing samples were thin-coated with carbon prior observations with a Zeiss Auriga Scanning Electron Microscope (SEM). The SEM was equipped with a Field emission Electron Gun (FEG) at 15 keV with a SE-Inlens detector.

7.2.4.2 Leachates composition

The concentration of major elements in filtered samples was determined using ICP-AES (ICAP 6200 Thermo Fisher), whereas HR-ICP-MS (Thermo Scientific Element II) was used for trace elements analysis. Detection limits were typically between 0.6 and 74 ng L^{-1} and the standard deviation associated to the measurements was smaller than 5%. Fe speciation in the leachate was measured with the ferrozine method (Viollier et al., 2000).

7.2.4.3 Protein determination

In order to establish the growth of the bacterial community, the Lowry protein test (Rodríguez-Vico et al., 1989; Waterborg and Matthews, 1984) was performed in the supernatant collected in the leaching experiments. For the calibration curve, protein standards were prepared with bovine serum albumin at concentrations between 10 and 500 µg mL^{-1}. 0.1 mL of 2 N NaOH was added to 0.1 mL of sample or standard. The mixture was hydrolysed at 100°C for 10 minutes in a boiling water bath. After cooling the hydrolysate to room temperature, 1 mL of the complex-forming reagent was added and the solution was left for 10 minutes at room temperature. After that 0.1 mL of Folin reagent was added to the mix using a vortex mixer. After 30 to 60 minutes,

the absorbance was read at 750 nm for protein concentrations below 500 µg mL^{-1} (Waterborg and Matthews, 1984).

7.2.4.4 Siderophores essay

Quantitative estimation of siderophores produced by *P. putida* was done by the CAS-shuttle assay (Payne, 1994). This method is based on the high affinity of siderophores for iron(III) (Schwyn and Neilands, 1987). The CAS reagent was prepared using: 1) 0.06 g of CAS in 50 mL of distilled water; 2) 0.0027 g of $FeCl_3 \cdot 6H_2O$ in 10 mL of 10 mM HCl; 3) 0.073 g of HDTMA in 40 mL of distilled water. Solution 1) was mixed with 9 mL of solution 2) and after with solution 3). The CAS reagent was autoclaved and stored in a plastic bottle (Lynne et al., 2011). For the quantification of the siderophores, 0.5 mL of supernatant (sample) was mixed with 0.5 mL of CAS reagent, and absorbance was measured at 630 nm. The siderophore content was calculated by using the equation (2) proposed by Sayyed et al. (2005).

$$\%\ siderophore\ units = \frac{A_r - A_s}{A_r} * 100 \qquad \textbf{(7.1)}$$

Where A_r and A_s correspond to the absorbance of the reference and sample at 630 nm, respectively.

7.2.4.5 Geochemical modeling

Visual MINTEQ 3.1 equilibrium modelling program was used to identify the major mineral(s) controlling the chemistry of fresh tailings. The Saturation Index (SI), which is defined as the logarithm of the ratio of the ion activity product and the solubility product (K_{sp}) (SI= log IAP/K_{sp}), was calculated with the program. Positive SI values indicate that the solution is oversaturated and precipitation is possible, negatives values indicate that it will tend to dissolve and zero shows equilibrium of the solution with a mineral phase. The input data for MINTEQ 3.1 included the pH, temperature, total cation (Ca, Mg, Na, K, Ni, Fe(II), Al, Cr(VI)) and anion (SO_4^{2-}, NO_3^-, Cl^-, PO_4^{3-}) concentration. No adsorption parameters were included within the calculations.

7.3 RESULTS

7.3.1 Tailings and concentrated ore characterization

A detailed chemical composition of the samples is given in Table 7.1. X-Ray Fluorescence analysis shows that in the fresh tailing sample 18 wt% is chromium oxide and 56 wt% is iron oxides. For the concentrated ore sample the proportion of Cr_2O_3 increases up to 33.17 wt%. The XRF composition is consistent with XRD results, which shows the presence of goethite (α-

FeO(OH)), hematite (Fe_2O_3), gibbsite ($Al(OH)_3$), chlorite ($(Fe,Mg,Al)_6(Si,Al)_4O_{10}(OH)_8$) and chromite ($FeCr_2O_4$), as the main crystalized mineral phases in the fresh tailing sample.

Table 7.1 XRF results of the fresh tailing and chromite concentrated ore sample collected in the beneficiation plant (Sukinda valley) in May 2017.

Oxide rate (%)	Fresh tailings	Chromite concentrated ore
Al_2O_3	8.7	9.4
SiO_2	13.4	3.7
Cr_2O_3	18.1	33.2
Fe_2O_3	56.7	52.0
Total	96.9*	98.4*

*The 3.1% and 1.6% leftover for tailings and concentrated ores, respectively correspond to traces of Mn, Mg, V, Ti, Ca, P and S.

Dwari et al. (2018) found additional mineral phases, in chromite tailings from Sukinda valley, including kaolinite ($Al_2Si_2O_5(OH)_4$), quartz (SiO_2) and magnesioferrite ($Mg(Fe)_2O_4$). The concentrated ore sample is enriched in chromite with some traces of lizardite, hematite and goethite.

SEM-EDX images collected on the fresh tailing sample are displayed in Figure 7.2. As was previously shown by the XRF results, the tailings are dominated by the presence of Fe, followed by Cr, Al and Si oxides (Figure 2(a)). In the fresh tailing sample Cr is found as chromite (Figure 7.2(d)).

In Sukinda chromite tailings, Tripathy et al. (2013) found two different types of chromite grains: the first one is rich in Cr with minimum amount of Fe, Al and Mg, whereas the second one is rich in Fe, Al and Mg along with Cr. The grain display in Figure 7.2(b) corresponds to the second group, where there is a 63 wt% of Cr_2O_3, 18 %wt of FeO, 9 wt% of MnO, 6 wt% of Al_2O_3 and 4 wt% of MgO. Other Cr-bearing phases are goethite, FeO(OH), aluminum oxides and other colloids with a positively charged surface where hexavalent Cr species, which are negatively charged (e.g. CrO_4^{2-} and $HCrO_4^-$), can be adsorbed (Kotaś and Stasicka, 2000). In the tailings gangue minerals enriched in Fe oxy(hydroxides) (81 wt%) are identified with the presence of Cr (Cr_2O_3 9 wt%), Si (SiO_2 5 wt%) and Al (Al_2O_3 5 wt%) (Figure 7.2(c)). Al oxide is also present in the fresh tailing sample, with a lower Cr content (6 wt%) (Figure 7.2(d)).

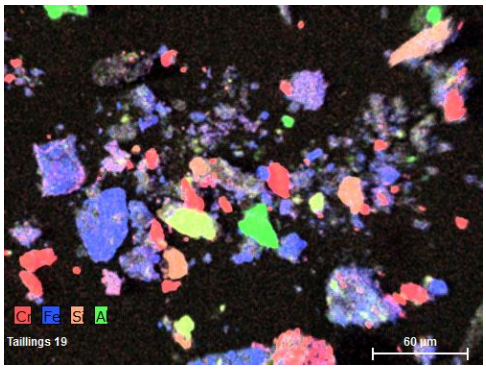

(a)

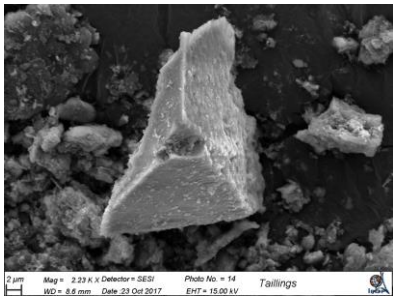

(b)

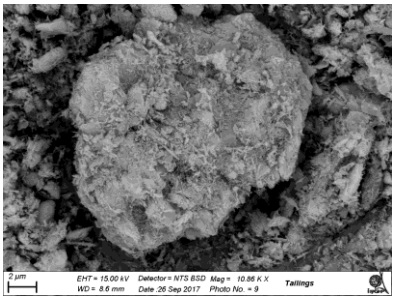

(c)

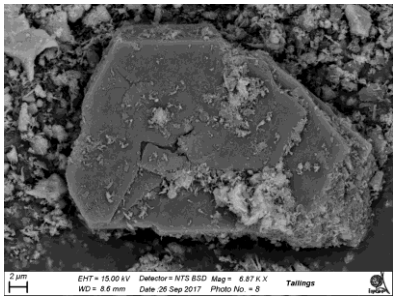

(d)

Figure 7.2 Chromite tailing (a) elementary map of EDS showing the dominance of Cr, Fe, Si and Al. SEM images of (b) chromite (Cr 63 wt%), (c) iron oxide (Cr 9 wt%) and (d). aluminum oxide (Cr 6 wt%).

7.3.2 pH profiles

The change of pH observed in the biotic and abiotic leaching experiments in distilled water and growth medium with *P. putida* and *A. thiooxidans* are presented in Figure 7.3. The leaching of the fresh tailing sample with distilled water shows a stable pH close to 7, and is 0.2 units higher for the pulp density at 30 g L^{-1} compared to 5 and 10 g L^{-1} (Figure 7.3(a)).

For *A. thiooxidans*, in the control (growth medium pH adjusted to 3.5) pH is higher at a higher pulp density. For 5 g L^{-1} the pH varies from 3.8 to 4.3, for 10 g L^{-1} it varies from 4.1 to 5.2 and for 30 g L^{-1} from 5.3 to 6.0. When *A. thiooxidans* is inoculated the pH is consistently low (1.6 in average) for all pulp densities. The low pH is the result of the sulfur oxidation by *A. thiooxidans* using dissolved oxygen as the electron acceptor, and the resulting H_2SO_4 production (Gleisner and Herbert, 2002). In the case of *P. putida*, the control (growth medium pH adjusted to 7) has a pH close to 7 and no differences were observed according to the pulp densities. However, in the reactors where *P. putida* is inoculated the pH increases significantly from 7 to 9.2 in the first 5 days whatever the pulp density.

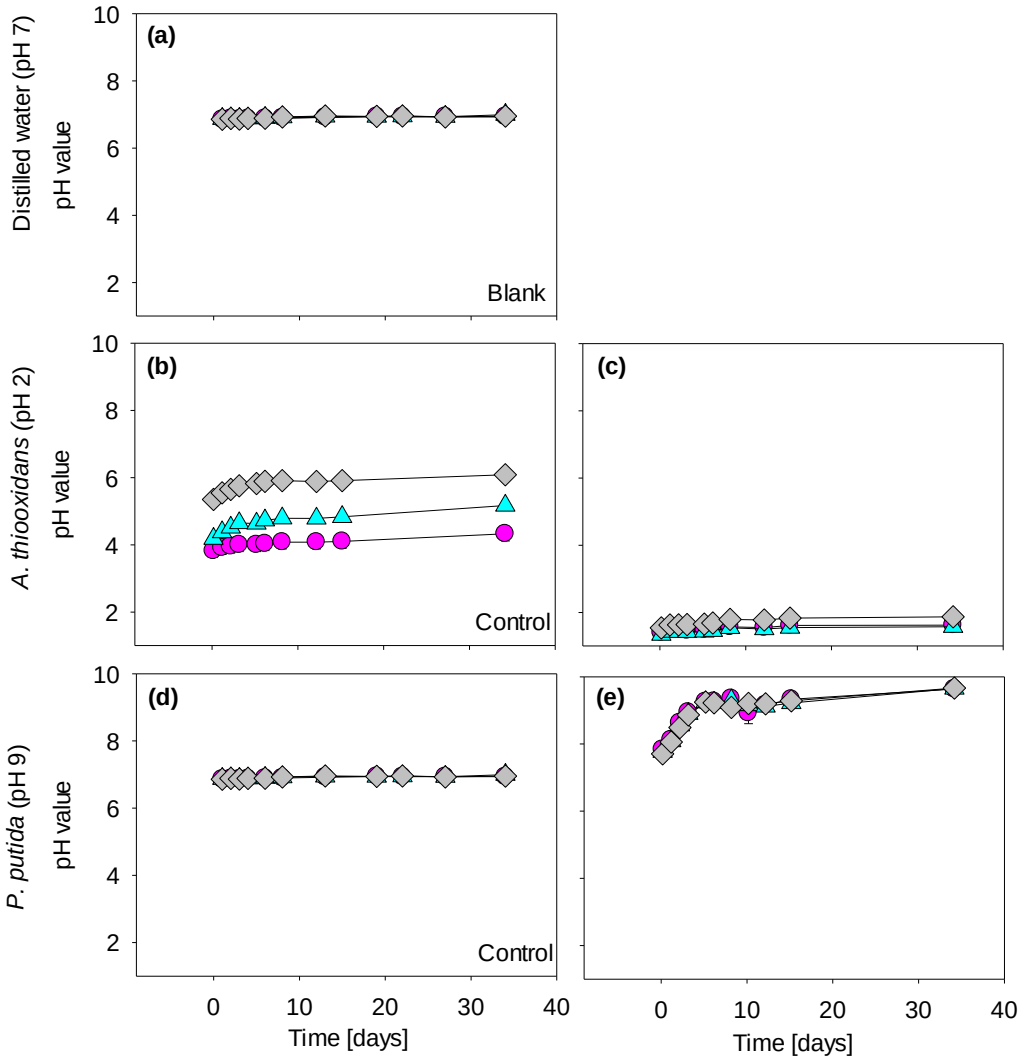

Figure 7.3 pH evolution in leaching experiments of the fresh tailings sample with distilled water (blank) (a), incubation with *A. thiooxidans* (c) and *P. putida* (e). Controls for *A. thiooxidans* and *P. putida* are display in (b) and (d), respectively. Three pulp densities were evaluated: 5 g L^{-1} (—●—), 10 g L^{-1} (—▲—) and 30 g L^{-1} (—◆—).

Van Hullebusch et al. (2015) explained the pH increase in slag leaching as a result of the initial dissolution of cations such as Ca^{2+} and Mg^{2+}, followed by neutralization by H^+ from H_2O. Potysz et al. (2016) also reported a pH increase in Cu slags leaching due to H^+ replacing Fe^{2+} during fayalite dissolution. In batch reactors inoculated with *P. putida*, dissolved oxygen increases from 0 on the first day to 4.7 mg L^{-1} on the fifth day and remains constant for the rest of the sampling time (supplementary data Figure S7.1).

7.3.3 Elements released during leaching experiments

The behavior of Cr, Fe, Ni, Mn and Al during the bioleaching of the fresh tailing sample is presented in Figure 7.4 to Figure 7.8 and the units are expressed in mg of element released per kg of tailings. The use of *A. thiooxidans* as a leaching agent facilitates Fe dissolution. At a pulp density of 5 g L^{-1}, Fe extracted from the fresh tailings sample increases from 421 to 1234 mg kg^{-1}, for 10 g L^{-1} the range is narrower with values between 510 to 940 mg kg^{-1} (Figure 7.4).

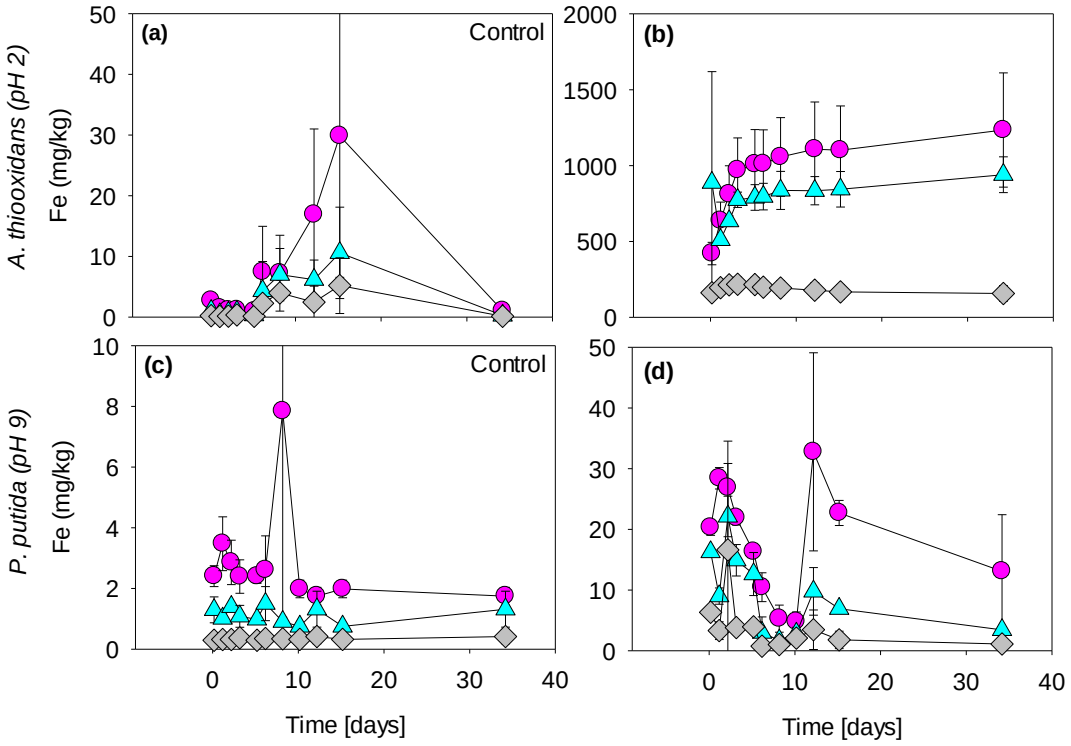

Figure 7.4 Fe concentration in the leachate as a function of time, during (bio)leaching experiments of the fresh tailing sample with *A. thiooxidans* (b) and with *P. putida* (d). Controls for *A. thiooxidans* and *P. putida* are display in (a) and (c), respectively. Three pulp densities were evaluated: 5 g L^{-1} (—●—), 10 g L^{-1} (—△—) and 30 g L^{-1} (—◇—).

For 30 g L^{-1} no significant fluctuations were observed with an average value of 190 (± 21) mg kg^{-1} over time. In the reactors with *A. thiooxidans* for the 3 pulp densities the pH is always below 4 and for the first day Fe^{2+} is the dominant species, however after that, Fe(III) species are more abundant caused by the oxidation of Fe^{2+} by *A. thiooxidans* (Liu et al., 2015). The same Fe speciation is observed in a leaching test using fresh tailings sample done with distilled water acidified with H_2SO_4 and without bacteria (Figure S7.2). Liu et al. (2015) performed leaching experiments of chalcopyrite with *A. ferrooxidans* (pH 2-2.5) and they found total Fe concentrations up to 0.6 g L^{-1}, which was present as Fe^{2+} and Fe^{3+} the first 6 days, but

afterwards only Fe^{3+} was detected. In the control of *A. thiooxidans*, at higher pH (6; pulp density 30 g L^{-1}) the Fe extracted is lower, compared with the lower pH (4; pulp density 5 g L^{-1}) where total iron reaches 7 mg kg^{-1} the 6th day of leaching. This result suggests that the medium effect is negligible compared to the leaching produced by the presence of *A. thiooxidans* and more specifically by the sulfuric acid produced.

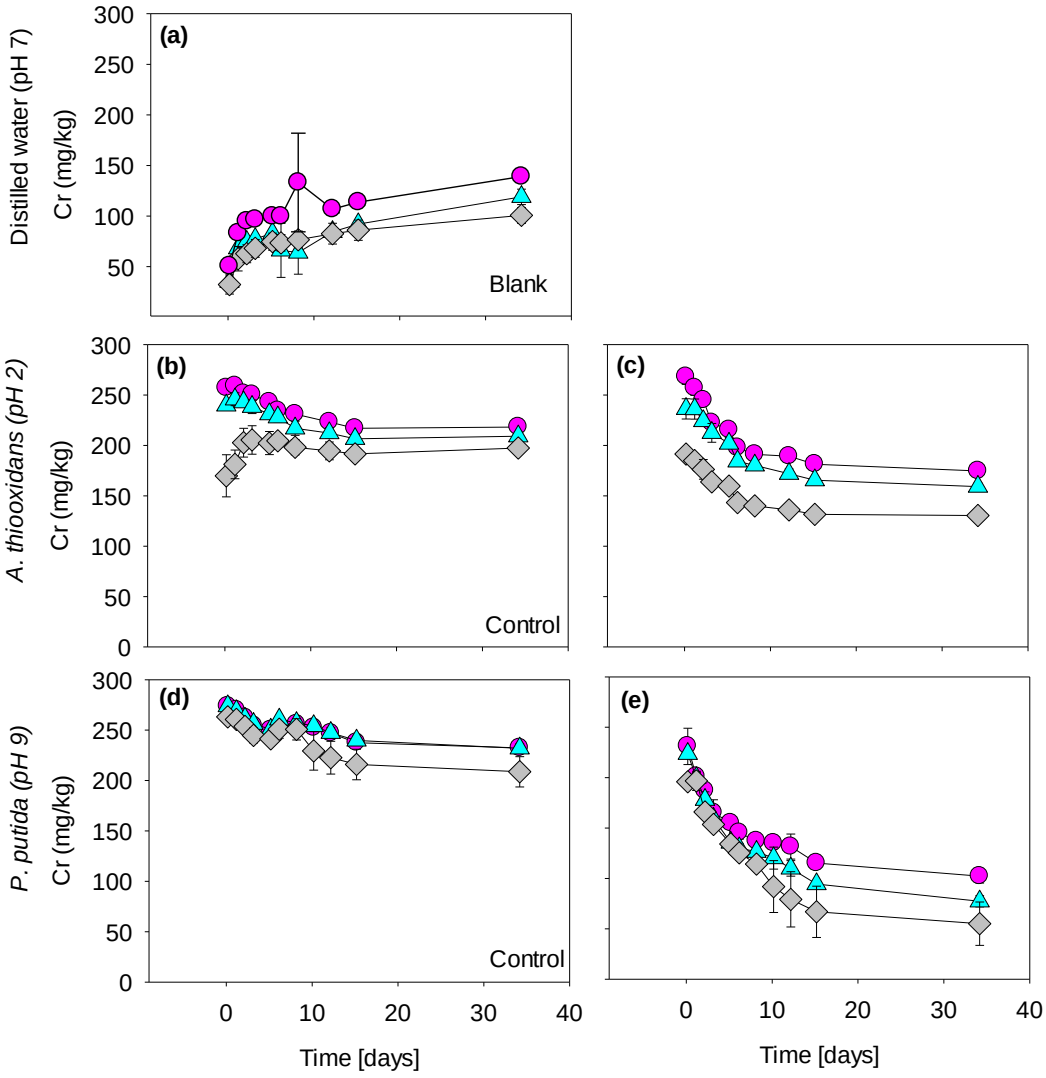

Figure 7.5 Cr concentrations in the leachate as a function of time during (bio)leaching experiments of the fresh tailing sample with distilled water (a), incubated with *A. thiooxidans* (c) and *P. putida* (e). Controls for *A. thiooxidans* and *P. putida* are display in (b) and (d), respectively. Three pulp densities were evaluated: 5 g L^{-1} (—●—), 10 g L^{-1} (—▲—) and 30 g L^{-1} (—◆—).

Because of its toxicity, mobility and enrichment in chromite and other Cr bearing phases in chromite tailings, the leaching behavior of chromium is of particular interest. With distilled water,

a maximum of chromium is leached from the fresh tailing sample in the first three days for all pulp densities, reaching values of 94.8 (± 1.41), 74.45 (± 0.35) and 62.70 (± 8.87) mg kg^{-1} for pulp densities of 5, 10 and 30 g L^{-1}, respectively.

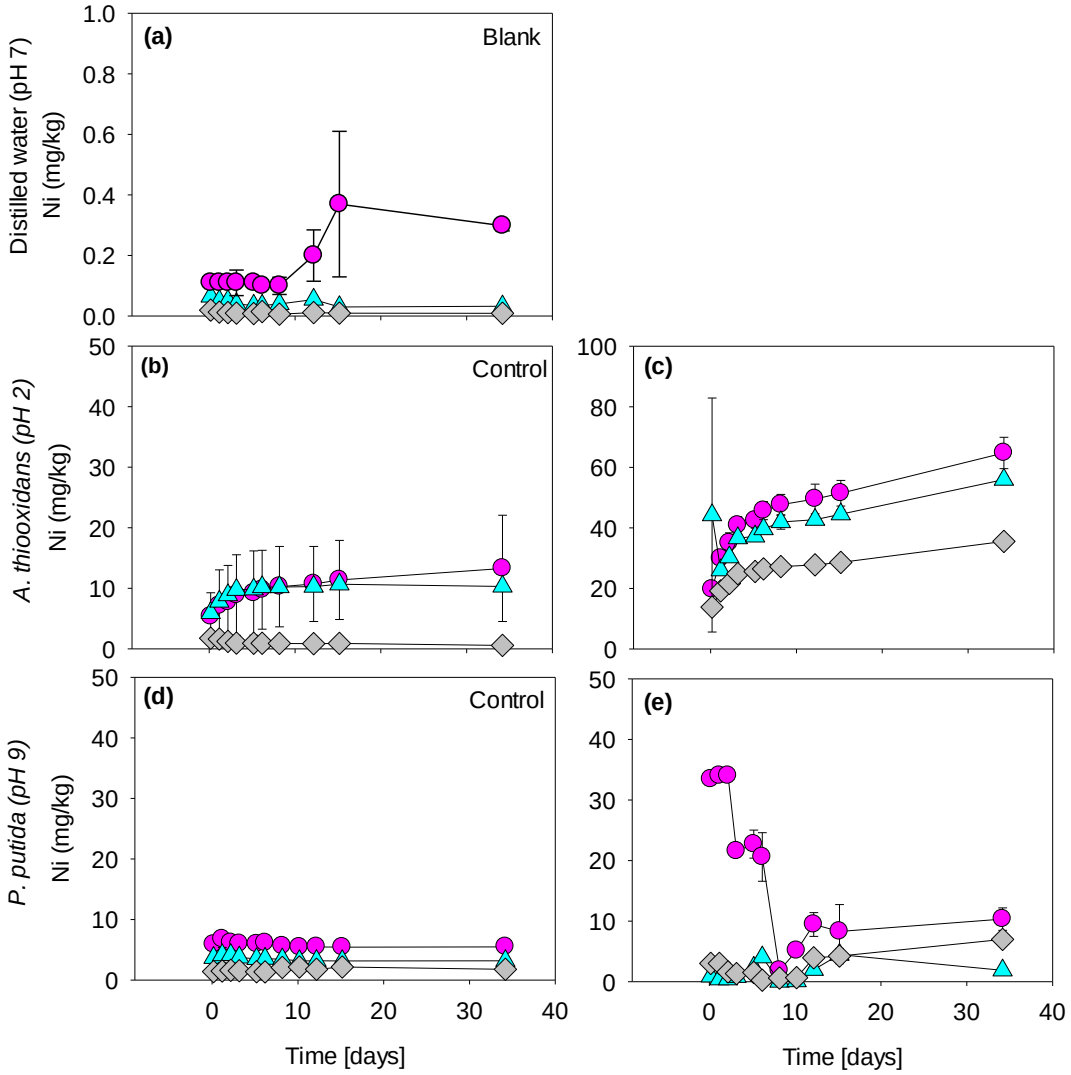

Figure 7.6 Ni concentrations in the leachate as a function of time during (bio)leaching experiments of the fresh tailing sample with distilled water (a), incubated with *A. thiooxidans* (c) and *P. putida* (e). Control for *A. thiooxidans* and *P. putida* are displayed in (b) and (d), respectively. Three pulp densities were evaluated: 5 g L^{-1} (—●—), 10 g L^{-1} (—▲—) and 30 g L^{-1} (—◆—).

After the third day, chromium extracted slowly increases until day 34. When *A. thiooxidans* is present in the batch reactor, chromium is leached from the fresh tailing sample in the first hours and then the curve decreases. The pulp density at 5 g L^{-1} presents the higher Cr content (174 – 268 mg kg^{-1}), followed by 10 (159 – 236 mg kg^{-1}) and 30 g L^{-1} (130 –191 mg kg^{-1}). In the control

of *A. thiooxidans*, the maximum chromium extracted for the 5 (259 mg kg^{-1}) and 10 g L^{-1} (245 mg kg^{-1}) pulp density is similar to the batch incubated with *A. thiooxidans*, for the same pulp densities. For the pulp density at 30 g L^{-1} in the control for *A. thiooxidans*, the chromium concentration slightly increases in solution from 170 to 202 mg kg^{-1} in the first two days and then remains stable (Figure 7.5).

In the case of the fresh tailing sample incubated with *P. putida*, for all pulp densities the maximum amount of chromium extracted (217 mg kg^{-1} in average) is reached in the first hours and then chromium concentration slowly decreased. Starting from the day 10, the differences between pulp densities become relevant being Cr extracted higher for a pulp density of 5 g L^{-1} (135 mg kg^{-1}). In the control for *P. putida*, chromium decreases by 15% at 5 and 10 g L^{-1} and 20% at 30 g L^{-1}, from day 1 to 34.

For both *A. thiooxidans* and *P. putida* the maximum Cr concentration is observed at the beginning of the incubation, and is influenced by the presence of KH_2PO_4 in the growth medium. Phosphates (PO_4^{3-}) can promote the desorption of anions including chromate ions, even if they are tightly bound compared with other anions such as chloride, nitrate and sulfate (Beukes et al., 2017; Sueker, 1964). However, not only the presence of phosphates promotes the presence of chromium in solution, because almost 150 mg kg^{-1} of Cr is extracted in the leaching with distilled water after 34 days (Figure 7.5).

It is known that lateritic chromite overburden contains nearly 0.4 - 0.9 % Ni which is entrapped within the goethite (FeOOH) matrix (Biswas and Bhattacharjee, 2014). Also is known that Ni and Cr are elements characteristic of ultramafic areas, and both of them have species with a certain grade of toxicity. For this reason, the leachability of Ni is also evaluated. Figure 7.6 presents the Ni behavior in the leachate over time.

The leaching of the fresh tailings sample with distilled water showed Ni in the leachate lower than 1 mg kg^{-1} for all pulp densities. In the incubation with *A. thiooxidans*, the extracted Ni concentration increased over time. For a pulp density of 5 g L^{-1}, the Ni extracted goes from 20 to 65 mg kg^{-1}, for 10 g L^{-1} is between 44 and 56 mg kg^{-1} and for 30 g L^{-1} between 14 and 36 mg kg^{-1}. The *A. thiooxidans* medium composition (Figure 7.6(b)) induces Ni leaching from the fresh tailing sample, however it only corresponds to the 20% of the Ni extracted under acidic in the batch reactor incubated with *A. thiooxidans*. This indicates that growth of *A. thiooxidans*

promotes the leaching of Ni. In the leaching experiments with *P. putida*, Ni tends to decrease for the first day (33 mg kg^{-1} for 5 g L^{-1}, 6 mg kg^{-1} for 10 g L^{-1} and 3 mg kg^{-1} for 30 g L^{-1}) to the day 6 (20 mg kg^{-1} for 5 g L^{-1}, 0.5 mg kg^{-1} for 10 g L^{-1} and 0.2 mg kg^{-1} for 30 g L^{-1}) and after part of it is re-solubilized and/or more Ni is leached from the tailings. The *P. putida* medium composition effect is negligible.

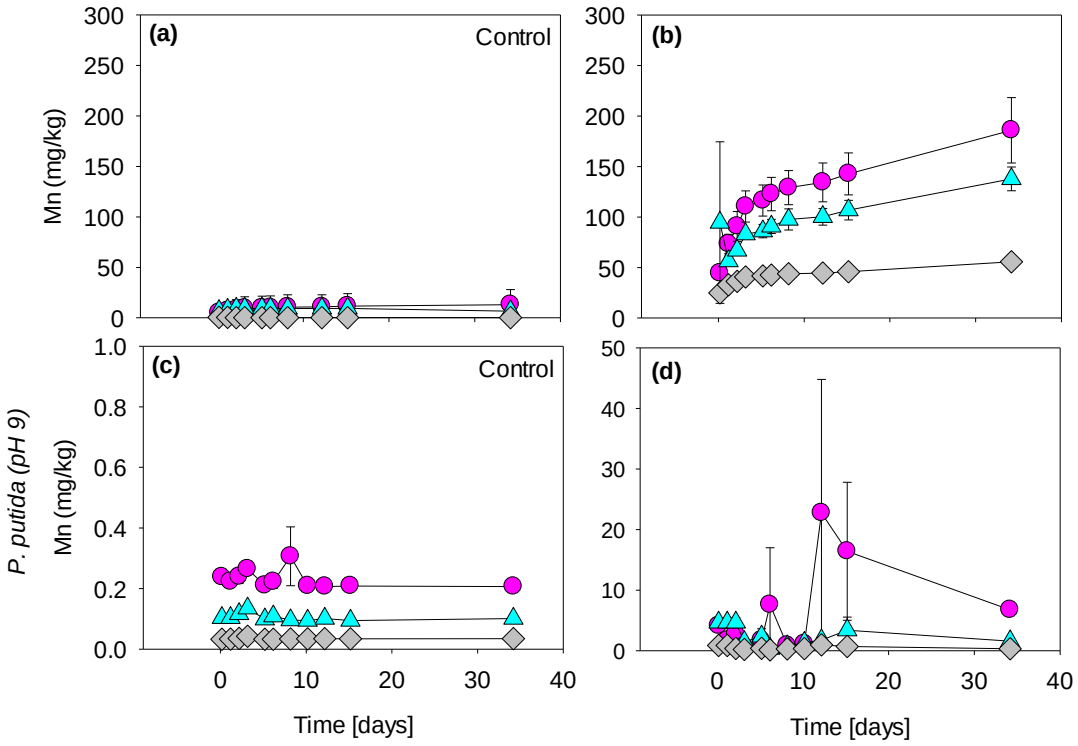

Figure 7.7 Mn concentration in the leachate as a function of time, during (bio)leaching experiments of the fresh tailing sample with *A. thiooxidans* (b) and with *P. putida* (d). Controls for *A. thiooxidans* and *P. putida* are display in (a) and (c), respectively. Three pulp densities were evaluated: 5 g L^{-1} (—●—), 10 g L^{-1} (—▲—) and 30 g L^{-1} (—◆—).

As it occurs with other elements, manganese is released from the fresh tailing sample under incubation with *A. thiooxidans*. At a pulp density of 5 g L, Mn increases at a rate of 21 mg kg^{-1} day^{-1} in the first 3 days and after continues the increase at a rate ten times lower (2 mg kg^{-1} day^{-1}). For 10 g L^{-1}, Mn extracted varies from 94 to 138 mg kg^{-1}. For the pulp density of 10 g L^{-1}, in the first 3 days the Mn extracted increases at a rate of 8 mg kg^{-1} day^{-1} and in the period remaining decreased to 1.6 $mg^{-1}kg^{-1}day$. For 30 g L^{-1}, the range of variation is smaller (25 to 56 mg kg^{-1}), and it also increases over time. The manganese chemically extracted by the medium without incubation of *A. thiooxidans* corresponds to 10% of the total amount extracted after incubation. For the incubation with *P. putida*, the Mn concentrations are considerably lower than

for *A. thiooxidans*, due to the instability of Mn^{2+} at pH higher than 7. The Mn variation, during incubation of the fresh tailing sample with *P. putida*, is higher for the pulp density at 5 g L^{-1}, with values between 0.6 and 23 mg kg^{-1} (Figure 7.7).

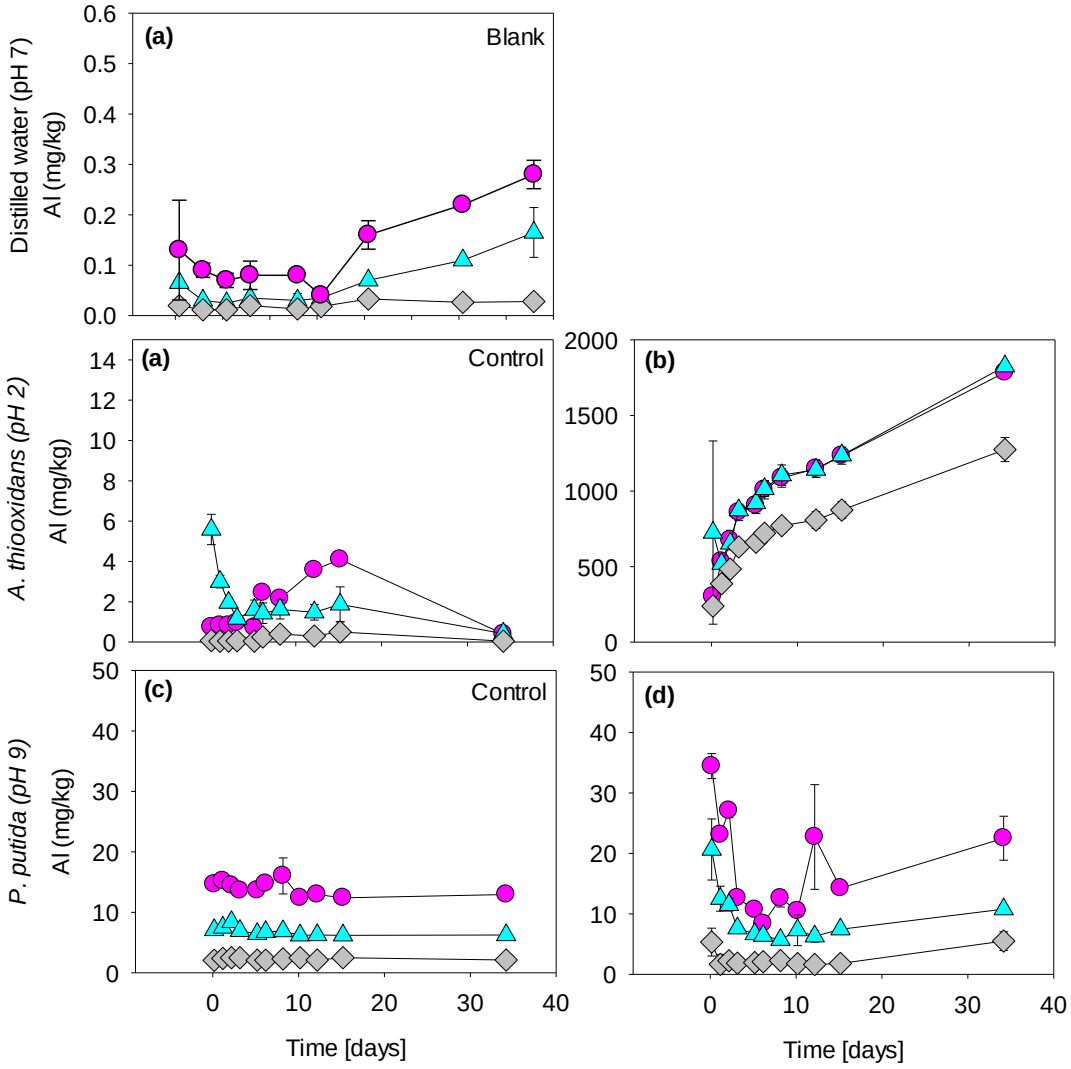

Figure 7.8 Al concentrations in the leachate as a function of time during (bio)leaching experiments of the fresh tailing sample with distilled water (a), incubated with *A. thiooxidans* (c) and *P. putida* (e). Control for *A. thiooxidans* and *P. putida* are displayed in (b) and (d), respectively. Three pulp densities were evaluated: 5 g L^{-1} (—●—), 10 g L^{-1} (—▲—) and 30 g L^{-1} (—◆—).

Aluminum is the fourth most abundant element present on the chromite tailings, and it remains present in the concentrated ore after the beneficiation process. Leaching of the fresh tailings sample with distilled water, shows that Al in solution is released in the first hours during the first

6 days. However, after this period of time, Al starts to continuously increase within 40 days of incubation, except for pulp density of 30 g L^{-1} where the concentration remains constant.

When the fresh tailing sample is incubated with *A. thiooxidans*, there is a release of Al starting from 302 to 1784 mg kg^{-1}, from 725 to 1826 mg kg^{-1} and from 239 to 1274 mg kg^{-1}, for the pulp densities of 5, 10 and 30 g L^{-1}, respectively. This is due to the production of H_2SO_4 by *A. thiooxidans* and the dissolution of amorphous mineral phases containing Al.

Chromite tailings of a beneficiation plant in India were characterized by Tripathy et al. (2013) and they found kaolinite ($Al_2Si_2O_5(OH)_4$) in addition to the Al mineral phases, such as gibbsite and chlorite, found in the chromite tailings used in the present work. The control of *A. thiooxidans* reveals no medium effect in Al dissolution. The incubation of the fresh tailing sample with *P. putida* shows notably less Al alteration, compared with the incubation with *A. thiooxidans*. In addition, Al does not dissolve continuously, on the contrary, two phases were identified. An initial Al precipitation, which incubation period lasts approximately 10 days, followed by Al dissolution in the time remaining. In the first phase, 50% of Al precipitates for the pulp density at 5 g L^{-1}, 64% for 10 g L^{-1} and 73% for 30 g L^{-1}. In the second phase, Al is dissolved again (Figure 7.8).

7.3.4 Chemical extraction

The chemically exchangeable pool of hexavalent chromium ($E_{Cr(VI)}$) for fresh and stockpiled old tailing and chromite ore, in mg of Cr(VI) per kg of tailing, is presented in Table 7.2. For the chromite ore samples, the total Cr content in the solid ranges between 203 and 236 g kg^{-1}. For the chromite ore 1, Cr(VI) extracted with water is equivalent to total Cr extracted with KH_2PO_4 with an average value of 3.4 mg kg^{-1}, while the Cr(VI) extracted with KH_2PO_4 ($E_{Cr(VI)}$) remains lower (2.3 mg kg^{-1}). In the case of chromite ore for band 6, the Cr(VI) extracted with water and KH_2PO_4 has the same value (1.6 mg kg^{-1}) and corresponds to 50% of the total Cr extracted with KH_2PO_4.

Table 7.2 Results of chemical extraction for the tailings and chromite ore sample.

Sample		Total Cr (g kg^{-1})	Cr(VI) water (mg kg^{-1})	Cr(VI) KH_2PO_4 (mg kg^{-1})	Cr(tot) KH_2PO_4 (mg kg^{-1})
Chromite ore 1		203	3.5	2.3	3.4
Chromite ore 2		236	1.6	1.6	3.1
Fresh tailing		96	63	223	240
Old tailing	7-10 cm	99	36	149	158
	15-20 cm	105	19	85	89
	>30 cm	101	3.7	31	31

In the fresh tailing sample, total Cr content in the solid (96 mg kg^{-1}) is approximately 50% of the total Cr contained in the chromite ore sample, however Cr(VI) extracted with KH_2PO_4 ($E_{Cr(VI)}$) (223 mg kg^{-1}) is 100 times higher compared with the chromite ore sample. In the fresh tailings sample, Cr(VI) extracted with KH_2PO_4 corresponds to 93% of the total chromium extracted with KH_2PO_4.

Total chromium in the stockpiled old tailing sample does not change significantly with the depth (102 ± 3 g kg^{-1}), however Cr(VI) extracted with KH_2PO_4 ($E_{Cr(VI)}$) decreased from the top to the bottom. For the Cr(VI) extracted with KH_2PO_4 ($E_{Cr(VI)}$), the range of variation goes from 36 and 149 mg kg^{-1} in the surface to 3.7 and 31 mg kg^{-1} in the deepest layer for extraction with water and KH_2PO_4, respectively. Between 94 and 100 % of extracted Cr with KH_2PO_4, is present as a Cr(VI).

7.4 DISCUSSION

7.4.1 Cr leachability and interaction with other ions

Among the main chromium bearing phases in chromite tailings, iron and aluminum oxides can play an important role in Cr mobility and leachability. In leaching experiments of soils derived from chromium ore processing residue (CORP), Weng et al. (1994) found that Cr(VI) was not detected in the leachate (pH < 2.5), because of the adsorption of Cr(VI) onto soil surfaces or the reduction of Cr(VI) to insoluble Cr(III). Significant amounts of Cr(VI) were leached between pH 4.5 – 12. Accordingly Liu et al. (2013) reported an optimal pH between 3 and 4 for hexavalent chromium leaching of chromium slag. Besides the importance of pH in the presence of Cr(III) and/or Cr(VI) in the dissolved fraction, pH also impacts the dominance of oxyanions species. According to visual MINTEQ simulation results, Cr precipitates during the leaching experiments and the Cr remaining in solution is mainly present as Cr(VI) oxyanions (supplementary data Table S7.3). For leaching with *P. putida* growth medium (control) at neutral pH, CrO_4^{2-} and $HCrO_4^-$ are the main Cr forms in the leachate, accounting for about 86% of total dissolved forms. The dominance of those species remains over time (supplementary data Table S7.2). When *P. putida* is inoculated, the pH increases up to 9.6 and CrO_4^{2-} represents 93% of the dissolved chromium. This occurs for all the pulp densities evaluated. In addition, visual MINTEQ simulation results revealed that at pH 3.5 (control of *A. thiooxidans*) $HCrO_4^-$ dominates (94 %), and at pH 1.6 when *A. thiooxidans* is inoculated $HCrO_4^-$ decreases (83%), while $CrO_3SO_4^{2-}$ represent 13% of dissolved chromium (supplementary data Table S7.3). In the blank, when the fresh tailing sample was leached with distilled water (pH= 7), 66% of Cr is present as a CrO_4^{2-} and the 34%

remaining as $HCrO_4^-$. The oxidizing conditions and the pH explain the presence of Cr(VI) as $HCrO_4^-$ or CrO_4^{2-} (Stanin, 2004).

The leaching of Cr for chromite tailings can be explained by two main processes. The first main process for Cr leaching is associated with the presence of phosphate anions in solution, which can exchange with chromate and bi-chromate anions, promoting the presence of Cr(VI) (Garnier et al., 2006) in solution. According to the chemical extraction performed with KH_2PO_4 (Table 7.2) the chemically exchangeable pool of chromium in the fresh tailing sample is 223 mg of Cr(VI) per kg of tailing. Chemical extraction was also performed with concentrated ore and the value obtained is 100 times lower. Given that the concentrated ore is mainly composed of chromite, it can be concluded that chromite contained in the fresh tailings is not the main source of Cr(VI), at least in a short term. However, it is important to consider that in the chromite deposit, which is the raw material for the concentrated ore, serpentinization and magnesium (Mg) ion release during deuteric alteration of ultramafic rocks (and associated laterization) create alkaline pore water, which brings on Cr(VI) formation (Godgul and Sahu, 1995). Chromite and Cr-magnetite have also been proposed by Garnier et al. (2008) as a source of Cr in ultramafic soils, in spite of r-spinel resistance to alteration. This findings are supported with XANES evidences for oxidation of Cr(III) to Cr(VI) by Mn-oxides in a lateritic regolith in New Caledonia (Fandeur et al., 2009). In other words, Cr(VI) is potentially produced in the chromite deposit, and if is not removed during the chromite beneficiation process it can be still present in the concentrated ore and tailings. However, given the Cr release during leaching experiments with concentrated ore, in the tailings chromite does not seems to be the main source of Cr(VI), consequently Cr(VI) leached from the tailings is coming from other bearing phases, such as iron and aluminum oxides and silicates.

The second main process for Cr leaching that could explain the presence of Cr in the leachate is related with redox processes. Manganese oxide containing minerals act as a transporter of electrons between dissolved oxygen and Cr(III), and therefore, Mn indirectly oxidizes Cr(III) to Cr(VI) (Choppala et al., 2013). On the other hand, Cr(VI) can reduce to Cr(III) which is less toxic. In this process iron(II), reduced sulfur and organic matter are chief sources of electrons (Kotaś and Stasicka, 2000). Reduction of Cr(VI) by Fe(II) (aq) can be expressed by the following general reaction (Fendorf, 1995):

$$Cr(VI)_{aq} + 3Fe(II)_{aq} \rightarrow Cr(III)_{aq} + 3Fe(III)_{aq} \quad \textbf{(7.2)}$$

Given the visual MINTEQ calculations, during the leaching with *A. thiooxidans*, under acidic conditions (pH= 1.6), ferrous iron is in solution mainly as $FeSO_4$ (aq) and as a free ion Fe^{2+}. The presence of ferrous iron in the leachate could explain the decrease of Cr over time, because of its iron dominant role in the reduction of Cr(VI) to Cr(III), process which is 100 times faster than a biotic process (Choppala et al., 2013). In the case of Mn, is present mainly as Mn^{2+}, which is a non-stable species and it does not play a role in Cr(III) oxidation. At acidic pH Cr(III) precipitation is not expected to occur, as is the case at neutral pH, so one can expect to have precipitation of Cr(III) produced after Cr(VI) reduction in leaching with distilled water and *P. putida* (Oze et al., 2004). In the batch experiments with *P. putida*, due to pH (6.6 – 9.6) and oxidizing conditions, Fe is present in solution at really low concentration forming $FeHPO_4$. Fe low content indicates that no significant colloidal transport of particles occurred (Raous et al., 2010).

Other elements of interest leached from the fresh tailing sample are Ni and Al. Given visual MINTEQ results, in the presence of *P. putida* medium (control), Ni is complexed by phosphates, which are concentrated in the growth medium. 77% is complexed as $NiHPO_4$ (aq), 14% is present as a Ni^{2+} and 5% as $NiSO_4$ (aq). When incubating the fresh tailing sample with *P. putida*, $NiHPO_4$ remains dominant until day 4 where the pH reaches a value of 8.9. However the diversification of Ni species increases over time, and at the end of the leaching period Ni complexed with ammonia become dominant. Those species include $Ni(NH_3)_2^{2+}$ (31%), $Ni(NH_3)_3^{2+}$ (18%) and $NiNH_3^{2+}$ (17%). When incubating the fresh tailing sample with *A. thiooxidans* at pH 2, Ni is distributed 68% Ni^{2+} and 31% $NiSO_4$(aq) (supplementary data Table S7.1). The main Ni species in solution, according with visual MINTEQ results shows its strong affinity with sulfur, nitrogen and phosphorus compounds. A negative significant correlation between Cr and Ni (R^2=0.8) in the leachate is observed for all pulp densities during the leaching experiment with *A. thiooxidans* (pH=2).

For Al, the presence of KH_2PO_4 and K_2HPO_4 in the *P. putida* growth medium induces the formation of $AlHPO_4^+$ as dominant (97%) specie in solution. When *P. putida* was inoculated at the beginning of the leaching experiment, when pH is lower than 8, Al is present in three main species, $Al(OH)_3$, $Al(OH)_4^-$ and $AlHPO_4^+$ representing 3.4, 49.4 and 46.5%, respectively. After three days Al starts precipitating due to the high pH which varied from 8.9 to 9.6 between day 4 and 34. Visual MINTEQ simulation (supplementary data Table S7.2) results predict the precipitation of Al as Gibbsite ($Al(OH)_3$) and kaolinite ($Al_2Si_2O_5(OH)_4$).

Under more acidic conditions (leaching with the *A. thiooxidans* medium), with pH= 4, during the whole experiment Al distribution did not change. The main Al species are $AlHPO_4^+$ (50%), $AlSO_4^+$ (25%) and $AlSO_4^{2-}$ (22%). Precipitation of Variscite ($AlPO_4 \cdot 2H_2O$) is expected according with the thermodynamical modeling results (supplementary data Table S7.3). During incubation of the fresh tailings sample with *A. thiooxidans*, at pH 2, aluminum sulfate complexes ($AlSO_4^+$ and $AlSO_4^{2-}$) became the dominant species through all the leaching period accounting about 90% of the dissolved forms. Due to the acidic conditions, no precipitation occurs. In the leaching experiment with distilled water, Al is mainly present as $Al(OH)_3(aq)$ and $Al(OH)_4^-$, however part of the aluminum hydroxide could precipitate as a Gibbsite. Negative significant correlation between Cr and Al (R^2=0.8) in the leachate is observed for all pulp densities during the leaching experiment with *A. thiooxidans* (pH=2).

7.4.2 Bacterial effect on chromite tailings leachability

In the present work two bacterial strains, *A. thiooxidans* and *P. putida,* were used for acidic and alkaline leaching conditions, respectively. In the previous section, the leaching of chromite tailings has been discussed without including the possible bacterial effect. However, the differences on elements concentrations observed over time (Figure 7.4 to Figure 7.8) between blanks, controls and batch experiments inoculated with both strains, indicate that bacteria may play an important role on tailings leachability, other than a simple pH controller. Despite Schindler et al. (2018) found no direct bacterial effect on the release of Cr from altered chromatites, they affirmed that the presence of bacteria in tailings, mine waste piles and soils may control pH and Eh and indirectly control Cr redox chemistry. Under this premise, the role of bacteria on Fe and Cr mobility, as the most abundant compounds on tailings, were selected to discuss this point.

Initially, the only role of *A. thiooxidans* on Fe leaching was considered to be associated with the production of sulfuric acid, through oxidation of both elemental sulfur and sulfide. However, Marrero et al. (2017) demonstrated that *A. thiooxidans* is able to mediate reductive dissolution of laterite overburden coupled to the acidolysis under aerobic conditions. This chemolithoautotrophic bacterium has been also used to leach iron from low grade cobalt laterite (Simate and Ndlovu, 2014), tailings (Onchoke and Sasu, 2016; Świetlik, 1998) and laterite overburden (Marrero et al., 2017). As shown in Figure 7.4(c), in leaching experiments with *A. thiooxidans*, Fe is permanently leached for all pulp densities, with higher Fe concentrations for 5 and 10 g L^{-1}. Considering that the increase on total iron concentration does not evidence

bacterial effect, batch experiments inoculated with *A. thiooxidans* were compared with batch experiment with distilled water acidified at pH 2 with 1 N H_2SO_4 for a pulp density of 30 g L^{-1} (supplementary data Figure S7.4(b)). In the batch experiment with acidified distilled water (pH 2), for a pulp density of 30 g L^{-1}, Fe reached a total extracted of 479 mg kg^{-1} in 11 days, while at the same pulp density batch experiment inoculated with *A. thiooxidans* total Fe only reached 213 mg kg^{-1}. Nevertheless, when fresh chromite tailings leaching with *A. thiooxidans* was performed with a pulp density of 5 and 10 g L^{-1}, the total Fe extracted was 834 and 1108 mg kg^{-1}, respectively. This could suggest an inhibitory effect of *A. thiooxidans* at a pulp density of 30 g L^{-1} due to the release of toxic elements in the leachate such as Cr (946 µg L^{-1}) and Ni (843 µg L^{-1}). Jang and Valix (2017) reported a bacteriostatic effect of Ni and Cu on *A. thiooxidans* for leaching of saprolitic Ni laterite ores.

Total chromium extracted, in the batch experiment with *A. thiooxidans*, decreases over time. It has been reported that when *A. thiooxidans, A. ferrooxidans and Thiobacillus thioparus* are capable of Cr(VI) reduction when they are growing on sulfur compounds, due to the production of a series of sulfur compounds with high reducing power (Allegretti et al., 2006; Viera et al., 2003). According to Viera et al. (2003) in *A. thiooxidans* cultures, reduced glutathione is a required intermediate for the oxidation of elemental sulfur. The polysulfide formed is then successively oxidized to different compounds like sulfite, thiosulfate and finally sulfate. Sulfite and polythionates could be responsible for reductive reactions. In addition, reducing compounds associated with sulfur particles (less than 3 µm) could promote Cr reduction in *A. thiooxidans* cultures (Quintana et al., 2001). Steudel (1989) found that colloidal sulfur in cultures of *Acidithiobacillus* would be present as long-chain polythionates forming micelles of globules of up to few µm. Later Viera et al. (2003) observed that at pH 2 and 4, *A. thiooxidans* cultures reached higher free bacterial populations but lower chromium reduction values. Thus, the higher the pH, the higher the amount of reducing compounds associated to the colloidal sulfur and cells. Taking into consideration that in the present work the Cr(VI) leached out due to the presence of PO_4^{3-} in the medium, the Cr decrease could be explained by the reduction of Cr(VI) to Cr(III) mediated by the presence of *A. thiooxidans* and the low pH.

During the incubation with *P. putida*, the pH is above 8, where Fe does not exist in solution. Siderophores (supplementary data Figure S7.3(a)) produced by *P. putida* during growth in low-iron conditions solubilize and bind iron, and transport it back into the microbial cell, usually through siderophore specific membrane receptors (Payne, 1994). In spite of the presence of Fe

in the leachate, the Fe extracted remains considerably low (0.73 – 76 mg kg^{-1}) compared with the incubation with *A. thiooxidans*. The cell growth of *P. putida* was monitored with the total protein content in the leachate (supplementary data Figure S7.3(b)). In the first two days, the protein content doubles for all pulp densities with lower protein content for higher pulp density. *P. putida* has a high affinity for goethite. The bacterial adhesion increases with K^+ concentration and pH (2-7) (Rong et al., 2010). Given the fact that goethite is one of the main mineral phases on the tailings studied, adsorption of *P. putida* on the solids is highly possible, which represents a limitation of its effect in the liquid phase.

To establish the role of *P. putida* on the leachability of fresh chromite tailings, a batch experiment with distilled water at pH 9 (adjusted with 1N NaOH) was carried out (supplementary data Figure S7.4). Total Fe concentration on the leachate of the distilled water at pH 9 reaches 1.4 mg kg^{-1} after 262 hours of leaching, while in the batch experiment with *P. putida* the Fe extracted is higher (3.5 mg kg^{-1}) for the same pulp density. For Cr there is only 9 mg kg^{-1} difference between the extraction with distilled water at pH 9 and the batch experiment with *P. putida*, being higher for the last one. Reduction of hexavalent chromium by *Pseudomonas dechromaticans*, isolated from industrial sewage, has been reported, as it uses the chromate or dichromate as a terminal acceptor during anaerobic respiration. Under aerobic conditions, *P. fluorescens* uses a variety of electron acceptor for chromate reduction. Additionally, microbial metabolite extracellular polymeric substances (EPS) enhance Cr(VI) reduction efficiency and form organo-Cr(III) complexes to protect the cell and chromate reductase from inactivation (Jin et al., 2017). Nevertheless, the presence of anions such as SO_4^{2-}, SO_3^{2-}, MoO_4^{2-}, VO_4^{2-}, PO_4^{3-} and NO_3^- affects cellular chromate sensitivity (Park et al., 2005). Given the Cr(VI) reduction mechanisms by *Pseudomonas* spp. and the decrease of Cr concentration over time during incubation of the fresh tailing sample with *P. putida*, reduction of Cr(VI) to Cr(III) is likely to happen (DeLeo and Ehrlich, 1994; Desjardin et al., 2002). Besides, the Cr decrease in the leachate is accompanied by an increase in protein and siderophore content, which ratifies the role of *P. putida* in Cr(VI) reduction.

Nonliving biomass can also reduce Cr(VI) to Cr(III) through two different mechanisms. In the first case Cr(VI) is directly reduced to Cr(III) in the aqueous phase by contact with electron-donor groups of the biomass, and the second consists in three steps: a) binding of anionic Cr(VI) into the positively charged groups on the biomass surface; b) reduction of Cr(VI) to Cr(III) by

adjacent electron-donor group and c) release of the aqueous phase due to electronic repulsion (Park et al., 2005).

In the present work *A. thiooxidans* bacteria have shown to have a potential impact on chromite tailings leachability. Under aerobic conditions, *A. thiooxidans* promote Fe reduction, and acidic conditions associate to the production of sulfuric acid which promotes heavy metals dissolution. On the other hand, *P. putida* plays an important role in iron dissolution thanks to the production of siderophores, but the influence on Cr leaching is negligible. The role of those types of bacteria, could be seen not only as a potential pollution factor, but also as a remediation pathway, as well as the possible opportunity to recover leached metal from residues (tailings).

7.4.3 Does chromite tailings represent an environmental risk?

From previous sections, it is concluded that due to chemical and/or biological processes, chromite tailings can release elements such as Fe, Mn, Ni and Cr. Even if it has to be considered that some of the batch experiments do not represent the field conditions, previous studies have shown that the exposure of tailings to air, oxidation and climatic conditions favored the release of heavy metals which are often a threat to the environment (Kotaś and Stasicka, 2000; Sayyed et al., 2005). Meck et al. (2006) studied the impact of mine dumps, including chromite mines, on river water quality. Based on the fact that the effluents were not acidic, this study concluded that chromite dumps do not bring major risks to river water quality. However, water bodies in the surrounding of chromite mine areas are known to be impacted, in particular due to the presence of Cr(VI), which is toxic and highly mobile (Dhakate et al., 2008; Equeenuddin and Pattnaik, 2017; Pattnaik and Equeenuddin, 2016; Paulukat et al., 2015). The extent and degree of heavy metal release around the mines, vary depending the geochemical characteristics and the mineralization degree of tailings (Godgul and Sahu, 1995).

The environmental risk is directly related to the mineralogical composition of chromite tailings and its susceptibility to release toxic elements into the environment. Typically, chromite ore process tailings contains an heterogeneous mixture of iron and chromium oxides, silicates and aluminum silicate minerals (Dwari et al., 2018). In the tailings studies, mineral phases included chromite, which is the main Cr mineral on earth. In order to rule out chromite as a source of dissolved Cr, a leaching experiment with concentrated ore (product after the beneficiation plant) at pH 2, and a pulp density of 30 g L^{-1}, was performed (supplementary data Figure S7.5). The results show three fold less Cr in the leachate of the concentrated ore sample (47 mg kg^{-1})

compared with the leachate of the fresh tailing sample (147 mg kg^{-1}), suggesting that chromite is not the main source of Cr release from the tailings. Chromite nanoparticles can be released as a consequence of silicate weathering, however the production of Cr(VI) requires first a dissolution of the nanoparticle (Schindler et al., 2017). Other mineral phases such as iron and aluminum oxides, are able to adsorb chromium, especially Cr(VI) anions. In the ring of Fire (Canada) various Cr bearing minerals occurs such as clinochlore, phlogopite, amphibole and clinopyroxene with traces of Cr occurring in orthopyroxene, olivine, serpentine and carbonates. Preliminary leaching test indicated that Cr(VI) can be generated from those minerals in presence of birnessite (Mn-containing mineral) (Beukes et al., 2017). In the present study area birnessite was not detected.

Fresh and old tailings were compared in order to evaluate the potential release of Cr(VI) over time (Table 7.2). Chemically extraction with KH_2PO_4 showed that 93% of total Cr extracted with KH_2PO_4 is present as Cr(VI) with a total concentration of 223 mg kg^{-1}. In superficial tailings collected in a stockpile (old tailings), 94% of total Cr extracted is present as Cr(VI) which has a concentration of 158 mg kg^{-1}. The proportion of Cr(VI) compared with total Cr does not change with the depth, however the Cr(VI) concentration decreases from 158 mg kg^{-1} in the first 10 cm to 31 mg kg^{-1} at 30 cm. These results evidences that chemically exchangeable pool of Cr(VI) is higher in the fresh tailing sample compared with stockpiled old tailing sample, and in the stockpiled old tailing sample the pool of Cr(VI) decreases with depth. Stockpiled chromite tailings are susceptible to store CO_2 within the structures of minerals, process known as natural carbonation, which is enhanced in mine tailings by a dramatic increase in mineral surface area from crushing during ore processing (Borja et al., 2016). During accelerated mineral carbonation, Mg-carbonate mineral and Fe-oxyhydroxide phases sequester transition metals. Hamilton et al. (2016) demonstrated that upon precipitation, $MgCO_3 \cdot 3H_2O$ (a common product of mineral carbonation at Earth's surface conditions) rapidly sequesters transition metals (Cr, Ni, Mn, Co and Cu) in solution. The trace metal uptake appears to occur by substitution of Mg^{2+} in the crystal structure, and by incorporation into minor, metal-rich phases, such as Fe-oxyhydroxides. Additionally, the natural content of organic matter (NOM) in mine tailings exposed over long periods to atmospheric conditions, increases over time. The NOM can directly affect the extraction of metals, reducing the production of oxidizing agents required for metal dissolution (Silva et al., 2017). The natural carbonation and the NOM enrichment in old tailings could explain the lower exchangeable pool of Cr(VI), compared with fresh tailings were the content of organic matter is negligible (Santini and Banning, 2016). Mg-carbonate and hydromagnesite are

common weathering products of serpentine minerals, such as lizardite, which is present in the stockpiled old tailing sample in all depths. Further analyses have to be done to understand the possible role of new secondary phases, NOM and the passive carbonation on Cr(VI) mobility on chromite tailings.

A broad estimation of the exchangeable pool of total Cr and Cr(VI) release from chromite tailings (for an average mine) could be estimated based on the average production between 2016 and 2017 in all the chromite mines in Sukinda valley (Indian Bureau of Mines, Ministry of Mines, 2017) (Equation 7.3).

$$Cr(VI)\left(\frac{kg}{yr}\right) = E_{Cr(VI)}\left(\frac{mg\ Cr(VI)}{kg\ tailings}\right) * Tailings\ produced\ \left(\frac{kg}{yr}\right) * 10^{-6} \quad \textbf{(7.3)}$$

A total of 37.28×10^5 tons year^{-1} with a feed grade of Cr_2O_3 (dry) is processed on the beneficiation plant, and 4.72×10^5 tons year^{-1} of concentrated ore is produced (~50%) together with 5×10^5 tons year^{-1} (tailings produced) of tailings containing ~15% of Cr_2O_3 (Indian Bureau of Mines, Ministry of Mines, 2017). If the chemically exchangeable pool of Cr(VI) ($E_{Cr(VI)}$) in fresh tailings is considered, potentially 111,500 kg of Cr(VI) could be released per year. If now $E_{Cr(VI)}$ in the surface of stockpiled old tailings is considered, the Cr(VI) production decreases to 74,500 kg per year. This estimation suggests that the production and storage of chromite tailings could represent a risk for the surrounding soils and specially water bodies, which could be severely affected by the presence of Cr(VI). Given the results of the batch experiments of this study, we can conclude that chromite is not the main source of Cr(VI) for tailings, however other Cr bearing phases more susceptible to alteration could represent an important source of Cr(VI) in the environment. However, batch experiments with A. *thiooxidans* and *P. putida*, under the condition studied, showed that reduction of Cr(VI) to Cr(III) is a dominant process that is mediated by Fe and bacteria. In addition, the absence of Mn containing minerals such as birnessite, limits the oxidation of Cr(III) to Cr(VI). Those results suggest the important role of bacteria to reduce the toxic hexavalent chromium, as a natural mechanism in stockpiled tailings.

7.5 BIBLIOGRAPHY

Allegretti, P., Furlong, J., Donati, E., 2006. The role of higher polythionates in the reduction of chromium(VI) by *Acidithiobacillus* and *Thiobacillus* cultures. J. Biotechnol. 122, 55–61. https://doi.org/10.1016/j.jbiotec.2005.08.031

Beukes, J.P., du Preez, S.P., van Zyl, P.G., Paktunc, D., Fabritius, T., Päätalo, M., Cramer, M.,

2017. Review of Cr(VI) environmental practices in the chromite mining and smelting industry – Relevance to development of the Ring of Fire, Canada. J. Clean. Prod. 165, 874–889. https://doi.org/10.1016/j.jclepro.2017.07.176

Biswas, S., Bhattacharjee, K., 2014. Fungal assisted bioleaching process optimization and kinetics: Scenario for Ni and Co recovery from a lateritic chromite overburden. Sep. Purif. Technol. 135, 100–109. https://doi.org/10.1016/j.seppur.2014.07.055

Borja, D., Nguyen, K., Silva, R., Park, J., Gupta, V., Han, Y., Lee, Y., Kim, H., 2016. Experiences and Future Challenges of Bioleaching Research in South Korea. Minerals 6, 128. https://doi.org/10.3390/min6040128

BRGM, 1999. Development of Application Techniques in Relation to Environmental Management of Mnes and Waste Recoveries, Phase D - Task 1 Regional environmental impact assessment of Sukinda valley chromite mines (Orissa - India). https://doi.org/10.1017/CBO9781107415324.004

Choppala, G., Bolan, N., Park, J.H., 2013. Chromium contamination and its risk management in complex environmental settings, Advances in Agronomy. Elsevier. https://doi.org/10.1016/B978-0-12-407686-0.00002-6

Çiçek, T., Cöcen, I., Engin, V.T., Cengizler, H., Şen, S., 2008. Technical and economical applicability study of centrifugal force gravity separator (MGS) to Kef chromite concentration plant. Trans. Institutions Min. Metall. Sect. C Miner. Process. Extr. Metall. 117, 248–255. https://doi.org/10.1179/174328508X251897

Coto, O., Galizia, F., Hernández, I., Marrero, J., Donati, E., 2008. Cobalt and nickel recoveries from laterite tailings by organic and inorganic bio-acids. Hydrometallurgy 94, 18–22. https://doi.org/10.1016/j.hydromet.2008.05.017

Das, S., Mishra, J., Das, S.K., Pandey, S., Rao, D.S., Chakraborty, A., Sudarshan, M., Das, N., Thatoi, H., 2014. Investigation on mechanism of Cr(VI) reduction and removal by *Bacillus amyloliquefaciens*, a novel chromate tolerant bacterium isolated from chromite mine soil. Chemosphere 96, 112–121. https://doi.org/10.1016/j.chemosphere.2013.08.080

Das, S., Patnaik, S.C., Sahu, H.K., Chakraborty, A., Sudarshan, M., Thatoi, H.N., 2013. Heavy metal contamination, physico-chemical and microbial evaluation of water samples collected from chromite mine environment of Sukinda, India. Trans. Nonferrous Met. Soc. China 23, 484–493. https://doi.org/10.1016/S1003-6326(13)62489-9

Deakin, D., West, L.J., Stewart, D.I., Yardley, B.W.D., 2001. The leaching characteristics of chromite ore processing residue. Environ. Geochem. Health 23, 201–206.

DeLeo, P.C., Ehrlich, H.L., 1994. Reduction of hexavalent chromium by *Pseudomonas*

fluorescens in batch and continuous cultures. Appl. Microbiol. Biotechnol. 40, 756–759.

Desjardin, V., Bayard, R., Huck, N., Manceau, a., Gourdon, R., 2002. Effect of microbial activity on the mobility of chromium in soils. Waste Manag. 22, 195–200. https://doi.org/10.1016/S0956-053X(01)00069-1

Dhakate, R., Singh, V.S., Hodlur, G.K., 2008. Impact assessment of chromite mining on groundwater through simulation modeling study in Sukinda chromite mining area, Orissa, India. J. Hazard. Mater. 160, 535–547. https://doi.org/10.1016/j.jhazmat.2008.03.053

Dwari, R.K., Angadi, S.I., Tripathy, S.K., 2018. Studies on flocculation characteristics of chromite's ore process tailing: Effect of flocculants ionicity and molecular mass. Colloids Surfaces A Physicochem. Eng. Asp. 537, 467–477. https://doi.org/10.1016/j.colsurfa.2017.10.069

Equeenuddin, S.M., Pattnaik, B.K., 2017. Assessment of heavy metal contamination in sediment at Sukinda ultramafic complex using HAADF-STEM analysis. Chemosphere 185, 309–320. https://doi.org/10.1016/j.chemosphere.2017.06.131

Fandeur, D., Juillot, F., Morin, G., Livi, L., Cognigni, A., Webb, S.M., Ambrosi, J.P., Fritsch, E., Guyot, F., Brown, G.E., 2009. XANES evidence for oxidation of Cr(III) to Cr(VI) by Mn-oxides in a lateritic regolith developed on serpentinized ultramafic rocks of New Caledonia. Environ. Sci. Technol. 43, 7384–7390. https://doi.org/10.1021/es900498r

Fendorf, S.E., 1995. Surface reactions of chromium in soils and waters. Geoderma. https://doi.org/10.1016/0016-7061(94)00062-F

Garnier, J., Quantin, C., Guimaraes, E., Becquer, T., 2008. Can chromite weathering be a source of Cr in soils? Mineral. Mag. 72, 49–53.

Garnier, J., Quantin, C., Martins, E.S., Becquer, T., 2006. Solid speciation and availability of chromium in ultramafic soils from Niquelândia, Brazil. J. Geochemical Explor. 88, 206–209. https://doi.org/10.1016/j.gexplo.2005.08.040

Gleisner, M., Herbert, R.B., 2002. Sulfide mineral oxidation in freshly processed tailings: Batch experiments. J. Geochemical Explor. 76, 139–153. https://doi.org/10.1016/S0375-6742(02)00233-9

Godgul, G., 1994. Chromium, its analytical techniques, geogenic contamination and anthropogenic pollution, PhD thesis. Submitted to Indian Institute of Technology (IIT) Bombay, India. 194 p.

Godgul, G., Sahu, K.C., 1995. Chromium Contamination from Chromite Mine. Environ. Geol. 25, 251–257. https://doi.org/10.1007/BF00766754

Hallberg, K.B., Grail, B.M., Plessis, C.A.D., Johnson, D.B., 2011. Reductive dissolution of ferric

iron minerals: A new approach for bio-processing nickel laterites. Miner. Eng. 24, 620–624. https://doi.org/10.1016/j.mineng.2010.09.005

Hamdan, S.S., El-Naas, M.H., 2014. Characterization of the removal of Chromium(VI) from groundwater by electrocoagulation. J. Ind. Eng. Chem. 20, 2775–2781. https://doi.org/10.1016/j.jiec.2013.11.006

Hamilton, J.L., Wilson, S.A., Morgan, B., Turvey, C.C., Paterson, D.J., MacRae, C., McCutcheon, J., Southam, G., 2016. Nesquehonite sequesters transition metals and CO_2 during accelerated carbon mineralisation. Int. J. Greenh. Gas Control 55, 73–81. https://doi.org/https://doi.org/10.1016/j.ijggc.2016.11.006

Hullebusch, E.D. van, Yin, N., Seignez, N., Gauthier, A., Lens, P.N.L., Avril, C., Sivry, Y., 2015. Bio-alteration of metallurgical wastes by *Pseudomonas aeruginosa* in a semi fl ow-through reactor 147, 297–305. https://doi.org/10.1016/j.jenvman.2014.09.018

Indian Bureau of Mines, Ministry of Mines, G. of I., 2017. Indian Minerals Yearbook, Part III (Mineral Reviews), Chromite; Indian Bureau of Mines: Nagpur, India, 2017; 6-1,6-19..

Jang, H.C., Valix, M., 2017. Overcoming the bacteriostatic effects of heavy metals on *Acidithiobacillus thiooxidans* for direct bioleaching of saprolitic Ni laterite ores. Hydrometallurgy 168, 21–25. https://doi.org/10.1016/j.hydromet.2016.08.016

Jin, R., Liu, Y., Liu, G., Tian, T., Qiao, S., Zhou, J., 2017. Characterization of Product and Potential Mechanism of Cr(VI) Reduction by Anaerobic Activated Sludge in a Sequencing Batch Reactor. Sci. Rep. 7, 1–12. https://doi.org/10.1038/s41598-017-01885-z

Kaprara, E., Kazakis, N., Simeonidis, K., Coles, S., Zouboulis, A.I., Samaras, P., Mitrakas, M., 2015. Occurrence of Cr (VI) in drinking water of Greece and relation to the geological background. J. Hazard. Mater. 281, 2–11. https://doi.org/10.1016/j.jhazmat.2014.06.084

Kotaś, J., Stasicka, Z., 2000. Chromium occurrence in the environment and methods of its speciation. Environ. Pollut. 107, 263–283. https://doi.org/10.1016/S0269-7491(99)00168-2

Ledin, M., Pedersen, K., 1996. The environmental impact of mine wastes - Roles of microorganisms and their significance in treatment of mine wastes. Earth-Science Rev. 41, 67–108. https://doi.org/10.1016/0012-8252(96)00016-5

Liu, H.C., Xia, J.L., Nie, Z.Y., 2015. Relatedness of Cu and Fe speciation to chalcopyrite bioleaching by *Acidithiobacillus ferrooxidans*. Hydrometallurgy 156, 40–46. https://doi.org/10.1016/j.hydromet.2015.05.013

Liu, S., Chen, L., Gao, Y., 2013. Hexavalent chromium leaching influenced factors in the weathering chrome slag. Procedia Environ. Sci. 18, 783–787. https://doi.org/http://dx.doi.org/10.1016/j.proenv.2013.04.105

Lynne, A.M., Haarmann, D., Louden, B.C., 2011. Use of blue agar CAS assay for siderophore detection. J. Microbiol. Biol. Educ. 12, 51–53. https://doi.org/10.1128/jmbe.v12i1.249

Marrero, J., Coto, O., Goldmann, S., Graupner, T., Schippers, A., 2015. Recovery of nickel and cobalt from laterite tailings by reductive dissolution under aerobic conditions using *Acidithiobacillus* species. Environ. Sci. Technol. 49, 6674–6682.

Marrero, J., Coto, O., Schippers, A., 2017. Anaerobic and aerobic reductive dissolutions of iron-rich nickel laterite overburden by *Acidithiobacillus*. Hydrometallurgy 168, 49–55. https://doi.org/10.1016/j.hydromet.2016.08.012

Mcclain, C.N., Maher, K., 2016. Chromium fluxes and speciation in ultramafic catchments and global rivers. Chem. Geol. 426, 135–157. https://doi.org/10.1016/j.chemgeo.2016.01.021

Meck, M., Love, D., Mapani, B., 2006. Zimbabwean mine dumps and their impacts on river water quality - a reconnaissance study. Phys. Chem. Earth 31, 797–803. https://doi.org/10.1016/j.pce.2006.08.029

Murthy, Y.R., Tripathy, S.K., Kumar, C.R., 2011. Chrome ore beneficiation challenges & opportunities - A review. Miner. Eng. 24, 375–380. https://doi.org/10.1016/j.mineng.2010.12.001

Naresh Kumar, R., Nagendran, R., 2009. Fractionation behavior of heavy metals in soil during bioleaching with *Acidithiobacillus thiooxidans*. J. Hazard. Mater. 169, 1119–1126. https://doi.org/10.1016/j.jhazmat.2009.04.069

Nguyen, V.K., Lee, M.H., Park, H.J., Lee, J.U., 2015. Bioleaching of arsenic and heavy metals from mine tailings by pure and mixed cultures of *Acidithiobacillus spp*. J. Ind. Eng. Chem. 21, 451–458. https://doi.org/10.1016/j.jiec.2014.03.004

Onchoke, K.K., Sasu, S.A., 2016. Determination of hexavalent chromium (Cr(VI)) concentrations via Ion chromatography and UV-Vis spectrophotometry in samples collected from nacogdoches wastewater treatment plant, East Texas (USA). Adv. Environ. Chem. 2016, 10. https://doi.org/10.1155/2016/3468635

Osaki, S., 1983. The effect of organic matter and colloidal particles on the determination of chromium (VI) in natural waters. Talanta 30, 523–526.

Oze, C., Fendorf, S., Bird, D.K., Coleman, R.G., 2004. Chromium geochemistry of serpentine soils. Int. Geol. Rev. 46, 97–126. https://doi.org/10.2747/0020-6814.46.2.97

Özgen, S., 2012. Modelling and optimization of clean chromite production from fine chromite tailings by a combination of multigravity separator and hydrocyclone. J. South. African Inst. Min. Metall. VO - 112 112, 387.

Panda, L., Banerjee, P.K., Biswal, S.K., Venugopal, R., Mandre, N.R., 2014. Modelling and

optimization of process parameters for beneficiation of ultrafine chromite particles by selective flocculation. Sep. Purif. Technol. 132, 666–673. https://doi.org/10.1016/j.seppur.2014.05.033

Park, D., Yun, Y.S., Jong, M.P., 2005. Studies on hexavalent chromium biosorption by chemically-treated biomass of *Ecklonia sp*. Chemosphere 60, 1356–1364. https://doi.org/10.1016/j.chemosphere.2005.02.020

Pattnaik, B.K., Equeenuddin, S.M., 2016. Potentially toxic metal contamination and enzyme activities in soil around chromite mines at Sukinda ultramafic complex, India. J. Geochemical Explor. 168, 127–136. https://doi.org/10.1016/j.gexplo.2016.06.011

Paulukat, C., Døssing, L.N., Mondal, S.K., Voegelin, A.R., Frei, R., 2015. Oxidative release of chromium from Archean ultramafic rocks, its transport and environmental impact – A Cr isotope perspective on the Sukinda valley ore district (Orissa, India). Appl. Geochemistry 59, 125–138. https://doi.org/10.1016/j.apgeochem.2015.04.016

Payne, S.M., 1994. Detection, isolation, and characterization of siderophores. Methods Enzymol. 235, 329–344. https://doi.org/10.1016/0076-6879(94)35151-1

Potysz, A., Lens, P.N.L., Vossenberg, J. Van De, Rene, E.R., Grybos, M., Guibaud, G., Kierczak, J., Hullebusch, E.D. van, 2016. Applied Geochemistry Comparison of Cu , Zn and Fe bioleaching from Cu-metallurgical slags in the presence of *Pseudomonas fluorescens* and *Acidithiobacillus thiooxidans*. Appl. Geochemistry 68, 39–52. https://doi.org/10.1016/j.apgeochem.2016.03.006

Quintana, M., Curutchet, G., Donati, E., 2001. Factors affecting the chromium(VI) reduction by microbial action. Biochem. Eng. J. 9, 11–15.

Raghu Kumar, C., Tripathy, S., Rao, D.S., 2009. Characterisation and pre-concentration of chromite values from plant tailings using floatex density separator. J. Miner. Mater. Charact. Eng. Raghu Kumar Sunil Tripathy 88, 367–378.

Raous, S., Becquer, T., Garnier, J., Martins, É.D.S., Echevarria, G., Sterckeman, T., 2010. Mobility of metals in nickel mine spoil materials. Appl. Geochemistry 25, 1746–1755. https://doi.org/10.1016/j.apgeochem.2010.09.001

Rodríguez-Vico, F., Martínez-Cayuela, M., García-Peregrín, E., Ramírez, H., 1989. A procedure for eliminating interferences in the lowry method of protein determination. Anal. Biochem. 183, 275–278. https://doi.org/10.1016/0003-2697(89)90479-X

Rong, X., Chen, W., Huang, Q., Cai, P., Liang, W., 2010. *Pseudomonas putida* adhesion to goethite: Studied by equilibrium adsorption, SEM, FTIR and ITC. Colloids Surfaces B Biointerfaces 80, 79–85. https://doi.org/10.1016/j.colsurfb.2010.05.037

Salem, F.Y., Parkerton, T.F., Lewis, R. V., Huang, J.H., Dickson, K.L., 1989. Kinetics of chromium transformations in the environment. Sci. Total Environ. 86, 25–41. https://doi.org/10.1016/0048-9697(89)90190-3

Santini, T.C., Banning, N.C., 2016. Alkaline tailings as novel soil forming substrates: Reframing perspectives on mining and refining wastes. Hydrometallurgy 164, 38–47. https://doi.org/10.1016/j.hydromet.2016.04.011

Sayyed, R.Z., Badgujar, M.D., Sonawane, H.M., Mhaske, M.M., Chincholkar, S.B., 2005. Production of microbial iron chelators (siderophores) by *fluorescent Pseudomonas*. Indian J. Biotechnol. 4, 484–490.

Schindler, M., Berti, D., JR, M.F.H., 2017. Previously unknown mineral-nanomineral relationships with important environmental consequences : The case of chromium release from dissolving silicate minerals. Am. Mineral. 102, 2142–2145.

Schindler, M., Lussier, A.J., Principe, E., Mykytczuk, N., 2018. Dissolution mechanisms of chromitite: Understanding the release and fate of chromium in the environment. Am. Mineral. 103, 271–283. https://doi.org/10.2138/am-2018-6234

Schwyn, B., Neilands, J.B., 1987. Universal chemical assay for the detection and determination of siderophore. Anal. Biochem. 160, 47–56.

Shahid, M., Shamshad, S., Rafiq, M., Khalid, S., Bibi, I., Niazi, N.K., Dumat, C., Rashid, M.I., 2017. Chromium speciation, bioavailability, uptake, toxicity and detoxification in soil-plant system: A review. Chemosphere 178, 513–533. https://doi.org/10.1016/j.chemosphere.2017.03.074

Silva, R.A., Borja, D., Hwang, G., Hong, G., Gupta, V., Bradford, S.A., Zhang, Y., Kim, H., 2017. Analysis of the effects of natural organic matter in zinc beneficiation. J. Clean. Prod. 168, 814–822. https://doi.org/10.1016/j.jclepro.2017.09.011

Simate, G.S., Ndlovu, S., 2014. Acid mine drainage: Challenges and opportunities. J. Environ. Chem. Eng. 2, 1785–1803. https://doi.org/10.1016/j.jece.2014.07.021

Stanin, F., 2004. The transport and fate of Cr(VI) in the Environment, in: Chromium (VI) Handbook. pp. 161–204. https://doi.org/10.1007/978-94-007-4375-5

Steudel, R., 1989. On the nature of “elemental sulfur” (S°) produced by sulfur-oxidizing bacteria, in: Bowien, B. (Ed.), Autotrophic Bacteria. Berlin, Germany, pp. 289–303.

Sueker, J.K., 1964. Chromium, in: Murphy, B.L.B.T.-E.F. (Ed.), Environmental Forensics: Contaminant Specific Guide. Academic Press, Burlington, pp. 82–93. https://doi.org/https://doi.org/10.1016/B978-012507751-4/50027-6

Świetlik, R., 1998. Speciation analysis of chromium in waters. Polish J. Environ. Stud. 7, 257–

266.

Thacher, R., Hsu, L., Ravindran, V., Nealson, K.H., 2015. Modeling the transport and bioreduction of hexavalent chromium in aquifers : Influence of natural organic matter. Chem. Eng. Sci. 138, 552–565. https://doi.org/10.1016/j.ces.2015.08.011

Tinjum, J.M., Benson, C.H., Edil, T.B., 2008. Mobilization of Cr(VI) from chromite ore processing residue through acid treatment. Sci. Total Environ. 391, 13–25. https://doi.org/10.1016/j.scitotenv.2007.10.041

Tiwary, R.K., Dhakate, R., Ananda Rao, V., Singh, V.S., 2005. Assessment and prediction of contaminant migration in ground water from chromite waste dump. Environ. Geol. 48, 420–429. https://doi.org/10.1007/s00254-005-1233-2

Tokunaga, T.K., Wan, J., Firestone, M.K., Hazen, T.C., Olson, K.R., Herman, D.J., Sutton, S.R., Lanzirotti, A., 1999. In situ reduction of chromium(VI) in heavily contaminated soils through organic carbon amendment. J. Environ. Qual. 32, 1641–9. https://doi.org/10.2134/jeq2003.1641

Tripathy, S.K., Murthy, Y.R., Singh, V., 2013. Characterisation and separation studies of Indian chromite beneficiation plant tailing. Int. J. Miner. Process. 122, 47–53. https://doi.org/10.1016/j.minpro.2013.04.008

Viera, M., Curutchet, G., Donati, E., 2003. A combined bacterial process for the reduction and immobilization of chromium. Int. Biodeterior. Biodegrad. 52, 31–34. https://doi.org/10.1016/S0964-8305(02)00103-8

Viollier, E., Inglett, P.W., Hunter, K., Roychoudhury, a. N., Van Cappellen, P., 2000. The ferrozine method revisited: Fe(II)/Fe(III) determination in natural waters. Appl. Geochemistry 15, 785–790. https://doi.org/10.1016/S0883-2927(99)00097-9

Wang, Y.S., Pan, Z.Y., Lang, J.M., Xu, J.M., Zheng, Y.G., 2007. Bioleaching of chromium from tannery sludge by indigenous *Acidithiobacillus thiooxidans*. J. Hazard. Mater. 147, 319–324. https://doi.org/10.1016/j.jhazmat.2007.01.005

Waterborg, J.H., Matthews, H.R., 1984. The lowry method for protein quantitation. Methods Mol. Biol. 1, 1–3. https://doi.org/10.1385/1-59259-169-8:7

Watts, M.P., Coker, V.S., Parry, S.A., Pattrick, R.A.D., Thomas, R.A.P., Kalin, R., Lloyd, J.R., 2015. Biogenic nano-magnetite and nano-zero valent iron treatment of alkaline Cr(VI) leachate and chromite ore processing residue. Appl. Geochem. 54, 27–42. https://doi.org/10.1016/j.apgeochem.2014.12.001

Weng, C.H., Huang, C.P., Allen, H.E., Cheng, A.H.D., Sanders, P.F., 1994. Chromium leaching behavior in soil derived from chromite ore processing waste. Sci. Total Environ. 154, 71–

86. https://doi.org/10.1016/0048-9697(94)90615-7

Zachara, J.M., Ainsworth, C.C., Cowan, C.E., Resch, C.T., 1989. Adsorption of Chromate by Subsurface Soil Horizons, Soil Science Society of America Journal - SSSAJ. https://doi.org/10.2136/sssaj1989.03615995005300020018x

Zaitseva, N., Zaitsev, V., Walcarius, A., 2013. Chromium(VI) removal via reduction–sorption on bi-functional silica adsorbents. J. Hazard. Mater. 250–251, 454–461. https://doi.org/10.1016/j.jhazmat.2013.02.019

7.6 SUPPLEMENTARY DATA

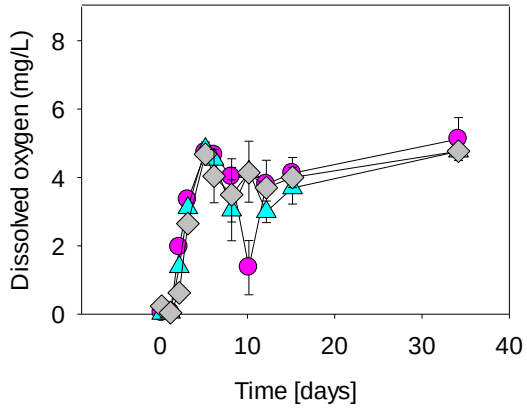

Figure S7.1. Dissolved oxygen evolution throughout the incubation of the fresh tailing sample with *P. putida* at different pulp densities: 5 g L^{-1} (—●—), 10 g L^{-1} (—▲—) and 30 g L^{-1} (—◆—).

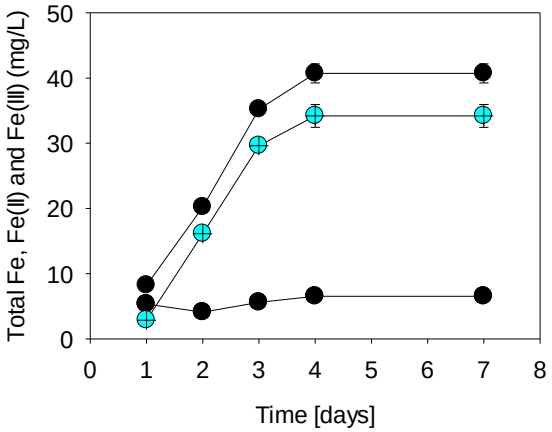

Figure S7.2. Total Fe (—●—), Fe(II) (—●—) and Fe(III) (—⊕—) evolution throughout the leaching of the fresh tailing sample with acidified (H_2SO_4) MQ water for a pulp density of 30 g L^{-1}.

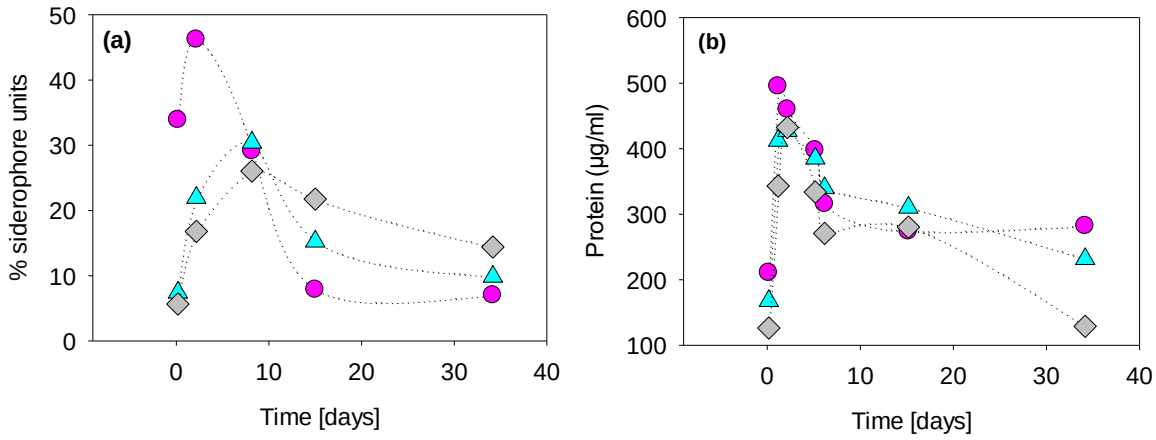

Figure S7.3. Siderophores content under incubation of the fresh tailing sample with *P. putida* (a) and protein content in the leached (b). The medium were *P. putida* was grown did not contain Fe in order to stimulate the production of siderophores. Three pulp densities were evaluated: 5 g L^{-1} (—●—), 10 g L^{-1} (—▲—) and 30 g L^{-1} (—◆—).

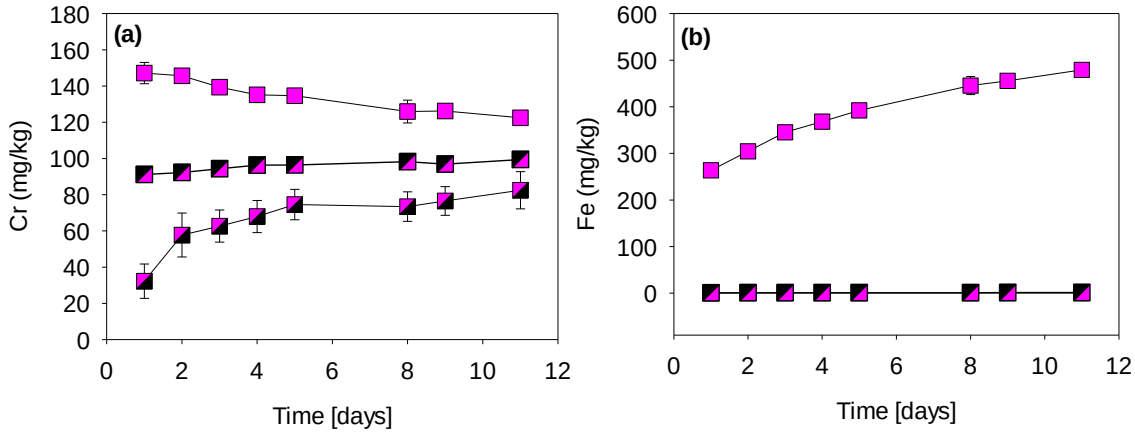

Figure S7.4. Cr (a) and Fe (b) extracted from the fresh tailing sample, after leaching with MQ water at pH 7 (—◪—), pH 2 with H_2SO_4 (—■—) and at pH 9 with NaOH (—◪—).

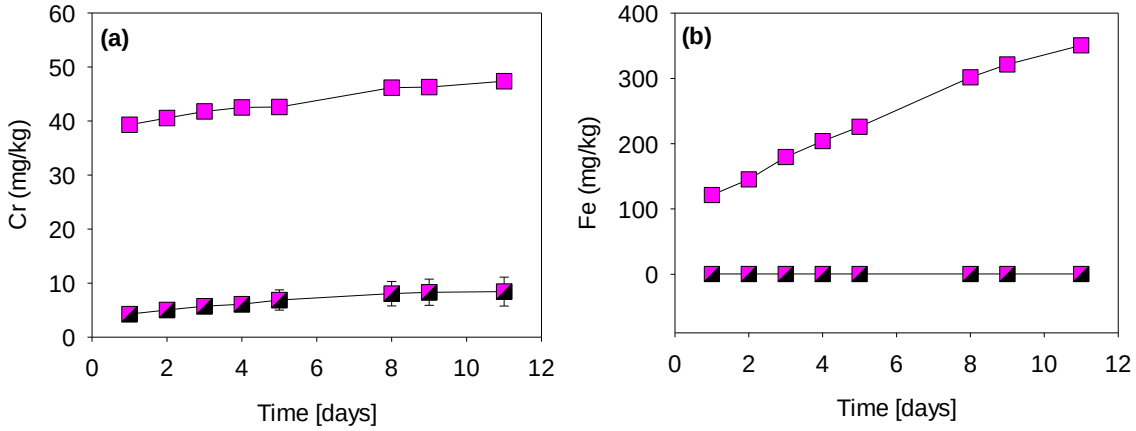

Figure S7.5. Cr (a) and Fe (b) extracted from the concentrated ores sample, after leaching with MQ water at pH 7(—◪—) and pH 2 with H_2SO_4 (—■—).

Table S7.1. Species distribution obtained in visual MINTEQ simulation, for the control and the leaching of the tailing sample with *A. thiooxidans* for a pulp density of 5 g L^{-1}.

Component	Species	Control *A. thiooxidans*	Batch *A. thiooxidans*
		% of total concentration	
Al(III)	Al^{3+}	1.71	10.67
	$AlOH^{2+}$	0.30	
	$Al(OH)_2^{+}$	0.04	
	$AlSO_4^{+}$	24.76	66.14
	$Al(SO_4)_2^{-}$	22.12	23.16
	$AlHPO_4^{+}$	51.02	0.03
	$Al_2PO_4^{3+}$	0.05	
Cr(VI)	CrO_4^{2-}	3.98	
	$CrO_3HPO_4^{2-}$	1.09	0.18
	$CrO_3H_2PO_4^{-}$		1.64
	$KCrO_4^{-}$	0.01	
	$HCrO_4^{-}$	94.62	82.93
	H_2CrO_4 (aq)		1.59
	$Cr_2O_7^{2-}$	0.26	0.21
	$NH_4Cr_2O_7^{-}$	0.02	0.02
	$CrO_3SO_4^{2-}$	0.02	13.40
	CrO_3Cl^{-}		0.02
Fe(II)	Fe^{2+}	36.81	61.11
	$FeCl^{+}$	0.01	0.02
	$FeSO_4$ (aq)	51.41	35.05
	$FeH_2PO_4^{+}$	11.49	3.82
	$FeHPO_4$ (aq)	0.28	
Ni(II)	Ni^{2+}	46.63	68.13
	$NiCl^{+}$		0.01
	$NiSO^{4}$ (aq)	52.93	31.76
	$Ni(SO_4)_2^{2-}$	0.08	0.02
	$NiNH_3^{2+}$	0.02	
	$NiH_2PO_4^{+}$	0.25	0.07
	$NiHPO_4$ (aq)	0.08	

Table S7.2. Species distribution obtained in visual MINTEQ simulation, for the blank, the control and the leaching of the tailing sample with *P. putida*. Results are presented for a pulp density of 5 g L^{-1} and three subsamples collected at 0, 5 and 34 days in the batch with *P. putida*.

Component	Species	Blank	Control *P. putida*	Batch *P. putida*		
			% of total concentration			
	Day	0	0		5	34
Al(III)	$AlOH^{2+}$	0.28	0.02	0.02		
	$Al(OH)_2^+$	8.79	0.20	0.64		
	$Al(OH)_{3\ (aq)}$	22.10	0.34	3.43	0.17	0.03
	$Al(OH)_4^-$	68.83	1.53	49.37	99.83	99.97
	$AlHPO_4^+$		97.90	46.54		
Cr(VI)	CrO_4^{2-}	66.45	71.78	86.89	93.49	93.62
	$CrO3HPO_4^{2-}$		8.31	1.48		
	$KCrO_4^-$		5.33	6.12	6.36	6.35
	$HCrO_4^-$	33.55	14.54	5.50	0.15	0.03
	$CaCrO_{4\ (aq)}$		0.04			
Fe(II)	Fe^{2+}		2.71	2.42	2.19	2.16
	$FeOH^+$				0.27	1.33
	$Fe(OH)_{2\ (aq)}$					0.03
	$FeSO_{4\ (aq)}$		1.20	1.03	0.93	0.93
	$Fe(NH_3)_2^{2+}$					0.06
	$FeNH_3^{2+}$				0.26	0.68
	$FeH_2PO_4^+$		30.22	12.42	0.36	0.07
	$FeHPO_{4\ (aq)}$		65.87	84.12	95.99	94.73
Ni(II)	Ni^{2+}	99.92	14.11	10.64	6.31	2.62
	$NiOH^+$	0.08		0.01	0.25	0.51
	$Ni(OH)_{2\ (aq)}$				0.10	1.07
	$Ni(OH)_3^-$					0.06
	$NiSO_{4\ (aq)}$		5.07	3.68	2.18	0.92
	$Ni(NH_3)_5^{2+}$					0.17
	$Ni(NH_3)_4^{2+}$				0.14	2.93
	$Ni(NH_3)_3^{2+}$			0.84	2.25	17.65
	$NiNH_3^{2+}$		0.36		15.64	17.30
	$Ni(NH_3)_2^{2+}$			0.02	10.42	30.72
	$NiHPO_{4\ (aq)}$		77.80	83.88	62.69	26.04
	$NiH_2PO_4^+$		2.66	0.92	0.02	

Table S7.3. Ion Activity Product (IAP) and saturation index (SI) of $MNHPO_4$ and variscite, obtained in visual MINTEQ simulation, for the control and the leaching of the tailing sample with *A. thiooxidans*. Results are presented for two pulp densities (5 and 10 g L^{-1}) and three subsamples collected at 0, 5 and 34 days.

Pulp density		**5 g L^{-1}**						**10 g L^{-1}**					
Time [days]		**0**		**5**		**34**		**0**		**5**		**34**	
Experiment type	**Mineral**	**log IAP**	**SI**	**log IAP**	**SI**	**log IAP**	**SI**	**log IAP**	**SI**	**log IAP**	**SI**	**log IAP**	**SI**
Control *A. thiooxidans*	**$MnHPO_4$(s)**	-24.44	0.96	-24.18	1.22	-24.06	1.34	-24.36	1.04	-24.18	1.22	-24.12	1.28
	Variscite	-20.821	1.25	-21.00	1.07	-21.20	0.87	-21.35	0.72	-21.74	0.32	-22.16	-0.09
Incubation with *A. thiooxidans*	**$MnHPO_4$(s)**	-27.77	-2.37	-27.30	-1.90	-26.76	-1.36	-27.07	-1.68	-27.17	-1.77	-26.96	-1.56
	Variscite	-26.52	-4.45	-26.05	-3.98	-25.35	-3.28	-25.86	-3.79	-25.77	-3.70	-25.45	-3.38

SUMMARY AND CONCLUSIONS

Nickel and chromite mining activities in ultramafic environments produce a large amount of metal-rich waste residues. In all the products and by-products, Cr is present, even in its hexavalent form which is known to be highly mobile and toxic. Thus, the aim of this research was to identify the impact of mining activities on Cr mobility, availability and isotopic composition in ultramafic environments.

i. INFLUENCE OF COLLOIDS IN CHROMIUM MOBILITY

Mining activities are known to increase the rate of erosion due to the removal of the plant cover in the exploitation area. The particles released are stored in ponds and/or streams in the mining area. Isotopic dilution techniques can be efficiently used to assess the impact of mining activities in water bodies, through the estimation of the labile pool of chromium in the suspended particulate matter (SPM) in water.

The isotopically exchangeable pool of chromium in ponds (2246 µ L^{-1} for pond 1, 872 µg L^{-1} for pond 2 and 373 µg L^{-1} for pond 3) is higher compared to the stream localized in the mining (stream 2 – from 74.3 to 164 µg L^{-1}) and in the pristine area (stream 1 – from 0.41 to 143 µg L^{-1}). However, when evaluating the impact of the pore size (cut-off) in the E^{W}_{Cr} value calculation (#E1), no differences between cut-offs were observed in ponds, while in the pristine area differences between the cut-offs were present. The contribution of particles (> 0.2 µm) due to mining activities was also reflected in a second experiment where the E^{W}_{Cr} was assessed in the SPM according to their specific range of size (0.2–0.7 µm, 500 KDa–0.2 µm and 1–500 KDa). The ponds showed differences in the E^{W}_{Cr} values and the exchangeable chromium was mainly associated with the particulate fraction (> 0.2 µm), indicating that the exchangeable chromium was directly related with the number of particles and their mineralogy.

Both in the pristine and in the mining areas, there was an overestimation of the exchangeable pool of chromium (E^{W}_{Cr} value) due to the presence of organic and inorganic colloids containing non-exchangeable chromium. We propose a method to calculate a “worst case” scenario for the colloidal contribution and a correction to overcome this discrepancy. After the correction, the E^{W}_{Cr} value in stream 1 showed that there are no differences in the available pool of chromium,

meaning that the presence of different sizes of colloids artificially decreases the isotopic ratio and increases the estimated E^W_{Cr} value. In the mining area, the situation is similar for the 0.2 µm, 500 kDa and 1 kDa cut-offs, while in the lasgest fraction (> 0.7 µm) the E^W_{Cr} value is less affected by the presence of colloids due to chromium binding to the particulate fraction. These results suggest that the presence of chromium associated to the colloidal fraction acts as a bias in isotopic exchange experiments, artificially decreasing the isotopic ratio in the filtrate with a consequent increase in the E^W_{Cr} value. This work reveals the importance of considering the presence of colloidal non-exchangeable chromium in order to avoid overestimating the E^W_{Cr} value.

ii. CHROMIUM MOBILITY AND AVAILABILITY IN MINING RESIDUES OF ULTRAMAFIC AREAS

Ultramafic systems display high chromium (Cr) concentrations. Cr is naturally leached from laterite to surface and groundwater. However, mining and metallurgical activities may considerably increase the amount of both trivalent and hexavalent chromium (Cr(III) and Cr(VI)) released into the environment, the later being highly soluble in water, bioavailable and toxic. In a nickel exploitation and metallurgic area in Goiás state Brazil (Barro Alto), Cr mobility and availability were evaluated.

The reconstruction of the stratigraphic column indicated the presence of material with different degrees of alteration (ultramafic index of alteration - UMIA). The results of the UMIA reflect an intense mineralogical transformation of the lateritic ores and soils, leading to the enrichment of Cr mainly in its trivalent form. By contrast, the less altered materials were the saprolitic ores and the bedrock which are composed mainly of Mg and Si. Sediments have an intermediary degree of alteration, located between lateritic and saprolitic ores, because they represent a mixture of particles coming from different sources (ores and soils for example). Therefore, UMIA on sediments likely represents an average of that on soils, ores and all the superficial materials from the area.

Total chromium is least concentrated (0.1 – 0.3 g kg^{-1}) in the bedrock. In the weathering products of the parent material, the chromium concentration depended on the degree of alteration, being the most altered materials and the one with higher chromium content. The high Cr content (10 – 18 g kg^{-1}) in the lateritic ores is accompanied by enrichment on Fe (85 – 536 g kg^{-1}). The exchangeable pool of Cr(VI) increases with the degree of alteration. However, it

does not necessarily mean that samples with higher total Cr will have a higher exchangeable pool of Cr(VI). Mineral phases control the release of Cr(VI), in particular Fe oxides. In addition, a significant positive correlation of total manganese with total chromium content (R^2=0.9) and UMIA (R^2=0.8), suggests the role of Mn oxides on Cr(III) oxidation.

The degree of alteration of the samples is also associated with the Cr isotopic signature. For the saprolitic ores, the δ^{53}Cr for the total chromium (+0.97 ± 0.08‰) and the extracted Cr(VI) (+1.34 ± 0.07‰) is positive and there is a small difference between both values, indicating that the losses of heavy Cr(VI) in the saprolitic ores are negligible. This statement is in agreement with the incipient degree of alteration of the saprolitic ores. By contrast, for the lateritic ores the difference between the Cr isotopic fractionation of total Cr (-0.76 ± 0.07‰) and Cr(VI) (+4.37 ± 0.06‰) is considerably higher. This occurs as a consequence of the loss of isotopically heavy and exchangeable Cr(VI) during weathering, leaving Cr negatively fractionated. On the contrary, the positive δ^{53}Cr in the saprolitic ores can be explained by re-deposition of mobilized isotopically heavy Cr.

Isotopically heavy chromium was found in the pristine (stream 1) and in the mining area (stream 2 and ponds). In stream 1, 97% of Cr is associated to SPM (0.02 ± 0.09 ‰). The dissolved fraction was enriched in ^{53}Cr (+2.60 ± 0.04 ‰). SPM concentration (3.3 – 316 mg L^{-1}) of water bodies inside the mine evidences the particles release due to extraction, transport and stockpiling of the residues produced during mining processes. In the mining area, chromium was found in the particulate (24 – 1064 µg L^{-1}) and in the dissolved fraction with concentrations up to 737 µg L^{-1}. In pond 1, particulate Cr (-0.38 ± 0.08‰) and Cr in the sediments (-0.50 ± 0.04‰) are negatively fractionated, the second being slightly lower probably due to the oxidation of Cr(III) and the release of Cr(VI) enriched in heavy isotopes. This hypothesis suggests that sediments in the ponds represent a source of isotopically heavy Cr(VI) for the water column.

The range of variation for the surface waters (+2.10 ± 0.04 to +3.66 ± 0.04 ‰) is within the range of the extracted Cr(VI) (+1.34 ± 0.07 to +4.37 ± 0.06 ‰). It indicates that the enrichment of ^{53}Cr in the surface and even in the groundwater is associated to the release of Cr(VI) from Cr(III) oxidation in the solid phases. Part of the contribution is related to natural weathering, where we observed an increase in the concentration of Cr(VI) in more altered materials and the correspondent depletion of ^{53}Cr in the solid remaining. But there is also an important contribution directly linked to erosion promoted by mining processes, accelerating natural weathering. In the

pristine area, stream 1, the total chromium concentration is lower (0.20 µg L^{-1}) compared with the rest of surface waters evaluated. However, the $\delta^{53}Cr$ remains within the range of variation of the Cr(VI) extracted. This suggests that $\delta^{53}Cr$ can potentially be used as a tracer of sources in the dissolved fraction, however, it is not a self-sufficient tool and its interpretation must be accompanied by other parameters like total chromium concentration in the dissolved fraction together with Fe, Mn, organic carbon and chromium speciation.

iii. CHROMIUM FATE IN SOILS AFFECTED BY MINING ACTIVITITES IN ULTRAMAFIC AREAS

The impact of historical chromite mining activities on chromium fate was evaluated in Cromínia mine. Cromínia mine presents several favorable attributes to achieve the aim, as the small size together with a high ability to define the impacted and non-impacted area meanwhile there are no artifacts related to recent activities.

The mineralogy of the soil profiles in the non-affected (T3) and affected area (S1) were characterized by the presence of serpentine, hematite and spinel (chromite and/or magnetite), as the main Cr-bearing phases. Chlorite was present in T3, but not in S1. Other mineral phases found were quartz, micas and talc 2M. Total chromium in the solid samples of the non-affected (T3) and directly affected (S1) soils are within the same range, with values between 0.3 and 5 g kg^{-1}. Surprisingly, the exchangeable pool of Cr(VI) ($E_{Cr(VI)}$-KH_2PO_4) is higher in the non-affected area, however in both T3 and S1 this pool is low compared to other studies in ultramafic areas (Garnier et al., 2009; Mills et al., 2011). Two main factors explain the discrepancies between the non-affected and directly affected soil profiles. Firstly, the geological variability within the chromite chemical variation, originally caused by fractional crystallization from a primitive magma. Secondly, in the non-affected soil profile (T3) Cr availability is probably controlled by Fe-oxides, such as hematite, which form inner-sphere chromate complexes (Rai et al., 1989), while in the affected soil profile, Cr is mainly associated with chromite. The material extracted after mining exploitation could contain more exchangeable Cr(VI), however, its exposure to open air would eventually wash the mobile Cr into the hydrosphere.

Chromium isotopic fractionation was particularly high in the affected soil profile (up to 3.87 ‰) in comparison with the non-affected area, which cannot only be explained by the reasons mentioned. Hydrothermal processes mayo have occurred in Cromínia, being an additional factor which may affect Cr isotopic composition. While several studies have shown that chromite is

systematically enriched in light isotopes (-0.08±0.06‰ according to Schoenberg et al. (2008)), if hydrothermal processes took place in Cromínia, hydrothermal chromite would be enriched in ^{53}Cr as a consequence of reduction of isotopically heavy Cr(VI) (Farkaš et al., 2013; Wang et al., 2016). Weathering is also a process which could favor the presence of isotopically heavy Cr in the solid phase. During weathering, Cr(VI) is released, with a consequent re-deposition, via Fe-oxide trapping, which later is reduced to isotopically heavy Cr(III). The $\delta^{53}Cr$ values reported in solid samples are never higher than +1‰, as a result of weathering or serpentinization processes. We hypothesize that exploitation mining activities, which implies mobilization and transport of a relevant amount of material, increase the heavy Cr(VI) mobilized and re-deposited as Cr(III), which could partially explain the heavy $\delta^{53}Cr$ values observed in the affected soil profile (>+3 ‰).

Hexavalent chromium released from non-affected and, in minor proportion, affected soil profiles can be transported into local creeks. The SPM in the creeks presents a similar, but slightly lower $\delta^{53}Cr$ value (+2.78 and +2.37 ‰) than the one of the top of the affected-soil profile (+3.08 ‰), while in the dissolved fraction $\delta^{53}Cr$ value was associated to the presence of the mobile hexavalent chromium. These results suggest that in the directly affected area, where chromite is one of the main Cr-bearing phases, the exploitation activities had left the area clearly exposed to environmental factors and due to erosion and eolian transport, the particles enriched in ^{53}Cr are transported into the creeks.

iv. CHROMIUM LEACHABILITY OF SAPROLITIC AND LATERITIC ORES

Ultramafic areas are enriched in heavy metals such as Cr and Ni, which explains why those areas are preferentially mined. Cr is present in Fe-Ni lateritic and saprolitic ores, waste rock and overburden. Most published studies focus on Cr mobility from mining waste materials and there is a lack of information regarding Cr fate in laterite mines localized in tropical regions. Leaching experiments of saprolitic and lateritic ores of ultramafic areas were conducted to evaluate the potential leaching of geogenic chromium and its isotopic composition.

The saprolitic ore (S3) is dominated by phyllosilicates, including minerals of the serpentine group, as well as clay minerals (smectite, chlorite). By contrast, Fe oxides (goethite and hematite) were dominant in lateritic ores which presented a higher degree of alteration (UMIA) compared with the saprolitic ore. The exchangeable pool of Cr was significantly higher in lateritic

than saprolitic ores, and it was mainly represented by the toxic Cr(VI). Thus, Fe oxides control the Cr availability in these lateritic ores.

The Fe oxides control ores Cr was also evident from leaching experiments with ores OL5 and OL8 which, according to XRD results, are composed of goethite and goethite and spinel, respectively. The Cr concentration in the leachate of ore OL5 (61 – 200 μg L^{-1}) is higher compared to the other lateritic and saprolitic ores (5 – 72 μg L^{-1}), increasing over time and becoming isotopically heavier (+1.93 ± 0.02 ‰ to +2.07 ± 0.02 ‰). In addition, Cr released from all the ores is present in its hexavalent form. Cr fate controlled by manganese oxides, which promote a first oxidation from Cr(III) to Cr(VI) followed by co-precipitation was observed during the leaching experiment with ore OL3 (composed mainly of hematite and chlorite).

While Cr in the leachate of ore OL3 was isotopically heavier compared to OL5 and OL8, Cr concentration in the leachate was lower (6 – 72 μg L^{-1}). In agreement with the differences in the isotopic composition in the leachate of ores OL3, OL5 and OL8, the δ^{53}Cr value of the original material was lower for OL3 (-0.76 ± 0.07 ‰) than for OL5 and OL8 (-0.43 ± 0.02 ‰ and -0.51 ± 0.06 ‰, respectively). In ore OL1 (quartz, spinel and goethite), Cr does not change over time during the leaching experiment and the Cr concentration in the leachate is the lowest among the lateritic ores (5 – 7 μg L^{-1}), however, the Cr isotopic in the leachate is the highest among all the ores (+4.84 ± 0.06 ‰.). Finally, in agreement with the exchangeable pool of Cr(VI) and the degree of alteration, the saprolitic ore OS3 presented the lowest Cr concentration in the leachate (< 6 μg L^{-1}), however the δ^{53}Cr value (+1.71 ± 0.02 ‰) was within the range of variation of the lateritic ores.

Despite weathering in ultramafic areas being well known as a natural source of Cr, mining activities acts a “catalyst” of this process. This study reveals that although lateritic ores in ultramafic areas are used to extract Ni, significant amount of Cr (mainly as toxic Cr(VI)) can be released due to the exposure of that material to environmental factors, such as rain and wind. In this process, pH, dissolved oxygen, manganese and iron oxides control Cr fate, speciation and isotopic composition. These results should encourage mining companies to focus on prevention and mitigation measures not only in Ni contamination, but also in other possible toxic metals such as Cr, which can be released from ores to ponds, surface and groundwater bodies.

v. (BIO)LEACHING BEHAVIOR OF CHROMITE TAILINGS

Chromite beneficiation operations in Sukinda valley (Odisha, India) produce large amount of tailings (3.7×10^5 tons $year^{-1}$), which are stored in open air. Several studies have been carried out to increase chromite extraction yield and therefore, to decrease the tailing production. However, the chromite tailings environmental impact has not been deeply studied so far. Hence, bio-leaching and chemical leaching experiments were performed to establish the leachability of chromite tailings.

XRD results showed that chromite tailings contain chromite, as well as gangue minerals such as lizardite, goethite, hematite, gibbsite and chlorite. Several elements are present in the tailings which contents decreasing as follows Fe > Cr > Al > Si > Mn. During incubation of the fresh tailings sample with *A. thiooxidans*, the sulfur oxidation using dissolved oxygen as electron acceptor produces sulfuric acid. The acidic conditions in the experiments with *A. thiooxidans* favor the dissolution of Fe > Al > Mn and Ni, compared with *P. putida* where the concentrations of these elements in the leachate are lower. Despite the production of siderophores by *P. putida*, Fe in the leachate was lower than for *A. thiooxidans*.

The Cr leached at the beginning of the incubation of fresh tailing with *A. thiooxidans* (pH 2) and *P. putida* (pH 9), corresponded to the concentration of Cr(VI) extracted with KH_2PO_4. Subsequently, Cr(VI) decreases in solution as a result of reduction to Cr(III) and prior precipitation, and adsorption onto Fe oxides phases. Comparing fresh tailings incubation with and without bacteria, it was noticed that both *P. putida* and *A. thiooxidans* are able to reduce Cr(VI) content in the leachate. Consequently, those types of bacteria could be seen as a remediation pathway, as well as the possible opportunity to recover leached metal from residues (tailings).

The source of Cr(VI) in the tailings is not chromite. Because: 1) chromite is a spinel resistant to alteration and even if some studies (Fandeur et al., 2009; Garnier et al., 2008) reported that chromite could be a potential source of Cr(VI), the duration of the leaching experiments of the present study was too short for Mn oxides to oxidize Cr. In addition, the concentration of Mn oxides was limited; 2) Cr(VI) extracted with KH_2PO_4 from chromite ore was negligible (~ 2 mg kg^{-1}), and probably the Cr(VI) extracted was coming from gangue minerals present in the mixed ore; 3) in the chemical leaching of the concentrated ore, with acidified MQ water (pH 2) (extreme

conditions), extracted Cr was more than 4 fold lower than the one obtained during the chemical leaching performed under the same conditions with the fresh tailing sample.

A total of 37.28×10^5 tons $year^{-1}$ of chromite tailings are produced containing 15% of Cr_2O_3. If the chemically exchangeable pool of Cr(VI) ($E_{Cr(VI)}$) in fresh tailings is considered, potentially 111,500 kg of Cr(VI) could potentially be released per year. Nevertheless, the Cr(VI) content in old stockpiles tailings (31 in the bottom – 149 mg kg^{-1} in the surface) is lower than in the fresh tailings (223 mg kg^{-1}), and Cr(VI) content decreases with depth. These results indicate that Cr(VI) released is attenuated over time, probably due to the presence of bacteria which reduce and immobilize the toxic hexavalent chromium, as a natural mechanism in stockpiled tailings mediated by the presence of organic matter.

vi. RESULTS OVERVIEW

The context of this PhD and the main findings of the research are displayed in Figure 1. Natural weathering takes place in ultramafic areas, where isotopically heavy and exchangeable Cr(VI) is released, leaving behind solids depleted in ^{53}Cr. Chromium released during weathering may reach the streams and ground waters. Cr can be present as Cr(III) or mobile Cr(VI). In pristine areas, non-exchangeable Cr (Cr(III)) is mainly associated with colloids. There, the presence of organic and inorganic colloids containing non-exchangeable chromium causes an overestimation of the E^W_{Cr} value.

Large amount of residues are produced by exploitation and beneficiation in mining activities of ultramafic areas. The potential release of Cr(VI) differs among mining residues, and depends on the Cr-bearing phases as well as the degree of alteration (UMIA). Fe oxy-(hydroxides) were identified as one of the main Cr-bearing mineral phase controlling Cr fate. The lateritic ores in Barro Alto, which are the most altered materials studied here have the highest chemically and isotopically exchangeable pool of Cr(VI) ($E_{Cr(VI)}$). This suggests that residues stored into the mining area could potentially be the main sources of Cr(VI), mobilized within surface waters and deeper soil profiles. The $E_{Cr(VI)}$ values are related to enrichment in ^{52}Cr in the solid phase. Chemical leaching of ores showed that in the leachate Cr was present in its hexavalent form which was enriched in ^{53}Cr. In ores OL5 and OL8, composed mainly by goethite, $\delta^{53}Cr$ increased overtime in the leachate.

Tailings produced after chromite beneficiation process showed a decrease in Cr(VI) leachability while they were stockpiled. Bioleaching experiments in batch reactors with *Acidithiobacillus thiooxidans* or *Pseudomonas putida* evidenced Cr(VI) reduction.

A. thiooxidans produced a series of sulfur compounds with high reducing power, while *P. putida* used a variety of electron acceptor for chromate reduction. In addition extracellular polymeric substances (EPS) enhance Cr(VI) reduction efficiency. Increase of natural organic matter (NOM) and mineral carbonation may be additional factors which explain the lower exchangeable pool of Cr(VI) in stockpiled chromite tailings compared to fresh tailings.

Isotopic exchange experiments confirmed the contribution of particulate matter and colloids containing Cr-bearing phases, mainly iron oxy(hydroxides), in streams affected by mining activities. Larger particles (>0.2 µm) were dominant in the impacted area. The contribution of Cr containing particles is related to erosion and eolian transport in mining areas, of material previously milled. This reflects an accelerated weathering, probably due to exploitation mining activities. In Cromínia, it is partially responsible of the high δ^{53}Cr values found in the affected soil profile. Natural weathering resulting in re-deposition of mobilized isotopically heavy Cr and the existence of hydrothermal chromite in Cromínia, might be the main causes. Finally, the gap between natural and accelerated weathering is reflected in the Cr isotopic composition in the dissolved phase of the pristine and mining area, respectively. The δ^{53}Cr in the Cr(VI) extracted from the mining residues and in the ores leachate, is within the range of variation of δ^{53}Cr in water bodies impacted by mining activities. This suggests that Cr isotopes measured in the dissolved fraction could be used as a tracer of sources in mining context.

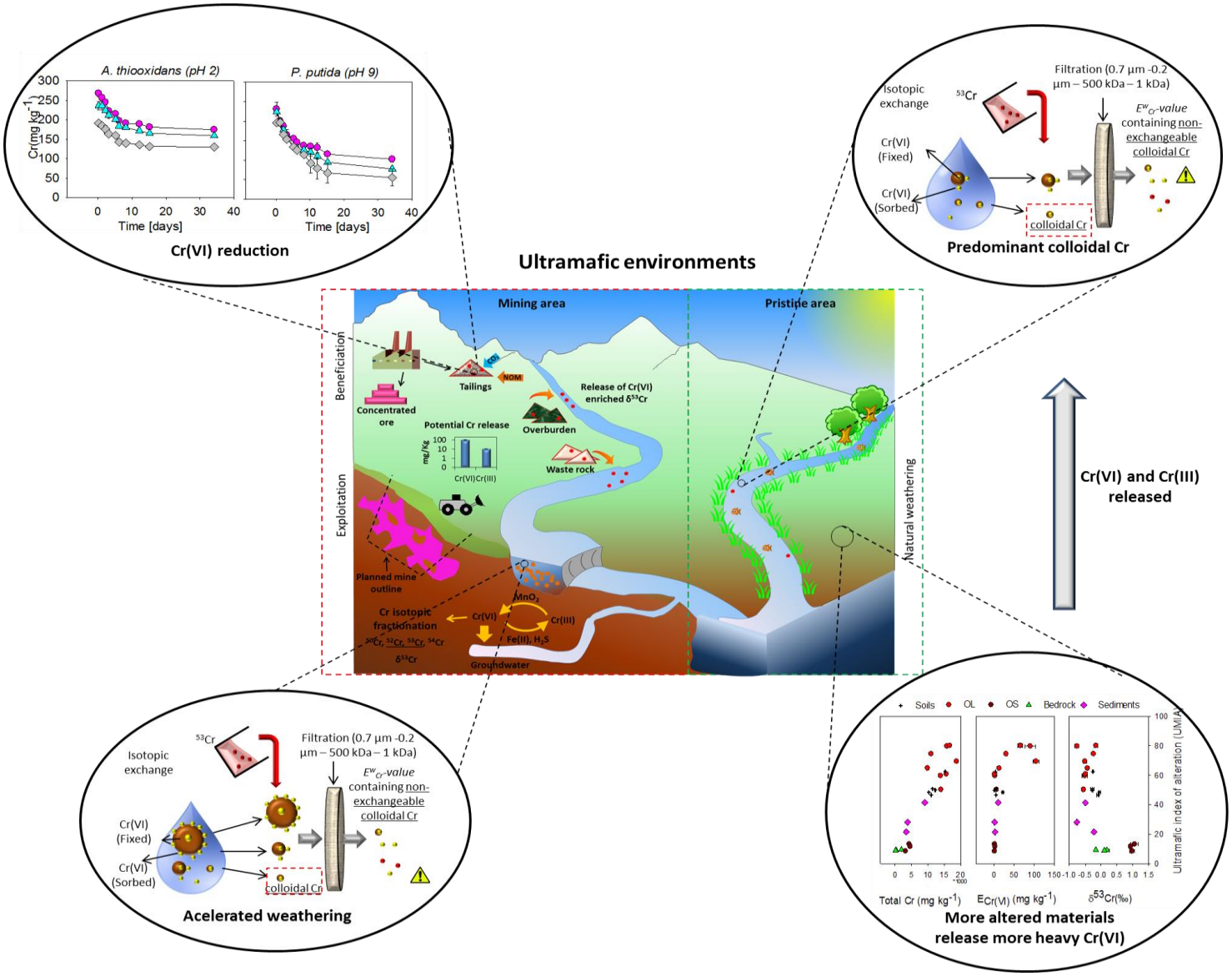

Figure 1. Understanding of biogeochemical processes controlling Cr mobility and availability in ultramafic environments.

vii. FUTURE PERSPECTIVES

While conducting this research, some difficulties were encountered, which might serve for the development of further research in this direction. The limitation lies within the following context:

- Future studies should systematically consider the presence of the non-exchangeable fraction of metals due to the colloidal contribution in water bodies, while calculating both corrected and un-corrected E values, in order to assess the importance of the potential bias for a given sample.

- The real Cr isotopic signature of individual phases present in mining residues has not been measured yet, as it is exceptionally difficult to physically isolate each phase. Similarly, the Cr alteration rate and kinetics of the main individual crystalline and amorphous phases present in mining residues such as overburden, waste rock and tailings, should be evaluated. This will help to understand the contribution of each phase to the overall alteration of mining residues.

- It is still unclear the gap between field weathering conditions and laboratory leaching experiments to predict long term reactivity of the material leached. *In situ* measurements will help to set precedents of field conditions.

- It is well known that bacteria could play an important role in the mobilization of metals. In this sense, bio-leaching experiments should be ideally performed with bacteria isolated from the mining waste residues. Bio-leaching experiments coupled with chemical leaching will give a more complete overview of the factors controlling metals mobility and availability.

- Chromite tailings studies have focused on the increase of the chromite yield, however the environmental risk that tailings represent for the environment has never been studied. This work is the first to evaluate the behavior of certain metals released from tailings, however many questions associated with the role of secondary phases on Cr mobility still remain. In addition, conditions closer to the field should be evaluated.

viii. REFERENCES

Fandeur, D., Juillot, F., Morin, G., Livi, L., Cognigni, A., Webb, S.M., Ambrosi, J.P., Fritsch, E., Guyot, F., Brown, G.E., 2009. XANES evidence for oxidation of Cr(III) to Cr(VI) by Mn-oxides in a lateritic regolith developed on serpentinized ultramafic rocks of New Caledonia. Environ. Sci. Technol. 43, 7384–7390. doi:10.1021/es900498r

Farkaš, J., Chrastný, V., Novák, M., Čadkova, E., Pašava, J., Chakrabarti, R., Jacobsen, S.B., Ackerman, L., Bullen, T.D., 2013. Chromium isotope variations (δ53/52Cr) in mantle-derived sources and their weathering products: Implications for environmental studies and the evolution of δ53/52Cr in the Earth's mantle over geologic time. Geochim. Cosmochim. Acta 123, 74–92. doi:10.1016/j.gca.2013.08.016

Garnier, J., Quantin, C., Echevarria, G., Becquer, T., 2009. Assessing chromate availability in tropical ultramafic soils using isotopic exchange kinetics. J. Soils Sediments 9, 468–475. doi:10.1007/s11368-009-0062-4

Garnier, J., Quantin, C., Guimaraes, E., Becquer, T., 2008. Can chromite weathering be a source of Cr in soils? Mineral. Mag. 72, 49–53.

Mills, C.T., Morrison, J.M., Goldhaber, M.B., Ellefsen, K.J., 2011. Applied Geochemistry Chromium (VI) generation in vadose zone soils and alluvial sediments of the southwestern Sacramento Valley , California : A potential source of geogenic Cr (VI) to groundwater. Appl. Geochemistry 26, 1488–1501. doi:10.1016/j.apgeochem.2011.05.023

Rai, D., Eary, L.E., Zachara, J.M., 1989. Environmental chemistry of chromium. Sci. Total Environ. 86, 15–23.

Schoenberg, R., Zink, S., Staubwasser, M., von Blanckenburg, F., 2008. The stable Cr isotope inventory of solid Earth reservoirs determined by double spike MC-ICP-MS. Chem. Geol. 249, 294–306. doi:10.1016/j.chemgeo.2008.01.009

Wang, X., Planavsky, N.J., Reinhard, C.T., Zou, H., Ague, J.J., Wu, Y., Gill, B.C., Schwarzenbach, E.M., Peucker-Ehrenbrink, B., 2016. Chromium isotope fractionation during subduction-related metamorphism, black shale weathering, and hydrothermal alteration. Chem. Geol. 423, 19–33. doi:10.1016/j.chemgeo.2016.01.003